DYNAMIC ANALYSIS OF THE CUTTING FORCES IN GEAR HOBBING

by

Ali M. Abood, BSc.

This thesis is submitted in fulfilment of the requirements for the degree of Doctor of Philosophy

School of Mechanical and Systems Engineering
University of Newcastle upon Tyne, UK

December 2002

ABSTRACT

The work reported in this thesis has been developed to predict and measure the cutting forces in the gear hobbing process. A review of past research in this area has highlighted the need to adopt a different approach to modelling the process in order to predict the cutting forces. The hobbing process has been described using six different co-ordinate systems and the kinematic relationships between these systems established. A single rack profile has been used to represent the profile of a single cutting tooth from the hob which was then extended to simulate the hob itself.

When the hob gashes pass through the cutting region surfaces are generated which, if mapped on a regular grid can give the basis to estimate the depth of cut, i.e. the instantaneous chip thickness produced by that particular tooth. The instantaneous cutting forces generated by that tooth then can be estimated by using the concept of a specific cutting force of the workpiece material. The estimation of cutting forces acting on a single tooth space was used to predict the cutting forces produced during machining of a full gear, by assuming that the forces acting in a particular tooth space are equal to those acting on the adjacent tooth space at an equivalent instant in the cutting cycle. In order to validate predicted results, a Churchill PH1612 hobbing machine was retrofitted with a CNC control system at Newcastle University, utilising a programmable multi axis controller (PMAC).

A specially made single toothed gear, and a full gear were machined, and cut on this machine, and the cutting forces measured in real time using a 3-axis dynamometer. The force signals produced by the dynamometer were measured utilising a 12-bit ADC card. Code, written in C, was developed to perform the many functions needed for the overall control of the machine, but additionally was used to capture both the cutting forces and axis position data. The results of the simulation and modelling have shown very good agreement with those obtained experimentally.

ACKNOWLEDGMENTS

It is not easy to list the many people who have helped me during the course of this project, as it is now presented. But my first thanks are to Dr. Robert Bicker, my supervisor, for his support, and his patience. But most of all for his constructive technical advice and many suggestions throughout this project, which has been invaluable.

Special thanks must be directed to Mr. Tony Pennell who has helped and guided me on the theoretical part of the project. His invaluable support cannot be adequately expressed by words.

I would also like to thank the Design Unit, especially Mr. Robin Ashby for making available the force-sensing dynamometer. Thanks are also due to all the technicians who have helped with this project, especially Mr. Robert Adamson, and Mr Derek Simm, and also Mr. David Glennie for his advice and support during his time at Newcastle University.

Finally I would like to thank and dedicate this thesis to my family, especially my wife and my daughters, Mariam, Sarah, and Monna.

NOMENCLATURE

Control system variables are referred to in chapter 5 are not listed here. They are defined where they first appear.

Symbol	Notation
$a(t)$	Distance between the vertical slide and the worktable *(mm)*
a_0	$a(t)$ initial distance *at t=0 (mm)*
b	Blank face width *(mm)*
c_f	Chamfer height *(mm)*
F_{cmk}	Cutting force acting in the cutting direction *(N)*
F_{nmk}	Cutting force acting normal to the workpiece *(N)*
F_{res}	Resultant cutting force *(N)*
H	Hob lead (*mm)*
h_0	Vertical height between the gear blank mid face and the worktable *(mm)*
h_{a0}	Hob addendum *(mm)*
h_c	Depth of cut *(mm)*
h_{f0}	Hob dedendum *(mm)*
h_{mk}	Chip thickness at *mk* grid *(mm)*
h_{nmk}	Normal chip thickness at *mk* grid *(mm)*
h_{pq}	Chip thickness at *pq* grid *(mm)*
i_1	Index ratio
i_{ref}	Hob reference tooth
K_c	Specific cutting force (in the cutting direction) (N/mm^2)
K_n	Specific cutting force (normal to the workpiece) (N/mm^2)
k	Number of point along the hob profile $(k_{min} \le k \le k_{max})$
l_k	Length of the k^{th} element on a hob tooth cutting edge *(mm)*
M_0	Hob moment *(N.m)*
M_1	Gear moment *(N.m)*
m	Number of steps of hob revolution
m_n	Gear module *(mm)*
n_0	Hob rotational speed *(rpm)*
n_1	Gear rotational speed *(rpm)*

P_1, P_2	Points on the hob
P_{ijk}	Point k (at r_k) on hob tooth i, and start j.
r_0	Hob base radius *(mm)*
r_{a0}	Hob tip radius *(mm)*
r_{a1}	Gear blank tip radius *(mm)*
r_k	Radius at P_{ijk} *(mm) (same for all i,j)*
s_a	Axial feed rate *(mm/gear revolution)*
s_r	Radial feed rate *(mm/gear revolution)*
s_t	Tangential feed rate *(mm/gear revolution)*
v_a	Axial feed rate *(mm/sec)*
v_r	Radial feed rate *(mm/sec)*
v_t	Tangential feed rate *(mm/sec)*
$x_z(t)$	Axial shift *(mm)*
z_0	Number of teeth (starts) on hob *(mm)*
z_1	Number of teeth on gear *(mm)*
$z_a(t)$	Axial travel of hob head along the hob slide *(mm)*
z_{a0}	Hob head height from base at *t=0 (mm)*
z_k	Axial offset of P_{jik} *from tooth axis (mm)*
α_{cf}	Chamfer angle *(°)*
α_n	Normal hob pressure angle *(°)*
α_{nk}	Normal flank angle *(°)*
β	Helix angle *(°)*
β_k	Side rake angle *(radians)*
γ_0	Hob lead angle *(°)*
ε_k	Rake angle *(°)*
η	Hob setting angle *(°)*
$\theta_{i,j}$	Angle between two consecutive hob gashes *(°)*
ρ_{a0}	Hob tooth tip radius *(mm)*
ϕ_0	Hob rotation angle *(radians)*
ϕ_1	Gear rotation angle *(radians)*
ψ	Profile slope*(radians)*
ω_0	Hob angular velocity *(rad sec)*

ω_1	Gear angular velocity *(rad/sec)*
$\hat{c}_k$	Cutting direction unit vector at P_k
$\hat{n}_{1(1)}$	Surface normal unit vector at P_{ijk}
$\bar{v}_{rel}$	Relative velocity between hob and gear
$\hat{t}_{0(1)}$	Tangent to the surface at P_{ijk}
$(0XYZ)_{(1)}$	Co-ordinate axis of a point in system (1)
$(0XYZ)_{(2)}$	Co-ordinate axis of a point in system (2), etc.

Note that $(OXYZ)_{(6)}$ refers to co-ordinate axis of a point in system (6), whilst $(OXYZ)_{(i)}$ is the co-ordinate axis of the reference tooth at system (6)

CHAPTER ONE

INTRODUCTION

Hobbing is regarded as one of the most accurate gear cutting processes, but because of the demands for improved performance gears, it is essential to manufacture better quality gears, preferably without using a further finishing process, such as grinding. Hobbing machines have traditionally been designed using mechanical transmission systems, whereas the new generation machines are based on computer numerical control (CNC) where the axes are synchronised using an 'electronic gearbox'.

The opportunity to manufacture gears to a high quality are much improved with CNC controlled hobbing machines, since they have reduced transmission error, reduced set-up time, better reliability, and thus reduced cost.

It is considered important to understand the kinematics of the hobbing process, in order to provide the researcher with an improved understanding of how the gear generation process works, and how to improve it. The kinematic generating process is rather complex and consequently it is difficult to perceive the interaction between the hob and the workpiece. Recent researches have shown that a better understanding of the cutting force behaviour, in relation to the dynamic stability of the machine and tool wear is also very important in the manufacture of gears to a high accuracy and surface finish.

1.1. OBJECTIVES

The main aim of the work reported in this thesis is to provide the research community with a better understanding of the hobbing process. In carrying out this work it has been necessary to re-engineer a Churchill PH1612 hobbing

machine by replacing its old NC control system with a new CNC control system, in an effort to produce a better quality gear with improved surface profile. However the main objectives of the study was to:

- Carry out an analysis of the gear hobbing process, and develop a functional kinematic model that realistically simulates the interaction between the hob and the gear blank during the cutting process.
- Use the kinematic model to predict the resulting instantaneous chip thickness.
- Compute the instantaneous cutting force throughout the full cutting cycle.
- To accurately measure the cutting forces on the gear blank, in real-time, for comparison with the predicted values.

1.2. THESIS LAYOUT

In order to study the hobbing process it was first necessary to understand the basic rules of gearing, which govern the generation process. In Chapter 2 all the hobbing process methods are described and the pertinent kinematic formulae are introduced and explained, primarily to give the reader a better understanding of the gear hobbing process.

Gear hobbing was invented many years ago, and the historical improvements associated with the process are covered in Chapter 3, including the development of the kinematic theory of cutting. This chapter provides the basis from which the main objective of the work could be realised, namely the study of cutting force behaviour in the gear hobbing process.

The kinematics of the hobbing process are rather complicated and require a full understanding of the kinematic inter-relationships between the different elements of the machine. Chapter 4 describes the machine element design and the resulting kinematic transformations between these elements.

There are many different types and sizes of hobbing machines. Chapter 5 discusses the design of the Churchill PH1612 hobbing machine used in this

study, and the stages in the development of re-engineering the machine from a mechanical transmission to a fully computer controlled machine at Newcastle University. The design of force dynamometer used in the investigation is also described, along with the data acquisition method.

Chapter 6 presents the main findings of this research. The results of both practical tests and theoretical analysis are reported separately. The experimental test programme involved cutting a two-tooth gear as well as several full gears. The results from the simulation study are also presented and include the generation of the basic rack profile, full hob profile, and the cutting profile. The chip cross-section, and computed forces acting on a single tooth gear are analysed, prior to the estimation of cutting forces on a full gear.

In Chapter 7, the results of the foregoing work are discussed in detail and the conclusions presented. Comparisons between the practical and the theoretical tests are investigated. Recommendations for future work, for example developing the modelling software to predict cutting forces for a range of parametric conditions, including wear behaviour of the cutting tool, are also included.

Additional material that is supplemental to the work presented in this thesis is included in several Appendices, including a comprehensive list of references and bibliography.

CHAPTER TWO

THE HOBBING PROCESS

2.1 INTRODUCTION

Most cylindrical gears are produced by the hobbing process, which is regarded as the most accurate gear cutting process. It is unlikely to be replaced by any other process in the near future, especially if large externally toothed cylindrical gears of high accuracy are needed. Some hobbing machines are capable of cutting any diameter up to 11.76-m (40-ft).

Hobbing is used for rough and finish machining of both soft and hardened gears. It is also suitable for one-off, small batch and mass production environments. Whilst it is the most common method for cutting external spur and helical gears, it is also extensively used to cut external splines, serrations and chain sprockets. It is the only practical method for producing wormwheels, using a hob similar to the worm with which the wormwheel is to mesh. Other components that can be produced on hobbing machines include worm type screw compressor rotors and ratchets wheels. Modern CNC hobbers are capable of producing non-circular and tapered gears.

2.2 BASIC PRINCIPLE OF HOBBING

Hobbing is a continuous generating process, in which the cutting tool (the hob) rotates continuously in mesh with the gear being hobbed, progressively cutting all the teeth at the same time, as shown in figure 2.1. As the hob rotates, its multiple cutting edges, which all lie on an enveloping helicoid worm surface, cut out in

space the flanks of a virtual generating rack of infinite length, see figure 2.2, which continuously rolls with the gear blank to generate the required tooth form.

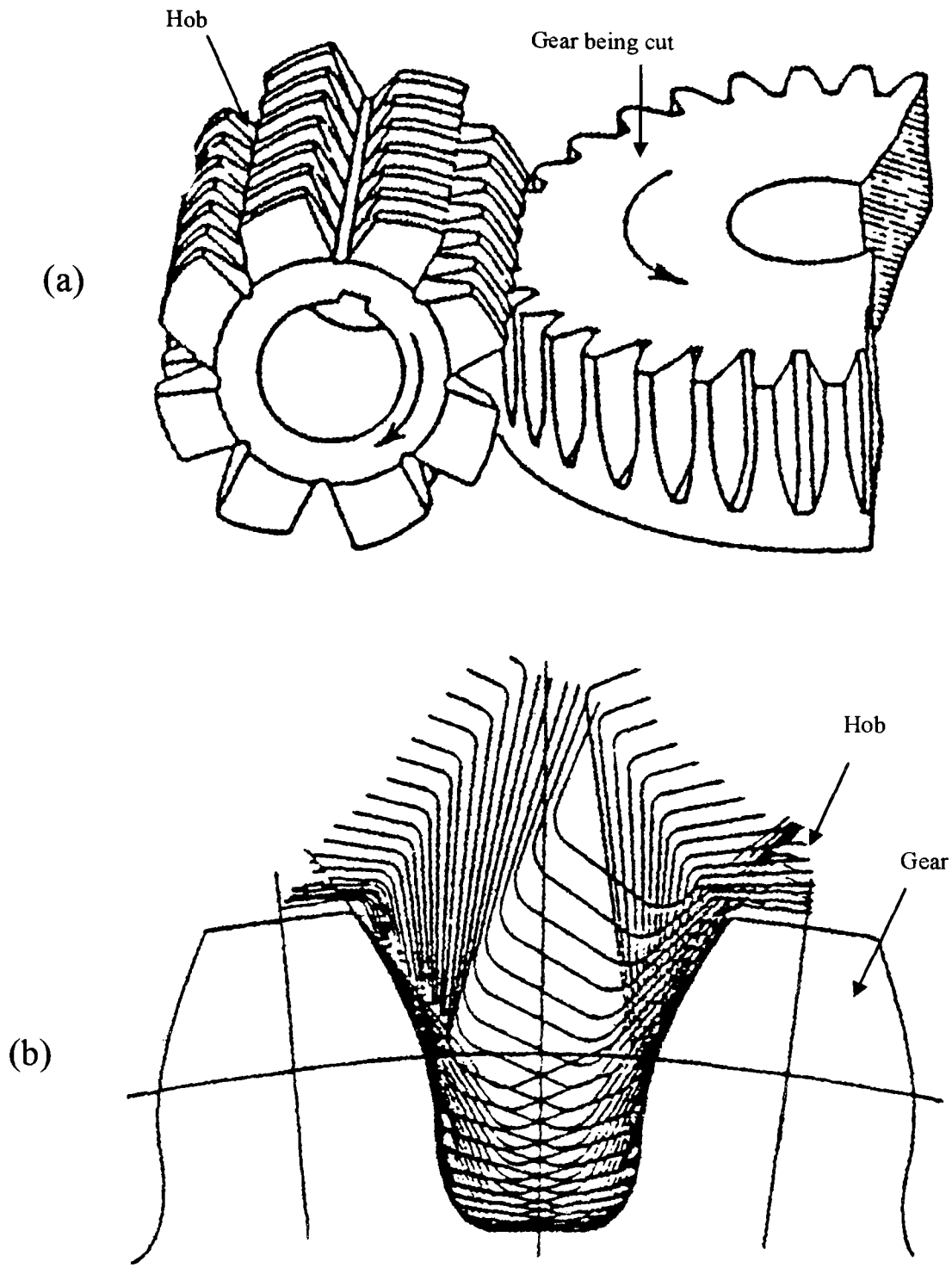

Figure 2.1: (a) The hobbing process, (b) gear generation, relative to gear [BGA].

Rotation of the hob in mesh with the workpiece in this way, with no other relative motion, would generate conjugate teeth on the gear. This would, however completely envelope the hob, like those of wormwheels. For spur or helical gear production, this tooth form is only correct along one generating line on each tooth flank, where the flank touches the virtual rack. To cut spur or helical teeth, it is thus also necessary to feed the hob slowly across the face of the blank, as they rotate in mesh so that each of these generating lines moves progressively across

the tooth flank. All the teeth are then generated simultaneously from one end. [Crockett]

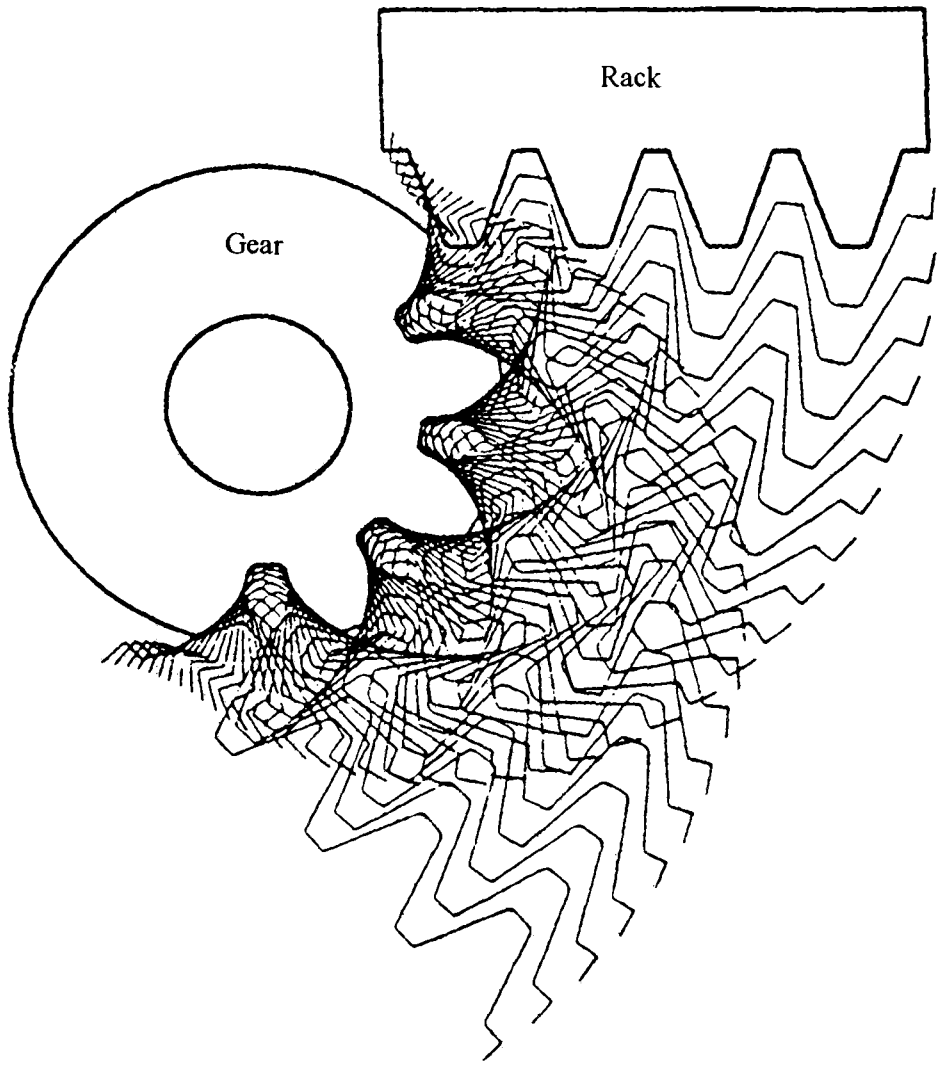

Figure 2.2: The gear generation process (BGA)

2.3 ADVANTAGES AND LIMITATIONS OF HOBBING

The main advantages of the hobbing process are:

- Versatility, which allows hobbing of spur or helical gears, sprockets, splines, serrations, worms, threads and wormwheels of virtually any tooth form on the same machine.
- Continuous rotation of the hob and the workpiece, allowing continuous cutting at high speeds without indexing or other intermittent motions, which cause errors due to the effect of backlash and other clearance.
- No loss of time on the return stroke, and no vibration due to heavy reciprocating masses, (as in gear shaping and planing).

- One hob with almost straight cutting edges will cut all external spur and helical involute gears of a given normal base pitch, so reducing tooling cost.

The main limitations of hobbing include the virtual impossibility of hobbing internal gears, which require a special hobbing head on the machine; an expensive globoidal hob and the gear diameter must be reasonably large. It is also impossible to hob close to a shoulder larger than the root diameter of the gear. Gears of this type can only be produced by shaping unless partial cutting away of the shoulder by the hob is acceptable, e.g. when hobbing splines. For the same reason, double helical gears can only be hobbed if there is a sufficiently large gap at the centre to provide run-out for the hob.

In practice, there are few limitations on tooth form, provided all the teeth are identical. Thus, splines and serrations with a blocked 'master' tooth cannot be hobbed and must be shaped or broached. There may be a restriction on the maximum/minimum number of teeth that can be cut caused by the limited range of table speeds and/or index ratios available on particular machines. [Pennell]

2.4 HOB DESCRIPTION

The conventional hob is made of high-speed steel, which is hardened and may be ground on the form. It can be likened to an involute worm provided with flutes or gashes usually at right angles to the helix and with the tooth profile suitably relieved behind the cutting edges thus formed, figure 2.3. The single start hob is the most common but a number of threads may be provided. The first is preferred for more accurate work while hobs of two or more starts are used in very high production where the gear is to be finished by some other operation.

Each cutting tooth is relieved to provide chip clearance behind the cutting edge. Therefore, the rake face of each tooth can be sharpened while the original tooth shape is maintained. Since hobbing is a generating process, the hob will not cut the shape of the cutting edges form. The law of gearing requires the tooth flank of

a gear and the tooth flank of the pinion to be shaped in such a way that the normal of each contact point of both flanks goes through the pitch point. Therefore, the tooth flank of the hob tooth is not straight, although the hob describes a virtual rack in space. The tooth flank of the gear is cut by the hob where the tooth flank of the hob touches the virtual rack. Effectively, the rack can be imagined to be the cutter.

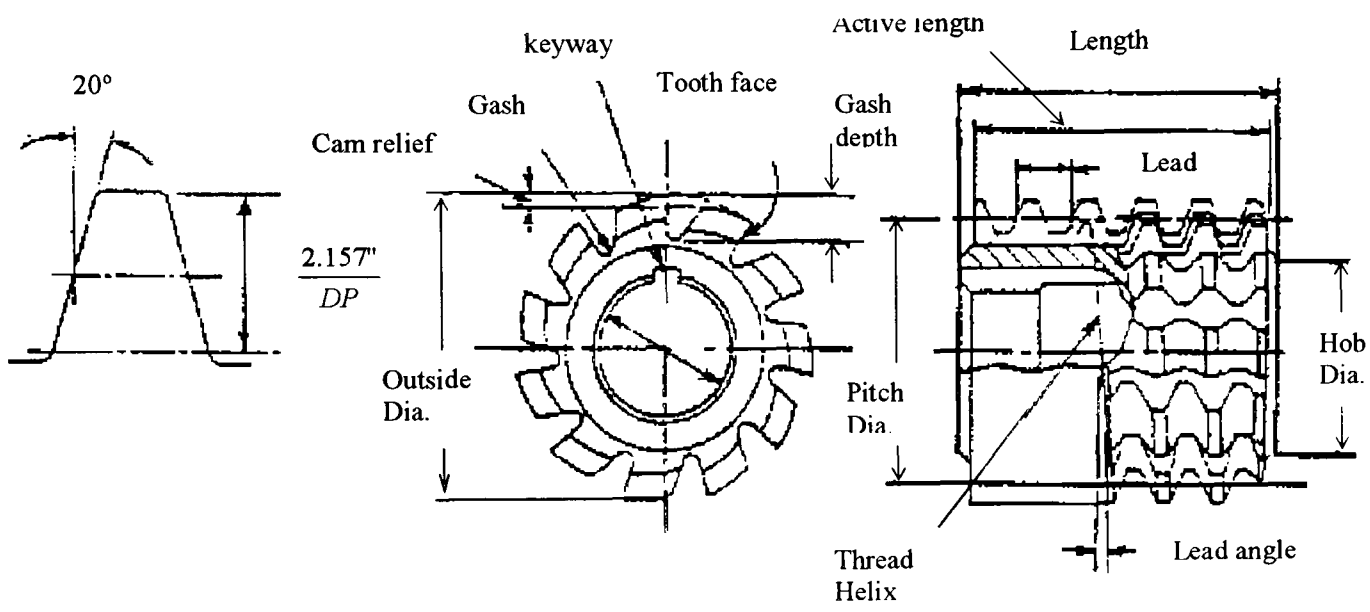

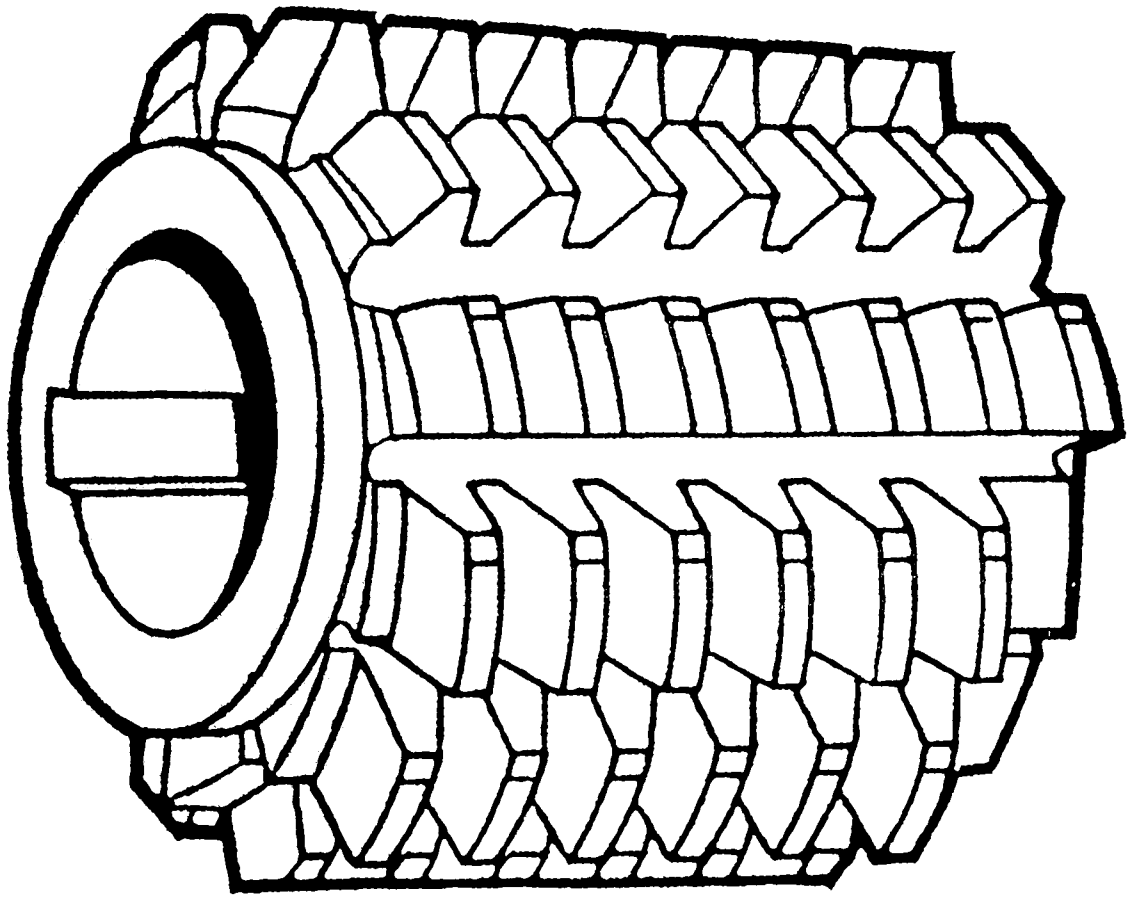

Figure 2.3: The hob [BGA]

2.4.1 Multi start hobs

Some gear hobs are made with two or three threads to reduce the cutting times. In a single start hob only one tooth does the maximum amount of work for any particular axial position of the hob. Whereas with a two-start hob, two teeth will carry the maximum load, provided that the hob has been mounted correctly. The accuracy of single and multi start hobs is the same, but because of the different manufacturing kinematics multi-start hobs do not usually produce gears as accurately as single start hobs. However the effect on the accuracy of the part produced may be of little importance if another finishing process is applied.

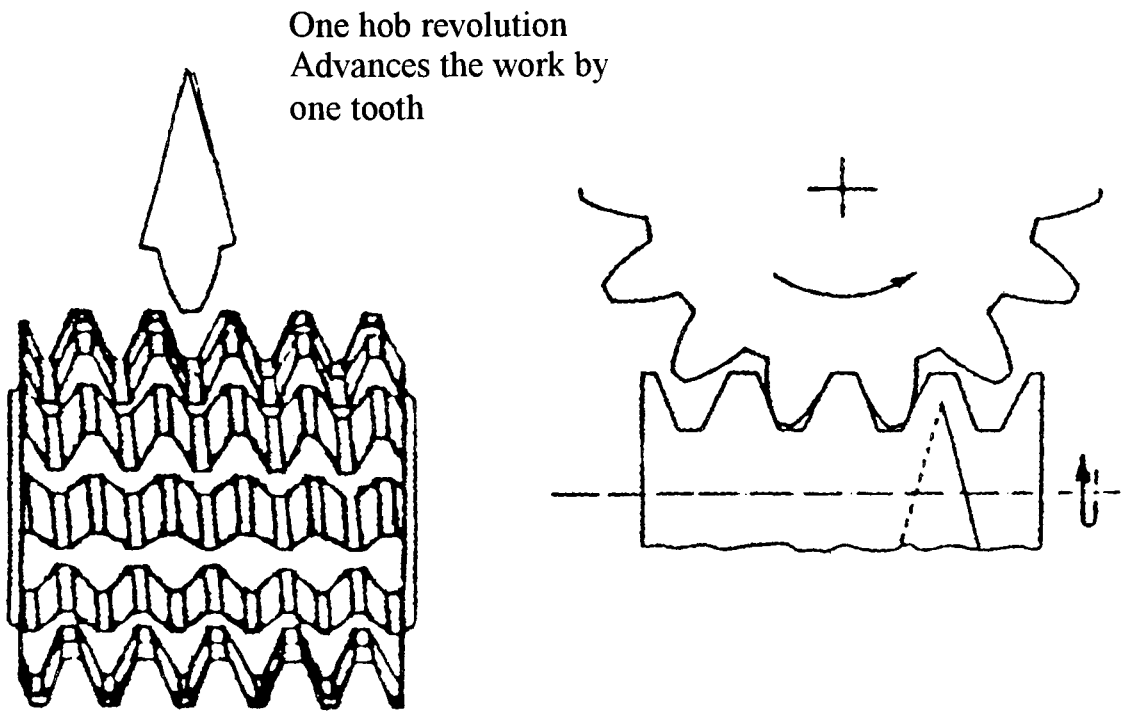

Figure 2.4: Single start hob [Gimpert]

The single start hob produces finer facets down the involute profile since it has more cutting edges available per tooth of the gear. However, for the same overall cutting time, it also produces a coarser feed mark along the tooth parallel to the gear axis. If the multi-start hob were made with more cutting edges it would produce finer facets on the involute profile. However, if it was possible to increase the number of cutting edges on the multi-start hob it would be also possible to increase number on the single start, which would then restore the status quo.

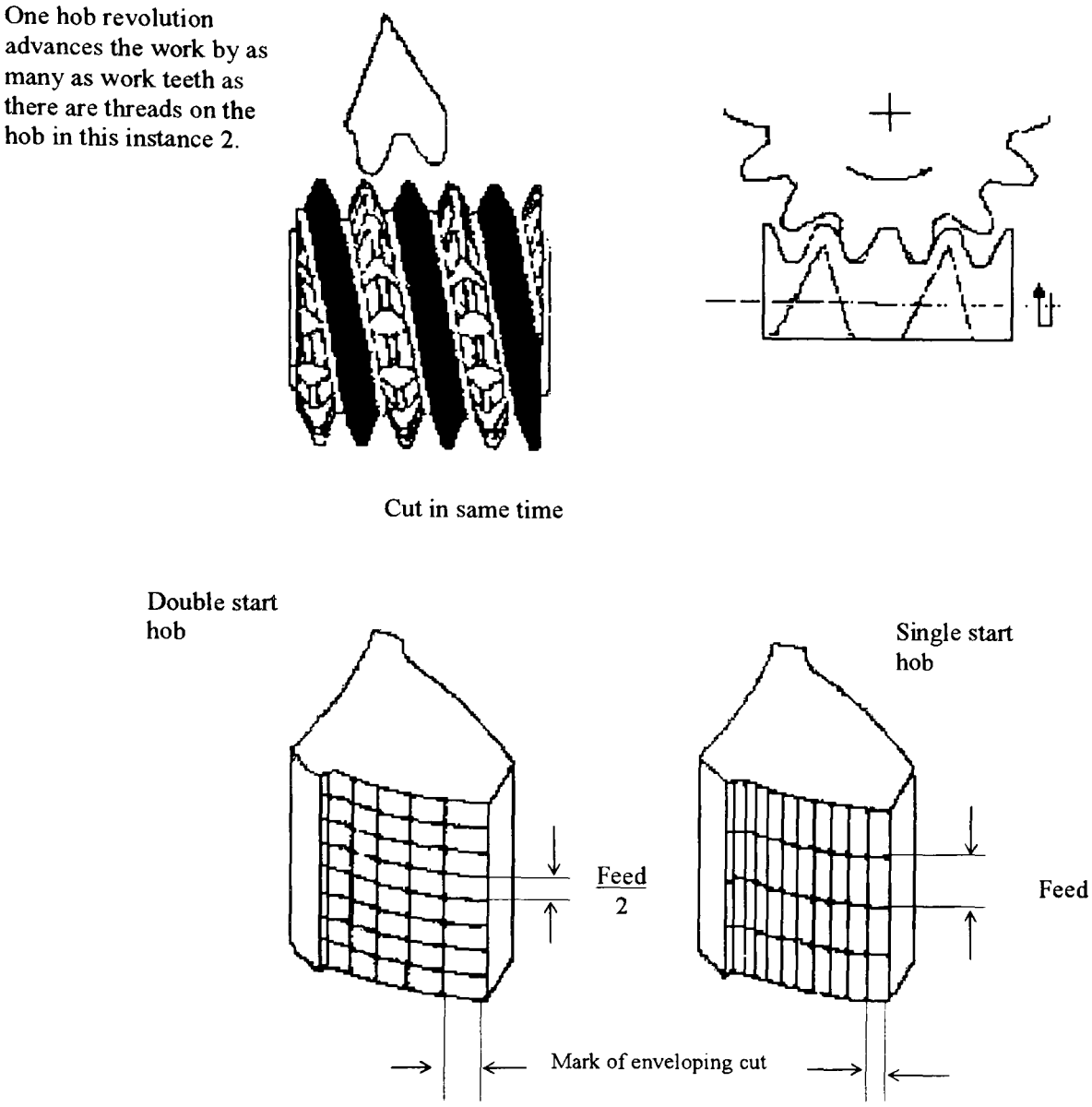

Figure 2.5: Cutting facets produced by single-start and 2-start hob for equal cutting time. [Gimpert]

With a multi-start hob the amount of metal removed per cut is larger, for a given axial feed rate, and because fewer cuts are taken to generate an approximate involute curve, this will reduce the period before sharpening becomes necessary. Multi-start hobs increase the tooth flank surface roughness, providing the hob diameter and the feed per revolution are maintained constant. Also, surface roughness will decrease by choosing a larger hob diameter. On the other hand multi-start hobs have the same pitch accuracy as single start hobs, and this eliminates a possible reason for not using them.

2.5 METHODS OF HOBBING

There are several ways in which gears can be produced by the hobbing process. Some of these techniques are briefly described as follows:

- Climb or conventional hobbing
- Axial hobbing
- Radial hobbing
- Tangential hobbing
- Diagonal hobbing
- Radial feed approach followed by axial feed
- Simultaneous axial and tangential feed
- Simultaneous radial and axial feed

The cutting tool can be fed in a way similar to milling machines, so both conventional and climb hobbing can be used, figure 2.6. In all cases, the cutting forces should be directed against the work spindle, never against the tail-stock. The directions of feed on a hobbing machine correspond to the work axis. In conventional type cutting, the hob is fed into the part in a direction that is in agreement with the tangential vector denoting the direction of hob rotation. Although the chips removed vary in size and shape, the centred hob tooth removes a chip that is comparable with those obtained in conventional milling. The chip starts out thin and becomes increasingly thicker as the hob tooth sweeps through the cut.

Climb cutting takes place when the hob is fed into the part in a direction that opposes the tangential vector denoting the direction of hob rotation. As well as with the conventional type cutting, the chips vary in size and shape. However, unlike conventional type cutting, the chip starts out thick and becomes increasingly thinner as the hob tooth sweeps through the cut.

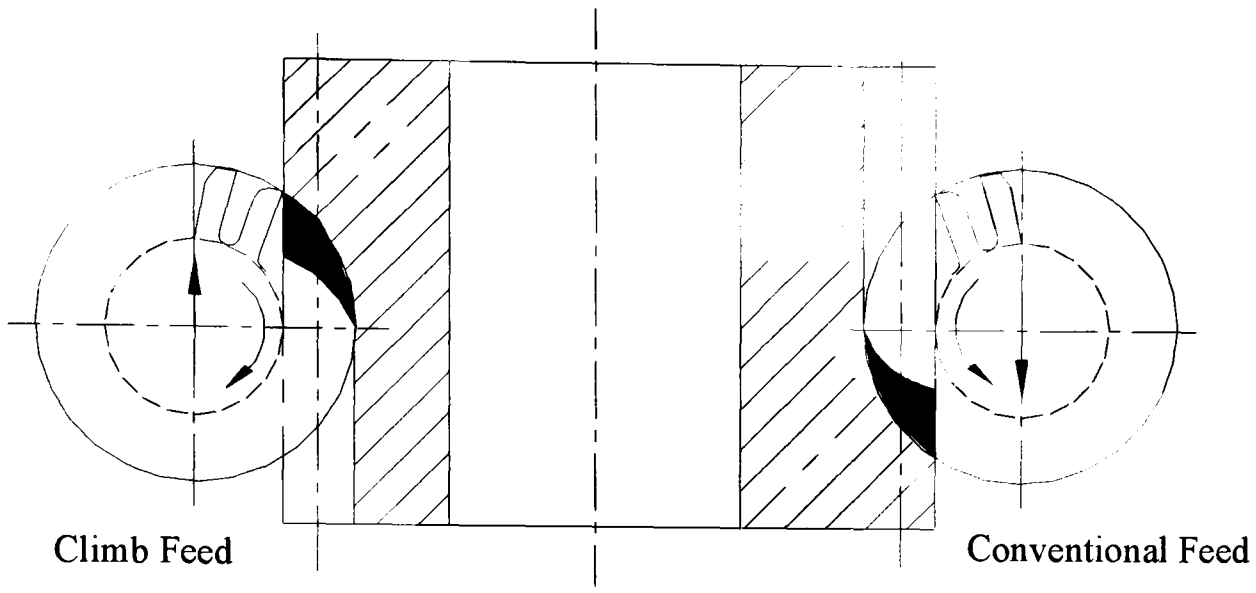

Figure 2.6: Climb and conventional hobbing

Surface finish is usually the main factor to consider when selecting climb or conventional cutting. There is no rule, which can be applied to choose which method will produce a better surface finish for a specific job. In many cases, climb cutting has been applied to replace conventional cutting because a better finish obtained, with equivalent hob life and accuracy, provided the machine is rigid and no backlash.

Tests have shown that in conventional hobbing the tool wear is higher than in climb hobbing especially on spur gears. But it is not the same case for gears with a larger helix angle as in the case of very large helix angles the conventional method is much better. This is helped by the better hob entrance conditions. In addition, the strength of the work gear material is likely to play a certain role.

A point worth mentioning is the fact that rough hobbing by the climb method frequently results in lead errors and poor surface quality. [Lichtenauer]. A general rule of thumb is that climb hobbing yields better tool life, and conventional hobbing yields a better finish. [Gimpert]

Three feed directions are possible, axial, radial and tangential, as shown in figures 2.7, 2.8 and 2.9, with a combination of more than one axis of feed successively or simultaneously during a machine cycle. A radial feed approach followed by an

axial feed across the face is used in fine pitch gear work or on a workpiece where an open axial approach is not possible, figure 2.10.

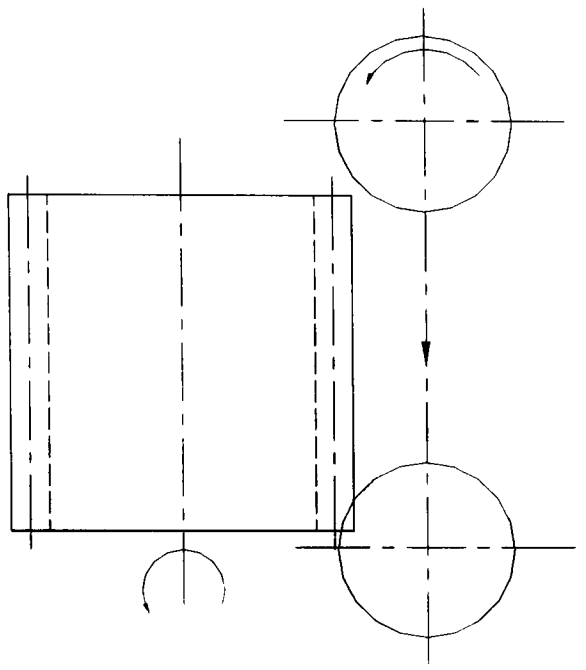

Figure 2.7: Axial feed (conventional)

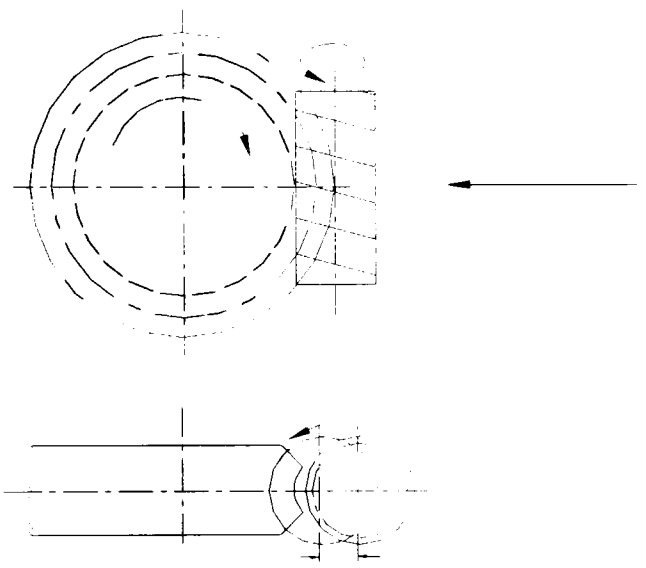

Figure 2.8: Radial feed

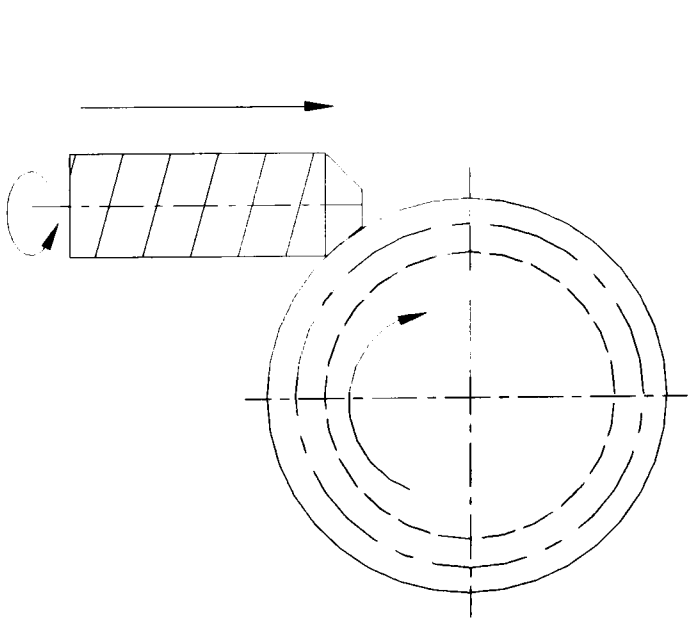

Figure 2.9: Tangential feed

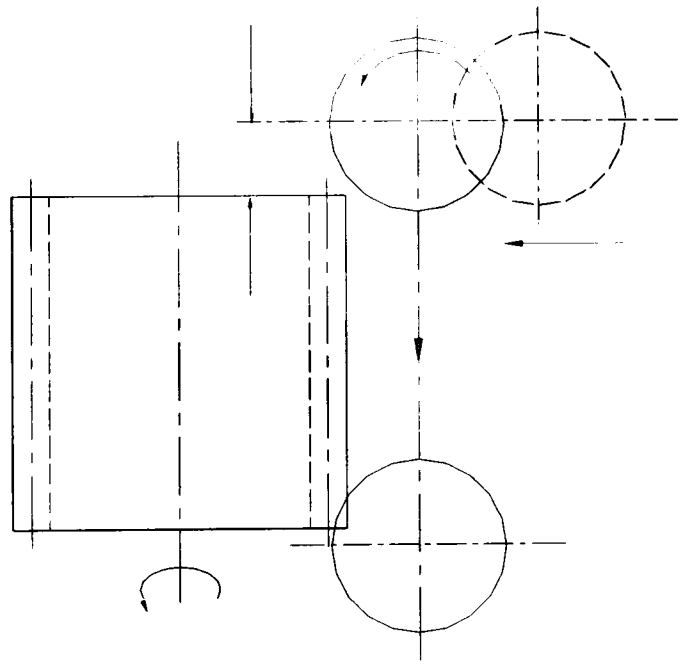

Figure 2.10: Radial feed approach with axial feed

Diagonal hobbing, which is a refinement of the tangential and axial feed method, as the hob moves tangentially along its axis while at the same time it moves axially across the face width of the gear.

Axial and tangential feed can be used simultaneously for very large gears with coarse pitch, and wide faced. The tangential feed presents a sharp portion of the tool as the axial feed cuts across the gear face, figure 2.11. Taper root splines are cut with simultaneous axial and tangential feed, figure 2.12. A 'jump' or 'skip' cycle is used to cut multiple gear elements on a single part. This may be required for gear tooth alignment or simple cutting efficiency, figure 2.13. Simultaneous radial and axial feed, figure 2.14 produce tapered gears or crowned gears.

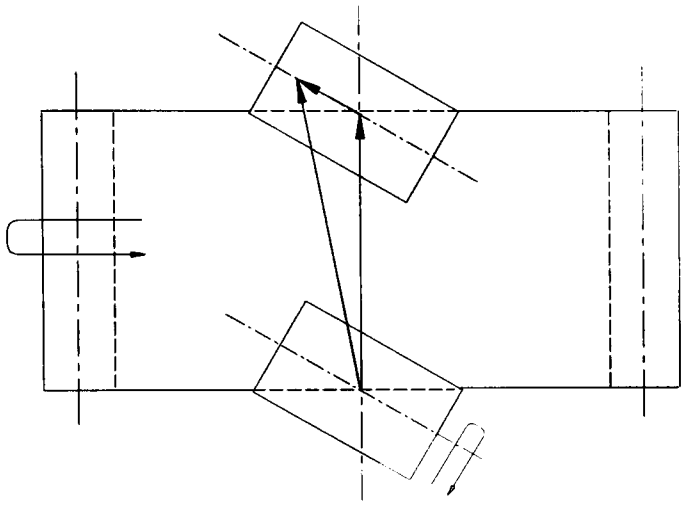

Figure 2.11: Axial and tangential feed

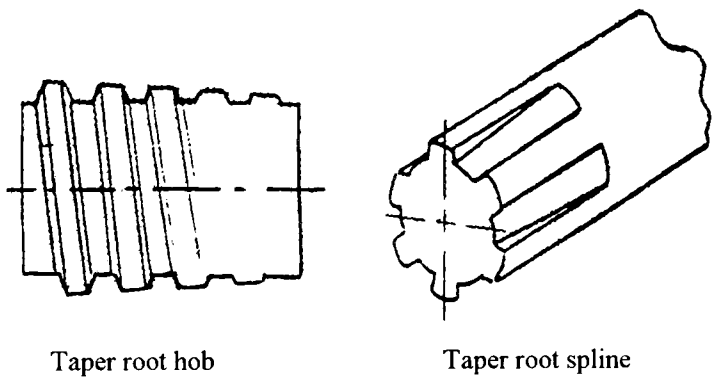

Figure 2.12: Axial and tangential feed used to cut root spline.

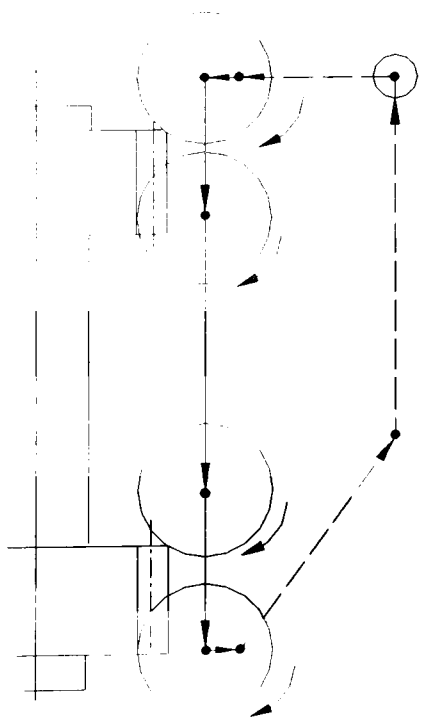

Figure 2.13: Jump cycle

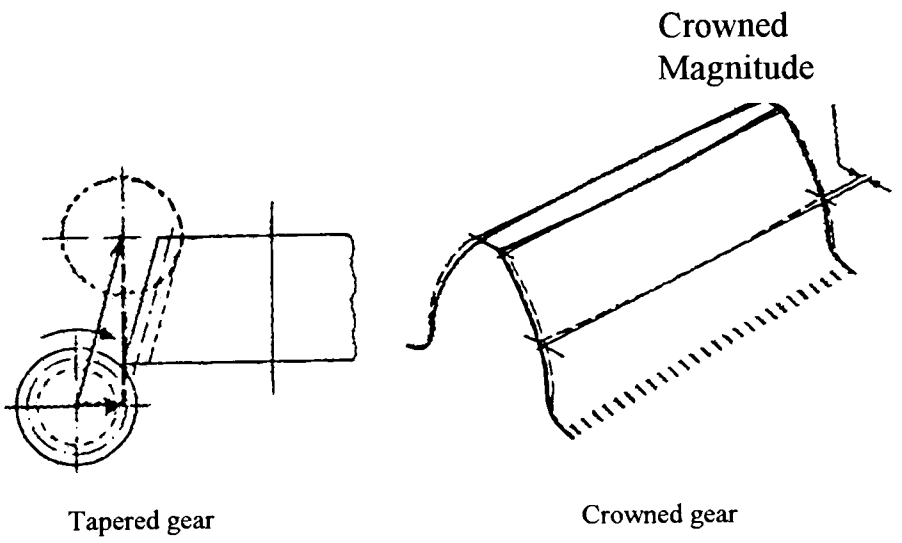

Figure 2.14: Simultaneous radial and axial feed

At the beginning of hobbing process, the hob will not produce the full depth of the gear tooth form, but only a small cut is made by each tooth as the hob feeds into the part. This is known as the (approach) portion of the cycle. It is possible to use different feed rates during this approach length with a reduction in process time, figure 2.15. During the hobbing of some gears or splines, the cutter will not feed completely through the workpiece face. This is known as a blind cut. To complete all the teeth evenly around the circumference of the gear, dwell is used. During a dwell the hob and workpiece continue to rotate in a timed relationship for one or two more work revolutions, but without feed, figure 2.16. [Gimpert].

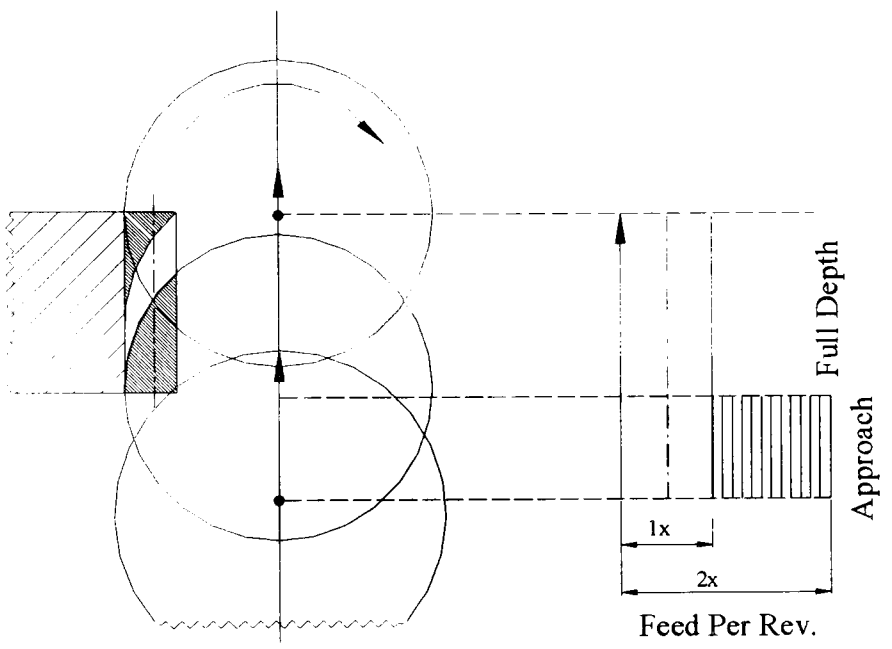

Figure 2.15: Approach portion of the cycle during climb hobbing

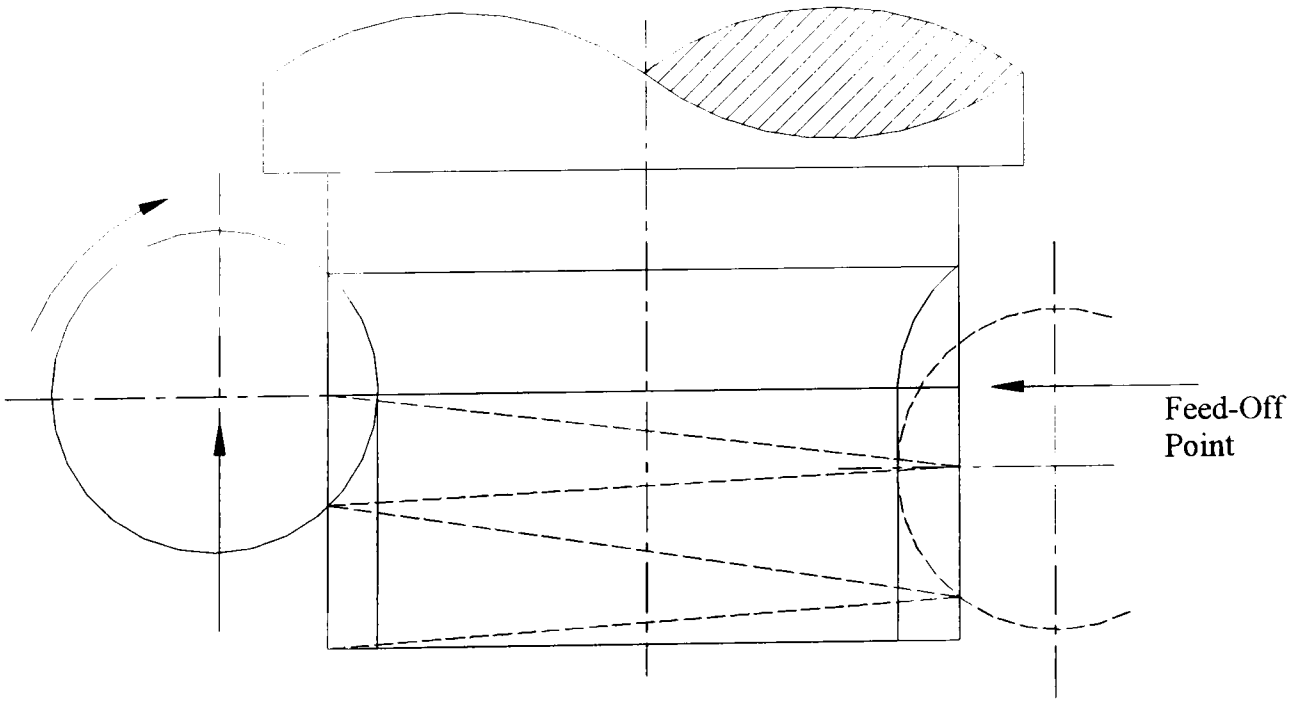

Figure 2.16: The Dwell operation

2.6 KINEMATICS REQUIREMENTS

The essential kinematics requirements of all hobbing processes are that the work must rotate in mesh with the moving virtual generating rack cut by the hob. This requires correct setting of the hob, and an appropriate selection of the hob-workpiece speed ratio and the radial, axial and tangential feeds. The settings required depend on the cutting method.

2.6.1 Hob settings

Since the tooth flanks of the hob effectively mesh with those of the rack, which are inclined at the helix angle β, the hob axis must be tilted, as shown in figure 2.17, at the hob-setting angle η given by

$$|\eta| = |\beta| \pm |\gamma_0| \qquad (2.1)$$

Where γ_0 is the lead angle of the hob at its reference diameter and β is the reference helix angle of the gear. The positive sign is used above when the hob and gear helix angles are both of opposite hand, while a negative sign denotes when they are both right handed or both left handed as shown in figure 2.17.

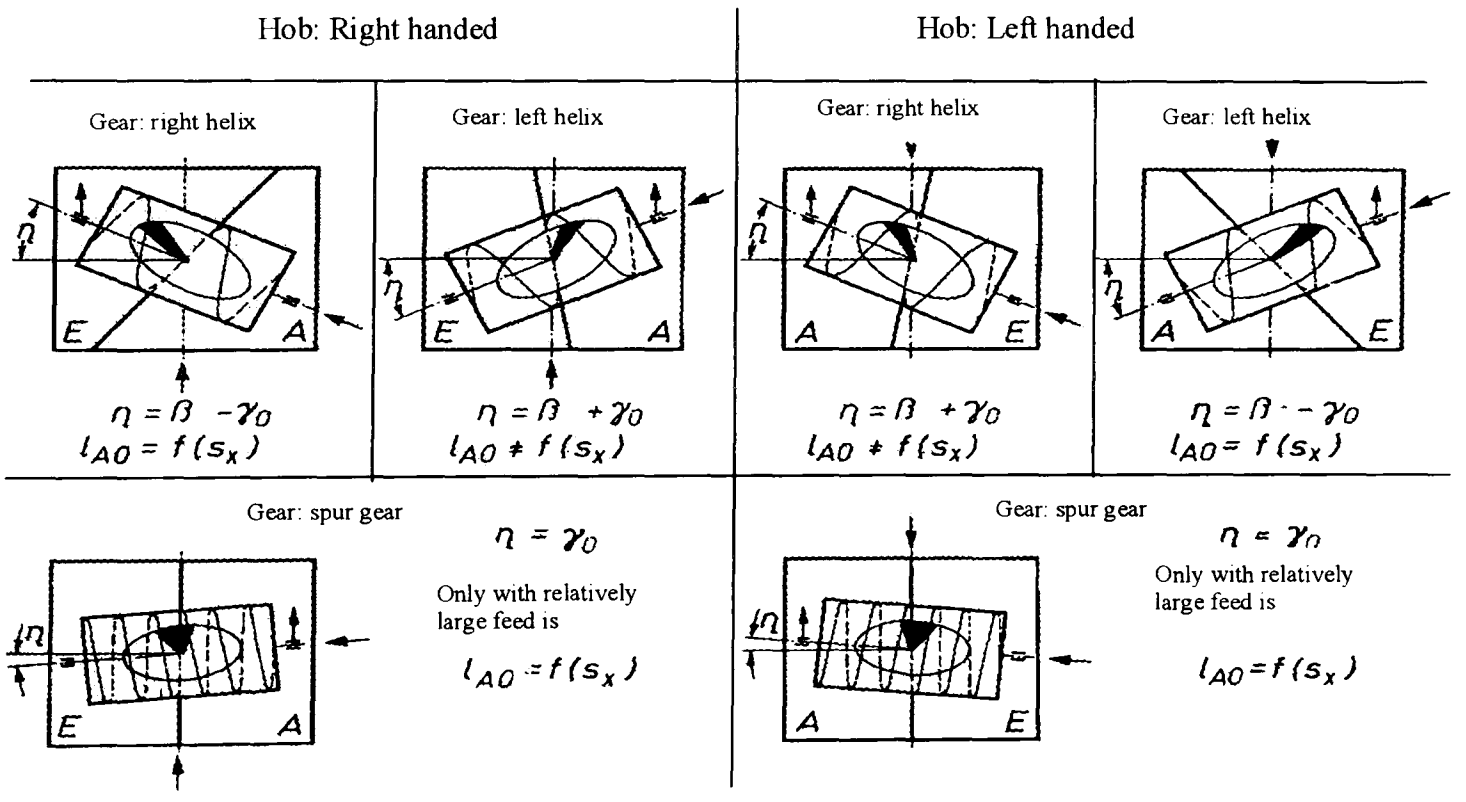

Figure 2.17: Possible combinations of gear and hob [Pfauter]

2.6.2 Index ratio

If the hob and the workpiece were both simply rotating about fixed axes, an index ratio $i_I = n_I/n_0 = z_0/z_I$ would be required, where n_I *and* n_0, z_0 and z_I are the rotational speeds and number of teeth (starts) on the hob and workpiece, respectively. This satisfies the meshing equation by ensuring that the normal velocities of the hob and gear flanks are equal at the pitch point. During normal axial feed hobbing, however, the hob is also moved across the facewidth of the gear at an axial feed rate of s_a mm per workpiece rotation. So that, on generating a helical gear, an additional rotation of the workpiece is necessary to compensate for the axial motion of the hob relative to the tooth helices. Since a helix makes one complete rotation in an axial distance equal to the lead H_a of the gear, and the axial feed per minute is $s_a n_I$, the additional rotational speed needed is $s_a n_I / H_a$ *(rpm)*, so that the meshing condition becomes

$$n_1 = \left(\frac{z_0}{z_1}\right) n_0 \pm \frac{s_a n_1}{H_a} = \left(\frac{z_0}{z_1}\right) n_0 \mp \left(\frac{s_a \sin\beta}{\pi z_1 m_n}\right) n_1 \qquad (2.2)$$

Where m_n is the normal module of the gear. This gives the required *index ratio* i_I as

$$i_I = \left(\frac{n_1}{n_0}\right) = \left(\frac{z_0}{z_1}\right) \cdot \frac{1}{\left(1 \mp \frac{s_a \sin\beta}{\pi z_1 m_n}\right)} \qquad (2.3)$$

On spur gears, the required index ratio is still simply z_0/z_I, regardless of the axial feed.

During tangential hobbing, which is used to generate wormwheels, there is no axial feed, but the hob is given a 'tangential' feed, along the hob axis, at a rate s_t mm per workpiece rotation. The additional hob rotation required to compensate for this motion is $s_t n_I / H_t$ where $H_t = \pi m_n z_0 / \cos\gamma_0$ is the axial lead of the hob, so that

$$n_1 = \left(\frac{z_0}{z_1}\right)\left(n_0 \mp \frac{s_t n_1}{H_t}\right) = \left(\frac{z_0}{z_1}\right) n_0 \mp \left(\frac{s_t \cos\gamma}{\pi z_1 m_n}\right) n_1 \qquad (2.4)$$

When

$$i_I = \left(\frac{n_1}{n_0}\right) = \left(\frac{z_0}{z_1}\right) \cdot \frac{1}{\left(1 \mp \frac{s_t \cos\gamma}{\pi z_1 m_n}\right)} \tag{2.5}$$

During diagonal hobbing, axial and tangential feeds are applied simultaneously, so that the hob moves obliquely at an angle determined by the feed ratio s_t/s_a. In this case, both the extra terms appear in the kinematics equation, giving the index ratio

$$i_I = \left(\frac{n_1}{n_0}\right) = \left(\frac{z_0}{z_1}\right) \cdot \frac{1}{\left(1 + \frac{\mp\left(s_a \sin\beta \mp s_t \cos\gamma_0\right)}{\pi z_1 m_n}\right)} \tag{2.6}$$

Oblique hobbing, also known as the Grant process, is a special case of diagonal hobbing in which the hob feed direction is parallel to the tooth helix, at the helix angle β. In this case it is easy to show that

$$s_a \sin\beta \mp s_t \cos\gamma_0 = 0 \tag{2.7}$$

so that the required index ratio is always simply z_0/z_1, for both spur and helical gears, regardless of the magnitude of the oblique feed rate. This fact was used to good effect in some early hobbing machines without a differential, e.g. David Brown Hydrax No. 7 & 14, Michigan Type 1445, in which the hob feed slide could be swivelled precisely to the helix angle, independently of the hob setting angle.

2.7 HOBBING MACHINE

In this section, an overview of conventional and CNC hobbing machine is given

2.7.1 Conventional hobbing machine

A conventional gear hobbing machine consists of the following common elements:

- A work spindle to rotate the work.
- A hob spindle to rotate the hob.
- The hob and the work are driven by the same motor and must be able to rotate at a constant index ratio of rotation between the gear and the hob.
- The hob or the workpiece must be able to move in the axial, tangential or radial directions.
- A rigid fixture on which to mount the hob and the workpiece.
- Coolant and swarf removal system.
- A rigid machine frame.

Hobbing machines are available in a number of different sizes, configurations and forms, but the principle remains the same. Actually, the most popular form is the vertical machine where the axis of the gear to be produced and the axial feed motion are vertical. It is suitable for most sizes of machines from small to large diameter and makes for easy work handling. The Churchill PH1612, as used here, is a typical example of such form. Designed with special rigidity in the structure to allow the conventional tie bar to be avoided and thus to give greater access for loading, see figure 2.18. Another shape is the horizontal type, which is useful for shaft work since by varying the length of the bed and hob traverse, long shaft components can be handled with ease.

An accurate kinematic relationship between various elements of the hobbing machine is very important in this generating process in order to produce the desired results. All the motions of the machine must be accurately related to each other, since from equation 2.6, it is the relationship between the rotation of the hob, the rotation of the work and the amount and direction of feed, which determine the gear to be cut.

Change gears are necessary to hob many different gears with different normal module since the index ratio depends on the number of teeth of the gear and the hob and the type of gear that has to be manufactured.

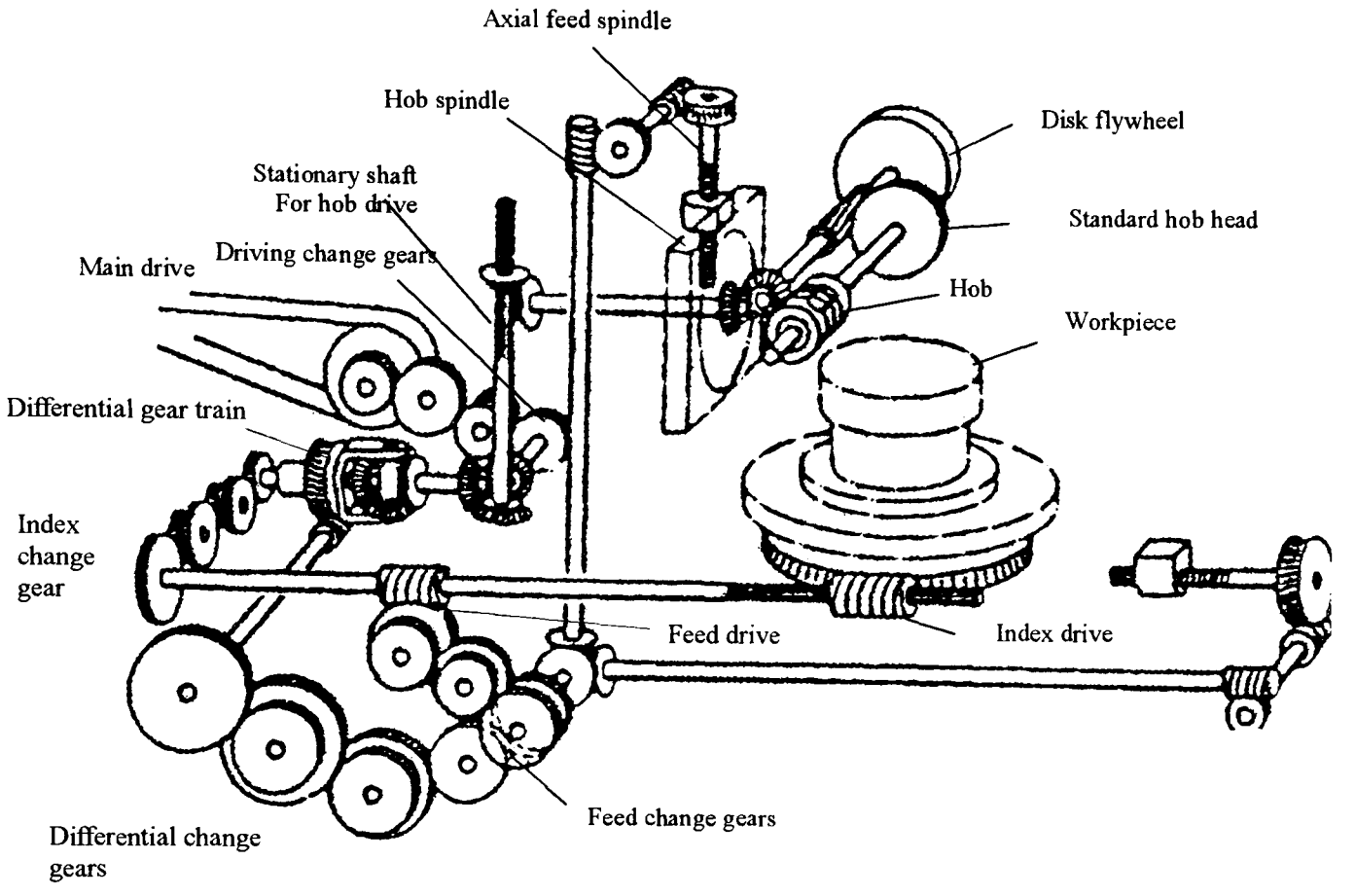

Figure 2.18: Mechanical arrangement of a conventional vertical hobbing machine. [Cluff]

Some conventional hobbing machines have means to change the feed rate automatically during the cutting process to reduce the cutting time. If helical gears were to be cut a change in the axial feed rate would affect the index ratio. Therefore, the machine tool must be capable of changing the index ratio simultaneously. A differential is used as an adding device in such a way that the index ratio can be changed during the cutting process in accordance with equation 2.6. Machines based on the Grant process do not need such a differential, since the axial and tangential feed rates do not influence the index ratio, although, the flexibility of these machines is limited. If a hobbing machine is not based on the Grant process, the differential is also essential if to add the extra rotation needed to cut a helical gear as a function of the axial /tangential feed rates.

2.7.2 CNC hobbing machines

The technological requirement of more accurate and reliable machines is increasing and the rapid increase in the computer technology made it possible to develop a new hobbing machine equipped with rotary encoders to control the transmission ratio between the hob spindle and the worktable. Electronically controlled drive units replaced the conventional mechanical gear train and differential. A rotary encoder coupled to the hob spindle generates impulses as the hob spindle rotates, while on the index gear shaft a second rotary encoder was mounted. Linear encoders fitted to the axial/tangential feed slides also produced impulses proportional to these motions. By using these and those from the hob shaft impulses an electronic differential was provided in place of the standard gear differential to drive the work spindle. This closed-loop system eliminates differential gears from the machine. In addition the machines are equipped with individual drives and associated incremental measuring systems for radial motion, axial motion and tangential motion.

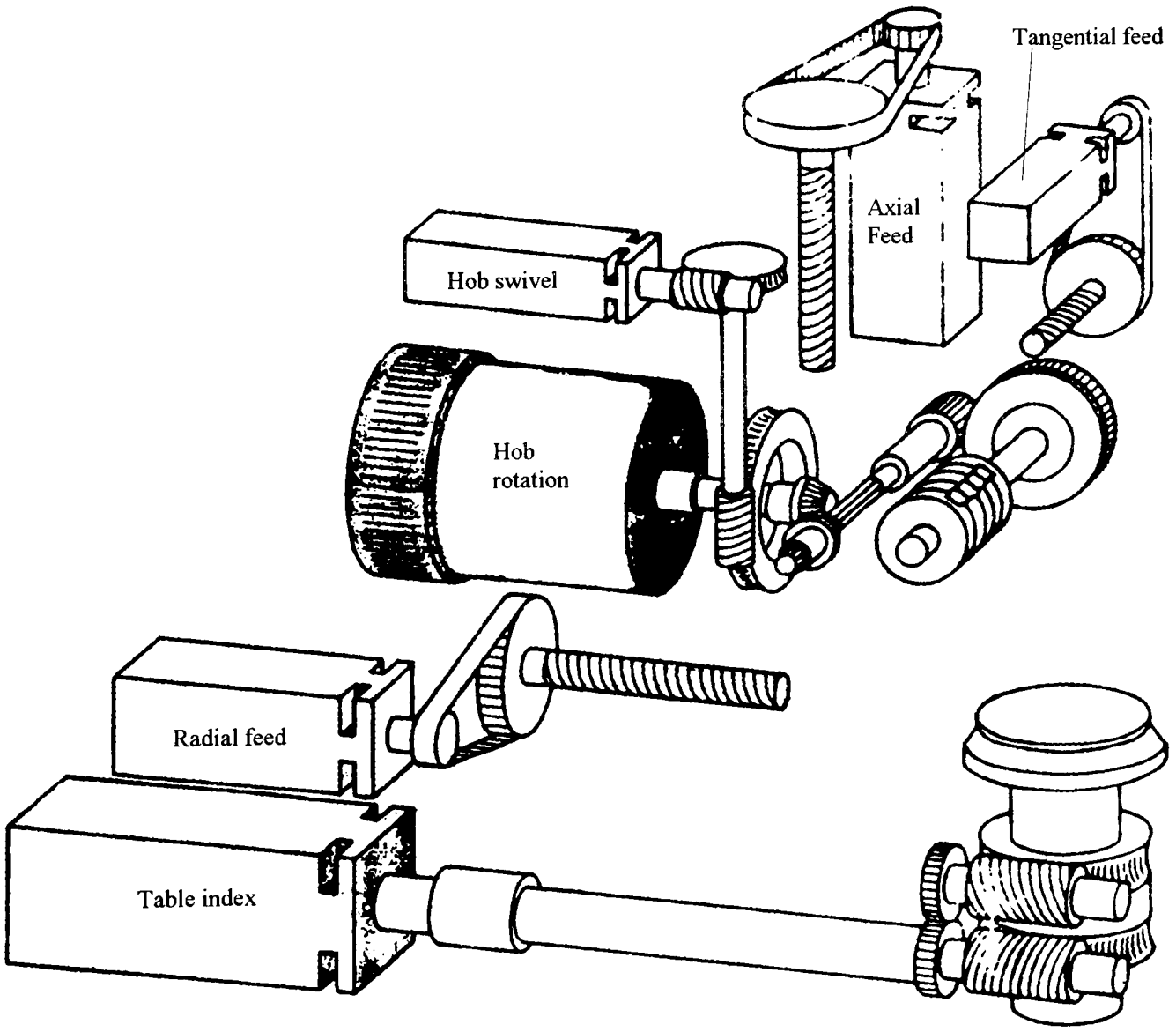

Figure 2.19: CNC hobbing machine [Cluff]

A six-axis hobbing machine offers many advantages to the user. The ability to calibrate axes and apply corrections by computer offers means of eliminating slight errors in lead screws and index so that, in effect, the machine will produce parts with greater accuracy than it was built for. Then hobs can be changed automatically, permitting dull hobs to be changed or even a different hob to be mounted, along with programs suitable for the new parts, and, if necessary, the work fixture can be changed. Automatic parts changing, automatic probing to control size, computerised control for management information, maintenance, diagnosis, optimisation for machine cycle, as well as other possibilities, gives the CNC user many advantages. In fact CNC hobbers are offered with as many control axes as needed to operate completely automatic hobbing centres.

The kinematics of hobbing machines was finally solved by the introduction of high-speed CNC controls. With development of electronics, CNC has provided an accurate substitute for the mechanical differential. The computer numerical controller provides a control board in which data necessary to cut a gear can be entered. Once the part data are entered in the keyboard they can be assigned a reference number. The reference number remains in the computer memory and can be recalled as needed.

The advantages of CNC hobbing machines can be listed as follow:

- Accuracy: The linear encoder, which controls the radial slide position, has a high resolution, which achieves good centre distance and tooth thickness control.
- Maintenance and safety: CNC control will display error signals on the display unit, drawing the operator's attention to potential problems. The elimination of change gears in the set-up of the CNC gear hobber eliminates a potential source of injuries.
- Flexibility: With the use of part programs a wide variety of hobbing cycles can be performed.

- Easier and faster set-up: The operator needs only concentrate on the positioning of the workpiece and run the part program.
- Reduced machining time: CNC hobbing machines have a higher dynamic rigidity than conventional, mechanical machines, plus ability to optimize feed rates etc.
- Greater repeatability: Numerical data inputs representing the motions are converted to electronic signals and used to move the hobbing machine elements. Positioning accuracy depends only on the resolution of the encoders and CNC control system.

The disadvantages of CNC hobbing machines are:

- Higher fixed costs and higher purchase costs.
- Time is saved by shorter set-up time, not by shorter cutting time since modern conventional machines can provide similar speed and feed rates.
- Higher training costs due to the introduction of new technology.

CHAPTER THREE

LITERATURE REVIEW

3.1 INTRODUCTION

The hobbing process was invented more than 150 years ago and struggled to become accepted. The earliest recorded hobs were made by Bodmer before 1840, [Watson]. Jungst and Reinecker were the first to design and successfully make special purpose hobbing machines capable of cutting helical gears. Later in 1897, Herman Pfauter patented his first universal gear hobbing machine. The earlier research concentrated on finding the periodic errors resulting from kinematic and transmission drive errors, [Broersma].

3.2 NUMERICALLY CONTROLLED GEAR HOBBING

In the Numerically Controlled (NC) machine the manual system is replaced by an electronic control system. The first NC milling machine tool was developed by MIT in 1950, but according to development engineers in Germany, the idea of (NC) hobbing machine tool was not new [Jablonowski]. Budnick's patent in the 1953 was the basis of the patent the Pfauter Company has registered on its NC gear hobbing. In the early 1960's, the first commercially available numerically controlled (NC) machine tools were introduced [Colin *et al*].

Figure (3.1) shows the gear train of a conventional hobbing machine. Whereas the gear train of a numerically controlled machine tool is shown in the figure (3.2)[Nagafune].

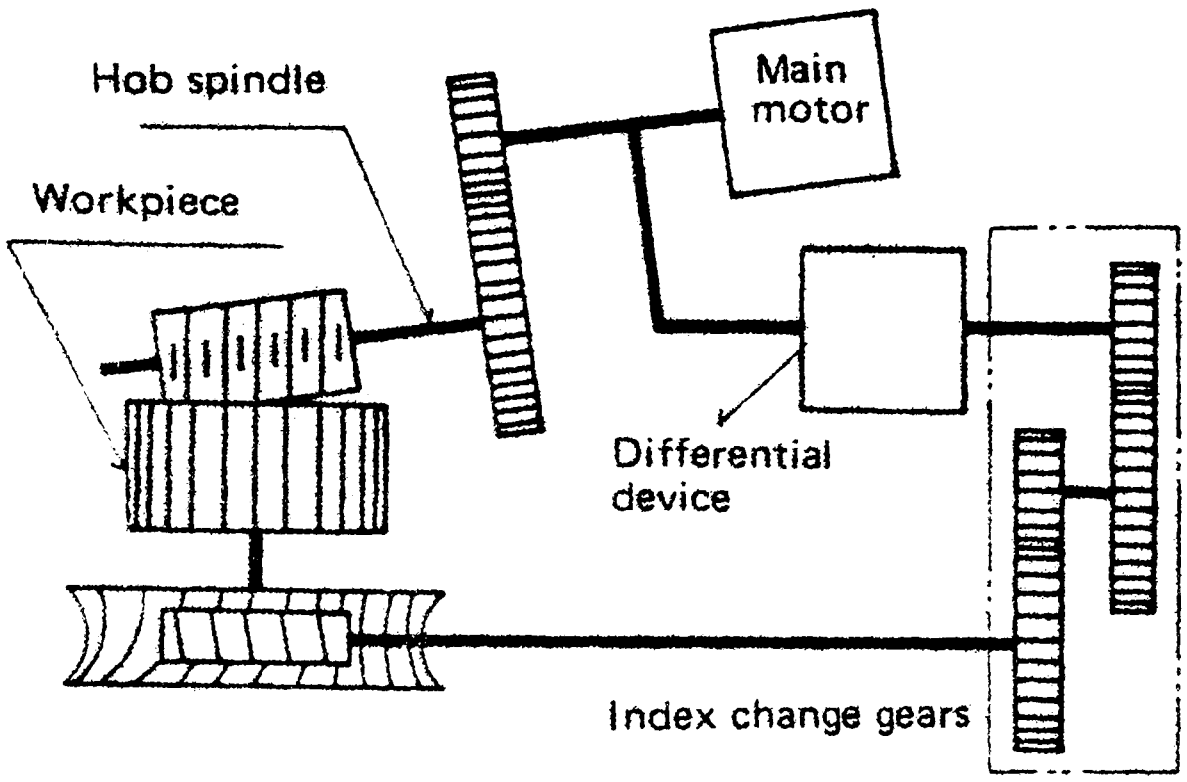

Figure 3.1 Gear train of a conventional hobbing machine index system [Nagafune].

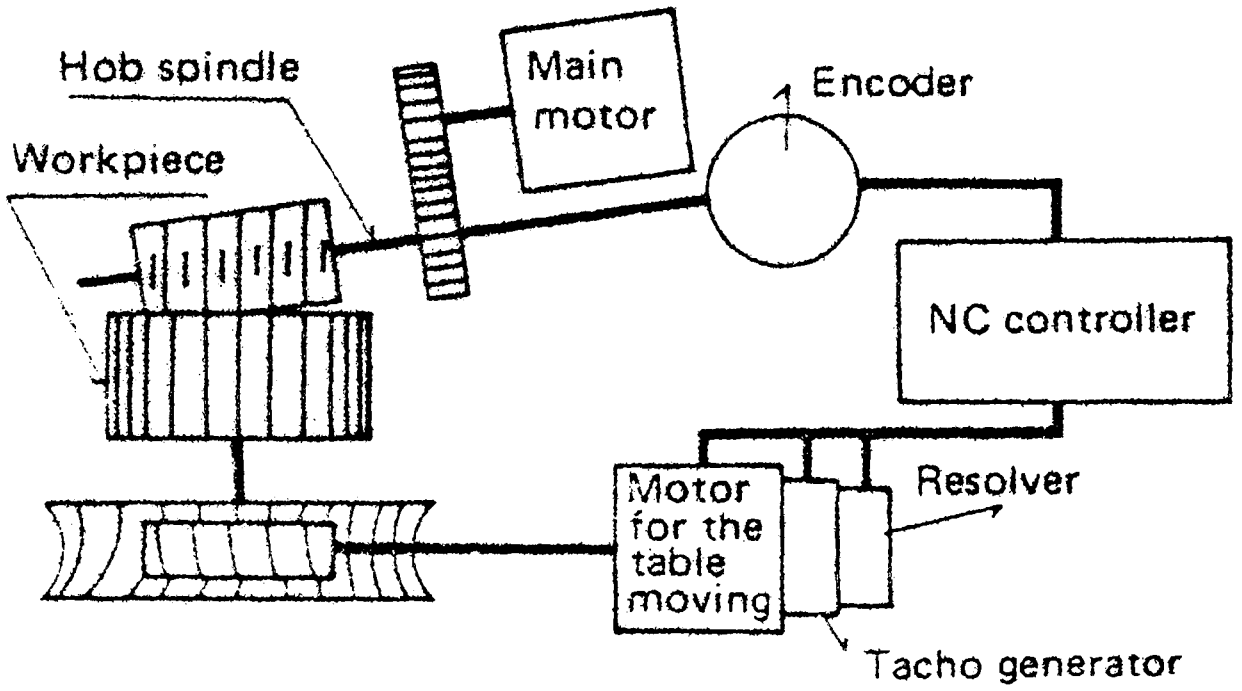

Figure 3. 2 Gear train of a numerically controlled hobbing machine [Nagafune].

Using an electronic control system instead of the kinematic connections in the NC gear hobbing machine results in a reduced number of elements, i.e. smaller mechanism, and significantly simplifies the machine structure and design, [Ramtirov]. This also helps to create fundamentally new machine tool

configurations. Microprocessor based NC systems can control many axes, and have no constraints on the number of controlled axes, and help automate the calculation of machine set-up parameters.

The cutting tool (hob) and the worktable must engage in a very precise synchronous rotation. The new NC system replaces the method of rotation of the hob with respect to the worktable, from a mechanical drive through gear trains using one main electric motor to an electronic synchronisation of two drives, which simultaneously drive the worktable and the hob. This new arrangement has improved machine performance, which results in an improvement in the quality of the finished gear. The new NC systems save a great deal on the amount of set-up time and improve the accuracy compared with the manual operation, and also ease adjustment of the machine.

3.3 CNC GEAR HOBBING

The early 1970's was an important era in numerical control of machine tools, as the microprocessor computer replaced the logic controller unit in early NC systems. The first CNC gear-manufacturing machine was introduced in 1980 by Pfauter [Kovar].

This produced both computer numerical controlled (CNC) systems and direct numerical controlled (DNC) systems [Koren]. Figure 3.3 shows a block diagram of closed loop CNC system.

A CNC system for a single machine tool includes a mini- or a micro-computer controlled by stored instructions to perform some or all of the basic numerical control functions. With DNC, a central computer directly controls several machine tools. CNC systems are widely used systems, because of the availability

and the reduced costs of the computer. The CNC closed loop systems control the velocity as well as the position. The tacho-generator may provide velocity feedback (with a voltage proportional to the velocity) and the encoder provides a position feedback. Alternatively, a pulse rate signal from the position encoders can be used a pseudo velocity signal.

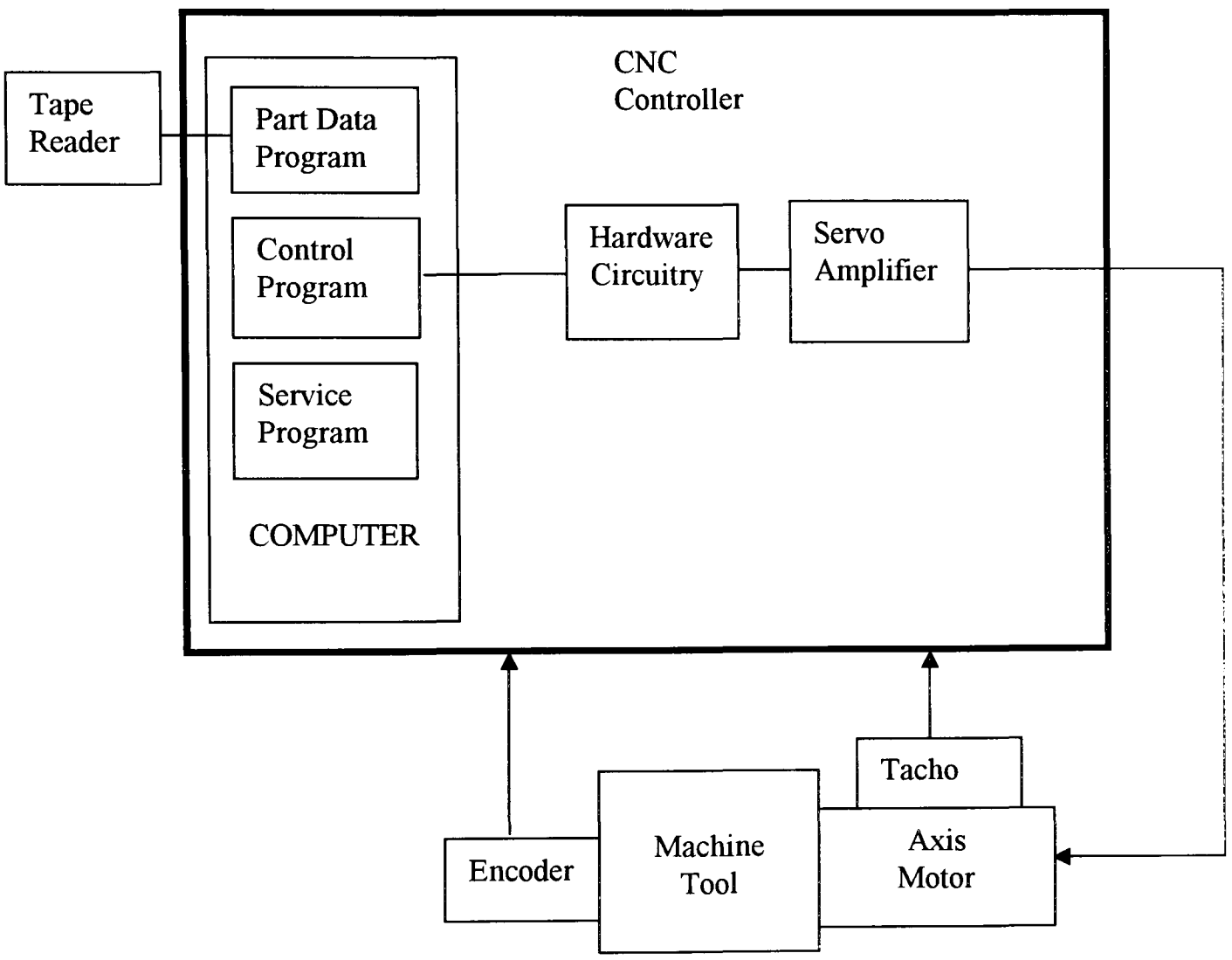

Figure 3.3 Diagram of a closed loop CNC system [Koren]

3.4 GEAR HOBBING KINEMATICS

The increasing demands for producing accurate gears make it necessary to determine the cutting forces and torques on the hob shaft. Recent research has indicated that the determination of the cutting force behaviour is important for analysing gear tooth accuracy and surface finish. The gear hobbing process has

not been analysed to the same degree as some other machining operations, because it is a highly complex process, geometrically.

Cutting conditions are very complex in hobbing, compared to orthogonal cutting. Several teeth of the hob are cutting simultaneously generating very different width and thickness of chip, which also vary during the rotation of the hob. It is not easy to determine the total width of the chip on the bottom and the flank, which have a great influence on torque and cutting forces, surface finish and even stability, [Slavicek]. These values depend on the parameters of the cutting process, i.e. blank diameter, hob diameter and number of gashes, axial feed rate, depth of cut etc.

3.4.1 Cutting zone and chip shape

Sidorenko, 1951, determined the shape and the size of the cutting zone graphically. It was concluded that the volume of the metal removed by the tip and the flank cutting edges of the hob teeth and the work done by the two edges were not equal. The hob tooth tips edges cut off most of the gear blank material whilst the side edges only shape the flank. The side edges do not cut exactly simultaneously and the length of cut is different. These conclusions were drawn from experimental data without any theoretical background.

Sunajev *et al*, 1954, determined the shapes of the side edges of chips by cutting a wax gear blank with a specially made single toothed hob. The wax chips were collected and unfolded to draw out their shapes. It was concluded that the mean width of chips on both side edges are equal, and mean width of chips cut by one side edge was approximately equal to that on the peripheral edge. It was also further concluded that the peripheral edge removes about 60% of the total chip volume while the side edges remove only 20% each, i.e. the chip thickness on the side edges is approximately three times smaller than that on the peripheral edge.

Slaviĉek, 1966, indicated that the determination of the cutting forces behaviour is very important to the stability of the gear hobbing machine. The study presented a theoretical analysis of chatter in hobbing and assumed that the sides and the root of a tooth space are straight sided, and that the chips cut from the opposite sides and the roots of a tooth space have equal widths. However, the study did not show any correlation between the theory presented and any cutting tests.

3.4.2 Hob geometry

Inozemtsev, 1961, investigated the effect of the hob cutting edge geometry on the cutting forces, and also measured all the three components of the cutting forces, but only concentrated on the tangential component. The analysis concluded that the radial rake has a significant effect on the cutting forces, as cutting forces are reduced with a positive radial rake angle. The peripheral clearance angle has an even greater effect on the cutting forces than the radial rake angle; so better dynamics of cutting can be gained by using a hob with a positive radial rake and a greater clearance angle. It was also concluded that the cutting forces are reduced by using straight gashes, which also increase the uniformity of cutting; and therefore it is recommenced that hobs be manufactured with straight gashes. The study was based on constant cutting conditions, which make the results of limited value.

Using a simplified, essentially 2-dimensional kinematic model, Wakuri, *et al*, 1966, discussed only the cutting of the tips of the hob teeth and how to reduce the fluctuations of the tip cutting forces by using the right form of hob. The authors analysed the cutting action at the tips of the hob teeth but did not consider the variations in the apparent depth of cut when the hob tooth enters the cutting zone. The study concentrated on hobbing of through hardened (350-400 H_B) gears in which tip wear is a problem. The wear distribution was assumed to be proportional to the rate of metal removed at each point on the hob. The study also assessed the effect of the cutting oil using milling tests with a fly-cutter, recommending oil that endures high pressure at low temperature. They also

assessed the hob material and the effects of using multi-start hobs in the research. The tests with a 2-start hob resulted in much lower wear rates, attributed by the authors to the thicker chips (and fewer cuts) associated with multi-start hobs.

Severilov, 1969, explained the relationship between the power when cutting spur gears with relieved (standard) and non-relieved hobs. A relationship was also established between the average and maximum cutting torques and the cutting parameters and concluded that the module size has a great effect on the torque. It also concluded that no function exists for average torque as a function of the Brinell number in a wide range of hardness variation.

Deb *et al*, 1980, studied the wear on the hob teeth using conventional and modified hobs, in which alternate tips and flanks were relieved. It was suggested that, in the hobbing process using conventional gear hobs, more metal was removed by the flanks of the hob teeth than the tips, but that the tips finish their task in fewer cuts. The chips removed from the uncut area have varying cross sections. The chip cross sections removed by the flanks have triangular shapes, but the chips removed by the tips have irregular, non uniform and quadrilateral shapes, similar results were gained from using modified hobs as far as the chip formation and shapes were concerned.

Kim, 2001, investigated theoretically the deviations of hob geometry and the hob alignment errors on the generated gears. The author proposed a method of representing the geometry of a generalised hob tooth profile in parametric form and determining the surface equation of a generated gear as a function of the hob design parameters and generating motion. The kinematic model was based on classical gear generation theory [Litvin] and considered only contact between the enveloped hob helicoids and the finished tooth surface. No results were presented.

3.4.3 Cutting force measurements and cutting parameters

A Japanese government report, 1961, [Honda], investigated the maximum and the average tangential cutting force acting on the hob. The report investigated the behaviour of the cutting forces for both climb and conventional hobbing. Different cutting parameters, with or without coolant, and different gear blank materials were studied. The report also attempted to calculate the chip thickness theoretically but no comparisons with the experimental results were made. The report showed the effect of each specific parameter on the cutting forces, one at time, but only shows this particular parameter effect on the response.

Sidorenko *et al*, 1961, and Adam, 1957, investigated the torque on the hob shaft. Nekrasov *et al*, 1966, also attempted to experimentally determine an empirical equation for the torque in the gear hobbing process, but there were some contradiction in their reports, which they wanted to investigate and compare.

Opitz *et al*, 1963, investigated the cutting geometry for hobbing a rack and worm or gear, where the hob and the blank axes are perpendicular and not perpendicular, which is the most usual case. Even though the research concentrated on hobbing a rack and worm, little mention was made of spur gears. An experimental evaluation was discussed but no analytical issue were discussed. The research also investigated the wear on the hob, especially on the tip, although wear on the flank was also noticed.

Cooke e*t al*, 1967 and 1968, investigated the cutting forces in the gear hobbing process for spur and helical gears respectively and measured the three cutting force components, tangential, separating (radial), vertical and torque, acting on the gear blank. For spur gears the cutting force components were measured for different hobbing parameters such as cutting speed, axial feed rate and diametral pitch, the tests were conducted for conventional and climb hobbing. The first finding was the smoothness of the forces with climb hobbing, and noted that the maximum force tangential to the hob was slightly greater in conventional than for

the climb hobbing; the resultant maximum force is about 25% greater and acts in a different direction. It was also claimed that the maximum torque on the workpiece remains almost unchanged despite the change of the cutting speed and the axial feed rate. Results also showed that the forces increase with the increase of the axial feed rate and decrease with the decreasing of the module.

For hobbing helical gears, the cutting force components were measured in respect of the variation of the helix angle. As expected, the peak forces increase significantly with the increase of the helix angle. The cutting power was also measured in relation to the helix angle, and again increased with increasing helix angle.

Khardin *et al*, 1967, investigated the cutting forces in hobbing worm wheels with both radial and diagonal (tangential) feed rates. A specially made dynamometer was used in order to measure the cutting force components and the torque. An empirical formula was used to estimate the forces, and the conclusions reached could be summarised into two parts for radial and tangential hobbing. The first part claimed that, in radial feed, the cutting force components and the torque were not constant in value, as they reach their maximum at the instant of full depth of penetration by the hob. It was then recommended to vary the feed rate by applying a greater feed rate at the start of operation and reduce it at the full depth of penetration. For the tangential hobbing it was claimed that both feed rate and cutting speed had very little effect on the cutting force components and torque.

Padham, 1972, also studied the relationship between the maximum cutting torques, the average power consumed and the cutting parameters such as axial feed cutting speed and material hardness. The study was conducted using different sizes of hobs to generate spur gears by conventional hobbing. The study concluded that the cutting torques decrease with the increase of the cutting speed and increase less than linearly with axial feed. It was also reported that the cutting power increases with the module increase as well as the increase of the hob speed.

Sakharov, *et al*, 1972, investigated the torque on individual teeth and individual cutting edges. Overall cutting force moments for cutting edges of complex form can be found without additional tests by summating the individual torques for the elementary cutting edges of the hob teeth. The behaviour was simulated on test using a lathe tool; the arrangement was, as shown in figure 3.4, using a single tooth hob mounted on the hob arbor and a single tooth blank. The torque was measured on the arbor where the dynamometer was attached. It was found that the torque increased by the increase in modules and pressure angle, whilst no changed was noticed with the increase of the number of teeth on gear. It was claimed that no direct proportional relationship could be found between the torque and the number starts on hob. The effect of the workpiece face width and the gear material were also investigated. Different shaped cutting edges and non-involute hob were also used.

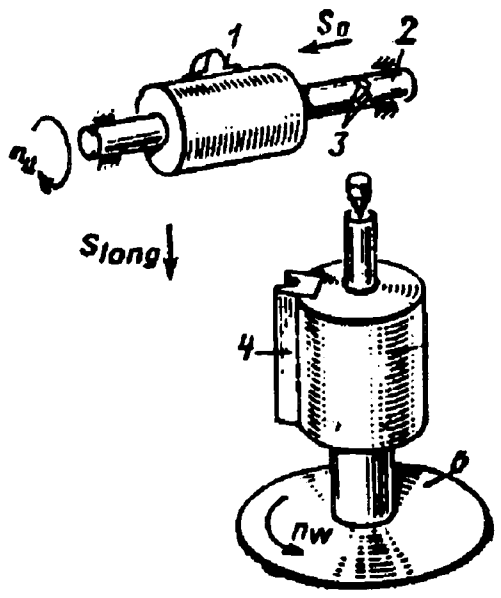

Figure 3.4 Diagram of rig for modelling the behaviour of hob cutting edges. 1-tool;2- tool arbor;3-strain gagues;4-workpiece;5-workpiece arbor;6-machine table; (Sakharov)

Milner *et al*, 1978, investigated the effect of the cutting speed in gear hobbing and concluded that the cutting speed has a great effect on both maximum torques on the hob shaft and the average power consumed during hobbing a spur gear. It was suggested to vary the feed rate during hobbing by applying a high feed rate at the start of cutting and reducing it toward the full of depth. The magnitude of the

cutting torque increased considerably with the increase in the gear module. Also an increase in the feed rate produces an increase in maximum torque at constant speed.

Khan, 1984, carried out an investigation to determine the relationship between the cutting forces on one hand and the cutting speed, and uncut chip thickness, in cutting worm wheels. An empirical formula was proposed for that relationship. The boring process was used to measure the forces as the study claimed that the geometrical parameters were similar.

3.4.4 Chip formation

Hannam, *et al*, 1968, analysed the chip formation in the conventional hobbing of spur gears. The process was analysed by considering relative rather than absolute motion, and was reduced to a two-dimensional problem. It showed the number of hob teeth engaged in forming a gear tooth space, the shapes of the chips and the volume of metal removed. It came to the conclusion that the flanks of the hob teeth remove greater volume of metal than the tips, but the tips complete their metal removal in fewer cuts and therefore are exposed to a very high load. The volumes of metal removed by, and hence the wear on; the two flanks of a hob tooth are unequal. The machining forces exert a fluctuating and reversing torque on the worktable. But this analysis was based on approximations and as mentioned before several parameters were not considered and did not give an exact solution to the problem. The study concentrated on three sections of chip in a single gear tooth space.

Terashima, *et al*, 1978, analysed numerically hobbing in an unfinished tooth space, which is the problem addressed in this thesis. The study described a method of calculating the length and the thickness to be cut on each point along the profile of each hob tooth without neglecting the tip roundness. The study claimed to be able to calculate the cutting zone, chip thickness and length and the cutting angles in hobbing of spur and helical gears. The method can be applied to any hobbing

process, i.e. spur or helical gears, climb and conventional hobbing. The authors compared their theoretical results with practical hobbing results on a right-hand gear. The hobbing mechanism was explained and co-ordinate systems equivalent to those used in this thesis were defined and the relationship between the moving elements was established. The hob tooth profile was calculated, and then the tooth numbered along the hob. A cutting zone in the tooth space was calculated, and the chip thickness determined at each point on the active hob teeth.

The 'cutting out' method used by the authors to define the chip thickness at each point is similar to that employed in this thesis and described in Chapter 4. However, the direct method of solution was preferred (see Appendix E) and the authors only explained in detail how the distribution of the cutting load round the hob teeth was calculated. Transformation of their results to a common time scale was not explained, although the authors have apparently done this, since they did present results showing an estimate of the cutting force waveform (based simply on the instantaneous rate of metal removed). No attempt was made to predict the cutting forces quantitatively.

Terashima, *et al*, 1980, also investigated hobbing in the unfinished tooth space using a simplified graphical approach based on the earlier numerical calculation. The procedure claimed to be able to estimate the cutting load on each tooth, chip thickness, the cutting width along the tooth profile, and the chip length. Wear causes are also analysed by relating the practical wear to the amount of metal removed, and the chip flow on the rake face. As in the previous paper, it was again claimed that cutting torque and vibration could be also analysed, although no data was provided.

The paper includes a valuable quantitative discussion of the cause of 'corner wear' on hobs, demonstrating that interfering chip flow occurs in the region where corner wear occurs, creating higher cutting pressure. The analysis procedure presented predicts this interfering flow, but can not take account of it

quantitatively to predict the wear or the cutting forces, although 'improved' hobs with reduced chip interference are discussed.

Sülzer, 1974, presented a mathematical model to calculate the chip cross-sections areas. The hobbing process was simulated and a 3-D model was used to describe the machine into 6 co-ordinate systems and an equation to relate the machine axes was introduced. As shown in figure 3.5 all the co-ordinate systems representing different part of the process starting with system (6) which is fixed in a hob tooth, ending with system (1) which is fixed in the gear tooth space. This approach is similar to that used in this thesis.

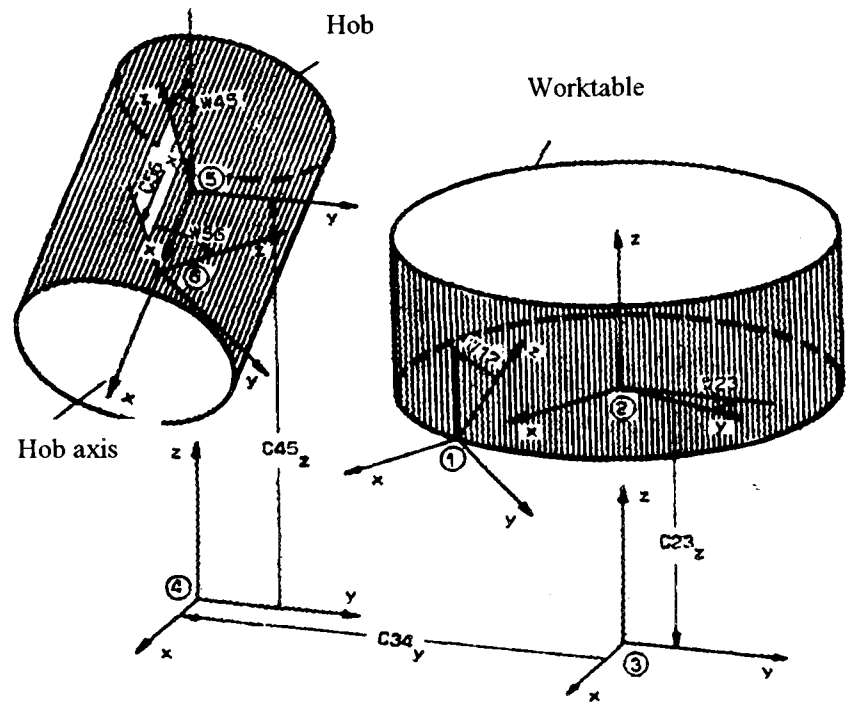

Figure 3.5 Co-ordinate systems in the hobbing machine (Sülzer)

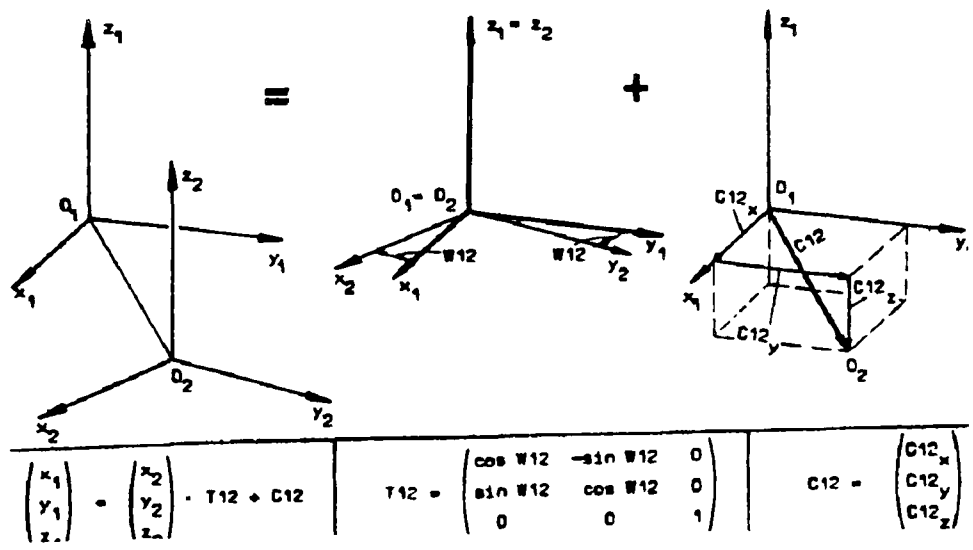

Figure 3.6 Co-ordinate transformations (Sülzer)

The chip cross section was estimated by dividing the region of intersection of the hob with the gear blank by 6 cutting planes. The chip cross section was calculated in those planes and illustrated against the layer (plane) number and along the hob length, figure 3.7. The study showed chip cross-sections for spur and helical gears for different teeth on the hob. It is not clear from the reference precisely how the chip thickness at each point on the hob was calculated. This is the most complex part of the analysis.

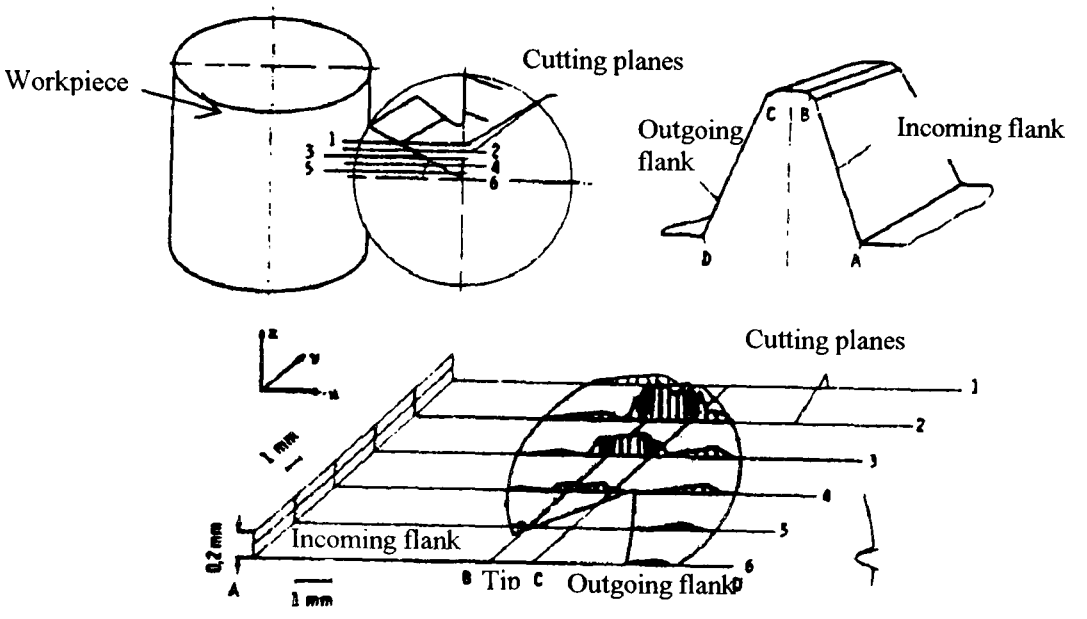

Figure 3.7 Chip cross section (Sülzer)

Bashkirov, *et al*, 1984, proposed a computer-aided calculation of the chip section in spur gears. The method calculates the chip section parameter removed by each cutting edge of the tooth and all edges of the whole hob, and is based on calculating the co-ordinates of boundary points representing the positions of the hob tooth cutting edges relative to the gear. The results were compared with experimental results by measuring the 'peripheral' force component. It was also claimed that the variation of cutting force is proportional to the variation of the chip width, but that the chip thickness has a less significant effect on cutting force. It was not very clear how the cutting forces were measured, and what the term 'peripheral' force meant (probably the component tangential to the hob).

Sidorenko, 1986, investigated the dimensions of chips removed by the cutting edges of a hob using a simplified model. The thickness, width and the length of

thin box shaped cuts (from the hob flanks) and thick 'comma' shaped cuts (from the hob tips) removed when hobbing gears having a high hardness value were studied. In gear hobbing the chip parameters were closely related to the dimensions of the hob and gear blank which, in their relative motion define the cutting zone. By establishing the boundaries of this zone (assumed to be elliptical) it was possible to estimate the chip parameters. It was claimed that the thickness of the box shaped chips depends mainly on the number of the teeth of the hob, whereas the thickness of the comma shaped chips depends on the feed rate. Equations based on the extent of the cutting zone were proposed and verified experimentally. On the basis of these equations an algorithm and program were written for computer calculation of rational hob cutting edge loads.

It was noted in the study that when a comparison was made with real chips collected from the hobbing process, that the 'comma' shaped chips comprised only about 1% of the swarf, but it is difficult to imagine how these chips were collected as the cutting oil usually sweeps the chips away and most of the swarf sticks in the machine ducts. It was not very clear if thermal distortion of the chips after cutting were taken into account, which changes the shape of the chips.

Suzuki, *et al*, 1993, investigated the chip interference, at the hob discussed by Terashima *et al* (1978), theoretically. In hobbing, the hob has many teeth and each tooth has three cutting edges, the tip and two flanks. When a gear is being cut, all three of the cutting edges of one tooth will generate chips simultaneously, at certain times. This will result in a phenomenon called 'interference of chips', and will lead to an increase in the specific cutting forces comparing to orthogonal cutting. As the chips flowing in different directions collide with each other, this will affect forces acting on the shearing area of the rake faces.

A simple basic model of chip interference was developed on the basis of cutting to full depth or non-full depth triangular cuts. Thus, the specific cutting forces in a non-full depth triangular cut made with a point nose straight tool were theoretically investigated in terms of various included angles. The results show

that the specific cutting forces become large when the included angle of the tool is small. The specific cutting force with an included angle of 90 degrees is about 1.3-1.35 times those produced by a flat tool.

3.4.5 Generation of finished tooth form

Yang Lin, 1994, proposed a mathematical model for the gear generation by hobbing, very similar to that later used by Kim (2001). The model was based on co-ordinate transformations similar to those used in Kim's paper and this thesis, and employed Litvin's theory of gear meshing. The hob axial section was also simulated, as in Kim's paper, and by calculating the surface generated by the hob the final tooth form of the gear was presented. The study also considered the generation of tooth helix modification.

Chang *et al*, 1997, proposed a mathematical model to simulate the gear generation process of a 6-axis CNC hobbing machine, based on the solution of Litvin's meshing equations. The control requirements for the six axes were shown to reduce, in all cases, to the solution of four scalar equations. Although different types of gears were discussed the detailed equations presented in the study were for special, 'Helipoid' gears, a new type of crossed-axes gearing. This paper and the previous research Yang Lin (1994) are only concerned with gear generation, based on meshing equations. No mention is made of the chip formation process.

3.4.6 Cutting forces

Bhattacharyya *et al*, 1970, estimated the cutting forces on the plane of the basic rack by 2-dimensional simulation of the metal cutting process. It was suggested that it was very difficult to estimate the instantaneous variation of the area of cut. A convenient approach for estimating the tangential cutting force was obtained from the specific energy of cutting. The cutting forces were also observed during the process of hobbing for different feeds and modules to find the tangential and

radial components of hobbing forces, as both forces increase with the increase in module and feed rate.

König reviews work of several researchers who have tried to use computation methods to determine the maximum and average cutting force components. He also reported on recent theoretical and experimental investigations at Aachen of the cutting force in gear hobbing. The previous formulae were based either on a limited number of cutting force measurements or, simultaneously, on the approximate determination of the chip cross sections. Several parameters in this earlier work were not considered so the resulting empirical formulae only apply to a narrow range of geometrical and technological machining data. According to König, the first attempt to determine the cutting force components in gear hobbing was made by Mitrovič, 1974.

In Germany and especially at Aachen Technical University (which König leads) many research studies were conducted to investigate the gear hobbing process kinematics and the cutting force component behaviour. Most of these studies were based on the kinematic method used by Sülzer.

König *et al*, 1980, developed a model to determine the time course of the cutting force components in gear hobbing. The calculation was based on Sülzer's, (1973), method of determination of the chip cross-section areas. The study calculated the penetration between the hob and the gear blank in 8 reference cutting levels in the gear space co-ordinate system, system (1), figure 3.5. The chip cross section area was calculated on the rake face of each individual chip in the 8 'revolving positions' and on all the generating positions of a hob tooth during the cutting of a gear tooth space.

Figure 3.8 shows how the cutting edges and the chip section were divided into small elements. The forces acting on each element were calculated, knowing the chip thickness and width of cut. The procedure for calculating the forces was investigated by Bouzakis, 1979, 1980. The study was conducted using a digital

computer program called FRDYN. The study also shows force components measured, on a single tooth gear space, using a 3-axis dynamometer, which was placed on the worktable.

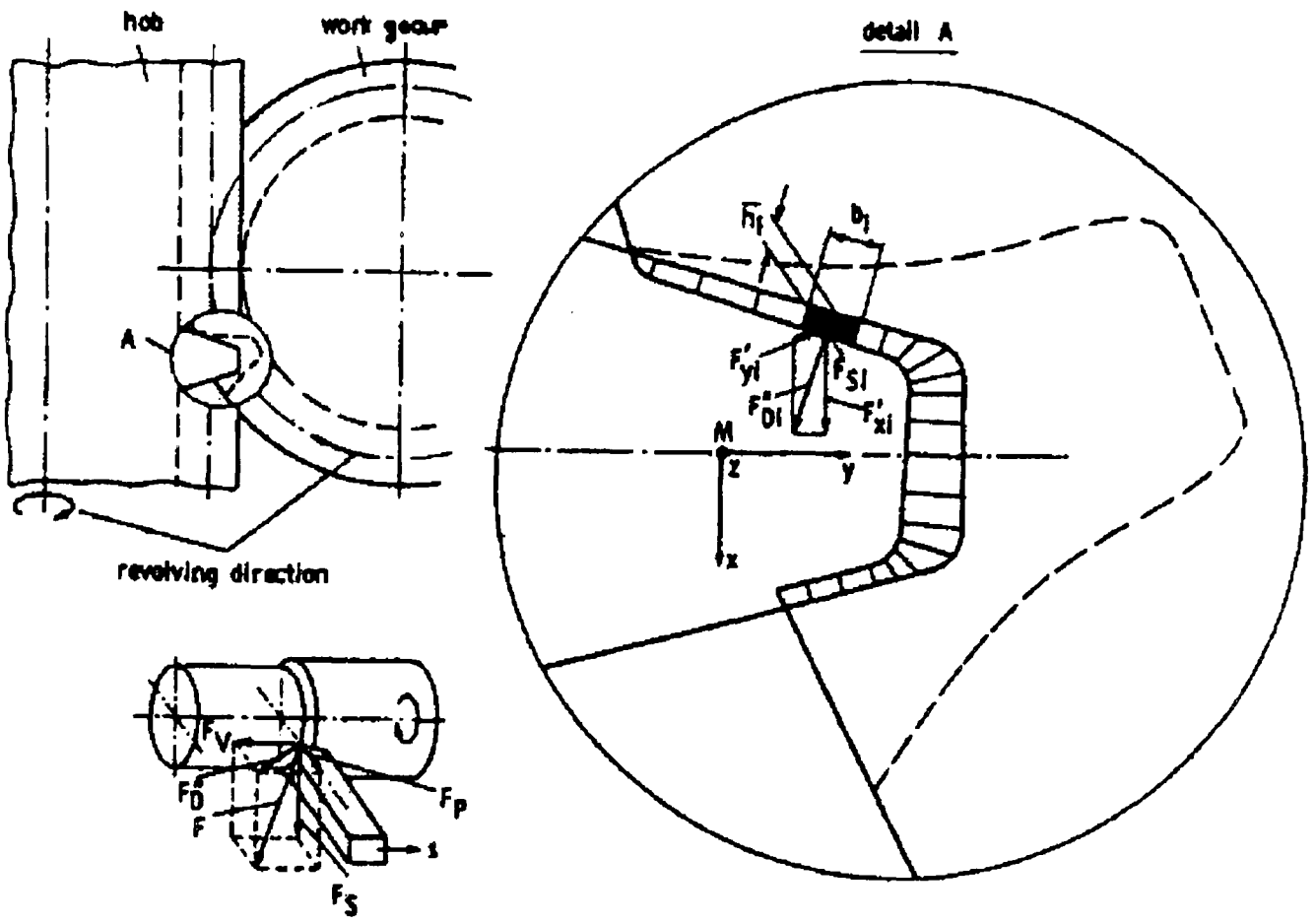

Figure 3.8 Forces acting on the chip cross section (König)

The study also investigated the effect of different parameters on the cutting forces. It was concluded that increasing the axial feed rate will lead to an increase in the resultant cutting force as it will increase the chip thickness and length and possibly causes an over lapping of active gashes cutting which would result in an increase of the cutting force on each hob tooth. It was noticed that forces acting in the Z and Y directions had been influenced by the increase of the axial feed. The study also investigated the force behaviour in climb and conventional hobbing and concluded that forces on the Y direction, see figure 3.8, are greater in the climb hobbing. The forces in the Z direction were found smaller, while the X direction forces only fluctuate around zero in both cases, due to the changes in chip formation on the tooth flanks on the individual hobbing positions during the hob rotation. Forces in hobbing helical gears were also studied and similar conclusions were reached, for climb and conventional hobbing.

Sidorenko, 1992, attempted to calculate the theoretical cutting forces in gear hobbing, based on a simplified model of cutting with a single cutting edge, and his earlier theory, Sidorenko (1986), in which the chip geometry in hobbing was analysed. This two dimensional theory based on a Russian paper by Rozenberg *et al* (1987) assumed that the chip was sheared along curve rather than along a straight shear line, during three dimensional oblique angled cutting. An ellipse was used for the shear line (as in Merchant's theory), with one semi-axis depending on the Brinell hardness of the workpiece material and the other on the cutting speed. No particular reasons are given for this assumption, and the numerical parameters used appear to be empirical 'curve fitted'. No comparison of the predicted cutting forces with test data were given.

Bouzakis *et al*, 2002, has investigated the wear on the hob tool and proposed a mathematical model to predict the wear, which relates the undeformed chip geometry and other cutting parameters with anticipated wear. A tangential shift of the hob, was also studied and a computational procedure to determine the optimal tangential shift amount was proposed in order to distribute the wear along the hob and prolong its life. The study considered the chip generation in full cut and in entry, exit and transient workpiece cutting regions. The undeformed chip geometries were calculated in various revolving and generation positions during the manufacturing of a gear tooth space, based on the method introduced by Sülzer. The undeformed chip cross sections on the cutting edges were presented at successive tool angles at every generating position, figure 3.9

In the full depth of cut the chips have the same geometry per tool rotation and with maximum dimensions, whereas in entry and exit conditions, only parts of the full cut chips are formed, figure 3.10. The study concluded that the length of chips in the successive tool entry cutting positions was increasing; in contrast the length of chip is decreasing in the exit region cutting positions. The study also established a relationship between the gear width, BR, and the length in the workpiece axial direction, QS, as shown in figure, 3.11, and it was claimed to affect the chip geometry and eventually hob wear. When the gear face width, BR,

is greater or equal to the distance QS, then the entry, full cut and the exit region can be clearly noticed, while if the face width, BR, is smaller than the distance QS, then a transient region between the entry and the exit region is apparent, in which the chip is always a part of the full cut.

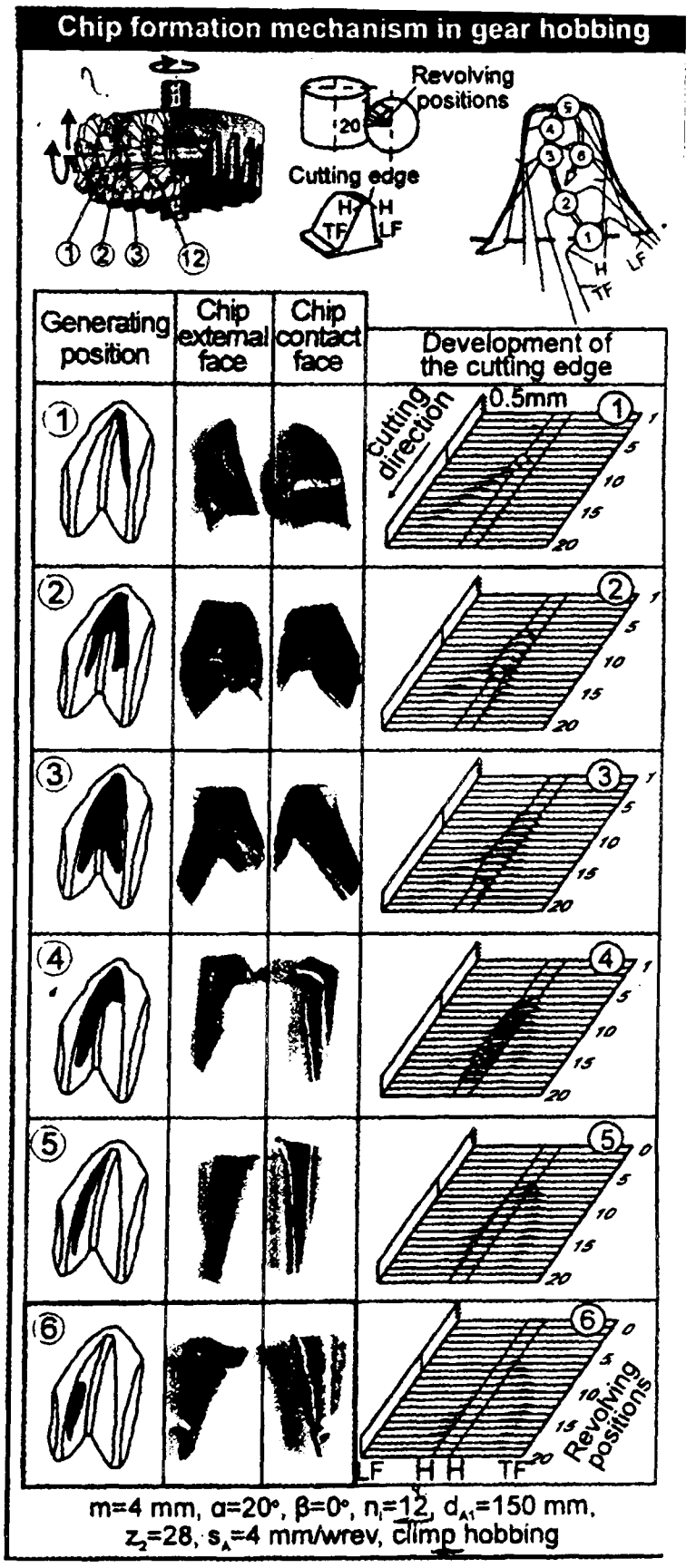

Figure 3.9 Chip formation at various generation positions in the gear hobbing, and the correspondent analytically determined chip cross section (Bouzakis)

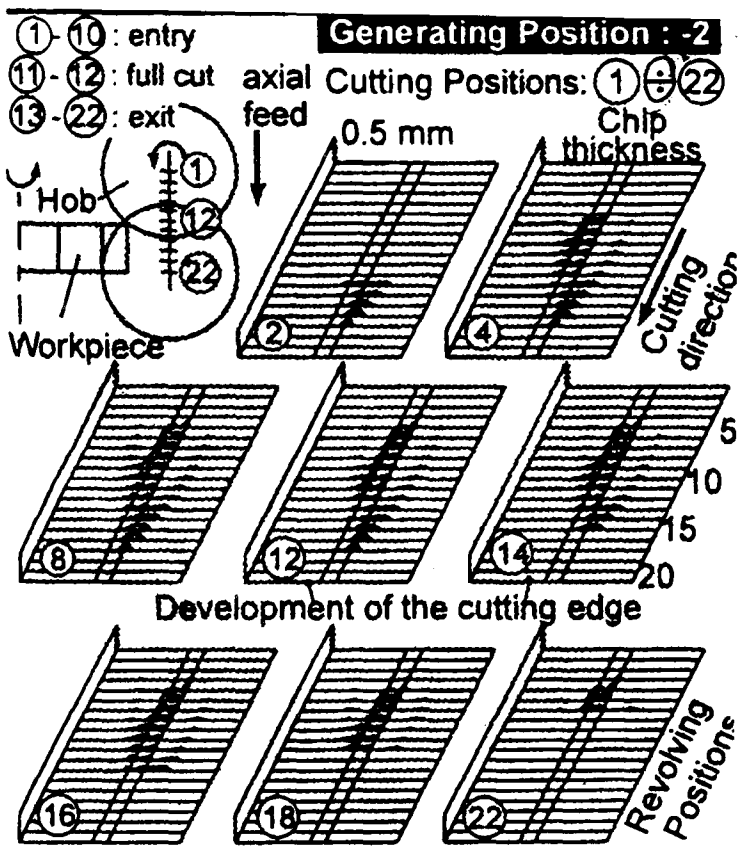

Figure 3.10 Undeformed chip cross sections in entry, full cut, and exit or transient cutting position in gear hobbing (Bouzakis)

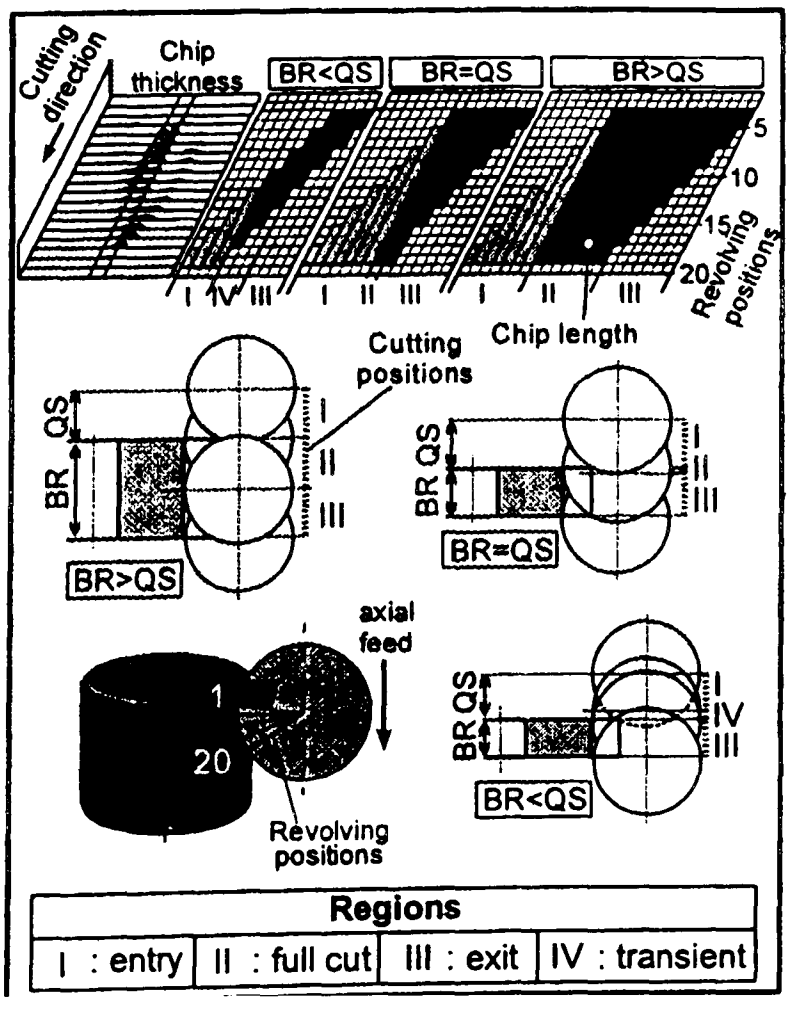

Figure 3.11 Undeformed chip length in various regions during hobbing versus the gear width, in a generation position (Bouzakis)

Weck, *et al*, 2002, estimated the wear in tool by simulating the hobbing process and calculated the chip geometry and effective relief angles during cutting and also estimated the geometry of the gear. The study was backed by experimental results, which was claimed to lead to establish an empirical method for the wear behaviour, and used a kinematic method to relate different co-ordinate systems.

The results of the simulation were split into basic results and process parameters. The basic results are the surface of the gear flanks, the chip thickness, the chip length, the chip width and the effective clearance angles. The process parameters were calculated by analysis of the basic results, and included the maximum chip thickness and the average chip thickness, maximum chip length, the number of cuts and the accumulated chip length.

The study illustrated a simulated chip shape and concluded that the largest value of the chip thickness occurs at the beginning of the cut at the tip of the cutting edge. The maximum values of the maximum chip thickness and average chip thicknesses are obtained at tip flank. For the chip thickness the maximum value is at the incoming tip radius and the values of the maximum chip thickness of the incoming side of the cutting edge are bigger than the outgoing side. It was concluded that during hobbing the number of chips with largest of thickness is small, which suggests only a few chips would cause damage on the hob. It was also concluded that the maximum of cumulative chip length is located on the tip radius of the incoming flank, but that the maximum number of cuts is in the area of the outgoing tip radius.

3.5 SUMMARY

The hobbing process has been used in industry for a considerable time, and has gone through several development stages, particularly with regard to reducing periodic errors. The machine itself has also gone through significant development on its transmission technique with the replacement of its mechanical transmission

with a fully automated CNC transmission technology, which has resulted in better quality products and mass production of gears.

As previously mentioned hobbing is a highly complicated process compared to other cutting processes, and this may explain why there is little published research on the cutting theory. Most of the available work has focused on the shape and the size of the cutting zone, the geometry of the cutting tool (hob), or the chip formation during the hobbing process. Some researchers have concentrated on the kinematics of the hobbing process and the relationship between the moving axes, whilst others have measured or even proposed mathematical models for the gear cutting forces in the gear hobbing. However the need for a comprehensive model, which includes all the above was felt still to be required, as well as the need to validate the model output with the experimental test data. During this project it has been possible to successfully develop the CNC control system for a gear hobbing machine as well as presenting a comprehensive model that is capable of predicting the cutting forces. The model was validated with the results obtained by cutting a single tooth space and also that for a full gear.

CHAPTER FOUR

KINEMATICS OF HOBBING

4.1 INTRODUCTION

Hobbing is a very complicated machining process as both the workpiece and the tool are rotating on oblique axes and engaged in a manner similar to two meshed gears. To understand the process and represent it mathematically it is convenient to define several different co-ordinate systems, within which to represent the different kinematic functions of the hobbing machine itself. The number of co-ordinate systems used is thus equal to the number of components of the machine-tool-workpiece system that have relative motion. These are described below for a vertical hobbing machine (one with a vertical workpiece axis), as shown in figure 4.1.

The first set of axes is fixed in the hob. The hob rotates $\phi_0(t)$ about its axis, but it is sometimes also necessary to move the hob along its axis (called hob shifting) to distribute the wear along the hob tooth or provide an additional generating motion $x_z(t)$ (eg. when cutting a worm wheel). To describe these two hob motions, a second set of axes is defined, fixed in the hob slide. The setting of the hobbing machine also requires the hob to be tilted by the setting (swivel) angle η, as explained previously, so this angle determines the orientation of this set of axes. In conventional (axial-feed) hobbing, the whole hob head travels vertically up (or down) the vertical hob slide, so two additional axis systems are defined, one fixed in the hob head at height $z_a(t)$, one in the vertical slide (attached to the machine base) to define this motion.

The worktable and the gear blank axes are displaced radially from the hob axis during most hobbing operations and may also move radially (in radial hobbing

and during radial in-feed). To model this motion, another co-ordinate system is fixed in the workhead, with its origin at the centre of the worktable. The final co-ordinate system is fixed in the gear blank itself to model rotation of the blank and worktable about their common axis.

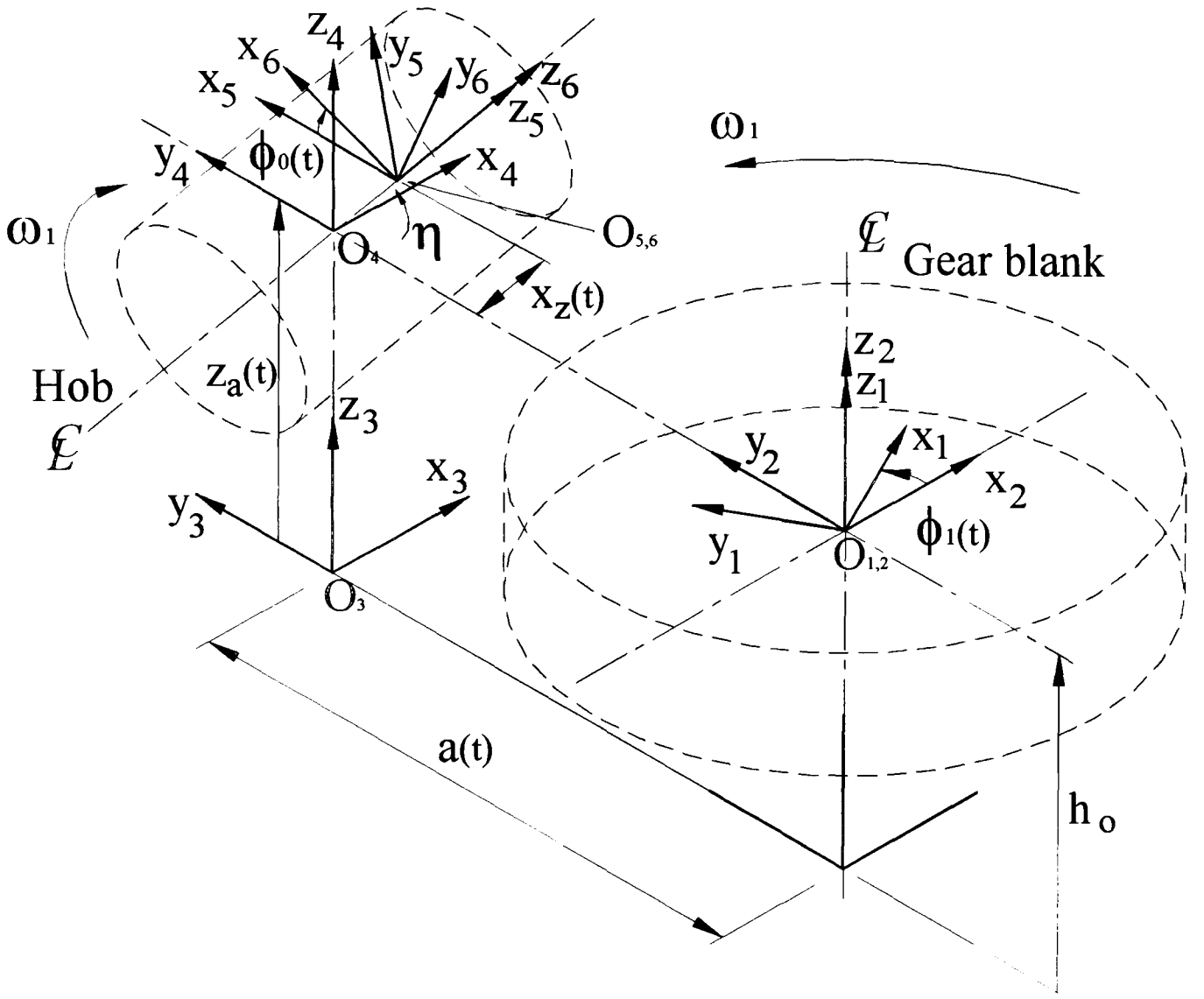

Figure (4.1): The co-ordinate system of a hobbing machine

All the co-ordinate systems are right-handed; the axis definitions are as follows:

(i) Co-ordinate system (1) is fixed to the gear blank, with origin O_1 and O_1Z_1 along the blank axis. It is rotated by ϕ_1 about O_2Z_2 relative to system (2) and coincides with system (2) when $\phi_1 = 0$.

(ii) Co-ordinate system (2) is fixed in the workhead with O_2Z_2 along the worktable axis and O_2Y_2 along O_3Y_3. It is translated by $a(t)$ radially and h_0 vertically relative to system (3) and coincides with system (3) if $a(t) = h_0 = 0$.

(iii) Co-ordinate system (3) is fixed in space with O_3 at the base of the vertical (hob head) slide, O_3Z_3 along this slide, intersecting the hob axis, and O_3Y_3 parallel to the radial slide.

(iv) Co-ordinate system (4) is fixed in hob head and coincides with system (3) when the vertical slide travel $z_a(t) = 0$.

(v) Co-ordinate system (5) is fixed in the hob axial slide with O_5 at the hob centre. When the hob head swivel angle $\eta = 0$ and the hob axial shift $x_z(t) = 0$, O_4 and O_5 coincide, O_5Z_5 is along O_4X_4 and O_5Y_5 is along O_4Z_4.

(vi) Co-ordinate system (6) is fixed in hob, rotated relative to system (5) by $\phi_0(t)$, so that it coincides with system (5) when $t = 0$ and $\phi_0(t) = \pi$.

4.2 TIME DEPENDANT KINEMATIC PARAMETERS

With respect to figure 4.1, the dynamic variables $x_z(t)$, $z_a(t)$, $a(t)$, $\phi_0(t)$ and $\phi_1(t)$ describe the instantaneous position of the system at time t and are discussed :

$a(t)$ is the centre distance between the vertical slide and the worktable and can be expressed as follows

$$a(t) = a_0 - \int_0^t v_r(t)dt$$

$$= a_0 - v_r t \quad \text{if } v_r \text{ is constant.}$$

Where a_0 is the initial distance at $t=0$, and it is the centre distance between the hob and the blank and can be written as

$$a_0 = r_{a1} + r_{a0} - h_c$$

r_{a1}, r_{a0} are the blank and the hob radii respectively.

h_c is the depth of cut which is represented at full depth as $h_c = 2.25m_n$.

v_r is the radial feed velocity (mm/sec). For any hobbing method which does not include radial feed $v_r=0$.

$z_a(t)$ is the centre distance between the hob and the hob slide, and may be written as

$$z_a(t) = z_{a0} \pm \int_0^t v_a(t)dt$$

$= z_{a0} \pm v_a t$ if v_a is constant.

v_a is the axial feed velocity (mm/sec); the sign ± denotes whether vertical federate is either positive (upwards) or negative (downwards) and z_{a0} denotes the hob height at $t=0$.

$x_z(t)$ is the axial shift (mm/s) of hob which is represented as

$$x_z(t) = x_0 + \int_0^t v_t(t)dt$$

$$= x_0 + v_t t$$

x_0 is initial hob shift at $t=0$.

η is the swivel angle where

$$\eta = |\gamma_0| \pm |\beta|$$

γ_0 is the lead angle of the hob, which can be calculated as

$$\gamma_0 = \sin^{-1}(\frac{m_n z_0}{2r_0})$$

Where m_n is the hob module, z_0 is the number of starts on hob and r_0 is the hob reference radius.

β is the helix angle of the gear, which is *zero* for spur gears.

The sign combinations of the angles represent the right or left hand hob and gear respectively as explained previously.

h_0 is the centre height at the gear blank above the worktable.

4.3 CO-ORDINATE TRANSFORMATIONS:

In Cartesian space, a point is defined by its co-ordinates relative to a specified set of axes. A co-ordinate transformation is the set of equations, which relate the co-ordinates of a point in one set of axes to those in a different set of axes. These two axis systems may either have a common origin and non-parallel co-ordinate axes (pure rotation), non-coincident origins but parallel axes (pure translation) or non-coincident origins and non-parallel axes (general rotation plus translation). In transforming the co-ordinates of points in the axes shown in Fig. 4.1, a general transformation (rotation plus translation) is needed in most cases. For this purpose the concept of 'homogeneous co-ordinates' is helpful.

The co-ordinates of a point in three-dimensional space are the vector $\bar{r} = (x, y, z)$. To use homogeneous co-ordinates, a 4-dimensional $\boldsymbol{r}$ vector is used, giving $\boldsymbol{r} = (x, y, z, 1)$. The transformation equations are best given in matrix form, in which the transformation only requires multiplication of matrices in a homogenous co-ordinate system with coincident origins, whereas both multiplication and addition are required for homogenous co-ordinate systems with non-coincident origins. [Litvin]

The transformation and translation vectors and matrices can be written as follows

$$\{r\}_{(2)} = [T_{2,1}]\{r\}_{(1)} \tag{4.1}$$

$$\{r\}_{(3)} = [T_{3,2}]\{r\}_{(2)} \tag{4.2}$$

$$\{r\}_{(4)} = [T_{4,3}]\{r\}_{(3)} \tag{4.3}$$

$$\{r\}_{(5)} = [T_{5,4}]\{r\}_{(4)} \tag{4.4}$$

$$\{r\}_{(6)} = [T_{6,5}]\{r\}_{(5)} \tag{4.5}$$

Or in their respective matrix form

$$\begin{bmatrix} x \\ y \\ z \\ 1 \end{bmatrix}_{(2)} = \begin{bmatrix} \cos\phi_1 & -\sin\phi_1 & 0 & 0 \\ \sin\phi_1 & \cos\phi_1 & 0 & 0 \\ 0 & 0 & 1 & 0 \\ 0 & 0 & 0 & 1 \end{bmatrix} \begin{bmatrix} x \\ y \\ z \\ 1 \end{bmatrix}_{(1)} \tag{4.1a}$$

$$\begin{bmatrix} x \\ y \\ z \\ 1 \end{bmatrix}_{(3)} = \begin{bmatrix} 1 & 0 & 0 & 0 \\ 0 & 1 & 0 & -a(t) \\ 0 & 0 & 1 & -h_0 \\ 0 & 0 & 0 & 1 \end{bmatrix} \begin{bmatrix} x \\ y \\ z \\ 1 \end{bmatrix}_{(2)} \tag{4.2a}$$

$$\begin{bmatrix} x \\ y \\ z \\ 1 \end{bmatrix}_{(4)} = \begin{bmatrix} 1 & 0 & 0 & 0 \\ 0 & 1 & 0 & 0 \\ 0 & 0 & 1 & -z_a(t) \\ 0 & 0 & 0 & 1 \end{bmatrix} \begin{bmatrix} x \\ y \\ z \\ 1 \end{bmatrix}_{(3)} \tag{4.3a}$$

$$\begin{bmatrix} x \\ y \\ z \\ 1 \end{bmatrix}_{(5)} = \begin{bmatrix} 0 & 1 & 0 & 0 \\ -\sin\eta & 0 & \cos\eta & 0 \\ \cos\eta & 0 & \sin\eta & -x_z(t) \\ 0 & 0 & 0 & 1 \end{bmatrix} \begin{bmatrix} x \\ y \\ z \\ 1 \end{bmatrix}_{(4)} \tag{4.4a}$$

$$\begin{bmatrix} x \\ y \\ z \\ 1 \end{bmatrix}_{(6)} = \begin{bmatrix} \cos\phi_0 & \sin\phi_0 & 0 & 0 \\ -\sin\phi_0 & \cos\phi_0 & 0 & 0 \\ 0 & 0 & 1 & 0 \\ 0 & 0 & 0 & 1 \end{bmatrix} \begin{bmatrix} x \\ y \\ z \\ 1 \end{bmatrix}_{(5)} \tag{4.5a}$$

4.3.1 Overall transformation matrix (position vectors $(\bar{r}_{(6)}, \bar{r}_{(1)})$

The overall transformation from co-ordinate system (1), down to co-ordinate system (6) is the result of the multiplication of all the transformation from system (1) to system (6) in order and is written as

$$\{\bar{r}\}_{(6)} = [T_{6,1}]\{\bar{r}\}_{(1)} \tag{4.6}$$

Where

$$[T_{6,1}] = [T_{6,5}][T_{5,4}][T_{4,3}][T_{3,2}][T_{2,1}] \tag{4.7}$$

To save multiple operations, in programming, when tangential hobbing occurs, it is useful to compute

$$[T_{5,3}] = [T_{5,4}][T_{4,3}] \tag{4.8}$$

Where $v_a, v_r = 0$ for tangential hobbing.

Similarly for axial hobbing with no hob shift and no radial feed. Thus $[T_{5,4}]$ and $[T_{3,2}]$ need be calculated only once.

The inverse transformation, from co-ordinate system (6) to co-ordinate system (1) is given by

$$\{\bar{r}\}_{(1)} = [T_{1,6}] \cdot \{\bar{r}\}_{(6)}$$

Where

$$[T_{1,6}] = [T_{6,1}]^{-1} \tag{4.9}$$

So both $[T_{6,1}]$ and $[T_{1,6}]$ will have the form

$$[T_{i,j}]=\begin{bmatrix} a_{11} & a_{12} & a_{13} & b_1 \\ a_{21} & a_{22} & a_{23} & b_2 \\ a_{31} & a_{32} & a_{33} & b_3 \\ 0 & 0 & 0 & 1 \end{bmatrix} \tag{4.10}$$

with $a_{ij} = -a_{ji}$ (i ≠ j).

4.3.2 Transformation of other vectors (e.g. velocities)

In this case, only the rotation terms are needed, since translation does not affect their components, the transformation matrices are thus

$$[R_{i,j}]=\begin{bmatrix} a_{11} & a_{12} & a_{13} \\ a_{21} & a_{22} & a_{23} \\ a_{31} & a_{32} & a_{33} \end{bmatrix} \tag{4.11}$$

so that for velocity $\bar{v} = \{v_x, v_y, v_z\}^T$

$$\{\bar{v}\}_{(6)} = [R_{6,1}] \cdot \{\bar{v}\}_{(1)}$$

or

$$\begin{bmatrix} v_x \\ v_y \\ v_z \end{bmatrix}_{(6)} = \begin{bmatrix} a_{11} & a_{12} & a_{13} \\ a_{21} & a_{22} & a_{23} \\ a_{31} & a_{32} & a_{33} \end{bmatrix} \begin{bmatrix} v_x \\ v_y \\ v_z \end{bmatrix}_{(1)} \tag{4.12}$$

Where

$[a_{i,j}]$ are the appropriate terms of $[T_{6,1}]$ from (4.14).

4.4 CUTTER PROFILE, TOOTH NUMBERING.

Consider a hob with z_g gashes and z_0 starts. Each tooth (cutting edge) of the hob is identified by two indices *i* and *j*. Index *i* denotes the number of the tooth, counted clockwise about the $(OX)_{(6)}$ axis and index *j* the start (thread) on which it is located. The reference tooth is that for which $i = i_{ref}$ on the reference thread for which $j = 1$. The centre line of the reference tooth is the $(OX)_{(6)}$ axis. When the

hob is in the datum position ($\phi_0(t) = \pi$ and $x_z(t) = 0$), the centre line of the reference tooth thus lies on the $(-y)_{(4)}$ axis (so that the reference tooth is cutting at maximum depth symmetrically in a tooth space of the blank). The centre line of tooth $[i, j]$ is on a radial line making an angle $\theta_{i,j}$ *with* $(OX)_{(6)}$, as illustrated in figure 4.2 where

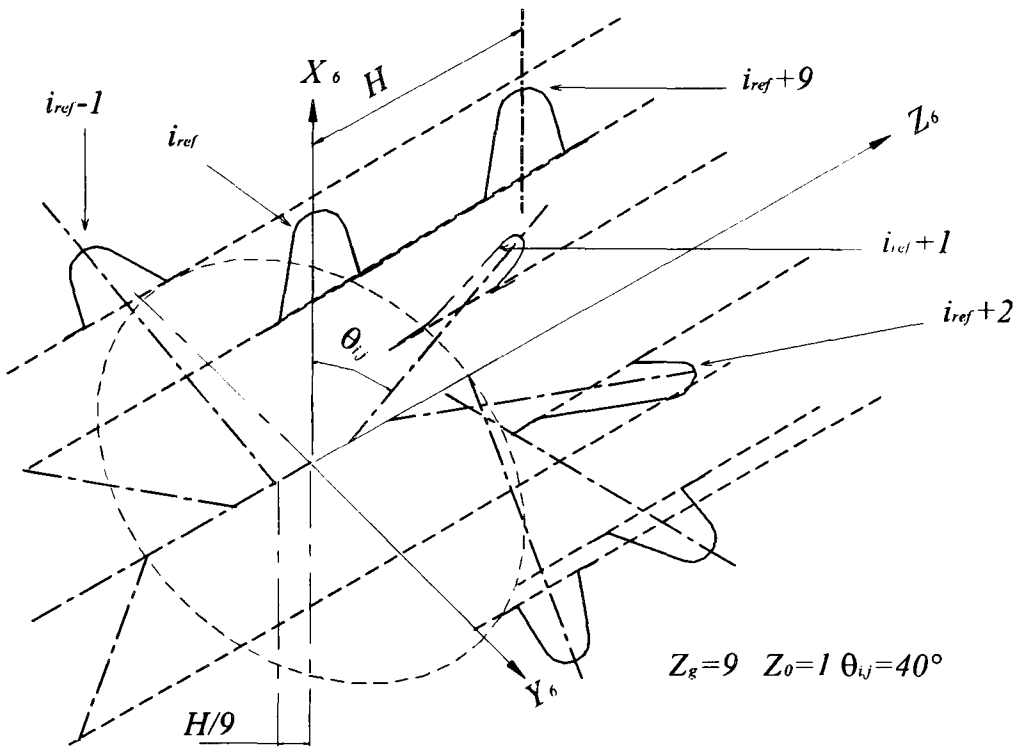

Figure 4.2 Tooth numbering on one-thread hob

$$\theta_{i,j} = \frac{2\pi}{z_0}(j-1) + \frac{2\pi}{z_g}(i - i_{ref}) = 2\pi\left[\frac{j-1}{z_0} + \frac{i - i_{ref}}{z_g}\right] \tag{4.13}$$

4.4.1 Tooth form

If the hob is cylindrical, all the teeth have the same symmetric profile. If the gashes in the hob are axial (as is usual on single and two-start hobs) the actual profile is that of the axial section of an involute helicoid worm [Buckingham]. However, for most gear hobs, this profile differs very little from that of a standard basic rack, so this simplified, straight-sided profile will be assumed.

In general, let the tooth thickness at radius r_y be given by (as shown in figure 4.3)

$s_y = f(r_y)$

Where s_y is determined by the type of profile, basic rack dimensions etc. The above formula is valid at any radius, whether the flank is involute, a tip radius etc., although the form of function s_y may change discontinuously.

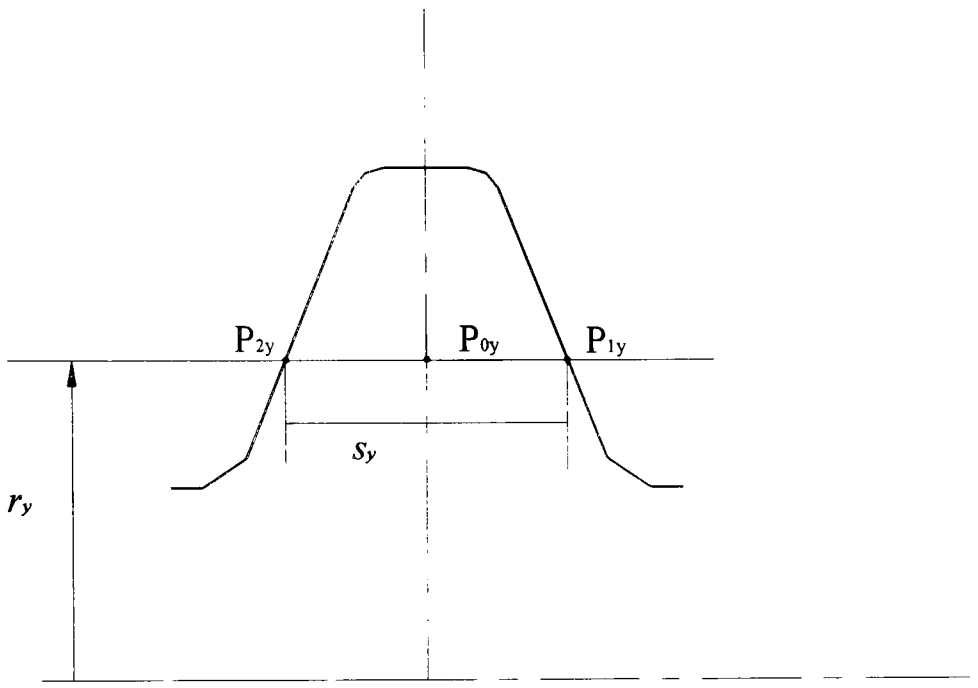

Figure 4.3 Tooth thickness (s_y) at radius (r_y)

In the polar co-ordinate of system (6), the co-ordinates of a point P_{0y} at r_y on the centre line of tooth i, j are

$$r_{0(6)} = r_y$$

$$\theta_{0(6)} = \theta_{i,j} = 2\pi\left[\frac{i - i_{ref}}{z_g} + \frac{j-1}{z_0}\right] \tag{4.14}$$

$$z_{0(6)} = H\left(\frac{i - i_{ref}}{z_g}\right) + \frac{H}{z_0}(j-1) = H\frac{\theta_{i,j}}{2\pi}$$

Where H is the hob lead given by $H = \dfrac{\pi m_n z_0}{\cos\gamma_0}$

The Cartesian co-ordinates of P_{0y} are thus

$$\{\bar{r}_{p_0}\}_{(6)} = \begin{bmatrix} x_0 \\ y_0 \\ z_0 \\ 1 \end{bmatrix}_{(6)} = \begin{bmatrix} r_y \cos\theta_{i,j} \\ r_y \sin\theta_{i,j} \\ H\dfrac{\theta_{i,j}}{2\pi} \\ 1 \end{bmatrix}_{(6)} \tag{4.14a}$$

It follows that the co-ordinates of the points P_1, P_2 on the cutting edges at r_y are

$$[\bar{r}_{p_1}]_{(6)_{i,j,k}} = \begin{bmatrix} r_y \cos\theta_{i,j} \\ r_y \sin\theta_{i,j} \\ \dfrac{H\theta_{i,j}}{2\pi} - \dfrac{s_y(r_y)}{2} \\ 1 \end{bmatrix}$$

$$[\bar{r}_{p_2}]_{(6)_{i,j,k}} = \begin{bmatrix} r_y \cos\theta_{i,j} \\ r_y \sin\theta_{i,j} \\ \dfrac{H\theta_{i,j}}{2\pi} + \dfrac{s_y(r_y)}{2} \\ 1 \end{bmatrix} \tag{4.15}$$

Where the suffix (6) denotes a quantity defined in co-ordinate system (6).

4.4.2 Basic rack profile in normal section.

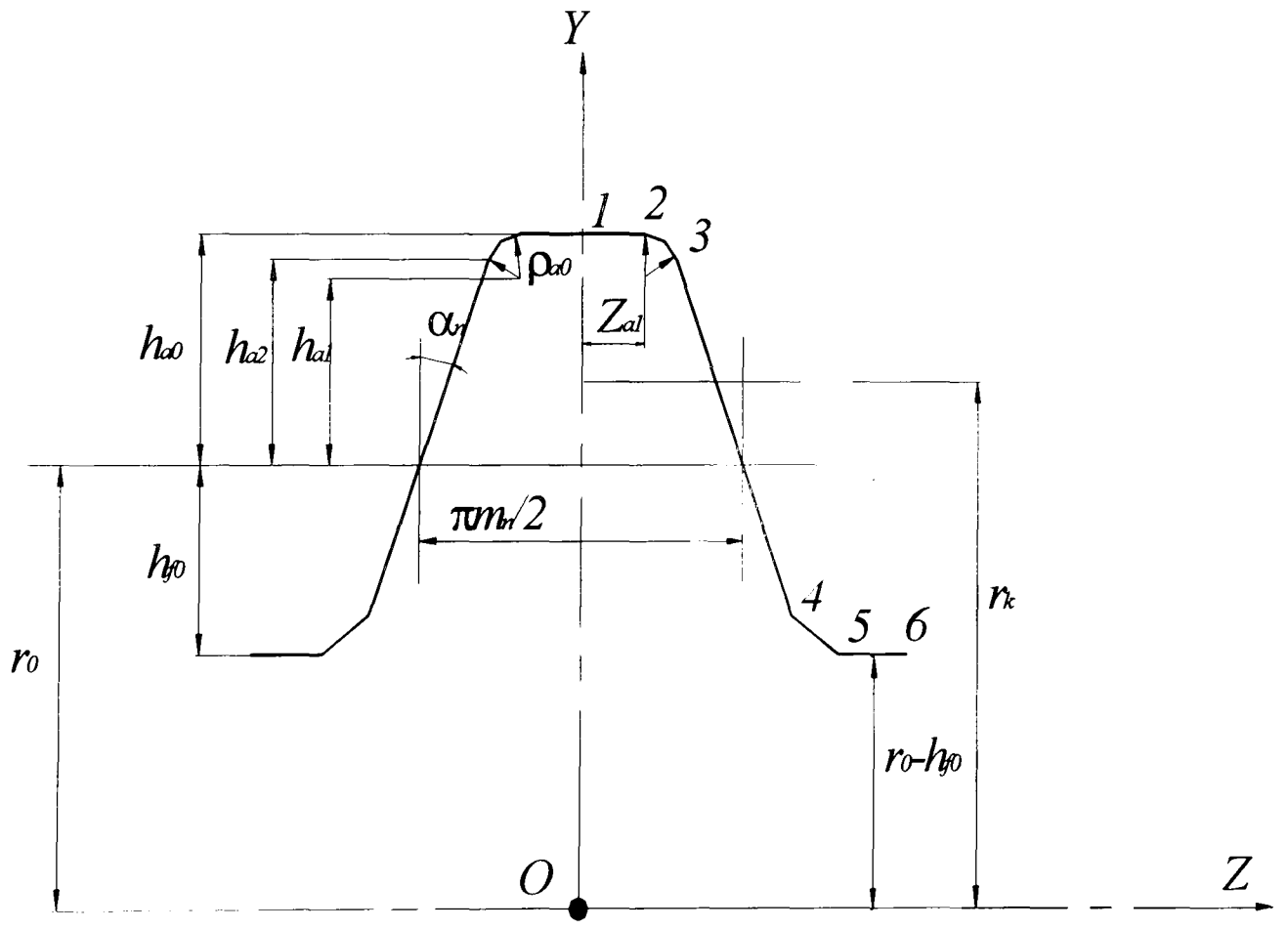

Figure 4.4 Boundaries on a tooth profile

The basic rack in the normal section has the general form shown in Fig. 4.4. For the *BS 436* basic rack, the addendum and dedendum are given by

$$h_{a0} = 1.25m_n \quad \text{and} \quad h_{f_0} = 1.0m_n. \tag{4.16}$$

where m_n is the hob normal module.

In order to calculate the co-ordinates of points on the hob tooth profile, it has been divided into five sections: the straight line (1-2), the curve (2-3), the straight line (2-3), the chamfer (4-5) and the straight line (5-6). The procedure for calculating the tooth profile is to consider a number of points P_k *(k_{min} <= k <= k_{max})* equally spaced at Δz along the z axis. Since the profile is symmetric, only points for $0 <= k <= k_{max}$ need be considered.

From Fig. 4.4

$$h_{a1} = h_{a0} - \rho_{a0} \tag{4.17}$$

where ρ_{a0} is the radius of the tooth tip *(= 0.39 m_n for BS436 basic rack)*, and

$$z_{a1} = \frac{\pi m_n}{4} - (h_{a1} + \rho_{a0}\sin\alpha_n)\tan\alpha_n - \rho_{a0}\cos\alpha_n \tag{4.18}$$

On the straight line section (4-3), for which

$$z_{a1} + \rho_{a0}\cos\alpha_n < z_k \le \frac{\pi m_n}{4} + h_{f_0}\tan\alpha_n \tag{4.19}$$

the axial co-ordinate is

$$z_k = \frac{\pi m_n}{4} - (r_k - r_0)\tan\alpha_n \tag{4.19a}$$

which gives (since r_y is to be calculated)

$$r_k = r_0 - \frac{z_k - \frac{\pi m_n}{4}}{\tan\alpha_n} \tag{4.20}$$

For the straight-line (tip land) section (5-6) for which

$$z_k > \frac{\pi m_n}{4} + h_{f_0}\tan\alpha_n$$

the radius is constant, so

$$r_k = r_0 - h_{f0} \tag{4.20a}$$

For the straight-line (root chamfer) section (4-5), with chamfer height $c_f = c_f^* m_n$ (c_f^* is the non-dimensional chamfer height: typically 0 <= c <= 0.1),

$$r_k = r_0 - \left[\frac{(z_{a3} - \frac{\pi m_n}{4})}{\tan(\alpha_n)} - \frac{(z_k - z_{a3})}{\tan(\alpha_{cf})} \right] \qquad (4.20b)$$

where α_{cf} is the chamfer angle (usually 45 °).

$$z_{a3} = \frac{\pi m_n}{4} + h_{Ff0} \tan(\alpha_n)$$

and $h_{Ff_0} = h_{f_0} - c_f$ is the profile form height

On the tip radius, curve (2-3),

$$z_{a1} \le z_k \le z_{a1} + \rho_{a0} \cos\alpha_n = z_{k*}$$

From Fig. 4.5, at a point defined by angle α_{nk}, for $90^\circ \le \alpha_{nk} \le \alpha_n$

$$z_k = z_{a1} + \rho_{a0} \cos_{nk} \qquad (4.21)$$

and

$$r_k = r_0 + h_{a1} + \rho_{a0} \sin\alpha_{nk} \qquad (4.22)$$

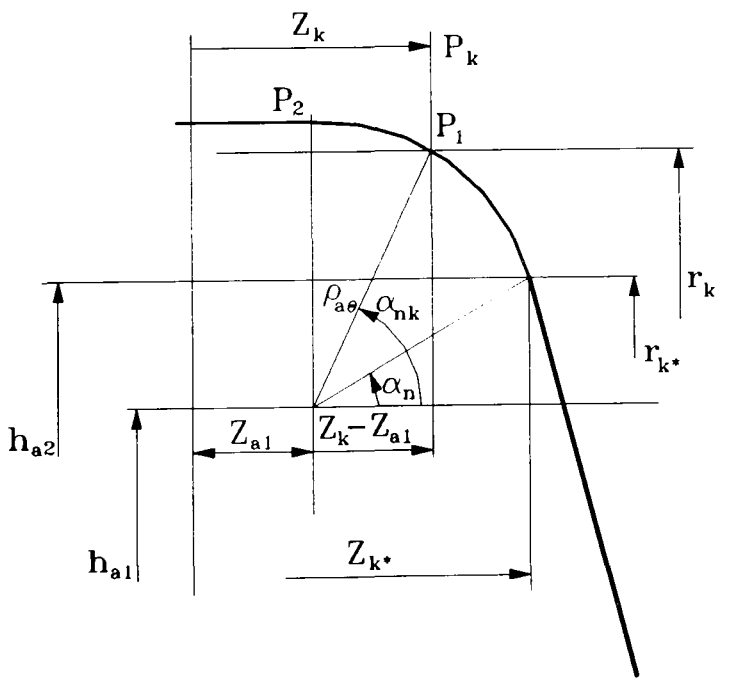

Figure 4.5 Boundaries of the radius tip on a tooth profile

$$r_k = r_0 + h_{a1} + \sqrt{\rho_{a0}{}^2 - (z_k - z_{a1})^2} \qquad (4.22a)$$

As for the tooth tip section, line (1-2), where ($|z_k| \le z_{a1}$)

$z_k = z_k$

$r_k = r_{a0}$

4.4.3 Reference tooth axial section

For small lead angles, the axial section of the hob approximates closely to the axial section of the equivalent generating rack with lead angle γ_0. [Buckingham]. The shape of the intersection of 'worm/rack' teeth with the rake face is thus the axial profile with sufficient accuracy as shown in Fig. 4.6.

For any point at radius (r_k, z_k) in the normal section, the corresponding values of z_k in the axial section are all increased by the factor $(1/\cos\gamma)$; r_k is, of course, unchanged. These co-ordinates of the axial section of the reference tooth can be defined in a local co-ordinate system, $(XYZ)_{(6)}$, fixed to the rake face of the reference tooth, as in Fig. 4.6.

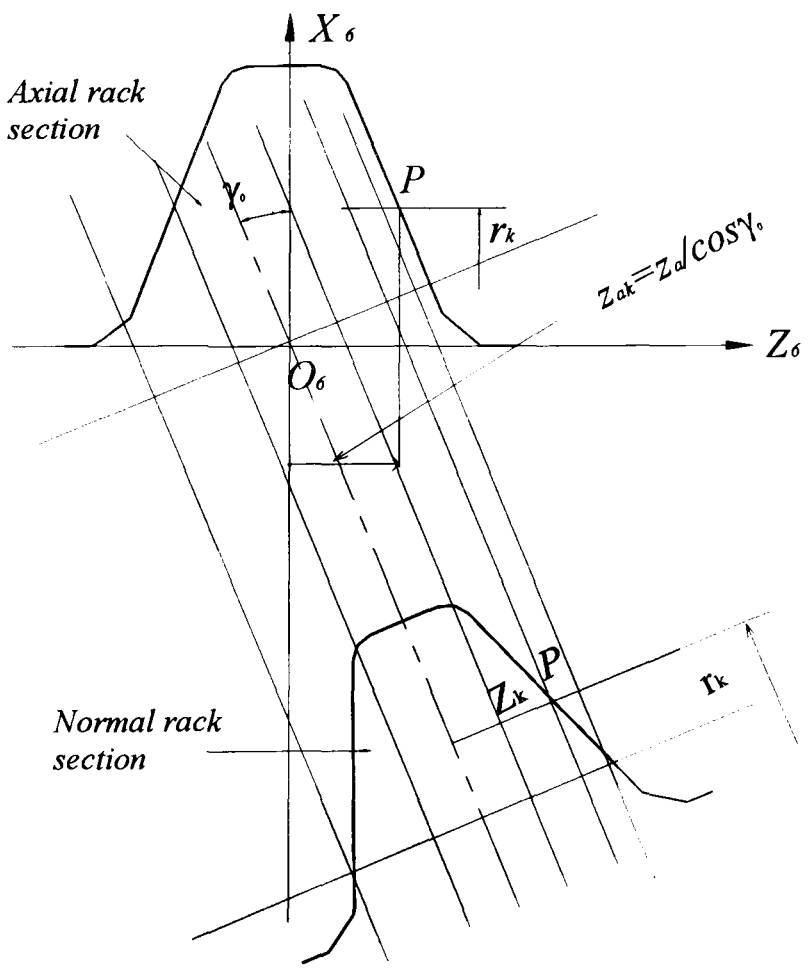

Figure 4.6 Profile the cutter in the axial and normal sections

4.4.4 Tooth numbering

Consider tooth *i* on the same thread (j = 1) as the reference tooth, with tooth axes *[i]=(OXYZ)$_{(i)}$* fixed in it, similar to axes *(OXYZ)*$_{(6)}$ in the reference tooth, so that O_iX_i is the centre line of tooth *i*. Axes *[i]* are translated by Z_i along *(OZ)*$_{(6)}$ relative to axes *[6]* and rotated by $\theta_i(i)$. The co-ordinates of point $P_{i,k}$ in system *[i]* are the same as those correspondent point P_{0k} on reference tooth in system *[6]*.

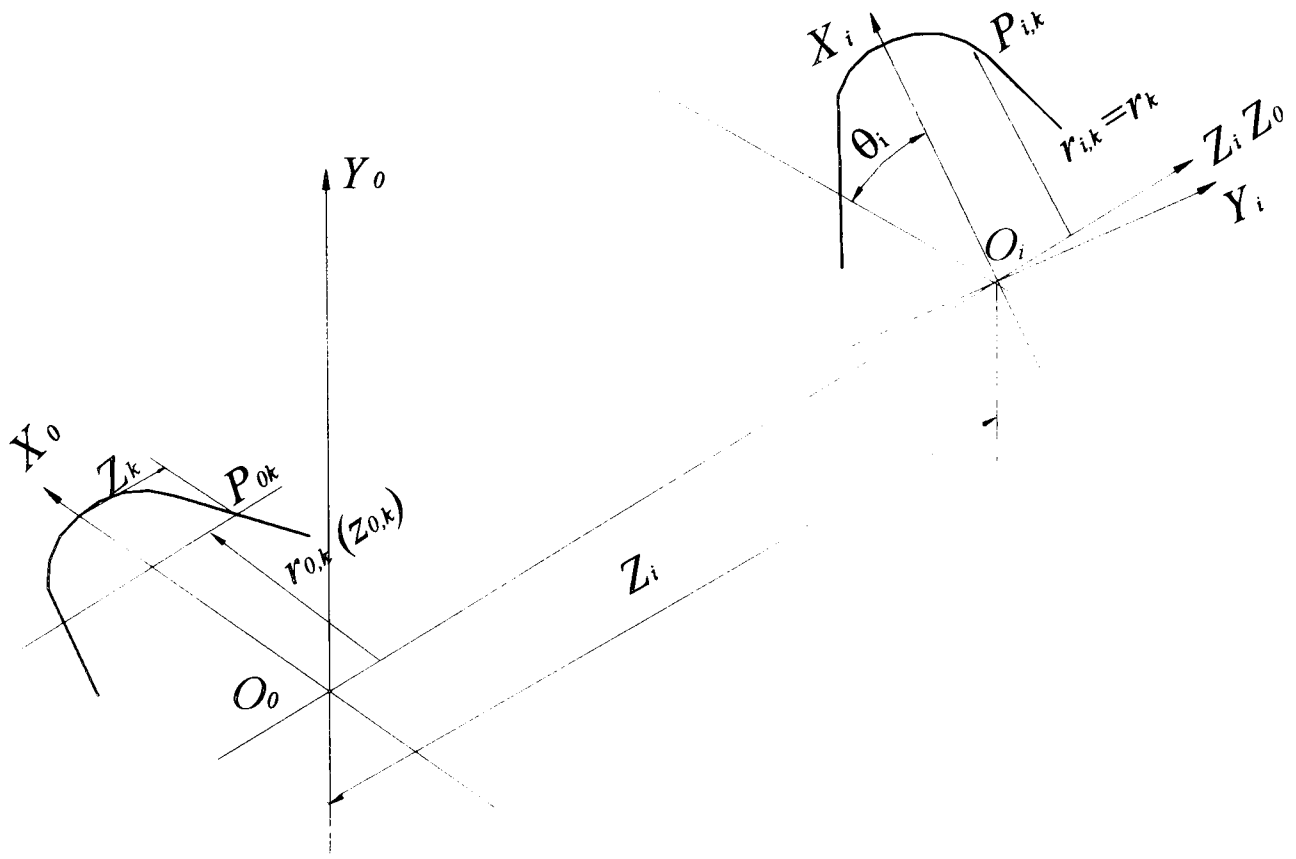

Figure 4.7 Co-ordinates of point $P_{i,j}$ on tooth i

The co-ordinates of $P_{i,k}$ in system [0] are given by

$$[\bar{r}_{i,k}]_{[0]} = [T_{0,i}][\bar{r}_{i,k}]_{[i]}$$

from which, since $[\bar{r}_{i,k}]_{[i]} \equiv [\bar{r}_{0,k}]_{[0]}$,

$$[\bar{r}_{i,k}]_{[0]} = [T_{0.i}][\bar{r}_{0,k}]_{[0]}$$

This gives

$$[Z_{i,k}]_{[0]} = Z_i + Z_{0,k}$$

$$[r_{i,k}]_{[0]} = \bar{r}_{0,k}$$

$$[\theta_{i,k}]_{[0]} = 0 + \theta_i = 2(i - i_{ref})etc$$

From the above, the co-ordinates $[r_{i,k}, \theta_{i,k}, Z_{i,k}]_{[0]}$ can be calculated provided $Z_{0,k}$ and $r_{0,k}$ are known and θ_i, Z_i have been calculated. To obtain $X_{i,k}$ and $Y_{i,k}$ of the point P_{ik} from $\bar{r}_{i,k}, \theta_{i,k}$

$$[X_{i,k}]_{[0]} = r_{i,k}\cos(\theta_{i,k})$$

$$[Y_{i,k}]_{[0]} = r_{i,k}\sin(\theta_{i,k})$$

4.5 TANGENT TO CUTTING EDGE.

The tangent at $P_{1,2}$ to the cutting edge is obtained by differentiating (4.15) with respect to r_y, so that, in system (6)

$$\left[\bar{t}_{0P_{1,2}}\right]_{(6)_{i,j,m,k}} = \begin{bmatrix} \cos\theta_{i,j} \\ \sin\theta_{i,j} \\ \pm\frac{1}{2}\frac{ds_y}{dr_y} \\ 1 \end{bmatrix}_{(6)} \tag{4.23}$$

The unit tangent $\left|\bar{t}_{0P_{1,2}}\right|_{(6)_{i,j}}$ can be obtained from

$$\left[\bar{t}_{0P_{1,2}}\right]_{(6)_{i,j}} = \frac{\left|\bar{t}_{0P_{1,2}}\right|_{(6)_{i,j}}}{\left|\hat{t}_{0P_{1,2}}\right|_{i,j}} = \frac{\left|\bar{t}_{0P_{1,2}}\right|_{(6)_{i,j}}}{\sqrt{1+\frac{1}{4}\left(\frac{ds_y}{dr_y}\right)^2}} \tag{4.24}$$

From which

$$\therefore \begin{bmatrix} t_x \\ t_y \\ t_z \\ 1 \end{bmatrix}_{(6)} = \cos\psi \begin{bmatrix} \cos\theta_{i,j} \\ \sin\theta_{i,j} \\ \pm\tan\psi \\ 1 \end{bmatrix} = \cos\psi \left[\begin{bmatrix} \cos\theta_{i,j} \\ \sin\theta_{i,j} \\ \pm\frac{1}{2}\left(\frac{ds_y}{dr_y}\right) \\ 1 \end{bmatrix}\right]$$

$$\text{since } \cos\psi = \frac{1}{\sqrt{1+\tan^2\psi}} = \frac{1}{\sqrt{1+\frac{1}{4}\left(\frac{ds_y}{dr_y}\right)^2}}$$

4.6 VELOCITIES AT P_1 AND P_2

The absolute velocities of the hob at the points P_1, P_2 result from rotation of the hob (the main component) plus small components due to the hob head feed rates s_a, s_r and s_t

Due to rotation of the hob at ω_0 (represented in (6) by the vector $\overline{\omega}_{0(6)}$ where

$$\left[\overline{\omega}_0\right]_{(6)} = \begin{bmatrix} 0 \\ 0 \\ \omega_0 \end{bmatrix}_{(6)} \tag{4.25}$$

the point P_1 has velocity $\left[\overline{v}_{p1}\right]_{(6)}^{(\omega_0)} = \left[\overline{w}_0 \times \overline{r}_{p1}\right]_{(6)}$ so that

$$\left[\overline{v}_{p_1}^{\omega_0}\right] = \begin{bmatrix} i_{(6)} & j_{(6)} & k_{(6)} \\ 0 & 0 & \omega_0 \\ x_6 & y_6 & z_6 \end{bmatrix}_{p_1,i,j} = \begin{bmatrix} -\omega_0 y_{(6)} \\ \omega_0 x_{(6)} \\ 0 \end{bmatrix}_{(6)}^{\omega_0} \tag{4.26}$$

The velocity of the hob head has components

$\hat{v}_{(4)}^{s_r,s_a} = \begin{bmatrix} 0 \\ -v_r \\ v_a \end{bmatrix}$ in system (4) due to the radial and axial feed rates s_a and s_r.

and a component $v_{(6)}^{s_t} = \begin{bmatrix} 0 \\ 0 \\ v_t \end{bmatrix}_{(6)}$ in system (6) due to s_t .

Continuing these transformations to system (6) gives

$$\overline{v}_{(6)}^{s_r,s_a} = \left[R_{6,4}\right] \cdot \overline{v}_{(4)} \tag{4.27}$$

Where, from (4.5), (4.4), (4.11) and (4.12)

$$\left[R_{6,4}\right] = \left[R_{6,5}\right] \cdot \left[R_{5,4}\right]$$

$$= \begin{bmatrix} \cos\phi_0 & \sin\phi_0 & 0 \\ -\sin\phi & \cos\phi_0 & 0 \\ 0 & 0 & 1 \end{bmatrix} \cdot \begin{bmatrix} 0 & 1 & 0 \\ -\sin\eta & 0 & \cos\eta \\ \cos\eta & 0 & \sin\eta \end{bmatrix} \tag{4.28}$$

and $\overline{v}_{(4)}^{s_r,s_a} = \begin{bmatrix} 0 \\ -v_r \\ v_a \end{bmatrix}$ (4.29)

This gives

$$\left[\bar{v}^{S_r,S_a}\right]_{(6)} = \begin{bmatrix} v_x^{S_r,S_a} \\ v_y^{S_r,S} \\ v_z^{S_r,S} \end{bmatrix}_{(6)} \tag{4.29a}$$

Adding the velocity components finally gives

$$\bar{v}_{0(6)i,j,k} = \begin{bmatrix} -\omega_0 \cdot y + v_x^{S_r,S_a} + 0 \\ \omega_0 \cdot x + v_y^{S_r,S_a} + 0 \\ 0 + v_z^{S_r,S_a} + v_t \end{bmatrix}_{(6)} \tag{4.30}$$

Note: v_a, v_r, v_t are velocities (mm/s) units . The feed rates s_a, s_r, s_t are usually defined as mm/rev. (of the work piece). The time for one work piece rotation is $t = \frac{2\pi}{\omega} = \frac{2\pi . i_0}{\omega_0}$ where i_0 is the index ratio.

Thus the feed velocities are $\begin{bmatrix} v_a \\ v_r \\ v_t \end{bmatrix}_{(6)} = \left[\frac{\omega_0}{2\pi i_0}\right] \cdot \begin{bmatrix} s_a \\ s_r \\ s_t \end{bmatrix}_{(6)}$ (4.31)

4.7 TIME SCALE, ACTUAL VELOCITIES.

This is a quasi-static model; so use of the actual velocities is unnecessary. Note that because of formula (4.31) all the velocity components of (4.30) are proportional to $|\omega_0|$, since (4.30) could be re-written as

$$\bar{v}_{0,i,j,k(6)} = \omega_0 \left[\begin{bmatrix} -y \\ x \\ 0 \end{bmatrix}_{(6)} + \frac{s_a}{2\pi i_0} \begin{bmatrix} v_{xa} \\ v_{ya} \\ v_{za} \end{bmatrix}_{(6)} + \frac{s_r}{2\pi i_0} \begin{bmatrix} v_{xr} \\ v_{yr} \\ v_{zr} \end{bmatrix}_{(6)} + \frac{s_t}{2\pi i_0} \begin{bmatrix} 0 \\ 0 \\ 1 \end{bmatrix}_{(6)} \right] \tag{4.30a}$$

Where v_{xa}, v_{xr} etc. are the appropriate terms in s_a, s_r, respectively from (4.29a), the factor $\frac{1}{2\pi i_0}$ could be included in these if required to give

$$\bar{v}_{0,i,j,k(6)} = |\omega_0| \left[\begin{bmatrix} -y \\ x \\ 0 \end{bmatrix}_{(6)} + s_a \begin{bmatrix} v_{xa} \\ v_{ya} \\ v_{za} \end{bmatrix}_{(6)} + s_r \begin{bmatrix} v_{xr} \\ v_{yr} \\ v_{zr} \end{bmatrix}_{(6)} + s_t \begin{bmatrix} 0 \\ 0 \\ \dfrac{1}{2\pi i_o} \end{bmatrix}_{(6)} \right] \tag{4.30b}$$

Note that an arbitrary value could be assigned to $|\omega_0|$ *(= 1, say)* or it could also be possible to simply work in terms of the "non-dimensional velocities" $\left(\dfrac{v_0}{|\omega_0|}\right)$, etc.

4.8 TOOTH CUTTING

4.8.1 Chip thickness (normal directions).

To determine the chip cross section, the depth of cut *h* (measured perpendicular to the cutting edge and the cutting direction) at each point $P_{i,j,k}$ on the cutter has to be calculated. Note that chip thickness is defined normal to the work piece surface. When a tool cuts, its velocity relative to the surface being cut must be along the surface, so that the relative velocity at $P_{i,j,k}$ must lie in the work piece surface, i.e. v_{rel} is tangent to the work piece. If cutting is occurring at $P_{i,j,k}$, the cutting edge tangent $\hat{t}_{0,i,j,k}$ (eq. 4.24) must also lie in the surface cut.

Thus $\bar{v}_{rel}$ and $\hat{t}_0$ are both tangents to the machined surface at $P_{i,j,k}$, if cutting is occurring. Both are thus perpendicular to the work piece surface normal $\hat{n}$, as shown in figure 4.8. The normal to the work piece (gear) tooth cut, could be found, at $P_{i,j,k}$, from

$$\hat{n}_{1(1)} = \hat{t}_{0(1)} \times \left[\frac{\bar{v}_{rel}}{|v_{rel}|} \right]_{(1)} \tag{4.32}$$

Where the vectors $(\hat{t}_0)_{(1)}$ and $[\bar{v}_{rel}]_{(1)}$ are defined with $\hat{n}_{1(1)}$ in the gear axis (1).

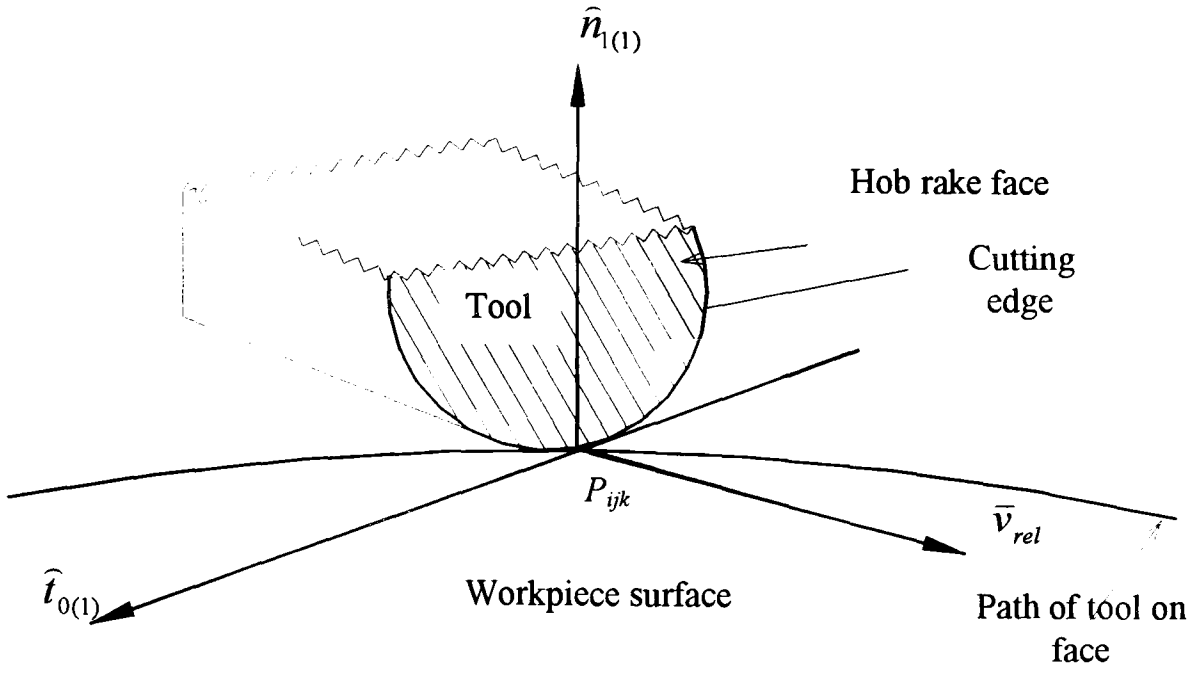

Figure 4.8 Normal and tangent at $P_{i,j,k}$

So far all the points and vectors are defined in the hob axis (6). To look at the gear teeth axis (1), it is necessary to transform all the position vectors, velocities, cutting edge tangents etc. to axis (1) in the gear, for each point *i,j,k* on the hob.

$$\left[\bar{r}_{0,i,j,k,}\right]_{(1)} = \left[T_{1,6}\right] \cdot \left[\bar{r}_{0,i,j,k}\right]_{(6)} \tag{4.33}$$

From (4.6, 4.15)

$$(\hat{t}_{0,i,j,k})_{(1)} = \left[R_{1,6}\right] \cdot \left[\hat{t}_{0,i,j,k}\right]_{(6)} \tag{4.34}$$

From (4.11 and 4.12) and (4.24)

$$\left[\bar{v}_{0,i,j,k}\right]_{(1)} = \left[R_{1,6}\right] \cdot \left[\bar{v}_{0,i,j,k}\right]_{(6)} \tag{4.35}$$

From (4.11 and 4.12) and (4.30) (or 4.30a 4.30b).

Note that $\left[\bar{r}\right]_{(1)}$ is the position of the point $P_{i,j,k,}$ on the cutting tooth in the gear axes (1), and is also the position of the corresponding point on the gear that is cutting. It is thus a point on the profile being cut at this instant (if cutting occurs at $P_{i,j,k}$).

The velocity of the point $P_{i,j,k,}$ on the gear at $\left[\bar{r}\right]_{(1)}$ is given by

$$\bar{v}_{1(1)} = \bar{w}_{(1)} \times \bar{r}_{(1)} \tag{4.36}$$

Where $\bar{w}_{(1)}$ is the, vector, angular velocity of the gear in system (1), which is a rotation about the $(OZ)_{(1)}$ axis so that

$$w_{(1)} = \begin{bmatrix} 0 \\ 0 \\ w \end{bmatrix}_{(1)} = w_0 \begin{bmatrix} 0 \\ 0 \\ \dfrac{1}{i_0} \end{bmatrix} \tag{4.37}$$

So that, from (4.25 and 4.26)

$$\bar{v}_{1(1)} = \begin{bmatrix} v_{1x} \\ v_{1y} \\ v_{1z} \end{bmatrix}_{(1)} = \frac{w_0}{i_0} \begin{bmatrix} -y_{(1)} \\ +x_{(1)} \\ 0 \end{bmatrix}_{(1)} \tag{4.38}$$

The relative velocity $\bar{v}_{rel}$ can then be calculated in system (1) using (4.35) and (4.38)

$$(\bar{v}_{rel})_{(1)} = \bar{v}_{0(1)} - \bar{v}_{1(1)} \tag{4.39}$$

The i,j,k notation can be dropped.

Using (4.32) (4.34) and (4.39) we can then calculate

$$\hat{n}_{1(1)} = \hat{t}_{0(1)} \times \left[\frac{\bar{v}_{rel}}{|v_{rel}|} \right]_{(1)} \tag{4.32a}$$

4.8.2 Cutting region

There is no point in looking at every point on every tooth on the hob, since only some points are able to intersect the gear blank, others do not reach the gear blank at all. The teeth which may cut can be determined as follows:

1- Calculate $\bar{r}_1$ for all $P_{i,j,k}$

2- Calculate the radius from the blank centre

$$R_{i,j,k} = \sqrt{x_{(1)}^{\ 2} + y_{(1)}^{\ 2}} \tag{4.40}$$

There no cutting if

$$R_{i,j,k} \geq r_a \tag{4.41a}$$

i.e. too far from workpiece axis to reach blank, where r_a is the tip radius of the gear blank, or

$$Z_{(1)}{}^2 \geq \frac{b^2}{4} \tag{4.41b}$$

i.e. above or below the end of the blank, where the origin of system (1) is at mid-face width. Where b is the gear face width.

4.9 CUTTING OUT SOLUTION

In this method, the surface generated in space by each hob tooth is first calculated, ignoring the problem of metal removal. The question of whether or not a particular hob tooth actually cuts at any particular point is then resolved separately, together with estimation of chip thickness, cutting forces, etc.. By comparing the different surfaces generated by successive hob teeth in a common co-ordinate system fixed in the gear, in this way, a picture of the actual instantaneous tooth shape is built up cut by cut, as the envelope of all previous cuts in each tooth space. With a single-start hob, each tooth space is cut out in about 3 hob rotations. This tooth profile then forms the starting profile for the next cut, one gear rotation later.

4.9.1 Tooth gash generated by one hob tooth

At any instant, defined by parameter m or corresponding hob angle $\phi_0(m)$, an arbitrary point $P_{i,j,k}$ on the hob may potentially cut a corresponding point on the tooth flank if either of equations (4.41a) or (4.41b) is satisfied. The co-ordinates of this point in the axes (1) fixed in the gear are given by (4.33), for each value of $\phi_0(m)$. Each point $P_{i,j,k}$ on tooth i,j will generate a succession of points, as it rotates through the potential cutting zone, on the tooth flank. All k points

($k_{\min} \le k \le +k_{\max}$) on it that are "active" according to 4.41a and 4.41b will generate trajectories in space, as shown in the figure 4.9, producing a grid of points on a surface, defined by m ($m=0 \ldots m_{max}$) positions of the cutting edges at each successive value of hob rotation angle $\phi_{0(t)} = \phi_{0(m)} = \phi_{0(0)} + m\Delta\phi_0$ *etc.* see figure 4.9.

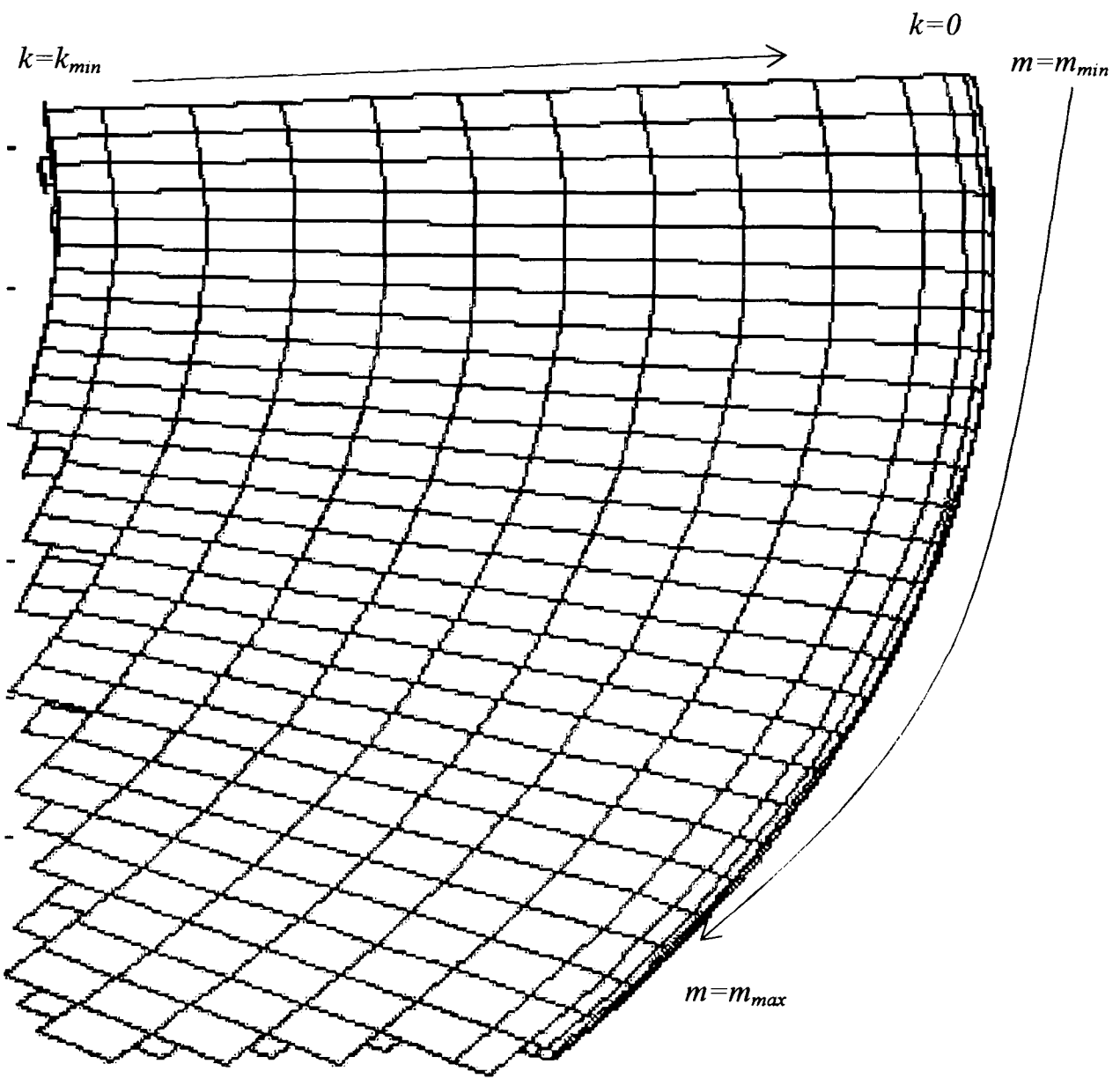

Figure4-9 Irregular curvilinear m,k grid in (x_1,z_1) plane

Note that surface points within and outside the blank boundary surface can all be calculated in the same way, and tested using (4.41a), (4.41b) to determine if there is any metal to cut. The surface generated does not "stop" at $r=r_a$ *or* $z=\pm b/2$.

The surface represented by the (m,k) grid of points can be approximated as closely as required by increasing the number of points (k_{max}) on each tooth and/or reducing $\Delta\phi_0$ (increasing m_{max}). However, although as fine a grid as required can be generated, the grid will not be uniformly spaced in the $(OXYZ)_{(1)}$ system of

axes, since none of the grid lines is oriented conveniently in this system, due to the relative screw motion of the hob and blank, and the hob setting angle η.

Much is nevertheless known about the geometry of the generated surface, since, at each potentially active point $P_{i,j,k}$ on each tooth *(i,j)*, the following are known

- Co-ordinate (position $\bar{r}_{1(1)}=(x_{mk}, y_{mk}, z_{mk})_{(1)}$ from (4.33)
- Surface normal $\hat{n}_{1(1)} = (n_{x(m,k)}, n_{y(m,k)}, n_{z(m,k)})_{(1)}$ from (4.32)
- The direction of the cutting edge $\hat{t}_{0(1)}$, which is a tangent to the surface at each point from (4.34)
- The cutting direction $\hat{v}_{rel(1)}$ from (4.39), which is also a tangent to the surface.

4.9.2 Superposition of gashes

The surfaces cut by each hob tooth can be superposed to create the generated tooth spaces. There is a problem, however, since the surfaces cut by successive teeth *i*. ($i_{min} \le i \le +i_{max}$) are all described by irregular *(m,k)* grids of points in axis (1),as in figure 4.9, but the grid points and grid lines for each tooth *i* all differ from each other.

It is thus necessary to transform each surface so that it can be represented by a different, common grid of points, regularly spaced in the $(OXYZ)_{(1)}$ system. Comparison of any two surfaces at corresponding grid points is then easy. A set of grid points capable of describing any 'partial' cut, of any depth, anywhere on the gear is needed. For a discussion of the alternative 'common' grids that could have been used for this purpose, see Appendix E. The one finally chosen was a rectangular x_1z_1 grid.

4.9.3 X_pZ_q Grid

Each surface is defined by the values of the y_{pq} on a regular grid of points $(x_p,z_q)_{(1)}$ where $(p=1... p_{max}, q=1..q_{max})$ in co-ordinate system (1) where

$$x_p = \frac{r_{a1}\sin(\frac{\pi}{z_1})(-1+2*p)}{p_{\max}-1}$$

$$y_{pq} = \sqrt{r_{a1}{}^2 - x_{pq}{}^2}$$

$$z_q = b(\frac{q-1}{q_{\max}-1} - 0.5)$$

where r_{a1} is the tip radius , z_1 is the number of teeth on gear and b is the face width. A comparison of any two surfaces to find where they intersect then merely requires comparison of the two values of y_{pq} at each point of the grid, see figure 4.10.

4.9.4 Interpolation- change of grid to *(x-z)*

The process of generating the surface produced by one cutting edge yields the co-ordinates in $[x_{(m,k)},y_{(m,k)},z_{(m,k)}]_{(1)}$ of each of the irregular grid points shown on figure 4-9. For each of these points, the position $\bar{r}_{m,k}$ is known (together with the surface normal $\hat{n}_{1(1)\,m,k}$).

To determine where cutting is actually occurs on a particular hob tooth, the surface it generates as it passes through the tooth space is compared with the surface representing the current tooth space (cut by previous teeth) mapped on a rectangular (x_p,z_q) grid. To facilitate this comparison, the MATLAB function 'griddata' was used to map the surface of figure 4.9, defined in the irregular (x_{mk},z_{mk}) grid, onto the common regular (x_p,z_q) grid.

The depth of cut can then be determined by comparing the y_{pq} values for the two surfaces. By checking a sufficient number of points (p,q) the depth of cut h_{pq} can be defined over the whole grid. Even negative values can be calculated, (the gap where there is no cut), so that subsequent interpolation is more reliable. If the

depth of cut is now plotted over the rectangular grid, a "surface" showing variation of h_{pq} over the grid is obtained, figure 6.8 shows an example.

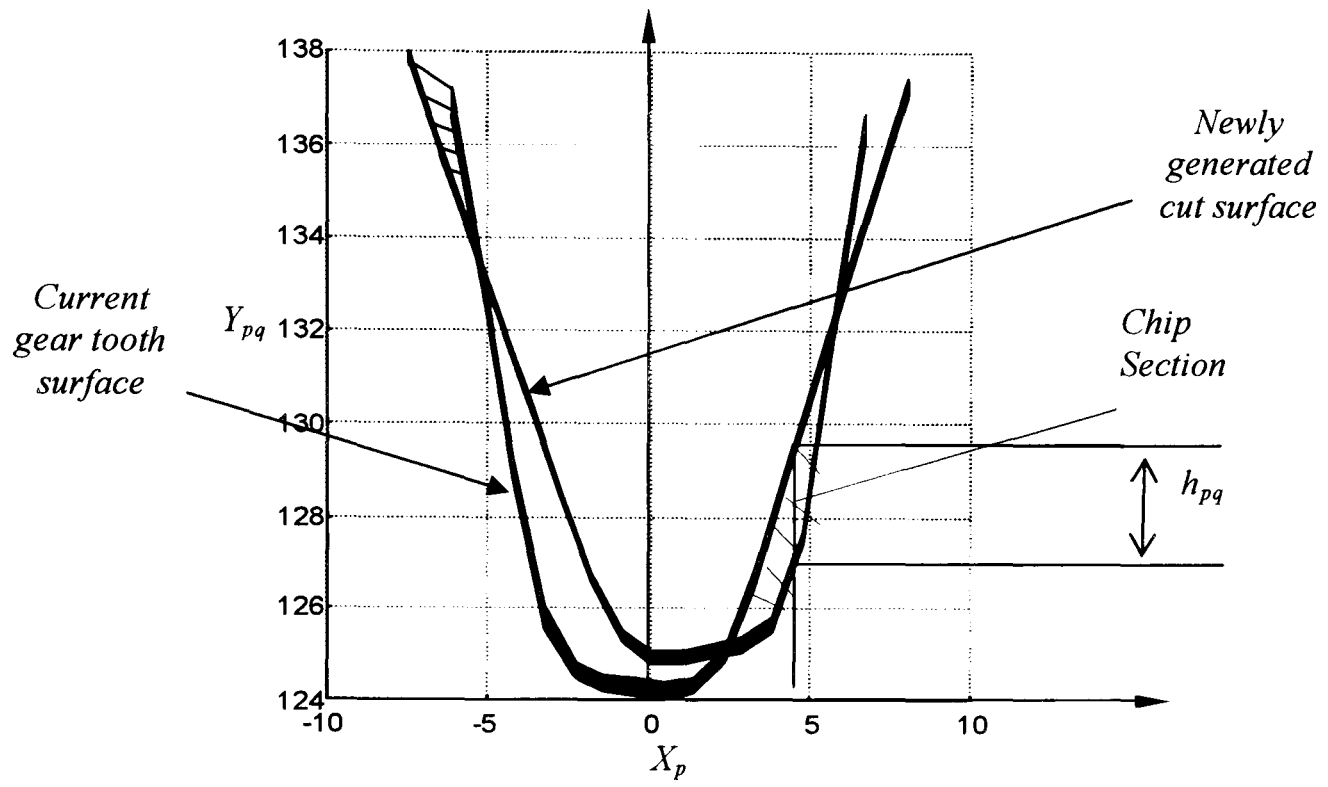

Figure 4.10 Surface generated by one hob tooth in a tooth space (equal increments of hob rotation)

Using the same (B-spline) interpolation procedure, the values of $h_{m,k}$ at each of the points $P_{m,k}$ of the original (irregular) grid can now be calculated, for each cutter tooth (i,j) at time instant m. These are derived by again using the 'griddata' function to map the values of $h_{pq}=h(x_p,z_q)$ onto the original rectangular (m,k) grid to give $h_{mk}=h(m,k)$.

Each value of m gives corresponding instantaneous values of $h(m,k)$ for each point k on the cutting edges. Since the index k corresponds to a particular point on each hob tooth, the total amount of cutting done by each part of each cutting edge can be summed (over the m time intervals of cutting action separately for each k). This allows estimation of the total cutting work at each point of each hob tooth, so providing a basis for estimating the hob wear distribution.

By summing the cutting forces at each point $P_{i,j,k}$ on the hob at the instant defined by m, the total cutting force on each tooth, and hence the hob torque and the total cutting force (summed over all teeth cutting at that time) can also be determined.

To calculate the cutting forces, the normal chip thickness $h_n(m,k)$ at each point is required. This can be calculated from the values of h_{mk} giving

$$h_{nmk} = \bar{h}_{mk\,(1)} \bullet \hat{n}_{1\,(1)} \tag{4.42}$$

where

$$\bar{h}_{mk\,(1)} = \begin{bmatrix} 0 \\ h_{mk} \\ 0 \end{bmatrix}$$

4.10 CUTTING FORCES

Each element of each cutting edge for which $h_{nmk} \geq 0$ will generate an element of cutting force $\bar{F}_{cmk}$ at time instant m (defined by ϕ_0) and whose magnitude is given by

$$\left|\bar{F}_{c(m,k)}\right| = l_k \cdot h_{m,k(av)} \cdot K_c \tag{4.43}$$

where l_k is the length of the k_{th} element of cutting edge given by

$$l_k = \sqrt{(x_k - x_{k-1})^2_{(1)} + (y_k - y_{k-1})^2_{(1)}} \tag{4.44}$$

Values of l_k can be pre-calculated, and are the same for all teeth

$$h_{mk(av)} = \frac{1}{2}(h_{nm,k} + h_{nm,(k-1)}) \tag{4.45}$$

K_c is the specific cutting force which, depends on the cutting tooth and workpiece materials, cutting speed $|v_c|$, rake angle ε_k, side rake angle β_k, etc. and can be derived empirically (from cutting data) using curve fits of the form [Bruins]

$$K_c = K_{c1,1}(\frac{h_k}{1})^{n_h} \bullet (\frac{v_c}{100})^{n_v} \bullet f(\beta_k, \varepsilon_k) \tag{4.46}$$

The force $\overline{F}_{cmk}$ acts in the cutting direction (on the work piece, parallel to $\bar{v}_c = \bar{v}_{rel}$)

The other main component of the cutting force acts normal to the workpiece surface and the cutting edge (i.e. along $\hat{n}_1$) this can also be estimated, using empirical data to give (4.43)

$$\left|\overline{F}_{n(m,k)}\right| = l_k \cdot h_{mk(av)} \cdot K_n \tag{4.47}$$

where

$$K_n = K_{n,1,1} \cdot (\frac{h_{kav}}{1})^{n'_h} \cdot (\frac{v_{ck}}{100})^{n'_v} \cdot f'(\beta_k, \varepsilon_k) \tag{4.48}$$

n'_h, n'_v etc. are empirical constants, and $K_{n,1,1}$ is a material parameter.

4.10.1 Resultant forces and moments on hob

At a particular instant, defined by hob rotation angle $(\phi_0)_m$, the resultant force caused by each cutting edge (i,j) is obtained by adding the relevant force components vectorially.

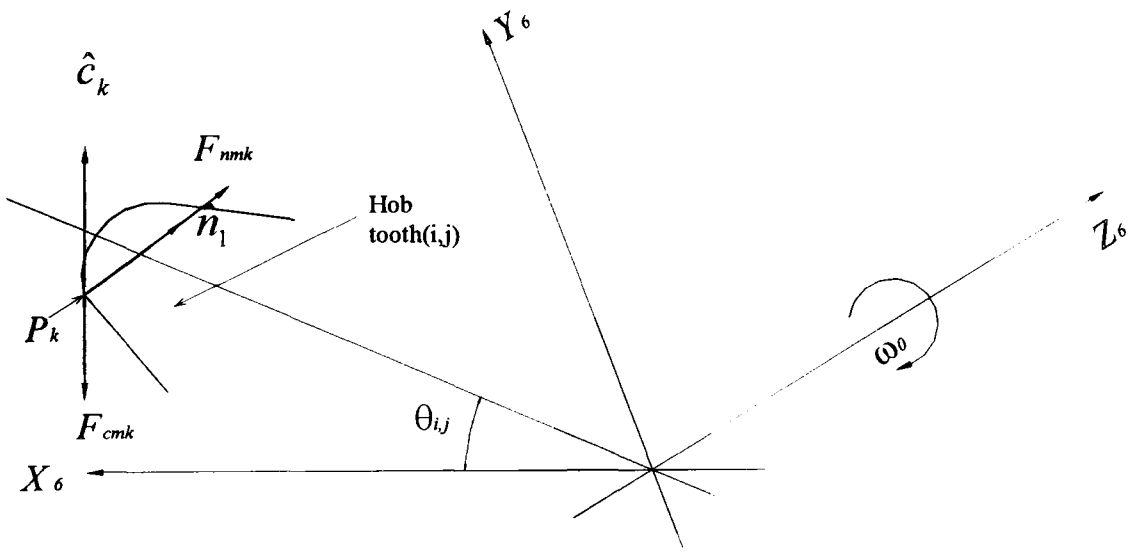

Figure 4.11 Forces acting on the hob at point P_k

The cutting directions at P_k and P_{k-1} are defined by the unit vectors ($\hat{c}_k$ and $\hat{c}_{k-1}$) parallel to $\bar{v}_{rel,k}$, see figure 4.8, and the surface normals by unit vectors $\hat{n}_{1,k}$ and $\hat{n}_{1,k-1}$. These are known: The mean cutting direction and surface normal for the element l_k at the cutting edge can be taken as parallel to

$$\bar{c}_{av.k(6)} = \frac{1}{2}(\hat{c}_k + \hat{c}_{k-1})_{(6)}$$
$$\bar{n}_{1av.k(6)} = \frac{1}{2}(\hat{n}_{1,k} + \hat{n}_{1,k-1})_{(6)} \qquad (4.49)$$

with $\hat{c}_{av,k}$ and $\hat{n}_{1av,k}$ the corresponding unit vectors ($\hat{c}_{av.k} = \frac{\hat{c}_{av.k}}{|c_{av.k}|}$) etc.

The cutting and thrust force can thus be represented as vectors in system (6)

$$\bar{F}_{c,k(6)} = F_{c.k} \cdot \hat{c}_{av.k(6)}$$
$$\bar{F}_{n,k(6)} = F_{n.k} \cdot n_{1av.k(6)} \qquad (4.50)$$

The resultant force on the hob is obtained by summing all the force components over k (to give forces $\bar{F}_{res,i,j,m}$) on each tooth *i,j* at $(\phi_0)_m$, and the over *i,j* to give the total instantaneous forces on the hob.

$$\bar{F}_{res,i,j,m(6)} = \sum_{k=k_{\min}}^{k_{\max}} (\bar{F}_{c,k(i,j)} + \bar{F}_{n,k,(i,j)})_{(6)} \qquad (4.51)$$

and

$$F_{tot.m(6)} = \sum_{j=1}^{z_0} \sum_{i=i_{\min}}^{i_{\max}} F_{res.i,j,m(6)} \qquad (4.52)$$

Clearly the summations need only to include those teeth *i,j* which are capable of cutting (eq. (4.10a) , (4.10b)).

The hob torque is calculated by summing the individual torques from each active element. The mean position vector at which the forces act is

$$\bar{r}_{av.k(6)} = \left[R_{6,1}\right] \cdot r_{av.k.(1)} \qquad (4.53)$$

where

$$\bar{r}_{av.k_{(1)}} = \frac{1}{2}(\bar{r}_{k_{(1)}} + \bar{r}_{k-1}) \qquad (4.54)$$

So that the element hob moment due to forces on segment *i,j,k* of the hob at time *m* is from (4.50)

$$\bar{M}_{0.ijmk(6)} = r_{av.k(6)} \times \left[F_{cijmk(6)} + F_{nijmk(6)}\right] \qquad (4.55)$$

the total moment on the hob is then

$$M_{0.tot.m(6)} = \sum_{i=-n_i}^{n_i} \sum_{j=1}^{Z_0} \sum_{k=-n_k}^{n_k} M_{0.ijmk(6)} \tag{4.56}$$

The hob torque is the (Z_6) component of $M_{0.tot.(6)}$.

4.10.2 Gear loading

The forces $F_{tot.m(6)}$ on the hob shaft give rise to corresponding reaction forces on the gear. A torque is also generated which can be calculated by summing the contributions from the individual force components $\overline{F}_{c.i,j,m,k}$ and $\overline{F}_{n,i,j,m,k}$ acting at the mid point of element l_k . In the gear axis system, the resultant torque due to these forces is

$$\overline{M}_{1,i,j,m,k_{(1)}} = \bar{r}_{av.k_{(1)}} \times (\overline{F}_{c,k_{(1)}} + \overline{F}_{n,k_{(1)}}) \tag{4.57}$$

The total torque on the gear is then

$$\overline{M}_{1,(m),(1)} = \sum_{i=-n_i}^{n_i} \sum_{j=1}^{Z_0} \sum_{k=-n_k}^{n_k} M_{1,i,j,m,k(1)} \tag{4.58}$$

The torque on the worktable is the 3rd $(Z_{(1)})$ component of $M_{1m(1)}$.

For component with measured values it is best to transform $F_{tot.m(1)}$ and $M_{1m(1)}$ into the "fixed" (non-rotating) axis system (2) to give

$$\begin{aligned} \overline{F}_{tot.m(2)} &= [R_{2,1}] \cdot \overline{F}_{tot,m(1)} \\ M_{1.m(2)} &= [R_{2,1}] \cdot M_{1.m(1)} \end{aligned} \tag{4.59}$$

4.10.3 Cutting in adjacent tooth spaces

Since cutting in a single tooth space extends over nearly three hob revolutions, during which the gear rotates through nearly three tooth pitches, see figure 4.17, it follows that at any time *m*, the hob may actually be cutting in up to three tooth spaces simultaneously. To find the total cutting force at time *m*, when cutting in a particular tooth space z, it is then necessary to add any forces generated at the

same time by hob teeth cutting in the adjacent (preceding or following) tooth space *(z+1)* and *(z-1)*. Investigation of these forces (in the adjacent tooth spaces, (z+1), (z-1), considered separately) showed that they followed almost exactly the same pattern as the forces in the central tooth z. (figure 4.17), but shifted (along the m axis) by $\pm m_{step}$ (equivalent of ±1 hob revolution).this is not surprising, since the axial feed rate is, in practice, very slow. It was thus, unnecessary to calculate these forces, since

$$F_{(z+1)}(m) \approx F_z(m - m_{step})$$

$$F_{(z-1)}(m) \approx F_z(m + m_{step})$$

so

$$F_{res}(m) \approx F_z(m) + F_{(z-1)}(m) + F_{(z+1)}(m)$$

or

$$F_{res}(m) \approx F_z(m) + F_z(m + m_{step}) + F_z(m - m_{step}) \qquad (4.60)$$

This equation is valid provided no cutting occurs in teeth (z±2), (z±3) etc. i.e. only over the central region of cut for tooth z. However, the resultant waveform is, in view of 4.60, periodic, so only one hob revolution need to be calculated, see figure 4.18.

4.11 MATLAB MODEL

The following section describes the development of the MATLAB model, used to predict the cutting forces in the hobbing process. It is hoped this will help to explain the unique nature of the complicated cutting process, and will also provide an understanding of how the many parameters affect the process and the cutting forces, before evaluating these changes experimentally.

It was decided to use MATLAB 5.0 to model the hobbing process. This software was chosen for its powerful ability of dealing with matrices, especially multi-dimensional arrays. Having developed the theory, the program was built to predict cutting forces in both a single tooth and full gear. The program consists of 4 main parts. The main program which calculates the instantaneous chip thickness, one routine which calculates the chip length along the flank, a second

routine which calculates the cutting forces acting on a single tooth, and a third routine which is used to calculate the cutting forces acting on a full gear.

To calculate the instantaneous chip thickness, many approaches were considered, but only three approaches were evaluated, of which one approach was finally chosen for this project. The other two approaches were rejected since they did not produce adequate results, either because the approach was not suitable for the process or due to programming difficulties.

The chosen method, as explained in section 4.9.3, computes the chip thickness by comparing the current surface of a tooth space with the surface produced by each passing hob tooth. The tooth-space surface is only updated when $h_{pq} > 0$, indicating that there was 'metal' removed.

The main program facilitates the input of basic gear and machining data, such as, module number, hob diameter, blank diameter, face width, hob speed, and axial feed rate, etc. Other gear parameters are subsequently calculated, such as depth of cut, index ratio, addendum, dedendum, chamfer depth, base radius, hob lead, etc. Additional programming parameters are also entered such the number of gear revolutions required to run the program, number of points along the hob tooth flank, and number of teeth on the hob.

The program is designed to run in five loops. The main loop controls the number of gear revolutions, whilst the second loop varies j, the number of the hob start. The third loop varies i, the number of the hob tooth, and the fourth loop is for the hob rotation increments $\Delta\phi_0$. The last inner loop is for the number of points on a hob tooth flank.

The first loop is usually calculated to cover the full operation from beginning to end, which depends upon the feed rate and the face width as well as the hob diameter. Cutting usually ends when the hob centre line coincides with the gear centre line. One revolution is added on top before cutting and another is added at the end as an extra precaution.

The second loop increments j from 1 to z_0, dealing with the number of starts of the hob, even though only a single start hob was eventually tested. Including this flexibility makes the model more general. The third loop increments i and deals with the number of teeth on hob. This is user defined, although a realistic number must be used. Within this loop the angle between the hob teeth is calculated as well the hob lead. The fourth loop increments the time parameter m through the cutting zone for each tooth. In this loop the incremental hob rotation angle ($\Delta\phi_0$) as well as the gear rotation angle ($\Delta\phi_1$) are calculated. Additionally the transformations for most of the co-ordinate systems are calculated. Some transformations or translations do not need to be calculated for every position of the hob as they depend on constants or parameters, such as the hob setting angle η, that are neither time nor position dependant. The last loop increments the number k of the point on the flank. The limits k_{min} and k_{max} are user defined as well the limits m_{min} and m_{max} in the previous loop. The higher this number is, the more accurate the output will be, but this has to be a compromise, since the calculation time increases rapidly with m_{max} and k_{max}.

Figure 4.12 shows a sample code for calculating the rack profile, at any time *(m)* and revolution of the table for tooth *(i)*.

```
for k = 1:k_max
   if abs(z(k)) <= za1
      rk = ra0;
   elseif abs(z(k)) <= za2
      rk = ro + ha1 + sqrt(rho_a0.^2 - (abs(z(k)) - za1).^2);
   elseif abs(z(k)) <= za3
      rk = ro -  (abs(z(k)) -(pi*mn/4))/tan(alphan);
   elseif abs(z(k)) <= za4
      rk = ro - ( za3 - pi*mn/4)/tan(alphan) - (abs(z(k))-
      za3)/tan(alphacf);
   else
      rk = ro - hfo;
   end
end
```

Figure 4.12 Sample code for calculating the rack profile.

The output of the sample code in figure 4.12 yields the radius of the rack profile at P_k, Note that, in the program, $k_{min}=1$ and the values of z(k) are pre-calculated, since the P_k are simply uniformly spaced over the hob axial pitch. In order to

obtain the co-ordinate axis of a point on the tooth, the rack profile is then transformed to $(OXYZ)_{(6)}$ co-ordinate axis, as explained in section 4.4.4. Note that the suffix (6) denotes the hob axes, in co-ordinate system (6), but the position of interest is in relation to the gear blank tooth space. The transformations and translations of these points from co-ordinate system (6) to co-ordinate system (1) is required, as discussed in section 4.3, by applying equations, 4.1- 4.7. Since not all points on hob intersect the gear, or pass through the cutting zone, each point needs to be tested against the boundaries of the possible cutting zone. Subsequently, only points of interest (that potentially cut), are stored and used to produce the surface of the generated gash, as shown in the code of figure 4.13.

```
delta_r=0.75*ra0*Nstep_rad;
delta_z=0.75/tan(alphan);
if (Z1^2 < (b/2 + delta_z)^2  & R1 < (ra1+delta_r))
   xcmk(m,k) = X1;
   ycmk(m,k) = Y1;
   zcmk(m,k) = Z1;
   mmk(m,k)  = m+ dmi(rev,i);
   kmk(m,k)  = k;
else
   xcmk(m,k) = inf;
   ycmk(m,k) = inf;
   zcmk(m,k) = inf;
   mmk(m,k)  = inf;
   kmk(m,k)  = inf;
end
```

Figure 4.13 Sample code for calculating the generated surface.

Note that b is the face width and $R_1 = \sqrt{x_1^2 + y_1^2}$ as explained in section 4.8.2, equation 4.40.The increments Δr and Δz extend the calculated generated profile a small distance beyond the actual boundaries of the blank. This was found necessary to allow reliable interpolation of the *mk* grid points (figure 4.9) by MATLAB 'GRIDDATA' at the edges of the cut. If Δr and Δz were too small (or omitted altogether), 'GRIDDATA' produced spurious interpolation 'spikes' in this region (see figure 6.3).

All points on all teeth of the hob that pass through the cutting region are now known and generate a surface on the original curvilinear *mk* grid, figure 4.9. This surface needs to be interpolated using the GRIDDATA function onto a regular *pq*

grid which was initialised at the beginning of the program. Figure 4.14 shows sample code for calling the interpolation function and comparing the current surface yz_{pq} and the surface produced by the passing gash y_{pq}. The difference is the depth of cut h_{pq}, and if there is a positive depth of cut the current profile is then updated.

```
y1pq=griddata(xcmk,zcmk,ycmk,xpq,zpq,'cubic');
m1pq=griddata(xcmk,zcmk,mmk,xpq,zpq,'cubic');
k1pq=griddata(xcmk,zcmk,kmk,xpq,zpq,'cubic');
for p=1:p_max
   for q=1:q_max
      hpq(rev,i,j,p,q) = yzpq(p,q) - y2pq(rev,i,j,p,q);
      if hpq(rev,i,j,p,q) < -1
         hpq(rev,i,j,p,q) = -1;
      end
      if hpq(rev,i,j,p,q) > 0
         yzpq(p,q) = y2pq(rev,i,j,p,q);
      end
   end
end
```

Figure: 4.14 Sample code for the interpolation onto a rectangular pq grid (showing a linear interpolation by 'griddata').

The second routine is used to calculate the mean distance between the points on the flank, as shown in the sample lines below

```
lk1=0.5*sqrt((rk(k)-rk(k-1))^2+(z6(i_ref,k)-z6(i_ref,k-1))^2);
lk2=0.5*sqrt((rk(k+1)-rk(k))^2+(z6(i_ref,k+1)-z6(i_ref,k))^2);
lkt(k)=lk1+lk2;
```

The third routine calculates the forces acting on the gear space. Having produced the instantaneous chip thickness in the rectangular *pq* grid, this has to be to interpolated again onto the original *mk* grid, and only the positive values of the chip thickness considered. Negative values are also calculated, however, restricted to -1, to allow accurate and reliable interpolation near the edge of the cut (where $h_{pq} \approx 0$). The normal chip thickness can be calculated using equation 4.42. Tangents and Normals to every single point are calculated using equations 4.24a and 4.32, respectively. The relative velocity between the gear and the hob is calculated as this will give the basis to estimate the instantaneous forces acting on the gear using equations 4.43 and 4.47. The resultant force is then calculated

using equations 4.51 & 4.52, as described in section 4.10.1. Figure 4.15 show a sample code to calculate the cutting forces.

```
Fc(m1,k1) = 850*lkt(k1)*hn_mk(m1,k1)^0.8;
Fmk = Fc(m1,k1) * (v_rel3(m1,k1,:) - 0.65*normal1a(m1,k1,:));
Fmk1(m1,k1,:)=Fmk;
if Fmk1(m1,k1,3) ~= 0
   Fmk3(m1,k1,1) = Fmk1(m1,k1,1);
   Fmk3(m1,k1,2) = Fmk1(m1,k1,2);
   Fmk3(m1,k1,3) = Fmk1(m1,k1,3);
else
   Fmk3(m1,k1,1) = 0;
   Fmk3(m1,k1,2) = 0;
   Fmk3(m1,k1,3) = 0;
end
F_res(m1+dm,1) = F_res(m1+dm,1)+ Fmk3(m1,k1,1);
F_res(m1+dm,2) = F_res(m1+dm,2)+ Fmk3(m1,k1,2);
F_res(m1+dm,3) = F_res(m1+dm,3)+ Fmk3(m1,k1,3);
t21a=t21(2:4,2:4);
F_res2=F_res(m1+dm,:)*t21a;
F_res3(m1+dm,:) = F_res2;
```

Figure 4.15 Sample code for calculating the cutting forces on a single tooth.

Line 2 of figure 4.15 is derived from equation 4.50, by assuming, in the absence of more detailed data of $K_{n1,1}, n'_h, n'_v$ etc for equation 4.48, that

$$K_n \approx K_{nc} \cdot K_c$$

with a typical value of $K_{nc} \approx 0.65$. [Kalpakjian]

Thus the cutting force on element k is (from equation 4.51) becomes

$$F_k = \left|F_{c,k}\right| \cdot (\hat{c}_{avk} + K_{nc} \cdot \hat{n}_{avk})$$

Since, $\left|v_c\right| \approx 36m/\min$ for the gears tested, the term $(\frac{v_c}{100})^{nv}$ in equation 4.46 becomes $0.36^{0.3} \approx 0.736$. For the gear steel tested $K_{c1,1} \times 0.736 = 850$ [Bruins].

Note that the forces are then transformed into co-ordinate system (2) which is fixed in space, for easier comparison.

Up until this point the forces acting on a single tooth space have been calculated. In order to calculate the forces acting on a full gear, further code is required which numerically sums these forces acting on a single tooth space at any instant

in time. Figure 4.16 illustrates sample code for the calculation of the forces acting on a full gear, according to equation 4.60, section 4.10.3.

```
for m=m_0:inc:m_0+m_step-1;
   F0(m,1) = F_res3(m,1) +F_res3(m+m_step,1)+F_res3(m-m_step,1);
   F0(m,2) = F_res3(m,2) +F_res3(m+m_step,2)+F_res3(m-m_step,2);
   F0(m,3) = F_res3(m,3) +F_res3(m+m_step,3)+F_res3(m-m_step,3);

end

nn=8;

for nm=1:nn
   for m=m_0:inc:m_0+m_step
      F0(m+nm*m_step,1) = F0(m,1);
      F0(m+nm*m_step,2) = F0(m,2);
      F0(m+nm*m_step,3) = F0(m,3);
   end
end
```

Figure 4.16 Sample code to calculate the forces on a full gear.

Note that the first part of the code adds (or subtracts) the forces acting on a single tooth space which act at time *m*, to form those occurring at the same time on the preceding and following hob teeth. The results are shown in figure 4.18.

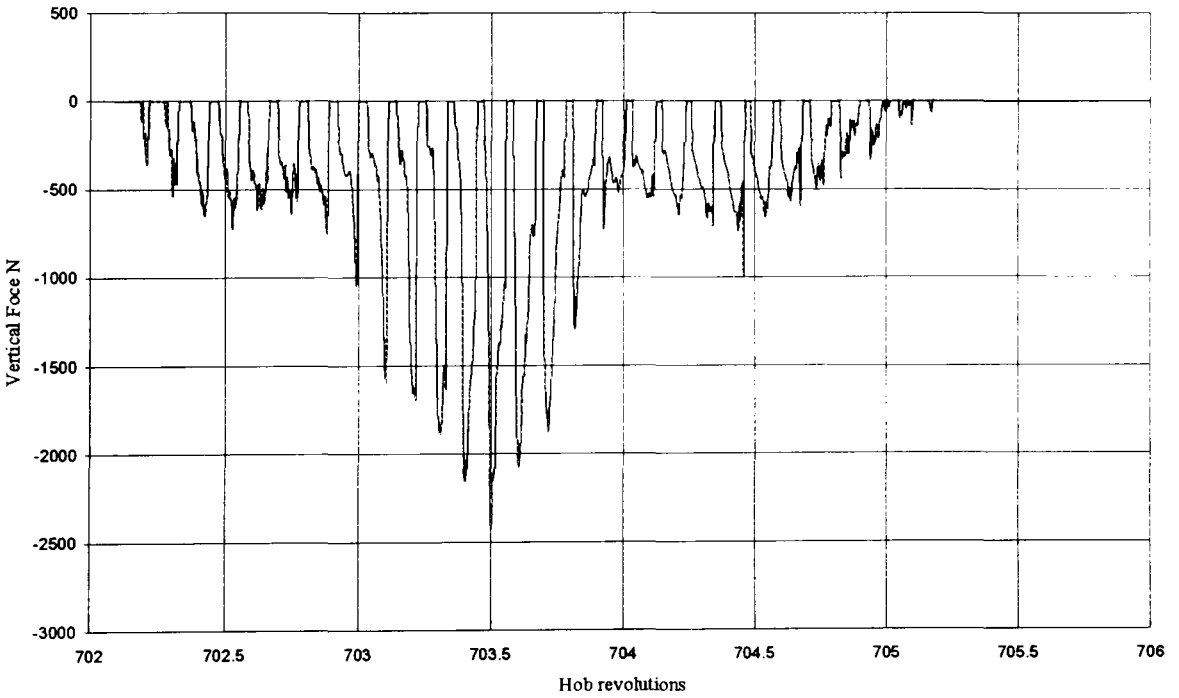

Figure 4.17 Vertical cutting forces for a single tooth space (mid face)

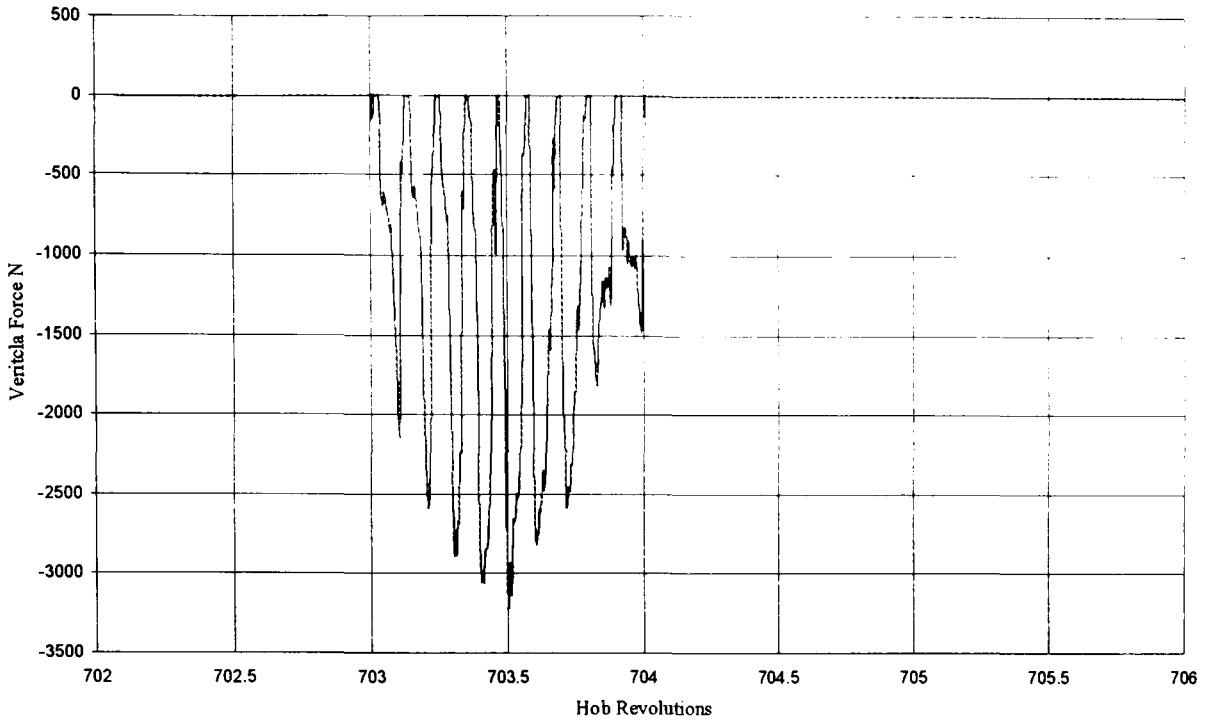

Figure 4.18 Vertical cutting force for a full gear tooth (mid face)

4.12 SUMMARY

The kinematical sub-systems of the hobbing process were described using 6 co-ordinate systems and the inter-relationship between these sub-systems was established. A rack profile in the normal and the axial sections was proposed, and a tooth numbering technique used to generate the full hob, and tangents and velocities of each single point on the hob were calculated. The cutting region was established to include only points on the tooth that intersect with the specified gear tooth space. By knowing every single point on each tooth, a 'cutting-out solution' was proposed by establishing the tooth space surfaces generated by every passing gash on their original curvilinear *mk* grid. Then by interpolating them onto a rectangular *pq* grid to compare the difference between the current tooth space surface and the one which is produced by each successive hob tooth, the difference will result in the instantaneous chip thickness. This was then re-mapped onto its original *mk* grid, allowing the normal chip thickness to be calculated. The cutting action generates two main forces: one acting in the cutting direction (on the workpiece); and another which acts normal to the cutting direction. By resolving the components of these two main forces the resultant cutting force acting on each tooth at any instant *m* gives the instantaneous cutting forces.

CHAPTER FIVE

MACHINE DESCRIPTION

5.1 INTRODUCTION

The Churchill PH 1612 universal gear hobbing machine was originally a conventional mechanical transmission machine, as shown in Figure 5.1. The machine was driven by a single main motor, with all motions of the machine, such as rotation of the hob and worktable achieved by using mechanical change gears and corresponding index ratios. In the late 70's Cranfield Institute of Technology developed the machine as a prototype CNC hobber by replacing the mechanical transmission by a new form of transmission, based on the new technology of a 'gearless' transmission, now referred to as an electronic gearbox. Separate DC motors were added to drive the worktable and the vertical axis, which carries the hob head. Feedback encoders were attached to the hob head, vertical drive and the wormshaft. The main AC motor was retained to drive the hob at a synchronous fixed speed. Circuit boards were designed to process the signals from the encoders as well as sending signals to both DC motor amplifiers. Cranfield adopted the use of their MIPROC microcomputer to carry out the closed loop velocity control and all mathematical calculations necessary to generate a gear. Limit switches were also used either as a safety cut out or basically as signal switches. Unfortunately, this system failed to work effectively, and could never have been a practical CNC hobber drive anyway. Since it was only a phased-locked loop velocity control system with no absolute position feedback. This meant it was impossible, for example, to restart the machine to continue hobbing after it had been stopped (e.g. to check tooth size) after the roughing cut, since the position of the teeth had been 'lost'. The machine

could not, either have been used to finish-hob hardened gears previously cut on another machine.

In carrying out this present research, the MIPROC computer was removed and replaced by a state of the art programmable multi axis controller (PMAC), which is able to control up to 8 axes. The same DC motors and encoders were utilised along with the signal conditioning circuit boards, as convenient for the inputs and outputs for PMAC. A prototype 3-axis force dynamometer was also incorporated to facilitate measurement of the cutting forces during the hobbing process.

5.2 HISTORICAL DEVELOPMENT OF CRANFIELD NC CONCEPT

5.2.1 Operating principle of the Churchill PH1612 hobbing machine

The Churchill PH 1612 hobbing machine is a typical hobbing machine, with a mechanical transmission and one main motor, which provides motion to all the machine axes. Figure 5.1 illustrates the mechanical transmission train of the hob, vertical slide and the worktable. The green dotted lines show the hob transmission, the red dotted lines show the vertical slide transmission, and the blue dotted lines show the worktable transmission. The hob shift arrangement, including the flywheel, are added to minimise the effect on the intermittent cutting action of the hobbing process. The main drive motor is a single speed 3-phase AC 7.5 hp motor. Different speeds can be achieved through a pulley belt. A tacho-generator is used to display the speed on an indicator mounted on the panel.

Index gears were used to change the index ratio between the worktable and the hob, and are located in the back of the machine. The mechanical drive to the worktable is via a single worm-wheel, and suits both right hand and left hand hobs, achieved by an extra gear in the indexing arrangement. The arrangement is also suitable for both climb cutting and conventional hobbing. A special nut is added for this operation. The feed rate could be changed during cutting, and was applied using an optional vari-feed system.

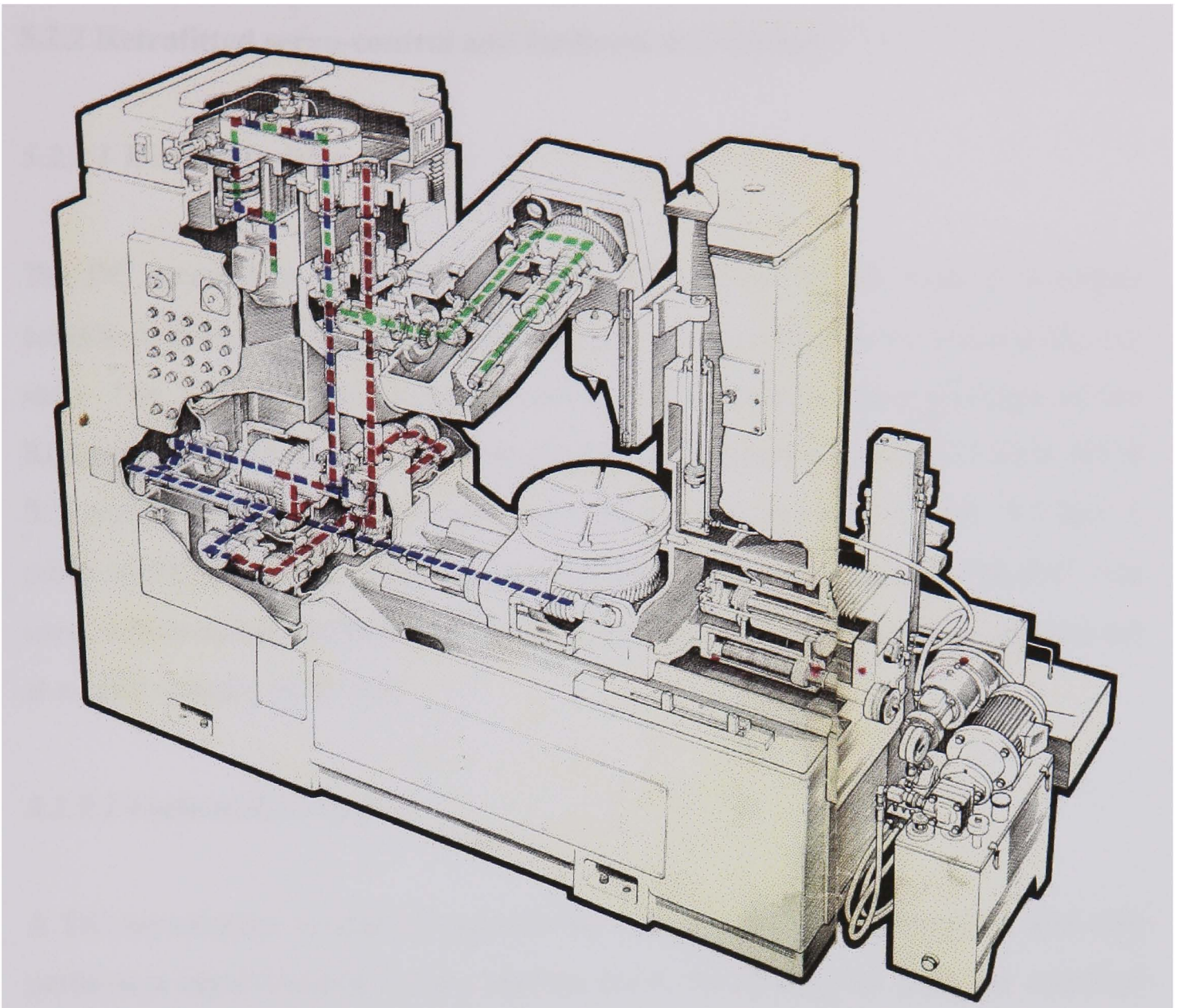

Figure 5.1: The conventional Churchill hobbing machine

Hydraulically powered movements are used to control the worktable slide feed, tailstock vertical motion, and hob shift. The worktable dead stop is controlled by two cylinders and adjusted by rotating a square ended shaft, to adjust the desired depth of cut for both rough and fine cuts. Electrically operated servo-valves are used to control the operation of the cylinders. An electric pump supplies the coolant oil to the hob head whilst cutting, and the swarf is collected and removed by an Archimedian Screw type conveyor which carries the chips from the work area to a collection box via a magnetic conveyor.

The electrical control gear cabinet is mounted on the machine rear and has the entire contactor switchgear and machine control relays. A push button panel is located in the front of the machine.

5.2.2 Retrofitted servo-control and feedback at Cranfield

5.2.2.1 Worktable drive system

The DC servomotor and drives were selected to cover the full range of operating conditions from one extreme of the high ratio worm to the other extreme of the low ratio. The TT5306B motor manufactured by the Inland Motor Division of the Kollmorgen was used to drive the worktable, with a peak torque of 111 N.M. (82 ft lb.), maximum speed of 2400 rpm and a horsepower rating of 4.1 kW (5.5 hp). A pulse width modulated amplifier manufactured by General Electric "HI-AK" was used, which makes available current up to 167-amp peak or 85 ampere (continuous) at a rated voltage. of 85 volt.

5.2.2.2 Vertical drive system

A DC servomotor is used to control the vertical feed of the machine, and also perform a rapid traverse of the vertical drive. In its original form the machine feed was driven by a main motor via screw and change gears, whilst the traverse was performed by a separate electric motor. The servomotor is controlled by a thyristor-controlled amplifier, rated at 2.2 kW (3 hp). The motor used is an Inland Motor Type TT5301A, which has a maximum speed of 2000 rpm and a continuous torque rating of greater than 27 N.M. (20 lb. ft). The matching controller type to drive the motor is TPAR 3340.

5.2.2.3 Hob and wormshaft encoders

The hob encoders and the wormshaft encoders have the same disc design, which consists of 250 holes and four reading heads, reference detectors, which contain photodiodes connected to dc pre-amplifiers. For a reference mark signal an opto-interrupter was used. The head signal processing circuit generates an edge at a point where a hole crosses the centre of the photo-detector; the edge is rising for anticlockwise rotation and falling for clockwise rotation. The four detectors are divided into two groups the (top and bottom, left and right), and processed to

produce the phase and the quadrant signal, which are 90° out of phase from each other.

5.2.2.4 Vertical encoders

The vertical encoder consists of a 35.56-cm (14-inch) etched stainless steel tape and a reading head, supplied with pre-amplifier, manufactured by Ferranti Ltd. The encoder is mounted adjacent to the hob head and has a line spacing of 0.02 mm. A moiré fringe reading head supplies phase and quadrature signal to a phase division module where the resolution is multiplied by 5.

5.2.2.5 Worktable encoders

The table encoder is a conventional glass grating with a resolution of 9000 lines/rev. It is mounted on a collar extending downwards from the underside of the worktable. This assembly was not used and it was only a back up for the wormshaft assembly. The only part, which is used, is the reference detector.

5.2.3 MIPROC controller

The MIPROC controller was developed by Cranfield, and adapted for the electronic gearbox, based on a phase locked loop. The MIPROC replaced the batch counters and the pulse phase comparator, i.e. all the calculations were carried out by the microprocessor. The real-time algorithm runs at a loop-frequency of 600 Hz, and was configured to support 8 interrupts, each with a separate priority, separate vector, and mask. Each interrupt was connected to a different source, i.e. power failure, hob encoder pulse, wormshaft encoder pulse, clock, hand-wheel pulse, vertical grating pulse and 2 spares. The functions of the interrupt handler are to save and restore all working registers, modify, save and restore interrupt mask states, support nested interrupts (interruption of an interrupt service routine), and prevent an interrupt interrupting itself.

The microprocessor also has six 16-bit I/O channels. The output channels were used to control the velocity feed forward, the position error and the vertical velocity demand as well as for ancillary functions such as operating the hydraulics and system control. The input channels provided inputs for the encoders and grating on the hob, wormshaft and vertical axis, and other discrete input functions such limit switches and system monitoring.

Because of the phase-locked loop system, used to control the table and hob motions, synchronised rotation can only occur when they are both rotating. When there is no rotation, there is no signal to detect the phase at, so synchronisation is lost, with the practical consequences already explained.

5.3 RE-ENGINEERED CNC HOBBING MACHINE AT NEWCASTLE

Figure 5.2 shows the Churchill CNC hobbing machine, as further developed at Newcastle University.

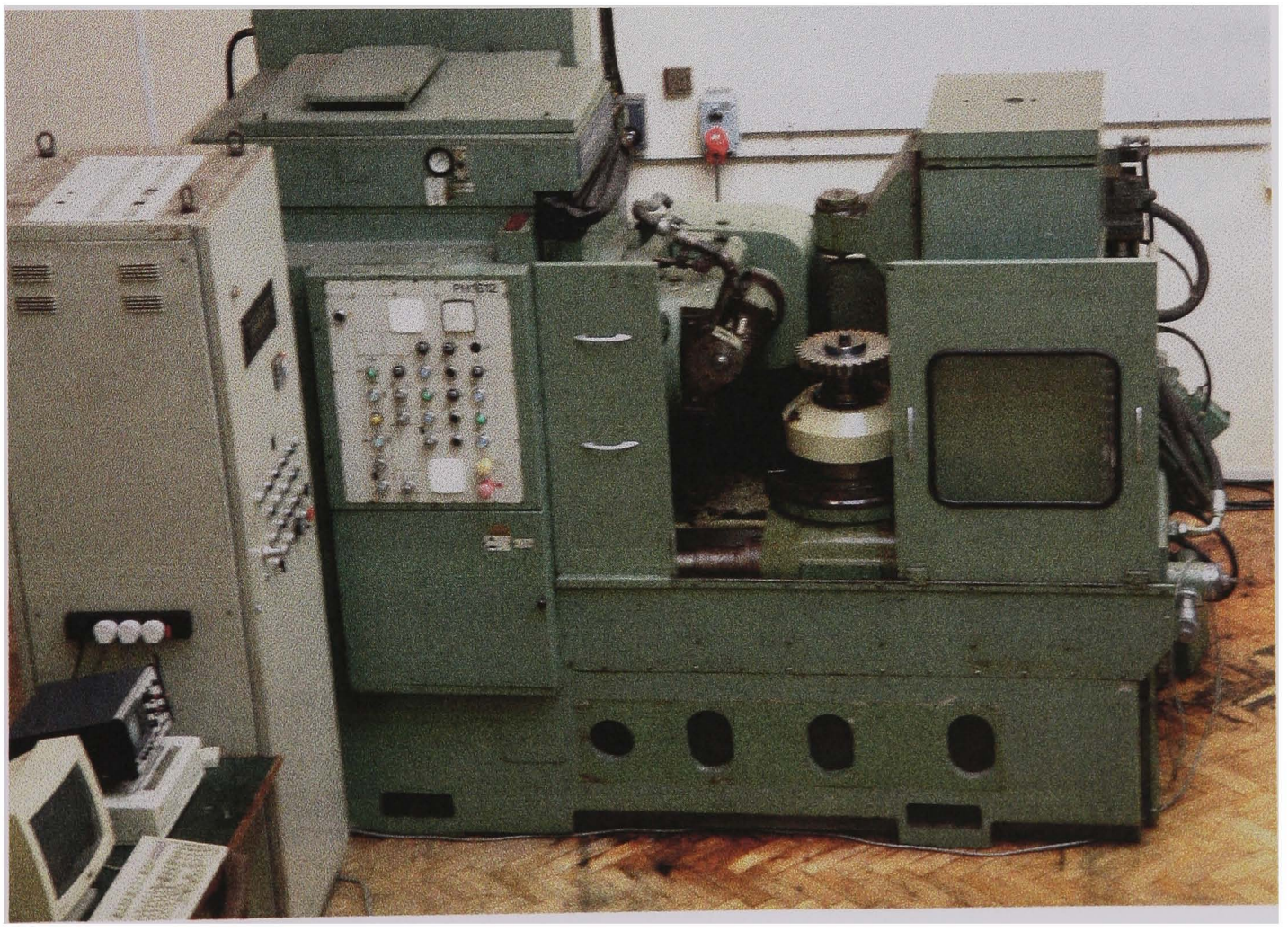

Figure 5.2: The Churchill PH1612 Hobbing machine arrangements at Newcastle

5.3.1 PMAC motion controller

PMAC (Programmable Multi Axis Controller) is a highly sophisticated motion controller card and has found use in a wide range of applications, which need a high precision, or on large machinery. A single PMAC board is capable of controlling up to 8 axes simultaneously.

In this project PMAC is integrated with 3 axes of the hobbing machine, namely the hob, worktable, and vertical drive. A 4^{th} axis is a mirror axis for the table to facilitate the climbing cut. PMAC has a number of inputs and outputs in order to control any individual axis independently or simultaneously with other axes. Each axis has a 16-bit DAC (digital to analogue converter) to generate an output voltage in the range +/- 10 V, differential encoder inputs for position feedback, positive and negative hardware limits to inhibit the motor, home flag (which sets the datum point of the axis and can return to it when homing the axis). There are also several discrete inputs on PMAC, which have not been utilised in this application, i.e. the amplifier fault input, which could be connected to the amplifier. PMAC also has 16 discrete I/O ports (8 inputs and 8 outputs), which have been used to switch on basic functions on the machine, or to inform PMAC of the status of input channels such as limit switches or push buttons. The PMAC card is installed in a PC and requires an external +/- 15-dc power supply for optical isolation. Further opto-isolation is provided through a dedicated printed circuit board, which was designed for this application. The circuit diagram is shown in appendix D. Figure 5.3 illustrates the schematic arrangement of the PMAC implementation.

As mentioned previously, the encoders, which are attached to the hob and wormshaft, have a resolution of 250 lines per revolution and the vertical slide encoder resolution of 250 lines/mm. PMAC has the ability of increasing the resolution by 4. The home flag facility on PMAC is an important feature to home (send the drive to its home position) at power on, or to send the drive to a required position. PMAC retains all the axis information stored in its memory as long as it is powered up and axes can be sent to any desirable position.

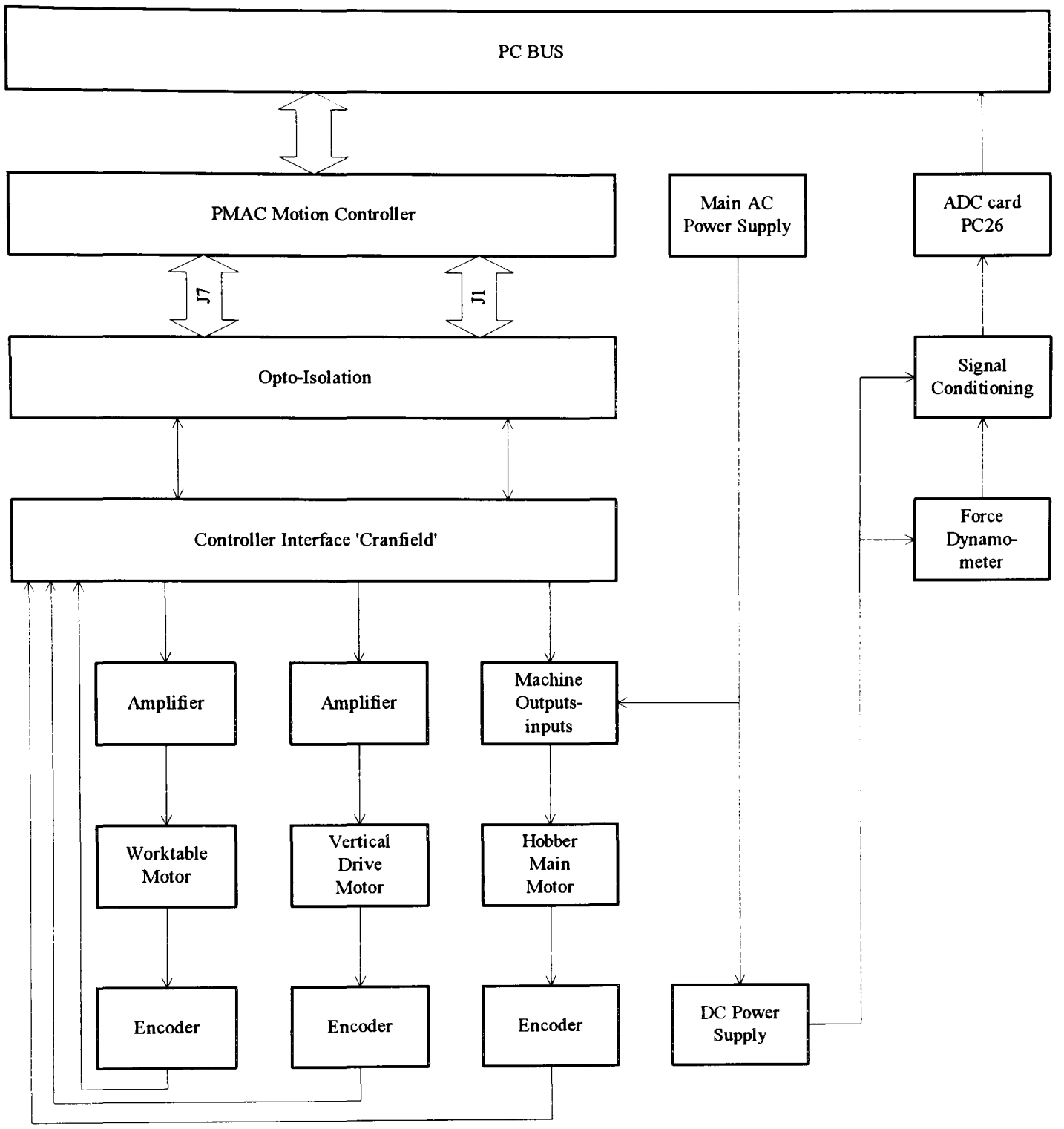

Figure 5.3: Schematic Diagram of PMAC implementation

There are two ways of communicating with PMAC, either using its executive software or via another programming language such as C. The PMAC executive program gives two options of programming either using motion programs (PMC) or PLC programs. It also provides the user with the ability of tuning the axes (which will be discussed later), as well as having a unique facility for data gathering, which is stored in memory for subsequent analysis. The executive program allows many operations to be carried out, such as moving the motor to any required position or executing a motion program, as well as displaying the instantaneous position of each motor. It also it has a self-diagnostic feature. If a motion program or a motor is not running this feature allows the configuration to

be displayed, along with all the possible warnings and definite faults causing problems preventing them from moving.

PMAC can have up to 8 co-ordinate systems and they are defined as &1-&8. Having 8 co-ordinate systems gives the user the freedom of choosing the best way to control an application. One motor can be assigned to every single co-ordinate system, 8 motors to one co-ordinate system, or 2 motors to 4 co-ordinate systems. A co-ordinate system must have at least one motor assigned to it in order to run a motion program. Grouping motors on different co-ordinate systems depends on the way an application can accomplish its job. If motors are to move independently from each other they can be placed in different co-ordinate systems, otherwise if they assigned on the same co-ordinate system they will run in a co-ordinated manner. Different co-ordinate systems can run different motion programs at different times, including overlapping, or even run the same motion program at different, or overlapping, times.

PMAC allows the user to define what are called M, P, Q and the I variables and gives the user access to PMAC memory and I/O space. Every M variable is defined by assigning it to a location. The size and format in this location can range from a single bit to a 48-bit double word, and can be an integer or floating-point type. There are 1024 M variables, which can be specified either as a constant or an expression, i.e. M575 or M (P1+20). M variables have to be defined and are only defined once for any application, M variables may take few types as specified by the address prefix in the definition, X: 1-24 bit fixed point in X memory. Typical M–variable definition can take the form M1->Y: $FFC2, 8,1. After it is defined the M variable can be used in the programs as a variable. The expression is evaluated by PMAC by reading the defined memory location, and calculates a value based on the defined size and format and utilises it in the expression.

P-variables are general-purpose user variables; they are 48 bit floating-point variables at fixed locations in PMAC memory, but with no predefined use. There are 1024 P variables, and all the co-ordinate systems have access to P variables

and are a useful way to pass information between different co-ordinate systems. P variables can be used in programs for any purpose desired, position, distance, velocities, times, etc. the P-variable is defined by P {data}, where {data} is either a constant or an expression, P234 or P (Q100+5*P10). Q-variables are the same as P-variables, but are only used for a specific co-ordinate system, and have not been used in this project.

I-variables are the most commonly used variables, initialisation, or set-up variables, and related to this application. They are in fixed locations in memory and have predefined meanings. Most of them have integer values, and their range depends on the particular variable. There are 1024 I variables, and they are divided into groups, I0-I75: general card set-up (global), I76-199: dual-speed resolver set-up, I100-I186: Motor #1 set-up, I187-I199: co-ordinate system 1 set-up, and so on I900-I979: encoder 1-16 set-up, I980 – I1023 are reserved, or not used. Using I-variables PMAC can be configured to handle the signals it is sending or receiving, for example to set the DAC range for any motor amplifier value of the DC which sending from –10 to 10 V, Ix69, which has a range of 0-32,767 (DAC unit), so the default value is 20,480 which gives a 6 V.

To have the resolution of any encoder multiplied by 4 the I900 variable should be changed to 3, or to set which of the flag inputs is used for position capture. Setting I903 to 0 tells PMAC that the home flag is the input to use.

The main function of PMAC in this project is what is called software gearing via a master-slave functionality, which permits position following. It is a motor-by-motor function, the signal coming from the master encoder (which may be in an open loop) is fed to other encoder inputs, usually under PMAC control. The slave encoder is 'told' that the encoder register is the master, by setting Ix05. Ix07 and Ix08 set the gearing ratio between the two motors, i.e. Ix07/Ix08 = i, where i: is the index ratio between the two gears (motors). This function can be turned on or off by setting Ix06 to 1/0, when on, the inputs from the master axis acts just like a trajectory generator, and commands the slave to move to the commanded position.

PMAC also has the ability of sending any motor to any required position either by using a jog command, e.g. #2 j=100000 or simply by typing the motor number and the position required. The jog speed and the direction can be set-up by the user via the assigned I-variables. All PMAC configurations can be saved in a file and restored at anytime.

The digital motion filter for each motor axis can also be easily tuned. This sets the control parameters of the motor amplifier, in order to achieve a fast and stable response. There are two parts to the tuning procedure. The first involves adjusting the feedback parameters to a step response, by setting the Proportional, Integral and Derivative (PID) filter parameters. The second stage involves setting the feed-forward parameters by using a parabolic move, in order to minimise the following error. By stimulating the amplifier and recording the system response this gives the user the option of changing any of the filter parameters. The user has to be careful of choosing the right step size, so as not to saturate the amplifier, or exceeding the motor limits.

During PMAC tuning the output response can be plotted graphically as position, velocity, acceleration, following error, and the corresponding DAC output. A step response is a commanded position, which will move it back to its new position. Studying the graph resulting from a step response tells the operator a great deal about the system characteristics. In the step response there are three major PID parameters, namely

K_p - Proportional gain *(Ix30)*, K_d - Derivative gain *(Ix31)*, K_i - Integral gain *(Ix33)*. The complete servo equation is

$$DACou(n) = \frac{Ix30 * Ix08 * [FE(n) - Ix31 * AV(n) + Ix32 * CV(n) + \frac{Ix35 * CA(n)}{64} + \frac{Ix33 * IE(n)}{2^{23}}}{2^{19}}$$

where

DACout (n) is the voltage output (+/- 10 volts) and limited by Ix69.

Ix08 is a scaling factor for any motor *x*, it is usually set to 96.

FE (n) the following error in servo cycles *n*, i.e. the difference between the commanded position and actual position cycle *CP (n) -AP(n).*

AV (n) is the actual velocity in servo cycle *n*, which is the difference between the last two actual positions, *AP (n) - AP (n-1).*

CV (n) is commanded velocity in servo cycle *n*, which is the difference between the last two commanded positions, *CP (n) - CP (n-1).*

CA (n) the commanded acceleration in servo cycle *n*, i.e. the difference between the last two commanded velocities *CV (n) -CV (n-1).*

IE (n) is the integrated following error in servo cycle *n*, or could be written in a mathematical term as

$$\sum_{j=0}^{n-1} FE(j)$$

There are three features by which a user can assess how the system responds. These are the rise time (which is the time the system takes to go to from 10% to 90% of the commanded step); Overshoot (which is the percentage that the system travels past the commanded step); and settling time (which is the time that the system takes to settle to within 5% of the commanded step). A well-behaved system is characterised by a quick rise time with little or no overshoot and a quick settling time. By examining the formula above it will be noticed that the *Ix30* variable is not strictly speaking a proportional gain *(K_p)*, as changing *Ix30* also affects the other two parameters of the PID filter, namely the integration and derivative gains. Changing K_p itself will not have that much effect on the system, when K_i and K_d are not equal to zero, i.e. changing the PID parameters should be done by changing all three parameters to get a stable system. Appendix B outlines the results of the step-response tuning procedures for the worktable and vertical axes of the machine.

The error between the commanded position and the actual position is called the following error, which is correlated to the velocity and the acceleration. PMAC's parabolic move will reduce this error by changing the velocity K_{vff} *(Ix32)*, and acceleration K_{aff} *(Ix35)* feedforward parameters. They add terms to the torque

command, which are proportional to the commanded velocity and acceleration. The correlation should be 1.0 in an ideal system, i.e. the closer the demanded trajectory correlates to the actual trajectory the better the correlation. The average ratio between the following error for both velocity and acceleration is calculated. The results of the parabolic tuning procedure for the worktable and vertical axes are given in Appendix B

PMAC also has the option of using an open loop tuning method, which is useful, especially for an amplifier with tachometer feedback, and uses the O command on PMAC. This is given as a percentage of the output voltage, and is determined by setting Ix69. The DAC parameters are denoted by the I-variables *Ix13, Ix14, Ix16, Ix29, Ix69. Ix13* and *Ix14* are the soft position limits, *Ix16* is the maximum permitted velocity and *Ix29* is the DAC offset bias, which has to be set to eliminate any drift when the axis is in open loop.

5.3.2 Multi axis force dynamometer

To study the behaviour of the cutting forces during the gear hobbing process a dynamometer was utilised. The hobbing process has a special cutting feature such that it is a continuous process and both the cutter (hob) and the work-piece (gear) are always engaged and meshed in a continuous motion. In order to be able to measure the cutting forces in the gear hobbing process, the signals must be transmitted using telemetry, or slip rings (as used in this application), in order to maintain an electrical contact between the dynamometer and the outside world. The slip rings are wired to the outputs of several strain gauges amplifiers, configured to measure the orthogonal cutting forces.

The rotating dynamometer has a four component arrangement, and measures the forces in *X, Y, Z* directions and a moment about the *Z-axis*. The *X* and *Y* axes are radial axes, while the *Z* axis is the axial (vertical) axis. General-purpose strain gauges were used and grouped in a four-gauge Wheatstone full-bridge arrangement to measure one component of force. Figures of the transducer arrangements are shown in appendix C. The signals from each bridge are

conditioned and processed using an INA-102 instrumentation amplifier with variable gain of each channel. The circuit board also has a dc-dc converter to provide a bi-polar supply for the amplifiers.

The dynamometer was originally designed for another application [Ashby], and substantial noise was evident on each signal channel. The hobbing machine is a large machine and has several AC and DC motors with switching amplifiers so the current and noise interference was very noticeable. It was decided to use a second-order low-pass active analogue filter, to reduce the noise. The filter was designed with a cut-off frequency of 200 Hz as it was constrained by the data-sampling rate of 466 Hz, to avoid aliasing, and thus complying with Shannon's sampling theorem.

The outputs from the dynamometer are analogue voltages in the range ±10 volts dc, and were captured using an Amplicon PC-26AT data acquisition card. The card has the capability to sample up to 8 differential input channels with a resolution of 12-bit at a sampling rate of 25 kHz per channel. In this instance the signal inputs were single ended, and the sampling rate was constrained to 466 Hz. Data acquisition software was written using C, and combined with data gathered from the PMAC motion control card to store positional and timing information.

Figure 5.4 shows the schematic diagram of the flow diagram for the data acquisition whilst figure 5.5 shows the flow chart of the data acquisition. Data analysis is explained in Chapter 6.

5.3.3 Software development

To be able to interact with the machine software code had to be written to control the machine and prepare it to cut a gear as well as acquiring the cutting force data from the dynamometer.

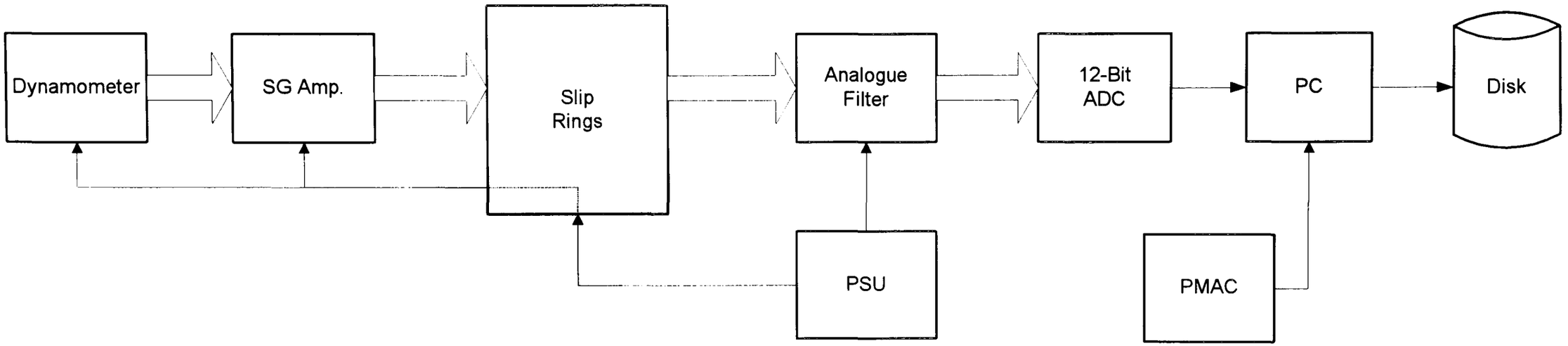

Figure 5.4 Schematic diagram of data acquisition from force dynamometer Data gathering flow chart

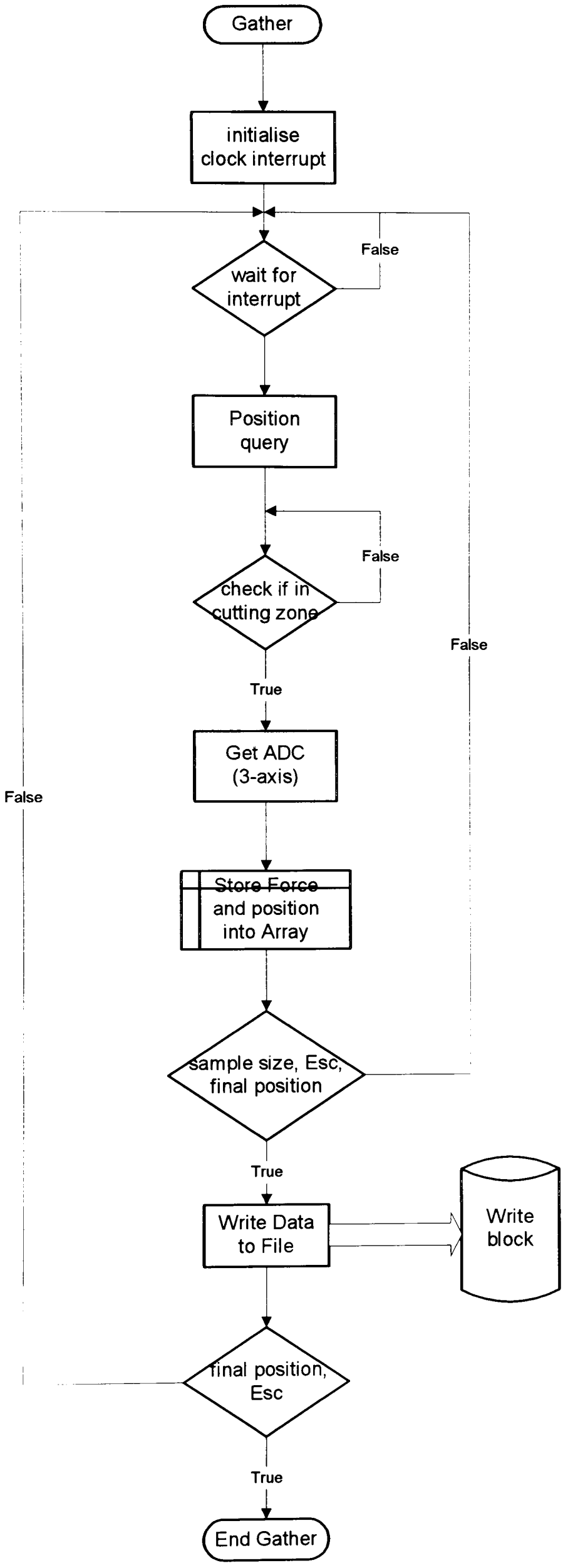

Figure 5.5 Data gathering flow chart

5.3.3.1 Axis co-ordinates for hobbing

PMAC provides motion programs that enable the user to perform simple tasks on the machine as well as setting appropriate co-ordinate systems for the machine axes. The definition of a co-ordinate system takes the form, for example *&1*, which defines the working co-ordinate system as number 1. The motors are defined in this co-ordinate system by symbols *X, Y, Z.* In this instance the machine has three motors, where: *X* is the hob motor; *Y* the worktable motor; and Z the vertical drive motor. The motors are assigned as follows *#1-> X, #2-> Y, #3->Z.*

Motor limits and M definitions have to be set for each axis in order to get the motor reading the appropriate data, and by setting and defining the correct values and definition. As far as the basic I/O ports are concerned they have an on-off function and only need setting of the appropriate M register definition.

All the above settings were carried out via the PMAC executive program. Having carried out all the related settings for the machine, and appropriately tuned each axis simple motion control programs were written to move any motor to the desired position. The line '#2 home' in a motion program will send motor 2 to its datum position, while the line '*Z1000*' will send motor *Z* (vertical to 1000 counts), 'M6=1' changes the status of register M6 which is ON while 'M6=0' will turn it off. Two lines such as 'while (M119 =1)', 'Endwhile', will force the program to wait for the flag M119 to become 1 and after which the loop will be satisfied. M119 is the home flag for the hob motor, and is very important, in order to know where the hob is as it set the start of cut for each start. The following show a simple motion program to advance and retract the work table every 30000 *ms*

```
;Program to advance the and retract the work table
DELETE TRACE DELETE GATHER
CLOSE                ; close previous programs
OPEN PROG 3
CLEAR
while (1<2)
```

```
M7=1                ;advance table
M8=0
DWELL 30000         ;wait 30000 ms
M7=0
M8=1                ;retract table
DWELL 30000
endw
CLOSE
```

5.3.3.2 Axis control

When the co-ordinate system is fully set-up, C language code was used to develop a machine control program, which provided an interface to PMAC and incorporated downloading of PMC programs. Several functions were written to facilitate the ease of development of the main programme. A pseudo flow diagram of the main programme is shown in Figure 5.6.

Prior to executing the program to cut a full gear there are few preliminary steps the user should do. These can be classified during the setting up of the machine, but need to follow a strict sequence. Depth of cut and how many cycles needed. Usually the machine takes two cycles, which are the rough cut, and the fine (finish) cut. To set up the depth of cut the worktable column has to be advanced very carefully to establish fine contact between hob and the gear blank. Prior to this, the vertical drive has to be lowered to a position where the two centres of the hob and the gear blank are parallel to each other. Setting the depth cut is done using hydraulic pistons, which are operated in an on/off manner, and using a switch. A short program was written, which only requires the operator to push a button. PMAC uses the status of the switch to activate the hydraulic piston and advance the table. While doing this the square nut adjuster, located at the back of the machine, is used to adjust the depth of cut and should be loose. As long as the gear blank just makes contact with the hob, the depth should be adjusted.

- Initialise interrupts
- Case
  - H: Home axes
  - D: Set dead Stop
  - E: Enter gear data manually
    - Gear diameter
    - Gear module
    - Helix angle
    - Rough cut feed rate
    - Finish cut feed rate
    - Blank thickness

    Save data into a file

    : Restore data from a file
  - S: Select Double cut
    - Advance table to rough cut position
    - Lower the hob head near the blank
    - Run the hob
    - Start gearing when hob home flag is found
    - Gather data
    - Stop when final position is reached

    -Start the fine cut cycle

    -Advance table to fine cut position

    -Repeat the same process above but with lower feed rate.

    -Gather data

    -Exit
  - F: Select Single cut
    - Same as double cut but only for rough cut
    - Gather data
    - Exit
  - P: display axis positions on screen
  - X: Exit

Figure 5.6 Pseudo chart of the main program

The gear data, gear diameter, number of teeth, gear module, helix angle and feed rate, should be entered to the computer. This data will be used to calculate gear-cutting parameters. The most important one is the index ratio, which instructs the machine how fast the table should rotate for each hob revolution, and is expressed in terms of how many times the hob rotates for each worktable revolution.

Because the hob is not under PMAC control, but is running in an open loop, it is important to know the number of revolutions, or teeth, which is basically the index ratio. For a 20-tooth spur gear the hob rotates 20 revolutions for each worktable revolution. In PMAC the index ratio for motor 2 (worktable) is determined by two I variables *I207* and *I208* as the index ratio is basically i = *I207/I208*. It is important to note that the worktable motor is not mounted directly on the worktable but is connected to the wormshaft where there is a 1/72 index ratio between the table and the wormshaft, i.e. for each revolution of the table the wormshaft has to do 72 revolutions. This makes the index ratio between the gear and the hob more complicated in order to get the exact index ratio between the table (wormshaft) and the hob this will involve computing a real number. This causes a problem, since PMAC will only accept integers for the I-variables. This problem can be overcome by using a look up table to find the right *I207* and *I208* parameters for each possible number of teeth in order to get the right (integers) for *I207* and *I208*.

A further problem results, as *I208* is an internal scaling factor, as mentioned before, which affects the PID algorithm. This may result in an erratic system, and was overcome by noticing the difference in *I208* and adding or multiplying that to the PID controller (I variables) to get the right parameter. In producing spur gears the axial feed rate is not a very important factor as it could be changed at any time and will not affect the cutting process, but a reasonable feed rate is required to reduce the wear in the hob and vibration. Three millimetre per revolution of the gear blank is considered a reasonable feed-rate for the rough cutting, whilst half that and less is suitable for finish cut, as the lower the feed rate the better the tooth profile is. While for a helical gear, where the helix angle is not zero, the feed rate plays a major part in the index ratio and it will not be practical to change it while

the machine is running. The vertical drive should follow the worktable, and the worktable will operate as the master to get the right feed rate.

A C program was written to produce both spur and helical gears, and for conventional and climbing gear hobbing. The program gives the user the option of either entering the data manually or retrieving them from a stored file, providing the same gear data as required, setting the depth of cut, the gear thickness is entered which will reduce the time by moving hob head, vertical drive to a position where it is just above the gear blank. The program also has the option of either using a one cycle cut or two-cycle cut. It shows the position of all the moving elements while cutting, and finally the program can be terminated at any time in the case of any error occurred.

5.3.3.3 Force sensing

A sub-program was written to handle the signals coming from the dynamometer. The analogue input was calibrated to give an appropriate measurement of force in newton (N). As well as acquiring the forces it was necessary to know the corresponding position of each motor so the forces can be analysed according to the position of the hob and the table. To obtain the axis positions a subroutine (called 'pos_query') was written which used the data gathering in PMAC. The sampling rate of the data for the cutting forces was restricted by many factors, but mainly the speed of the computer clock. It was decided that the best sampling rate was 466 HZ and maximum sample size of 6000, due to limitations the PC memory.

The subroutine, which handles the cutting forces, also stores the data in a series of files, which can then be analysed off-line to determine the various cutting forces namely on the 3-cutting axis of (*X, Y, and Z*). Although the signals were passed through an analogue filter some noise was still present due to the presence of the AC and DC motors, and switching amplifiers, which produce significant electrical noise. Tests, were carried out on the signals from the dynamometer, have shown that the machine has a quite effect on the signals. A running average filter was

employed in software to further reduce the level of noise and proved quite effective.

The cutting data, which stored in a series of files, represents the cutting forces on a moving co-ordinate, i.e. the worktable, rather than in a fixed co-ordinate system. The Z force is generally negative in the sense that the hob is always pressing on the workpiece while the X and Y forces are sinusoidal in nature, and 90^{o} out of phase, due to the rotation of the worktable. The transformation from the rotating co-ordinate system to a fixed co-ordinate system affect only the X and Y forces whereas the Z-force remains the same.

5.3.3.4 Overall software integration

The main software programme, which incorporates all the small subroutines also handles the machine set-up, entering gear data, and gives the user the option of either single or double cycle cut as required. It also facilitates the collection of cutting force data and storing them in files, which are named in a specific way so that the user can tell if they belong to the same set.

CHAPTER SIX

ANALYSIS OF RESULTS

6.1 INTRODUCTION

This chapter presents the results from both the kinematic analysis and the experimental cutting tests. The kinematic model of hobbing described in Chapter 4 was validated by carrying out cutting tests on the modified Churchill PH1612 hobbing machine described in Chapter 5. During these tests, the cutting force components were measured using the 3-axis dynamometer described in section 5.3.2, and are compared in this chapter with the values predicted from the model.

6.2 CUTTING FORCES IN A SINGLE TOOTH SPACE

In order to clarify the mechanism of the chip formation during cutting process it was felt appropriate to initially model theoretically and measure the cutting forces during the cutting of a single tooth, using a gear blank with only two diametrically opposed tooth spaces.

Producing a single tooth space gear will clarify two important factors in the process generating a specific tooth space; firstly it identifies the number of teeth on the hob, which actually take part in the cutting process; secondly it shows which part of these teeth is removing metal at each stage of the process.

6.2.1 Cutting force prediction

The kinematics of the hobbing process was successfully modelled with MATLAB, using the theory developed in Chapter 4. Further development of the

model facilitated prediction of the instantaneous chip thickness, from which it was then possible to determine the instantaneous cutting forces generated between the hob and the workpiece. The following sections present the results of the simulation, starting with the generation of the basic rack profile, and culminate in the estimation of the cutting forces in the gear hobbing process.

6.2.1.1 Basic rack profile

The basic rack profile of the hob teeth was generated by dividing a single rack profile into small sections, at interval Δz along the hob axis (z_6-axis), as previously explained in section 4.4.2. Fig 6.1 illustrates the basic rack profile in the axial and the normal sections, as explained in section 4.4.3. The lead angle is given by

$$\gamma_0 = \sin^{-1}(\frac{m_n z_0}{2r_0})$$

where m_n is the hob module, z_0 is the number of starts on hob and $r_0=r_{a0}-h_{a0}$, r_{a0} is the tip hob radius and h_{a0} is the hob addendum.

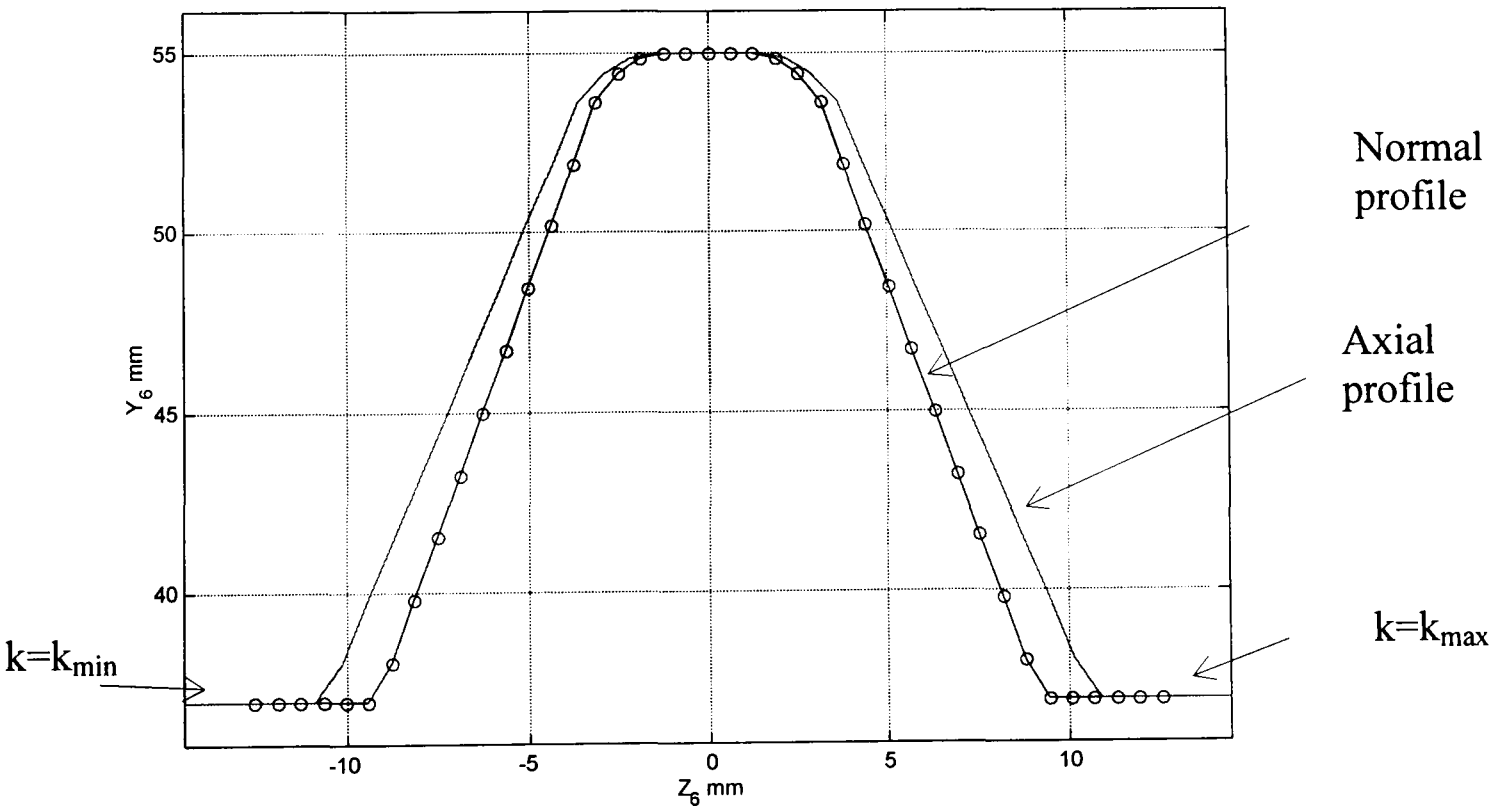

Figure 6.1 Basic rack profiles in axial and normal sections

$\gamma_0=30°$, $m_n=8mm$, $z_0=1$

Normally, γ_0 is very small, for example, for a hob with module of *8 mm*, $z_0=1$ and r_{a0} *=55 mm*, then $\gamma_0=5.097°$. This gives the value of $1/\cos(\gamma_0) = 1.0040$, so that the normal and axial rack profiles are virtually identical. But in figure 6.1 the value of γ_0 is exaggerated to show the difference, with a rack normal pressure angle $\alpha_n=20°$.

The figure also shows the number of points *(k)* along the rack profile. Negative values on the Z_6 correspond to the left side flank whilst the positive values give the right side flank. The centre line of the reference tooth coincides on the Y_6 axis.

6.2.1.2 Full hob

For single start hobs with low γ_0, the axial profile of the hob teeth, which lie on the surface of an involute helicoid surface conjugate to the basic rack, is virtually identical to the axial section of the rack shown in figure 6.1. For this reason, the software was developed on the assumption that the two axial sections are identical. The correct helicoid section could be calculated and substituted [Buckingham], but this would have very little effect on the mechanics of cutting.

The basic rack axial profile described in the previous section is thus taken as that of the hob reference tooth. However, this profile is then mapped to represent all other teeth by simply transforming it along the hob helix, by a rotation through an angle θ_i and a corresponding axial translation of distance $z_i=H/z_g$ as explained in section 4.4.4, where $H= \pi m_n z_0/\cos \gamma_0$, is the hob lead, *a*nd z_g is the number of gashes on hob. Figure 6.2 shows the profile of all the teeth on the hob, projected onto the y_6z_6 plane.

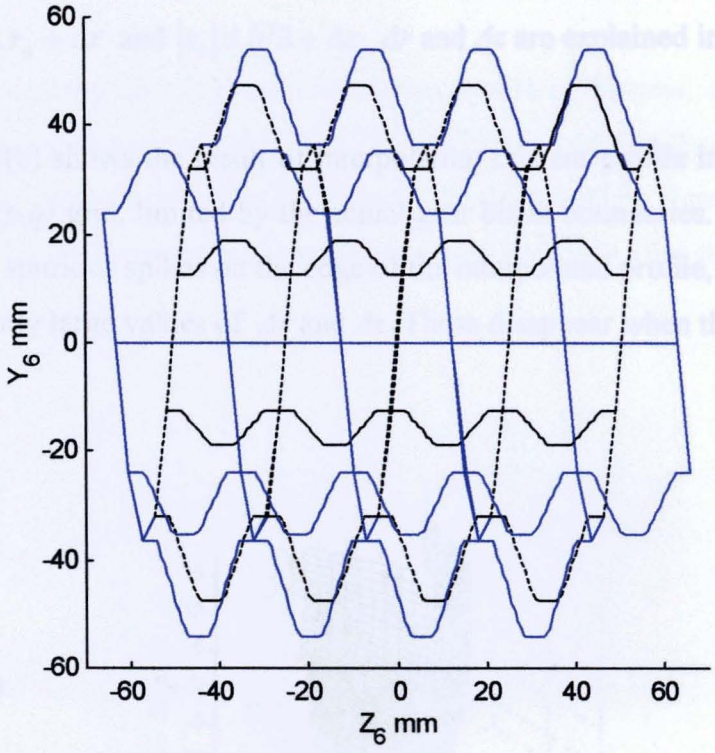

Figure 6.2 Full hob profile (z_g=9, z_0=1, m_n=8 mm, d_{a0}=110 mm)

6.2.1.3 Profile cut by one hob tooth

In order to generate the profile cut by each hob tooth it was first necessary to establish whether that particular tooth on the hob was within the cutting region on the blank, as described in section 4.8.2.

Figure 6.3 shows isometric views of the tooth space generated by one tooth of the hob after 23 of revolutions of the worktable. Figure 6.3(a) shows clearly how the tooth profile cut is generated by each point on the cutting edge *(k)* as it moves incrementally through the cutting region *(m)*. In this case, 40 points on each tooth profile, with rotation in increments of 1.5°.

To ensure that the original curvilinear *(m,k)* grid of points could be interpolated accurately to the boundaries of the gear blank at $r=r_a$ and $z_1=\pm\ b/2$, to give the

rectangular *(p,q)* points on the *(m,k)* grid were generated within the extended region $r \le r_a + \Delta r$ and $|z_1| \le b/2 + \Delta z$, Δr and Δz are explained in section 4.10.3.

Figure 6.3(b) shows the result of interpolating this cut profile into a rectangular (x_p, z_q) or *(p,q)* grid, limited by the actual gear blank boundaries. This figure also shows the spurious spikes on the edge of the interpolated profile, caused by using insufficiently large values of Δr and Δz. These disappear when the correct values are used.

(a)

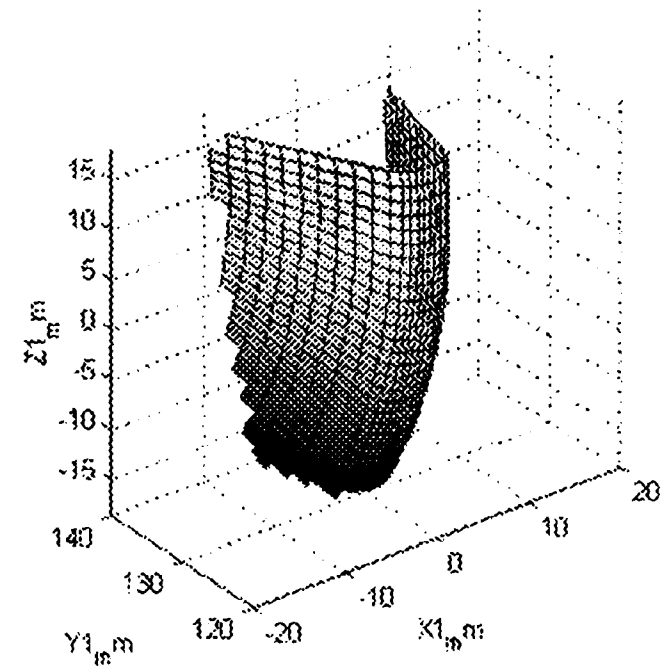

(b)

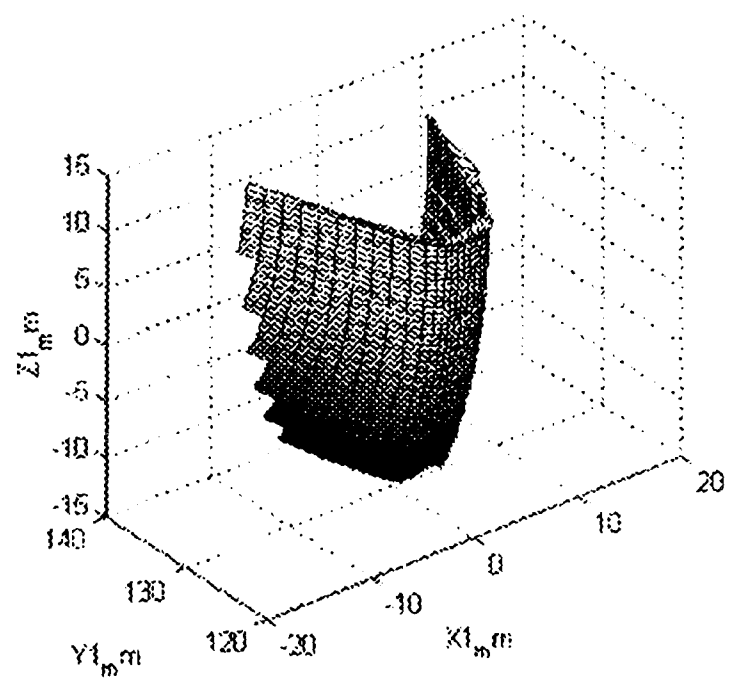

Figure 6.3 Model of generated (cut) surface (a) original (m,k) grid) (b) interpolated rectangular (p,q) grid, showing errors due to excessively small Δr and Δz

6.2.1.4 Tooth space profile

The tooth space profile is the instantaneous profile of the gear, as it is developed during the 'metal removal' process. The tooth space profile therefore eventually defines the final shape of the gear space, as illustrated in figure 6.4(b). Figure 6.4(a) shows the instantaneous tooth space profile shortly after the start of cut.

(a)

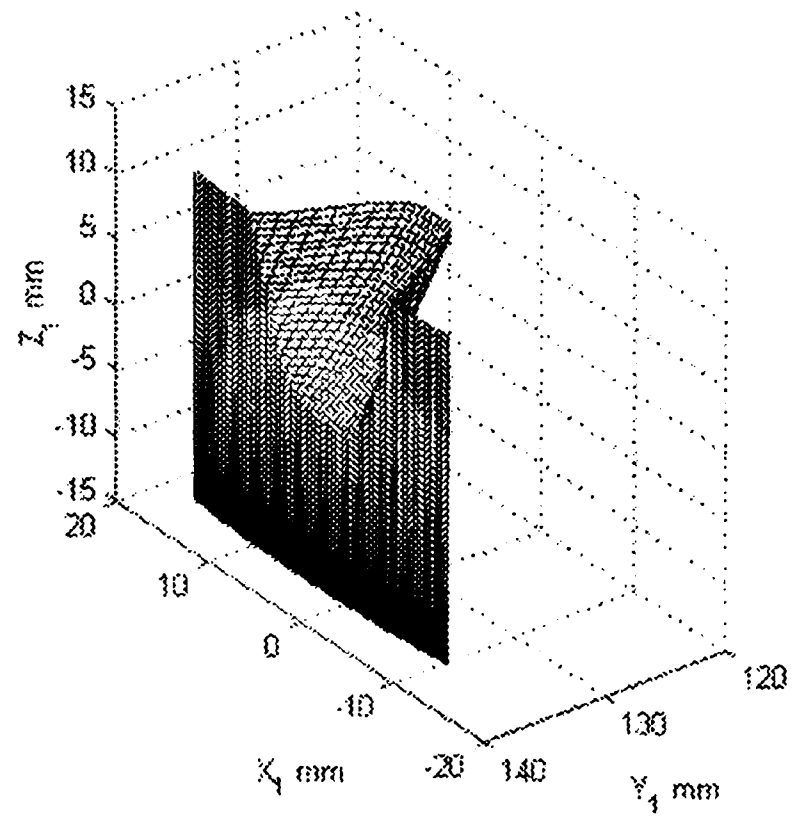

(b)

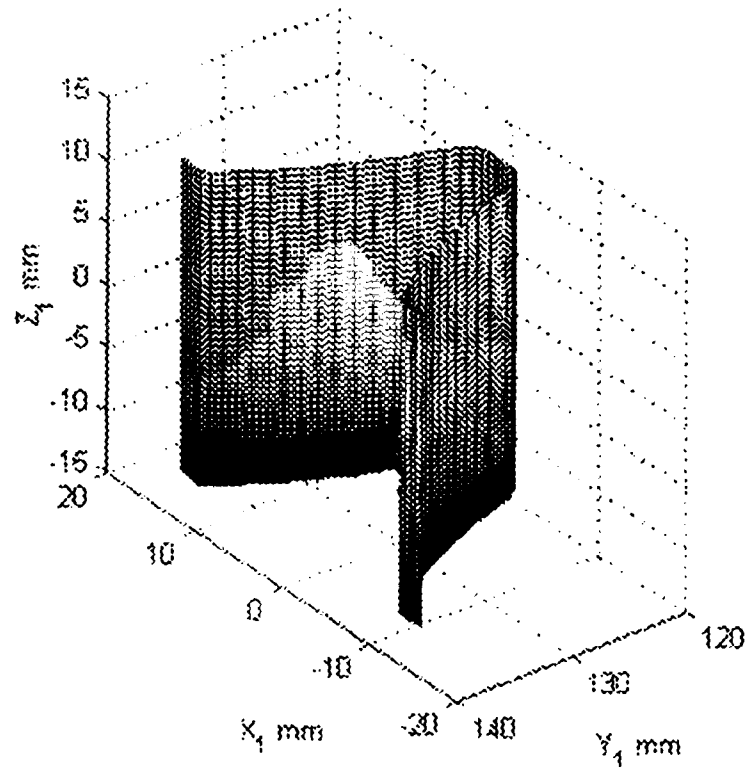

Figure 6.4: (a) Profile after 10 hob revolutions, (b) Final tooth space profile of a single space

To produce these tooth-space profiles, the cut surface shown in figure 6.3(a) has been mapped onto a regular *pq* grid, figure 6.3(b), using MATLAB's 'griddata', as explained in sections, 4.9.3 and 4.9.4. As each tooth passes through the tooth space, it generates a surface, similar to that of figure 6.3 which is first mapped onto this new rectangular *pq* grid and then compared with the current tooth space profile. This is only affected and updated if 'metal' removal is predicted, i.e. if the newly generated cut surface of figure 6.3 interferes with the current tooth space surface, as in figure 4.10.

So every time metal is removed the tooth space is updated to correspond with the newly cut surface in the regions where interference occurs. The new tooth space profile is then compared with the next cut space profile until there is no more metal to be removed. That produces the final shape of the gear tooth space profile, as shown in figure 6.4(b).

6.2.1.5 Instantaneous chip cross-section

The instantaneous chip cross-section is computed as the difference between the instantaneous cutting profile and the previously generated profile as shown in figure 4.10, provided the model indicates that there is interference between the two profiles, consistent with 'metal' being cut. The variation of the instantaneous chip cross-sections is most easily illustrated by viewing the rectangular *pq* grid, in which it is calculated, as shown in figure 6.5, although, once obtained, these values can also be interpolated back onto the original curvilinear (m,k) grid as shown in Figs. 6.6. These chip cross-sections are for the reference tooth after *23* revolutions of the worktable, roughly at mid face.

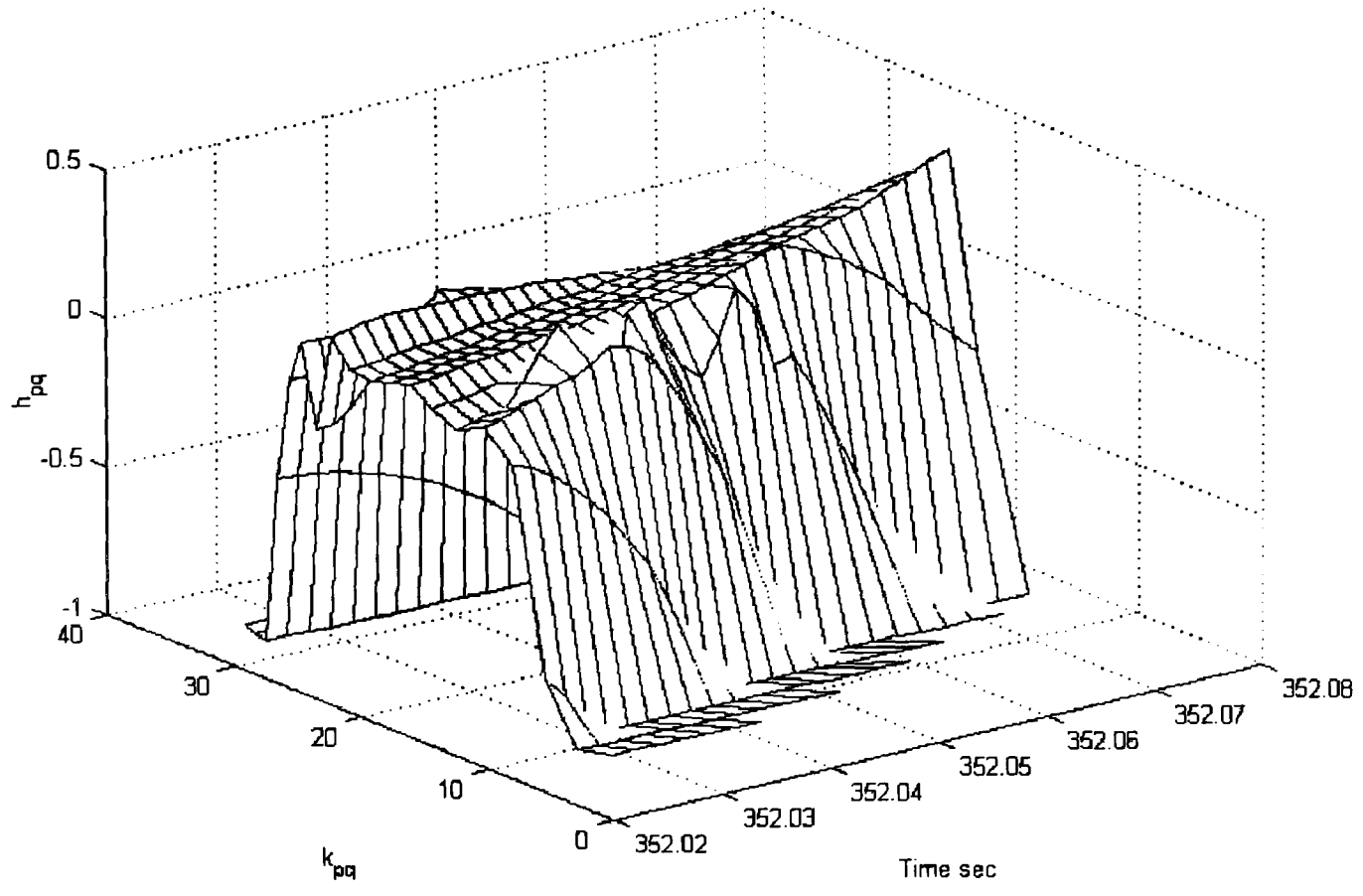

Figure 6.5 Chip cross-section on the pq grid

The chip cross-sections on both the *pq* rectangular grid and the *mk* original curvilinear grid includes the negative values of *h*. This is required to allow more reliable interpolation at small chip thicknesses. Early attempts to interpolate back to the *(m,k)* grid using only positive values of *h* resulted in missing some data, especially in the areas where only a small amount of metal is removed. It would have been possible to refine the grid to overcome the problem. However results have shown that increasing the number of grid points does not always mean a better outcome, while the amount of time it takes to perform the task is greatly increased.

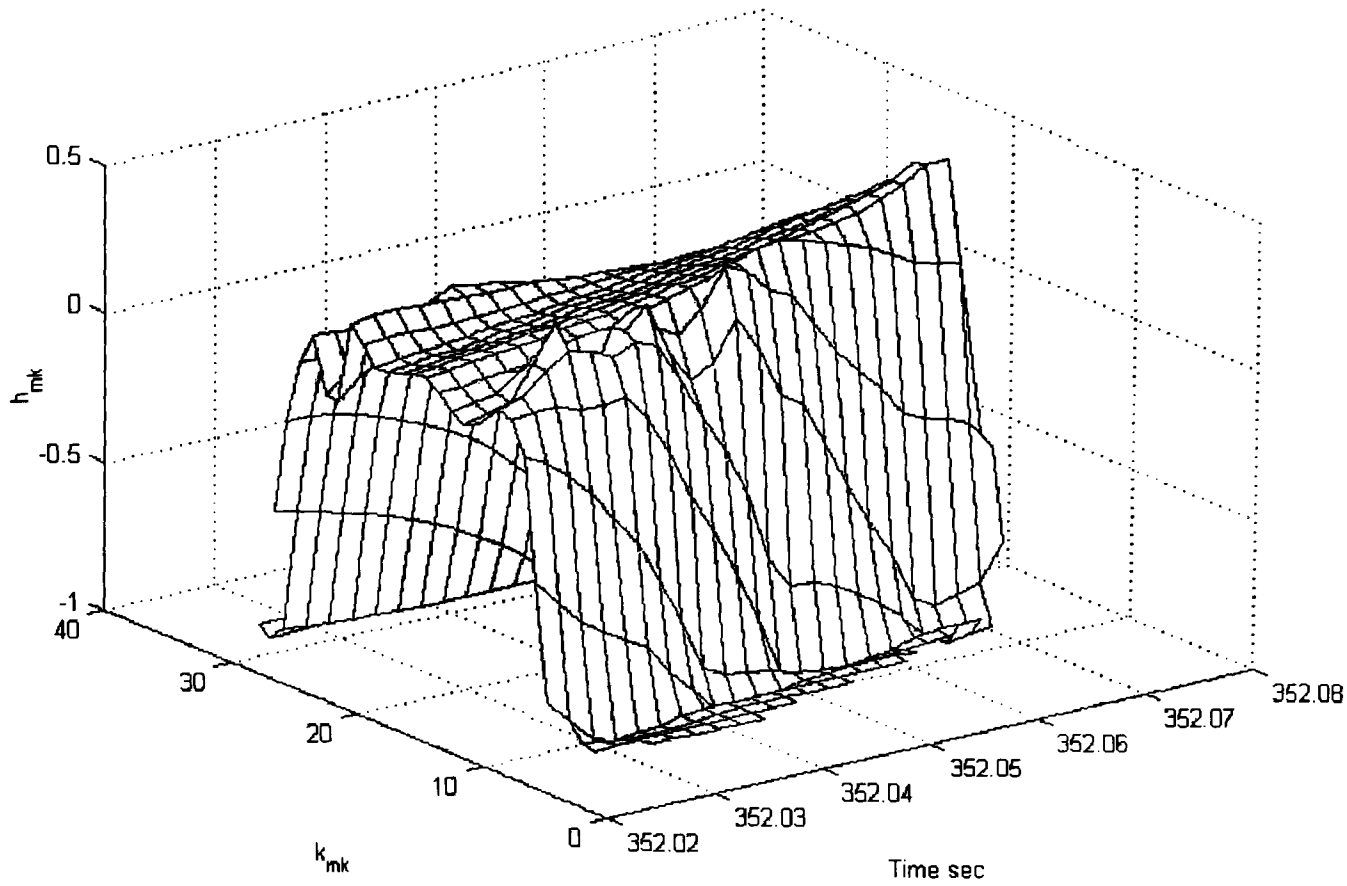

Figure 6.6 Chip cross-section on the mk grid

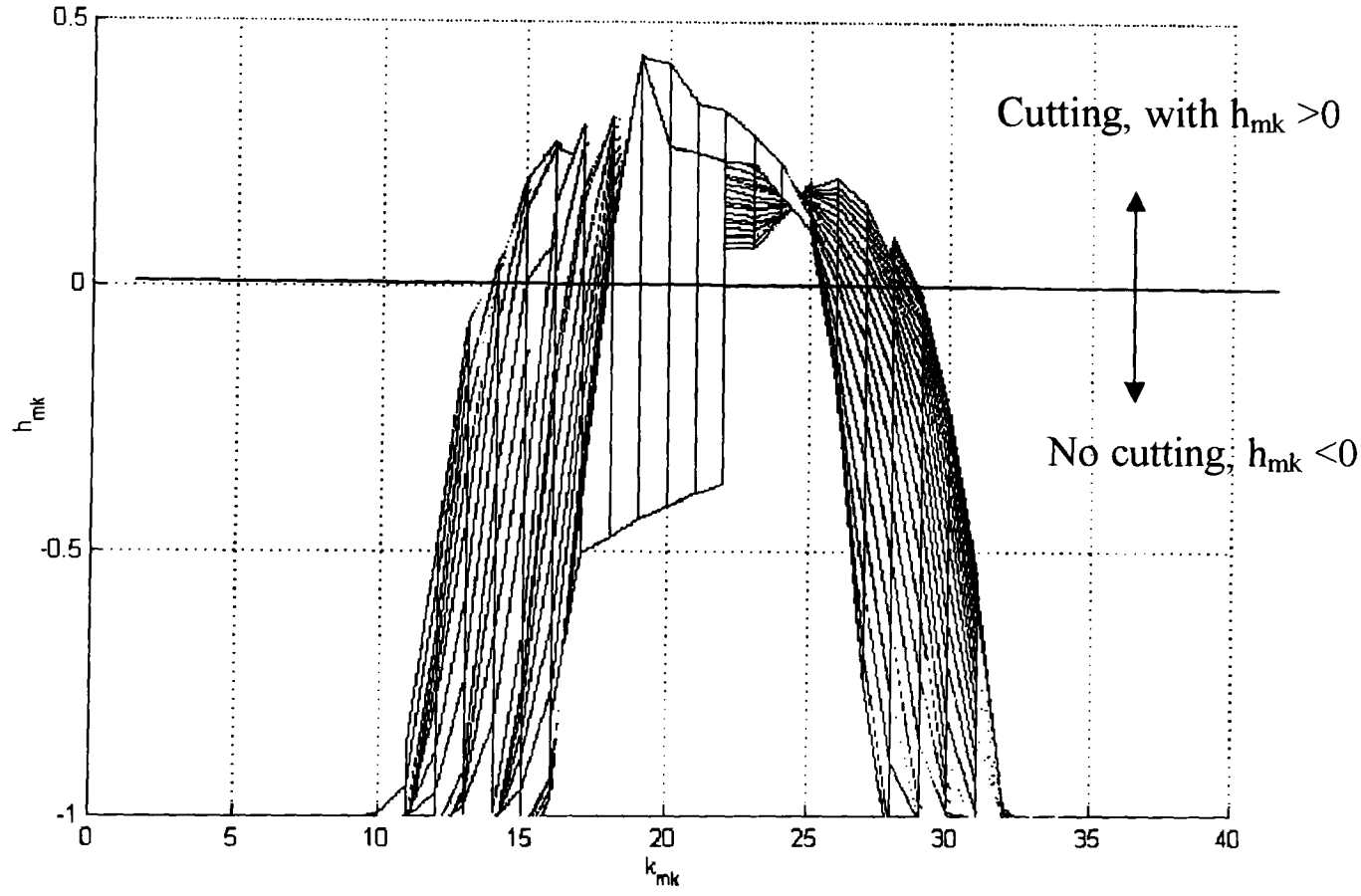

Figure 6.7 Chip cross-section on the (mk) grid (view of figure 6.6 along m axis)

Figure 6.7 shows the depth of cut as a function of position *(k)* on the hob tooth. Clearly most metal is removed by the tip of the tooth. The values on the abscissa show the number of points along the hob tooth flank *(k)*. This can be set to any number. In this particular case, the tooth profile was divided into *40* segments

points as $k_{min}=1$, $k_{max}=40$ so that the point *20* is lies on the tooth centre line. As this tooth is the reference tooth, it was expected to remove most of the metal using its tip and flanks (on both sides roughly equally). This is predictably what occurs (if only the positive values of h_{mk}, are taken into account, since this is the area of concern where cutting is really occurring.)

However other teeth along the hob which come into contact with the same tooth space do not engage with the gear in same manner. For example they might remove metal using only their left or right flank. This depends on many factors, namely the size of the gear, the face width of the gear and most importantly when contact is taking place. At any particular instant the tooth might be removing metal from anywhere along its cutting edge, but the amount of metal removed will vary from tooth space to tooth space.

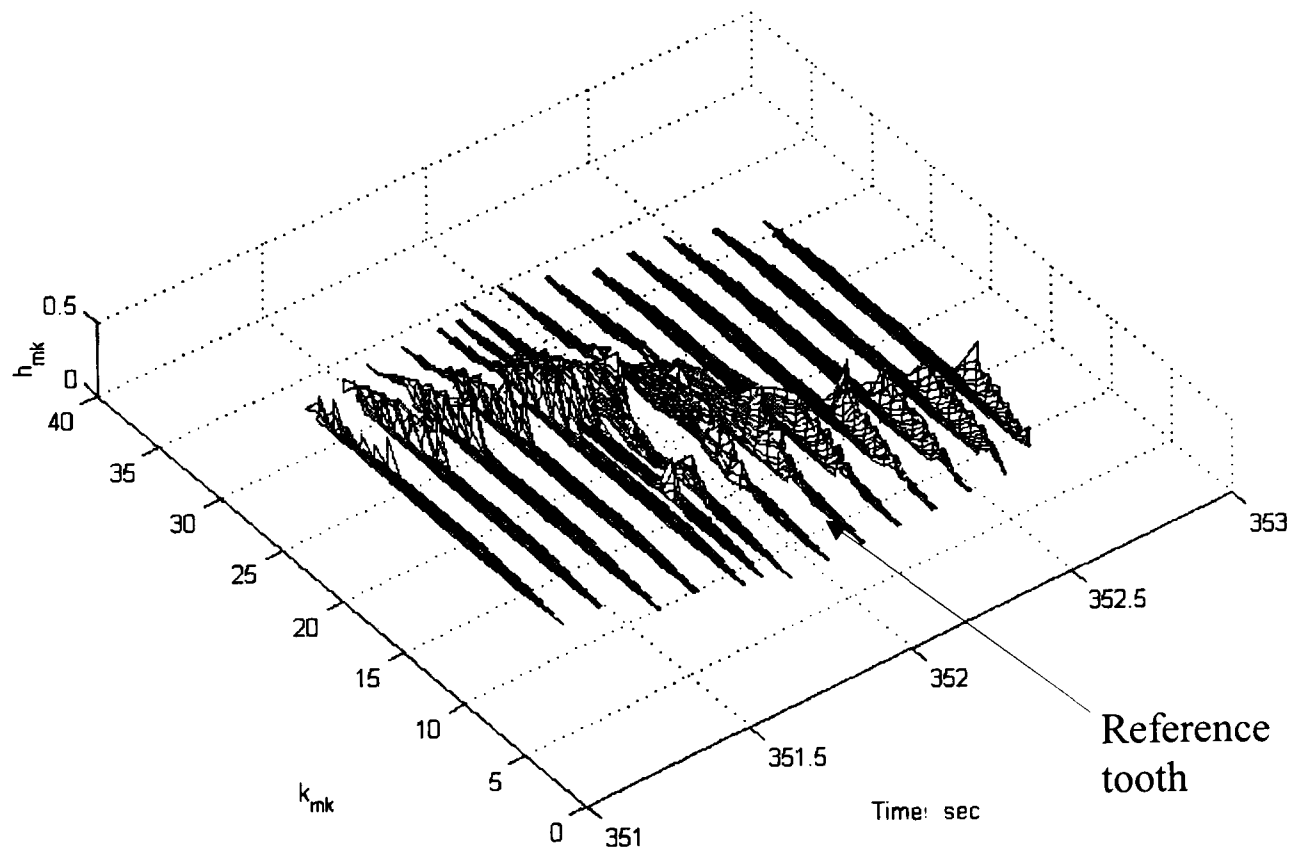

Figure 6.8 Chip cross-sections of even numbered hob teeth

This point is best illustrated in figure 6.8, which shows the variation in chip thickness whilst the gear is being cut at mid face, i.e. at a time of 352 seconds.

from start of simulation. For plotting purposes, and clarity, only selected even numbered teeth are shown. Note that this shows cutting along the hob teeth in one gear tooth space only. The first tooth begins to cut on its left flank only, with successive teeth cutting over a longer length of the flank, approaching the tip. At 352 seconds cutting can be observed to occur primarily along the tip, and on both flanks, simultaneously. This coincides with the reference tooth cutting (plus and minus one tooth position). As further cutting proceeds the chip thickness become progressively smaller until only the right flank remains in contact, and the hob teeth exit the tooth space. Altogether, 27 teeth cut in each tooth space, so that (since $z_g = 9$) tooth generation occurs over 3 hob revolutions.

Figure 6.8 indicates the reference tooth, and those right next to it. Even though this figure is only for selected teeth it is clear that only some hob teeth (actually, from tooth (9) to tooth (35)) are cutting. This number of active teeth depends on the number of teeth z and number of gashes z_g. The most important point here is that most of the cutting is performed by the reference tooth and the few teeth around it, so that the higher loads are on them. The figure only shows the metal removed by each hob tooth at mid face of cut, but in earlier stages of cut, where the hob makes only small contact with the metal, the number of teeth involved in removing metal is even less. The same situation arises when the hob moves away from the mid face position and starts to leave the gear blank. If the gears being cut are of thin section, or small diameter gears, the reference tooth and the teeth around it remove most of the metal and do not give other teeth the opportunity to participate in the cutting process. More teeth might take part for bigger gears. As a result, hob wear is much localised, especially on small gears, so that regular axial shifting of the hob is normally needed to distribute wear more evenly over all the hob teeth.

6.2.1.6 Prediction of cutting forces

The software was used to predict the cutting forces of the gear used in the cutting tests, with gear and cutting data as shown in table 6-1.

Parameter	Symbol	Value	Units
Module	m	8	mm
Hob tip diameter	d_{a0}	110	mm
Gear tip diameter	d_{a1}	278	Mm
Starts on hob	z_0	1	
Number of teeth	z	32	
Hob gashes	z_g	9	
Gear face width	b	25	mm
Depth of cut	h_c	$2.25m_n$	mm
Addendum of rack	h_{a0}	$1.25m_n$	mm
Dedendum of rack	h_{f0}	$1.0m_n$	mm
Hob speed	n_0	120	rpm
Helix Angle	β	0	^{o}
Normal Pressure Angle	α_n	20	^{o}
Axial feed rate	s_a	1.5	mm/rev(gear)
Chamfer angle	α_{cf}	45	^{o}
Hob shift	$x_z(t)$	0	mm
Depth of tip chamfer	c_f	$0.0m_n$	mm
Reference tooth	i_{ref}	22	
Number of revolutions	rev_{num}	47	

Table 6.1: Gear and cutting data

The simulation was run using $m_{min}=1$ and $m_{max}=20$ giving an increment of hob rotation of 1.5° between solutions. Each hob tooth profile was defined at 40 points $(k_{min}=1,\ k_{max}=41)$, the (p,q) grid was (40x40), the derived $(m,k)_{pq}$ grid could be 21x41 (like the original (m,k) grid or finer). Cutting forces parameters assumed (from Bruins) were $K_{c1,1}$ = 850 N/mm^2, and K_{nc} = 0.65.

6.2.2 Measured cutting forces

The dynamometer described in section 5.3.2 was checked and calibrated, and a fixture designed to mount it on the machine worktable. It was however noticed

that the signal to noise ratio from the dynamometer was rather poor, with most of the noise attributed to the dynamometer's on-board dc-dc converter. In the event it was decided to use an external dc power supply unit. The calibration procedure is explained in Appendix C.

The dynamometer was first tested using an oscilloscope and a voltmeter, but it was eventually connected to the host PC using an Amplicon PC-26AT data-acquisition card with 12-bit analogue to digital converter. Software was written to facilitate acquisition with the dynamometer, and a final calibration graph was produced for all three axes.

The gear blank material was mild steel normalised *BS970 080M40* with hardness of *240* H_B. The gear was aligned on the machine so that the centre line of the tooth to be cut coincided with the *Y-axis* of the dynamometer, which at the same time, coincided with the machine fixed axis when the table was at datum, at $t=0$. The hob was also adjusted so that the reference tooth centre line also lay on this axis when a maximum depth of cut (datum position). The first tests were carried out with a well used dulled hob, but all subsequent gear generation was conducted using a sharpened and re-furbished hob.

The machine was set-up as discussed in Chapter 5, using the main program to control the machine axes. The data acquisition software was modified to facilitate capture of force and position data only during cutting phase. Due to the nature of the hobbing process the hob makes contact with the particular tooth space well before the point when centre line of the tooth space coincides with the worktable axes. (Around one full tooth space before, maybe more for large diameter gears). The program was modified to allow extra 'clearance' of about one and half tooth spaces before and after the tooth space centre line coincided with the table axes, and ensures that all the data was captured. An approach length was estimated and used; this step is normally used in hobbing to accelerate the process as the hob head is moved to a position usually just above the blank.

The PMAC data gathering facility was used to simultaneously store the axes position information, as well as the force data, and then write it to disk. The data was subsequently analysed using Excel in three stages. Since the bridge outputs (for the three axes) were subject to an offset, it is first necessary to calculate these values under no cutting conditions. Secondly the raw integer values (in the range +2047 to -2048) were converted to real forces using the scaling factors, obtained during calibration. Thirdly a running average filter was incorporated which could be used to further reduce noise.

Data logging was initiated about 2-4 revolutions before cutting actually occurred, in order to compute the force offset values, and due correction made with respect to the collected data of this rotational offset.

6.2.3 Analysis of the cutting forces

To achieve a good comparison with the results obtained from the theoretical model it was felt necessary to obtain experimental data from a single tooth space, if at all possible. A number of specially prepared blanks were manufactured leaving only sufficient material to cut two diametrically opposed teeth spaces. Figure 6.9 shows the single tooth space gear being machined, and figure 6.10 illustrates its final shape.

Whilst the resulting cutting forces acting on the single tooth gear blank can be represented in either rotating or fixed axes, the relatively small difference in angle has a minimal effect, and to all intents and purposes, the two can be considered the same. In this instance the forces in the fixed vertical, radial, and tangential direction have been estimated. Figure 6.11 illustrates the magnitude of the forces at mid-face in the tangential, radial, and vertical directions.

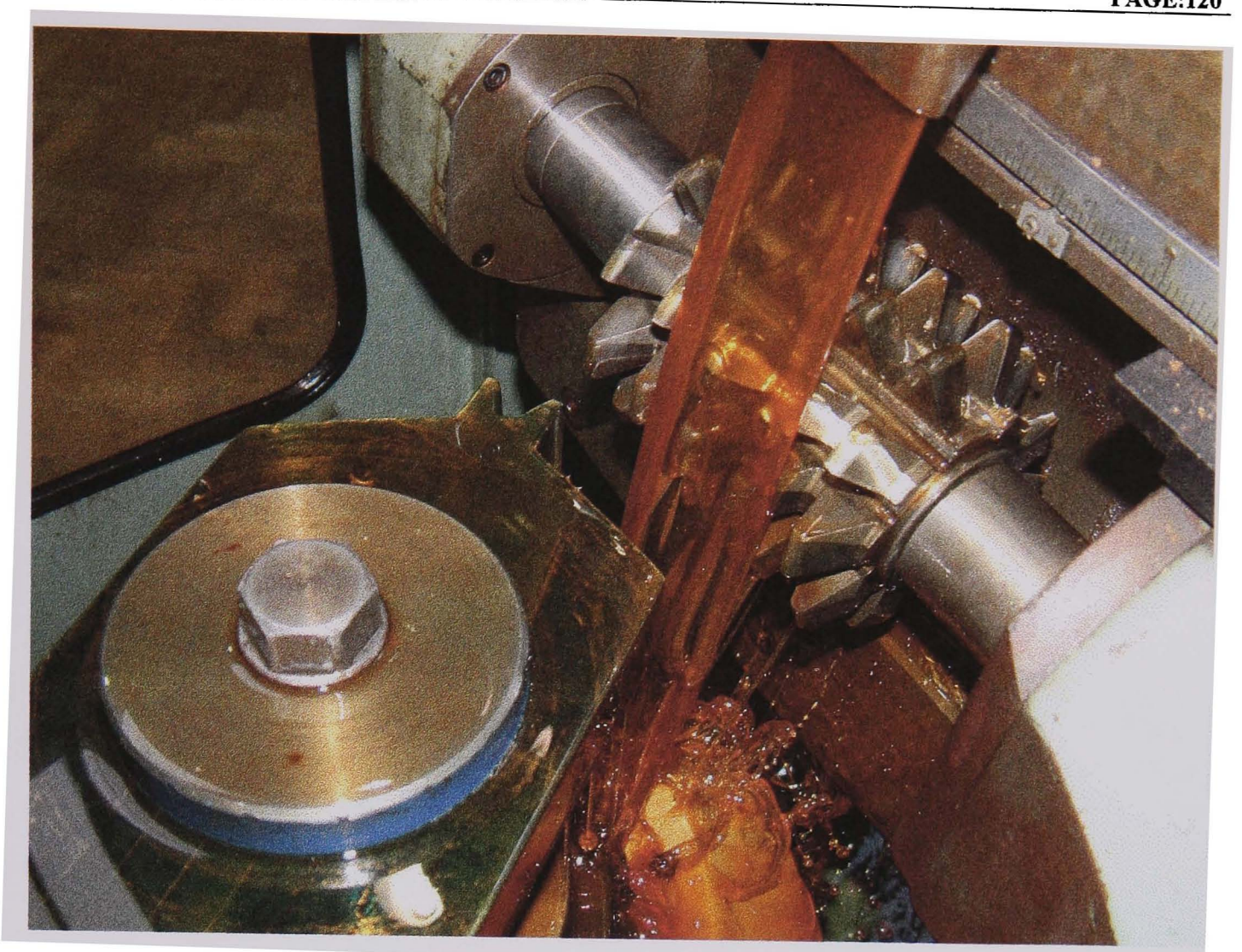

Figure 6.9: Single tooth space gear being machined

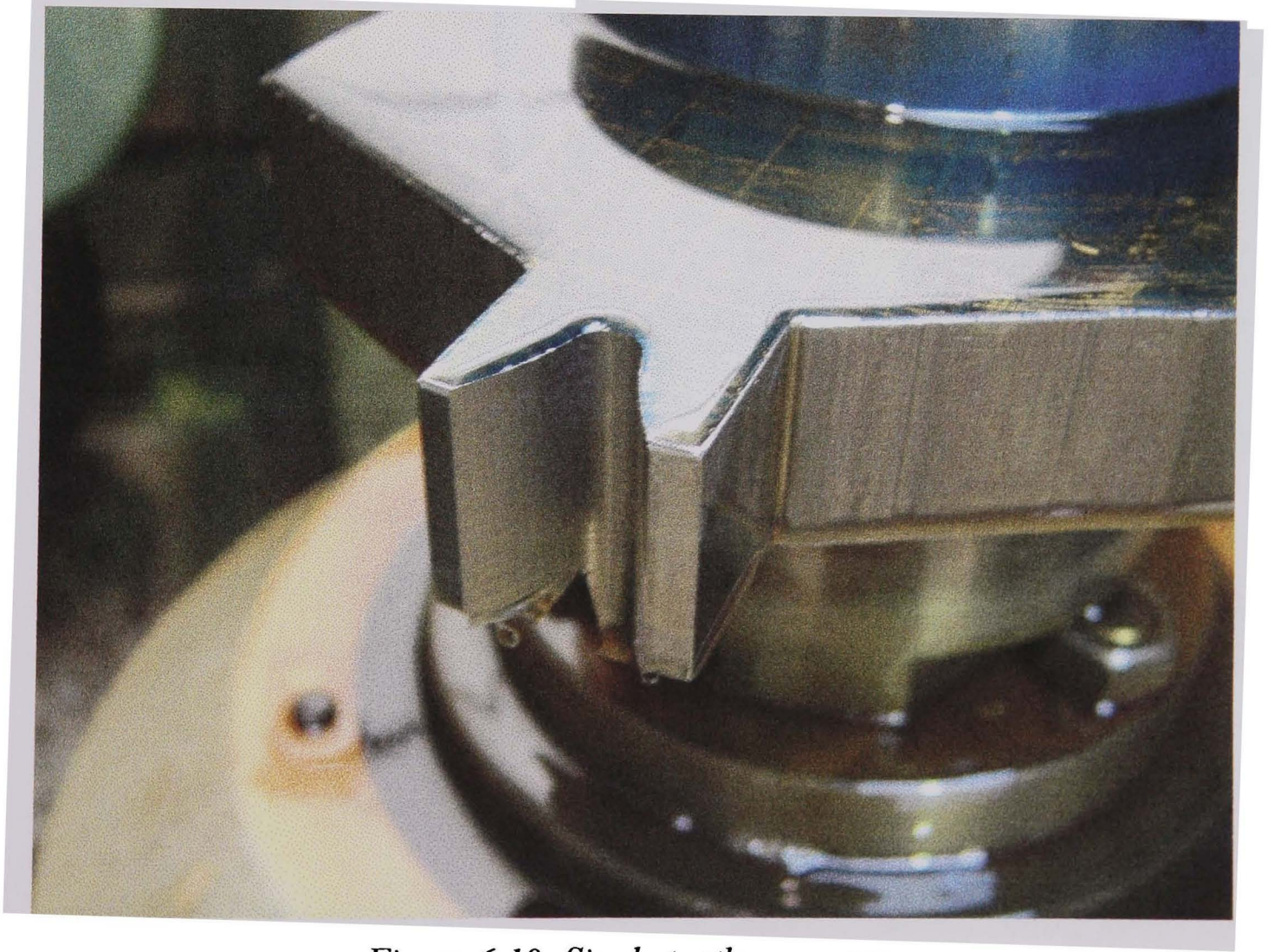

Figure 6.10: Single tooth space gear

Mid-face cutting occurred after approximately 670 hob revolutions (in this particular instance, a value highly dependant on the number of gear teeth, face width and the axial feed rate), and the intermittent nature of the cutting process is clearly illustrated. As each gash comes into contact with the tooth space, then loses contact, a force impulse is generated. The figure shows that 27 hob teeth cut in the tooth space. Since there are only nine gashes on the hob, the cutting takes place three hob revolutions during each cutting cycle.

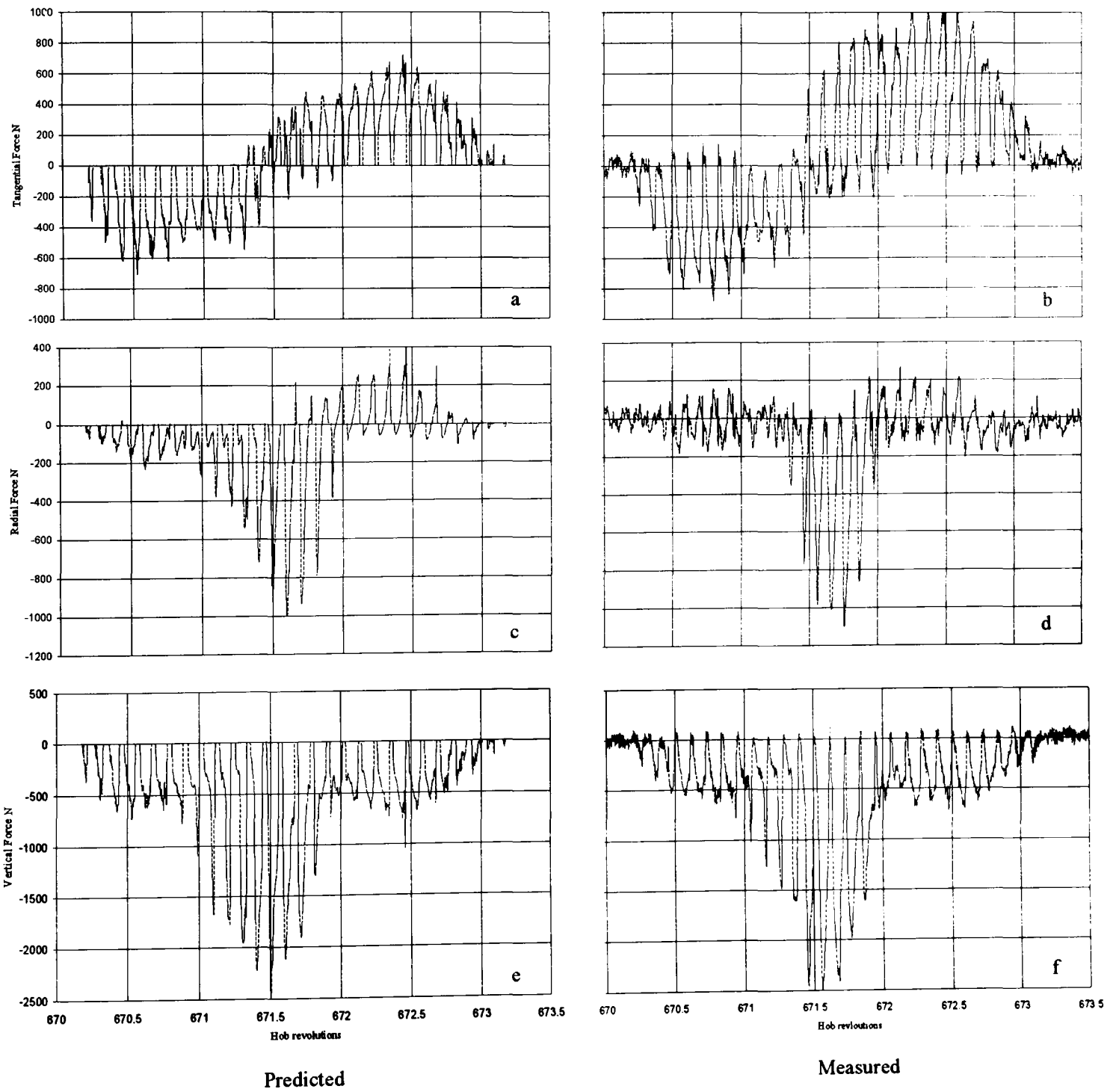

Figure 6.11 Comparison between theoretical and experimental cutting forces for a single tooth space (at mid face)

Notice that the first impulse coincides with the first hob tooth making initial contact with the blank several degrees before the centre of the tooth space is aligned with the hob tooth axis, when the reference tooth comes in contact. As explained in the previous section, the first tooth that comes into contact with the blank will only remove a small amount of metal, as it may only cut using its incoming flank, which explains the small magnitude of force, but as the hob goes deeper into the gear blank the magnitude of these forces increases, reaching its peak value when the reference tooth starts cutting. The forces will decline in magnitude as the following teeth cut using their outgoing flanks. This is only applicable to the axial and radial forces but not for the tangential force. It can be observed that the tangential force is almost negligible when the reference tooth is cutting but reaches its maximum and minimum values at either side of this point. When the reference tooth is cutting the tangential force components acting on both flanks tend to cancel each other out, as they are almost equal in magnitude, but opposite in direction, although the radial force components at each point are all in the same direction.

From Figure 6.11a, b, it can be observed that the fluctuating tangential force reaches a peak value of approximately ±1000N over the cutting cycle, changing direction as the tooth space centre line passes the axis Y_6, as expected. The envelope of the peak forces is roughly sinusoidal in nature, however the variation in the radial cutting forces, as shown in Figure 6.11c, d, is rather more complex, and the behaviour is difficult to analyse. The shape of the envelope suggests that initially only light cutting occurs along one of the flanks of the tooth space, when off centre, resulting in fluctuating radial force impulses. These forces are radially outwards, because cutting is mainly near the outer surface of the blank as the hob teeth leave the cut, and mainly on the tooth flanks, see figure 6.8.

In this region, at each active point, the normal cutting force F_n is predominantly axial so produces only as small (inwards) radial component, while the larger main cutting force F_c (in the cutting direction) has a significant radial outward component, see figure 6.12, as the hob tooth leaves the blank.

As the tooth centre space approaches the Y_6 axis, the magnitude of the radial forces alternates with significant cutting probably occurring more at the tip of the hob tooth. In this region, heavy cutting takes place on the cutter tip, see figure 6.8, producing large values of both F_c and F_n. However, in this region, F_n is predominantly radial with a greater inwards radial component that the outward radial component of F_c depicted in figure 6.12, so the resultant radial force suddenly increases and changes sign, as shown in figure 6.11c,d.

The variation in the vertical cutting forces, shown in Figure 6.11e, f, can be explained in the same way. The peak force occurs when the tooth space centre line is aligned with the Y_6 axis centre, as expected. Again only light limited cutting occurs along the leading and trailing flanks of the cutter at the start and end of the cut, prior to significant metal removal occurring when the tooth space is centred on the Y_6 axis.

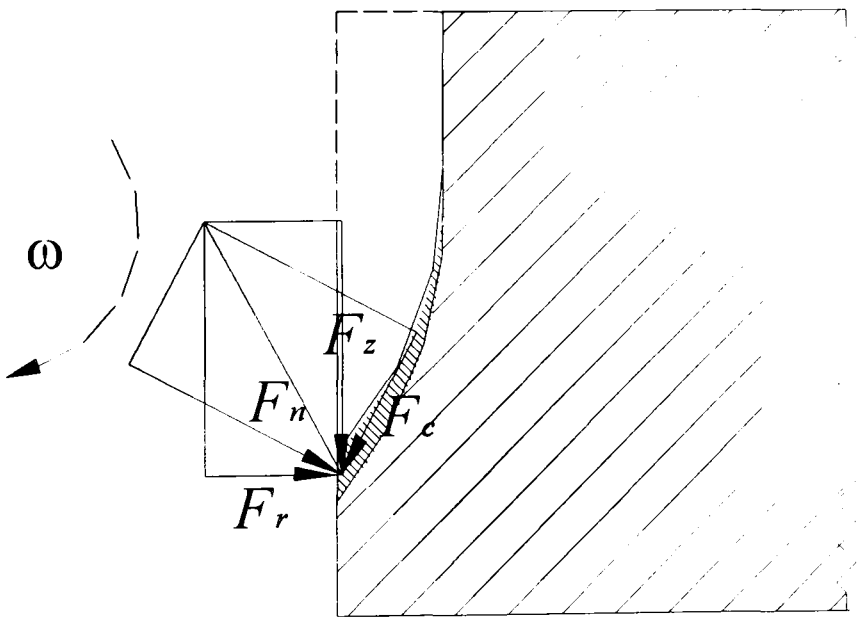

Figure 6.12: Cutting forces components at mid-face

At the early stages of cutting, the tangential cutting force component is again of a alternating nature as in full depth of cut, but the force magnitude is much smaller as less metal is being removed. However, the radial force component has a different behaviour at this stage, as the peak value (for the reference tooth as well as the other teeth) is very positive, implying that the hob is 'drawing' the gear blank towards it. This is because all the cutting forces are then at points near the blank surface, where the cutting velocity has a large radial outward component.

The vertical force component behaved much as was expected, with a peak value occurring at the reference tooth and for adjacent teeth.

Figure 6.13 shows the gear cutting forces components, predicted and measured, at an early stage of the cutting process, after about 95 revolutions of the hob. At this stage the hob has started to remove some metal, is not yet at full depth of cut, and there are only few gashes of the hob are effectively removing metal.

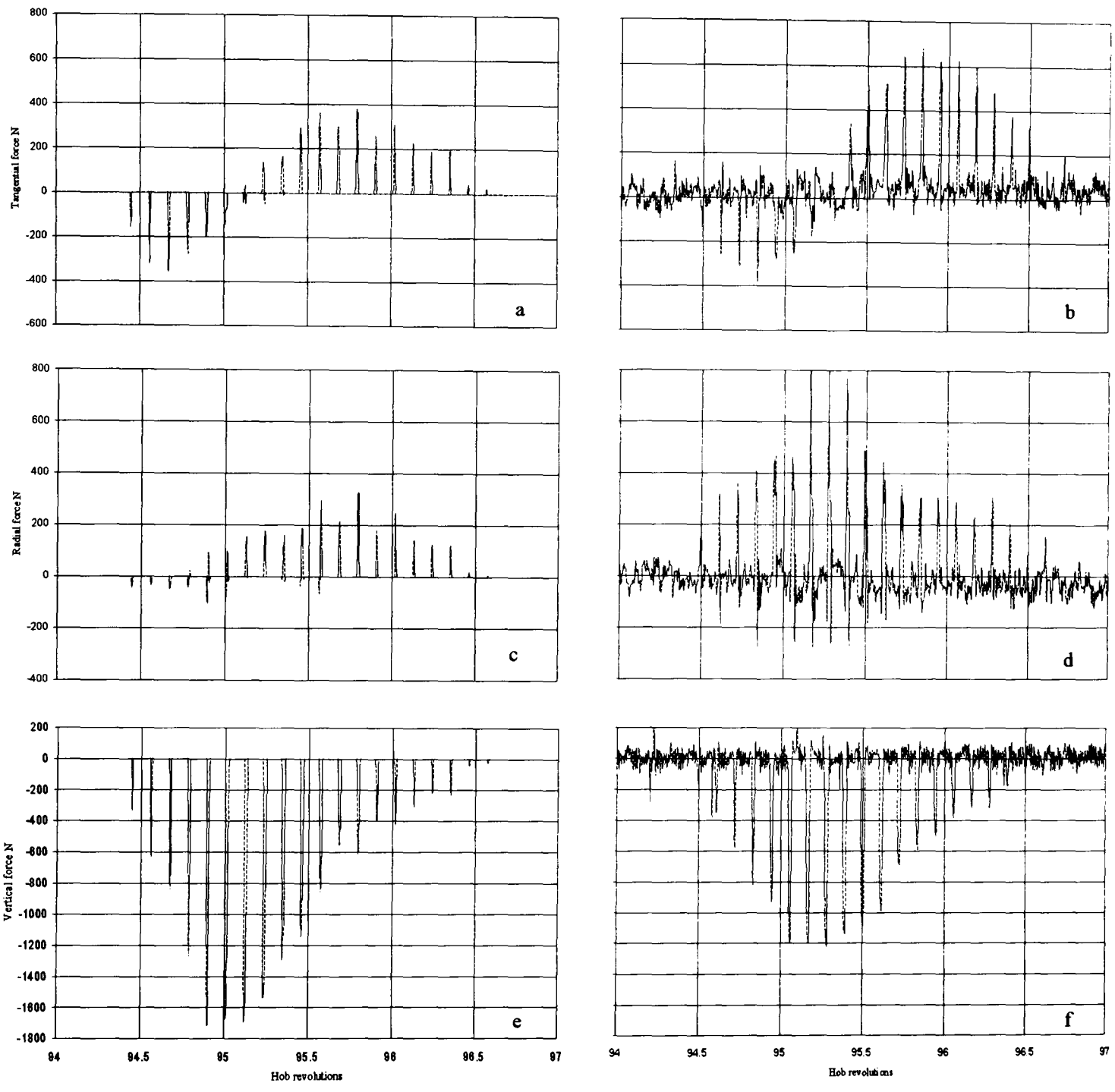

Figure 6.13: Comparison between theoretical and experimental results for a single tooth space (at start of cut)

Figure 6.14 shows the components of the cutting forces at a late stage of the process, i.e. after approximately 1200 revolutions of the hob. The tangential force component, fig 6.14a, b, maintains its alternating nature, but it is very

noticeable that the magnitude of the predicted tangential force is somewhat lower than that of the actual test data, particularly around the location of the reference tooth. This is because less cutting is occurring on the tooth tip, (compare figures 6.15 and 6.12). The radial force component, fig 6.14c, d, is very similar to that at mid face, but the magnitude of the predicted force is somewhat lower than the actual test data. There is good correlation between predicted and actual results for the vertical force component.

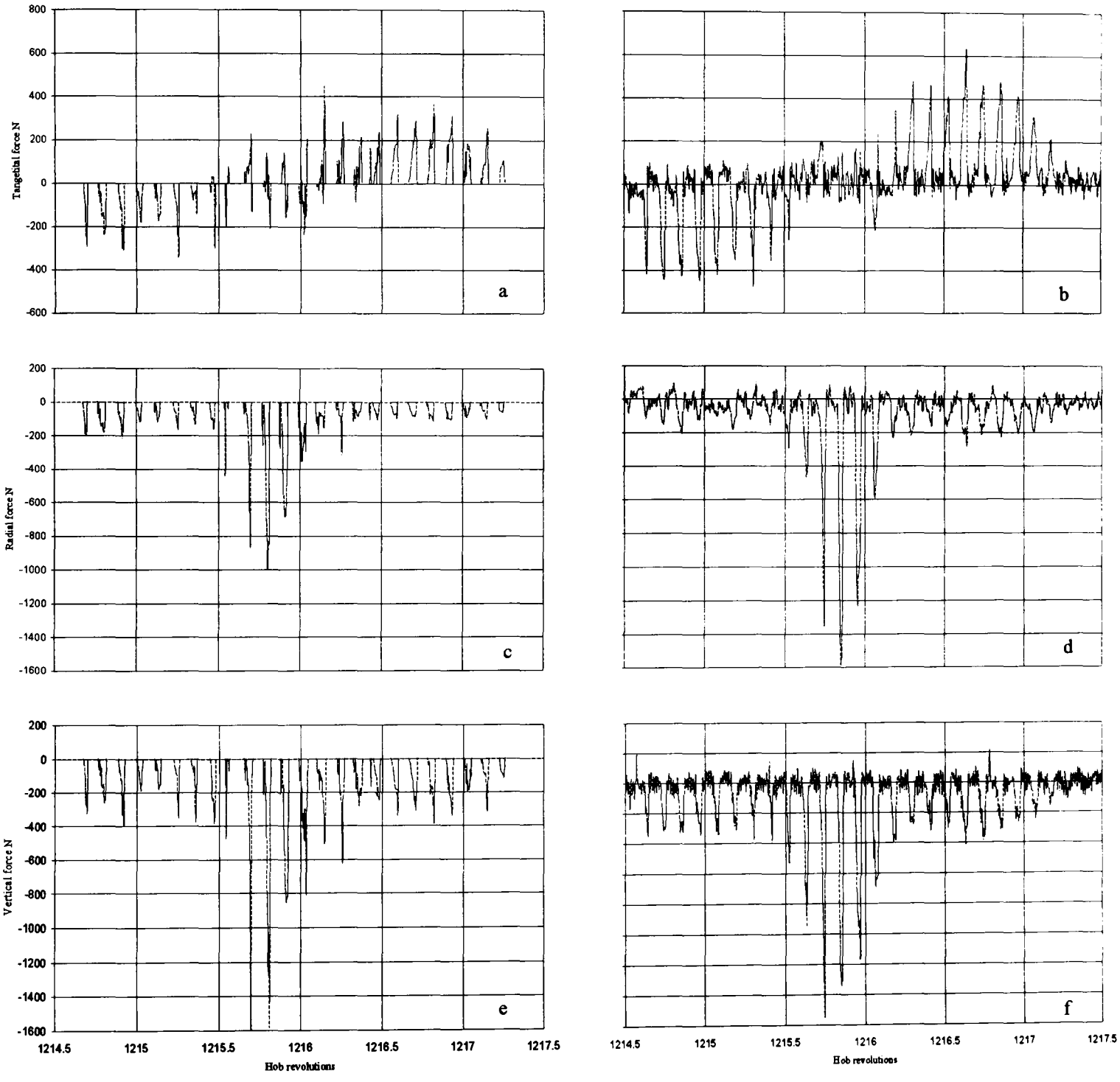

Figure 6.14 Comparison between theoretical and experimental results for a single tooth space (at end of cut)

In analysing the figures 6.11, 6,13 and 6.14, it is clear that both tangential and vertical force components behave in almost the same way from the beginning to the end of the process, but with different magnitudes, which depend on depth of cut. The radial cutting force component, though, has a unique behaviour, as this force has a positive value at the start of cut, for all the active gashes, as the hob 'pulls' the gear blank towards it. However this force changes direction when the hob depth increases. This sign changes does not apply for all teeth in contact with the gear blank. The sign change is only applicable to the reference tooth and adjacent teeth, as at mid face. The sign remains negative for all teeth, at later stages of cut, as shown, due to 'the inherent characteristics of the change in chip formation on the tooth flanks in the individual hobbing positions during the hob rotation.' [König]. During the early stage of the cutting cycle the hob is contacting the gear blank only on the tips of the hob teeth, and the tangential force component is negligible.

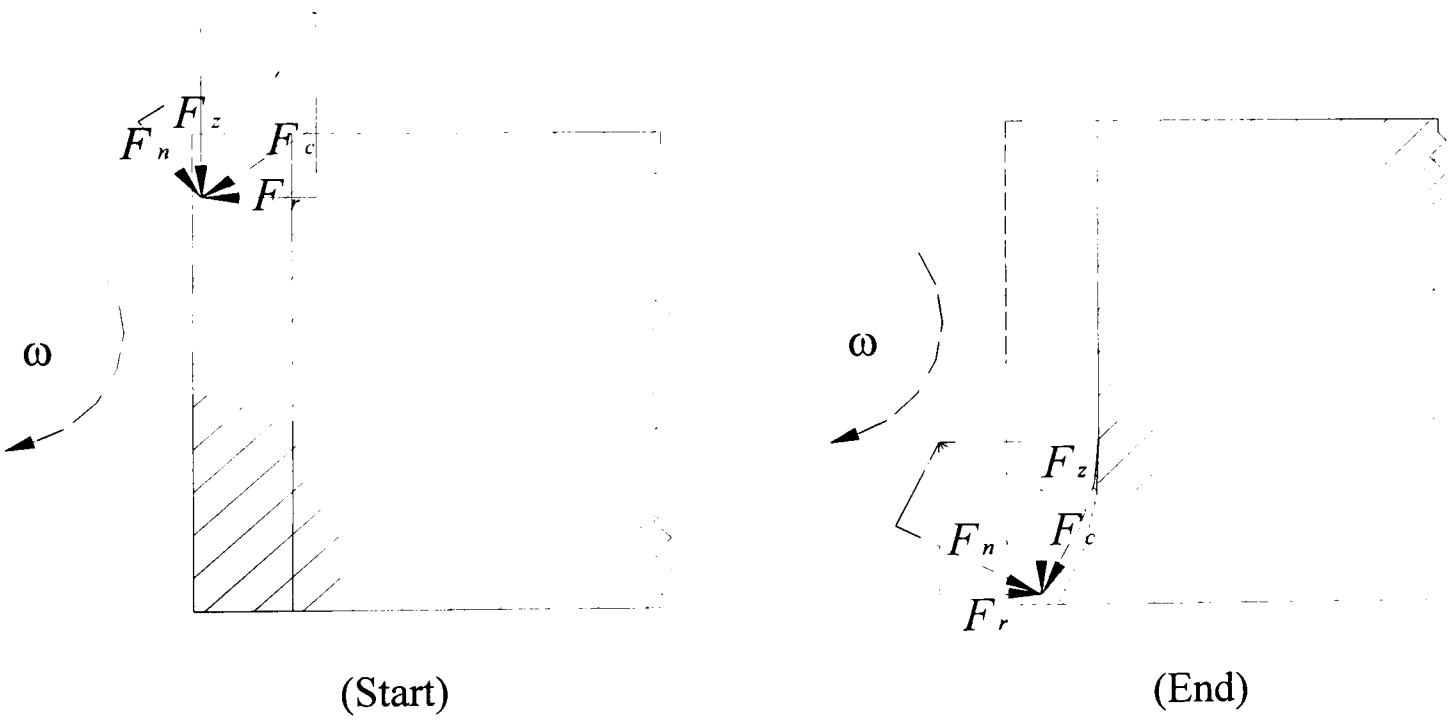

Figure 6.15: Cutting forces components at end and start of cutting

It is also noticeable that fewer teeth remove metal before the reference tooth than after it. This gives the impression that a hob shift is present, although the mathematical model shows the same results with no hob shift. This means that more cuts are made by the teeth which cut after the reference tooth, (see figure 6.8), even though these teeth are only used to shape the tooth space, as the magnitude of the forces shows.

6.3 CUTTING FORCES FOR A FULL GEAR

In normal gear hobbing, several hob teeth cut simultaneously and the forces acting at any instant is the sum of the individual forces acting at that instant on each hob tooth. The resultant force varies cyclically as each tooth space passes through the cutting region.

The single tooth space results discussed in pervious section show that multiple hob teeth are needed to generate a particular space. These teeth contact the tooth space at different times, with z_g teeth are cutting in this tooth space for every hob revolution. As a result, as shown previously, cutting in each tooth space (at full depth) extends over about three hob revolutions, during which time three adjacent tooth spaces will pass through/enter the cutting zone. It was thus assumed that, at any given time (represented by m), up to three teeth may be cutting simultaneously: one near the start of its cut cycle, one near mid-cut. and one near the end of its cut cycle. The total cutting force at time m will be the vector sum of the forces acting on these three teeth.

This was explained in 4.10.3, using equation 4.60, which could be simplified (for the tangential force for example), to

$$\sum_{m=0}^{\max} F_{total} = F_{res}(m,1) + F_{res}(m + m_{step},1) + F_{res}(m - m_{step},1)$$

where m_{step} is the time interval between two successive tooth spaces. In order to simplify the calculation of the total cutting force, use was made in equation 4.60 of the fact that the cutting force variation from one tooth space to the next is only slight, (this was verified theoretically by examining cutting in a number of 'adjacent' tooth spaces using the single-tooth model). As a result, the instantaneous cutting forces in an adjacent tooth space are simply $\bar{F}_{res}(m \pm m_{step})$. When the central tooth force is $F_{res}(m)$, provided the forces are all defined in the same fixed axis system 2.

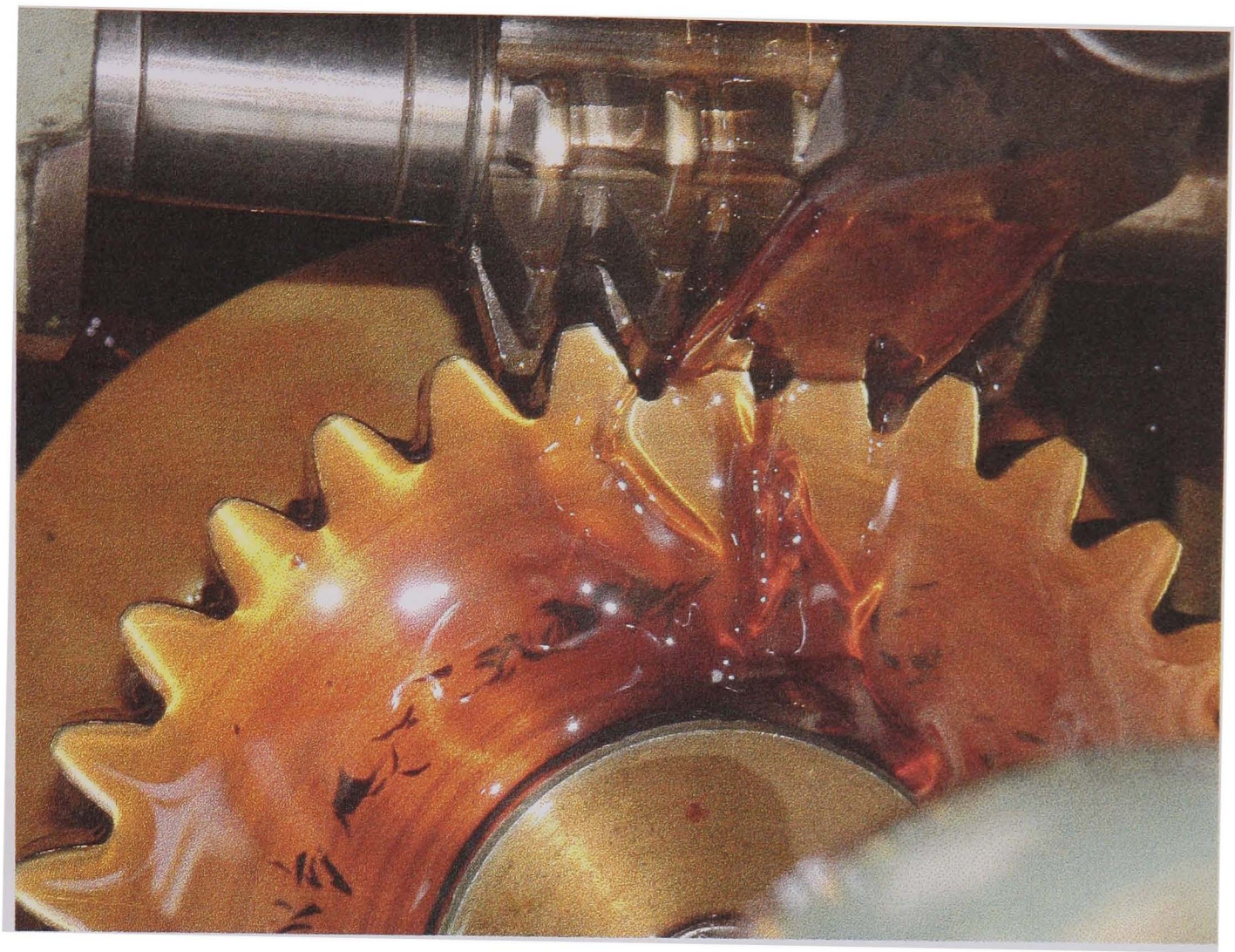

Figure 6:16 Full gear being cut

Section 6.2.2 discussed the measurement of cutting forces acting on a single tooth space. The same procedure was needed for a full gear, but with the forces and the gear positions recorded continuously. The PMAC data gathering facility was used to simultaneously store the axis position information, as well as the force data, and then written it to disk. However, because of the amount of data to be stored, an interrupt driven subroutine was written to optimise the storage of the data. The limited amount of on-board memory restricted the amount of data that could be held in memory at any time, so this required periodic transfer of data from memory to disk. During file transfer a limited amount of data was lost, but this did not inhibit the performance of the system, or restrict the value of the data stored. The parameters of the full gear (gear material, number of teeth, etc.), were all the same as those used in the single tooth-space cutting tests. Figure 6.16 shows a full gear being cut, near the end of cut.

Figure 6.17 shows the gear cutting forces acting on a full gear at mid face, after approximately 700 revolutions of the hob. The cyclic nature of the measured cutting forces is very noticeable, again justifying the assumption that the tooth-

space to tooth-space cutting force variations can be neglected. The agreement between the measured and the calculated components in regard to their general trend and magnitude is clearly evident. The deviations in the forces again can be attributed to the complex chip flow encountered in hobbing, especially near the tip of the tooth. In this region interference of chip occurs, which leads to an increase in the specific cutting forces. As chips flowing in different directions collide with each other, this will certainly influence the cutting forces acting on the hob teeth rake faces [Suzuki]. This phenomenon could not be included in the model since quantitative data is not available.

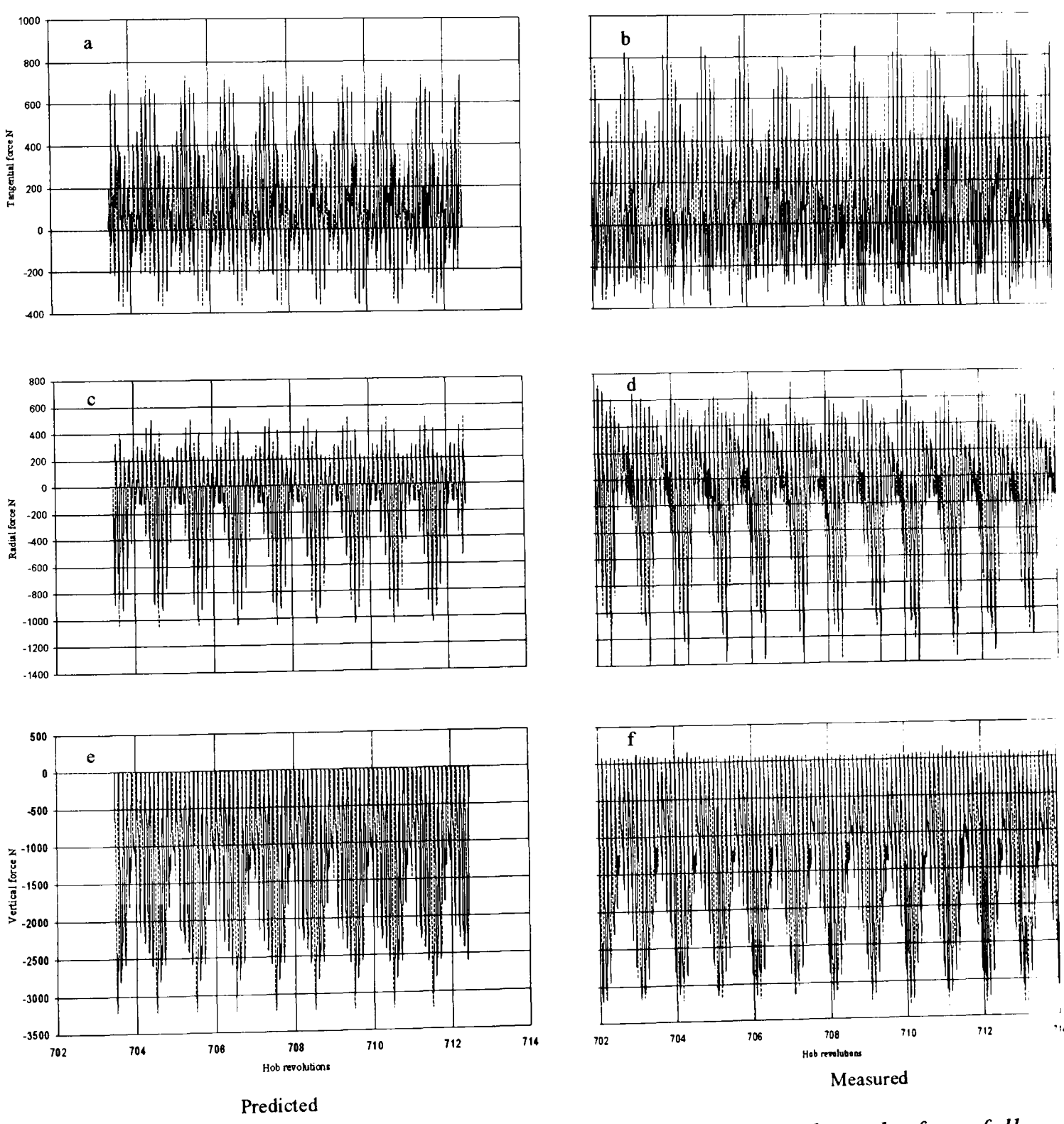

Figure 6.17: Comparison between theoretical and experimental results for a full gear (at mid face)

A further possible source of error is the fact that the normal cutting force component F_n is very sensitive to tool bluntness, especially at the shallow depths of cut that occur on the flanks. This could be the reason for the lower accuracy of the predicted F_x values which are mainly due to the tangential components of F_n.

Figure 6.18 shows the nature of the cutting forces acting during one full hob revolution, at one tooth space, and shows that the general behaviour is similar for all forces. It is very noticeable that when the hob row enters the tooth space it is cutting gradually using its incoming flank before suddenly leaving the tooth space. This process is repeated for the next row, but at increased depth, as cutting gradually involves the incoming flank and the tip but when the cutting reaches the reference tooth row. Here cutting is obviously taking place along the tip and both flanks. However, when the hob leaves the tooth space using its last rows the process is almost mirrored along the reference tooth, since only the tip and the outgoing flank are cutting, although later only the outgoing flank is removing metal.

From Figure 6.18 there appears to be an anomaly between the intuitive peak force values, which were expected to occur when the reference position coincided with the $cos(\phi_0)=1$, as shown by point A. From these results it can be observed that the peak forces do not coincide with point A and in fact a phase shift of approximately 40°, i.e. one full gash. The reason for this discrepancy is due primarily to difficulties aligning the reference tooth exactly at mid face position. As expected the model however does not exhibit the phase shift.

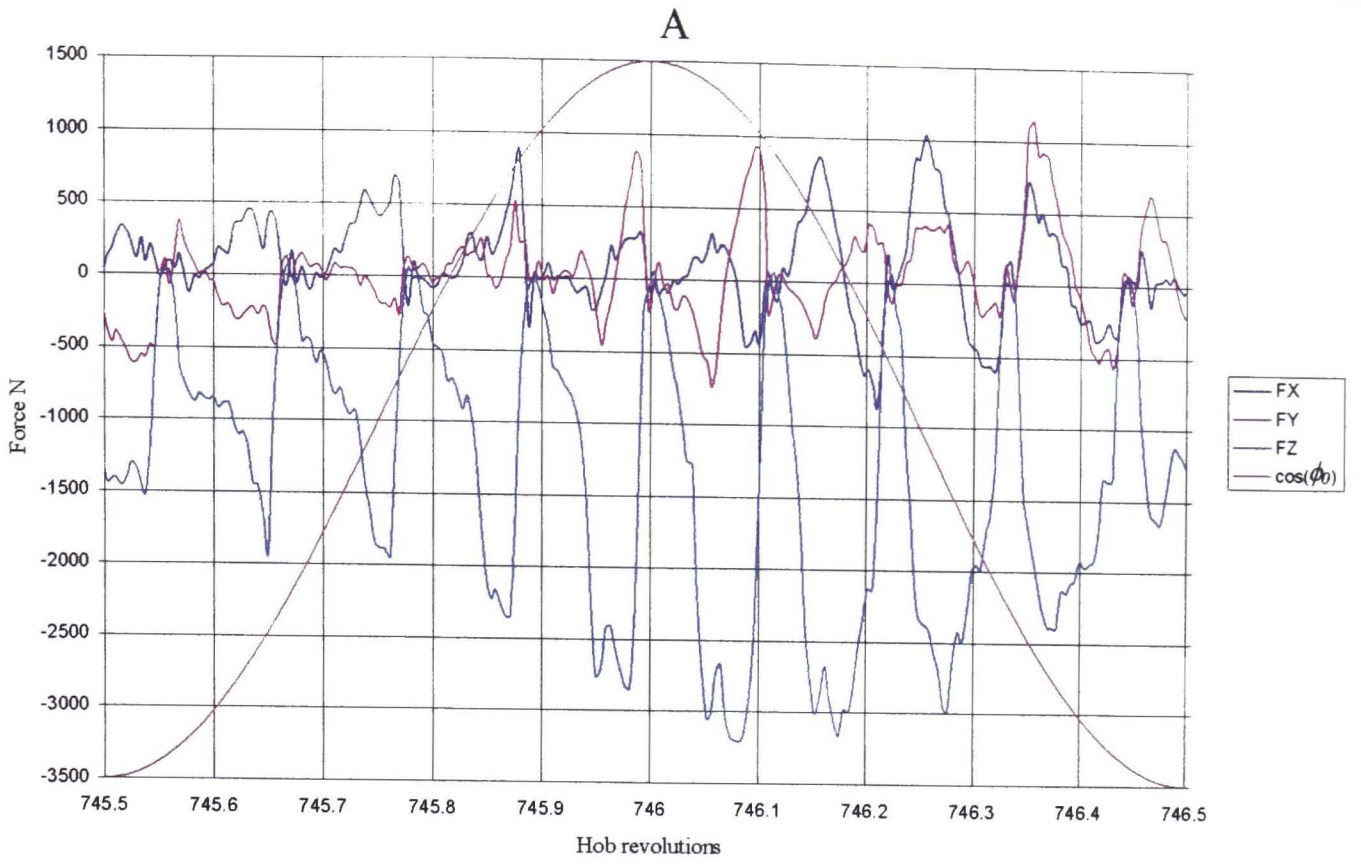

Figure 6.18: Cutting force for a full hob revolution (measured)

(Datum at No 746)

6.4 SUMMARY

The principal aim of the project was to develop a model, which was able to accurately predict the magnitude and nature of the cutting forces in the gear hobbing process. This has been achieved with some success. The predicted forces were estimated by calculating the instantaneous chip cross section produced by each passing gash in a particular tooth space. Experimentally derived results have also been obtained, from which it was possible to draw some good correlations. The actual cutting forces in a single tooth space as well as a full gear have been obtained. These results have in the opinion of the author shown good agreement with the forces theoretically predicted for both single tooth and full gear results.

CHAPTER SEVEN

CONCLUSIONS & RECOMMENDATIONS

7.1 CONCLUSIONS

The nature of the cutting forces in the hobbing process has been thoroughly investigated both theoretically and experimentally, as explained in the previous chapters. A Churchill PH1612 hobbing machine was used for the experimental part of the investigation. The prototype NC control system was significantly modified to allow full CNC control to be established via a PMAC multi-axis motion controller.

The machine was retrofitted with a specially designed 3-axis dynamometer with which to measure the cutting forces. The cutting forces were measured, in real-time, during the hobbing process, and several special gears were cut, including a single toothed gear as well as a number of full gears.

The kinematics of the hobbing process was also studied, and a theoretical analysis carried out in order to predict the instantaneous chip-thickness as well as the cutting forces. A MATLAB program was written and a simulation of the cutting process made. The cutting forces acting on a single gear tooth space were computed, and compared with those produced experimentally. The model was also able to predict the magnitude of the cutting forces during the generation of a normal full gear, and again these were compared with actual cutting data.

Whilst PMAC has the ability to operate with low-resolution encoders, which can be increased in resolution by a factor of four, the use of higher-resolution encoders might well have improved the performance of the control system. The control software was written to facilitate the interrupting of the cutting process at

any time, with the added functionality of being able to resume operation again even when the machine is switched off, as all motors can be homed and datumed, at anytime. This was a considerable improvement on the original MIPROC controller, which could not do this.

Close qualitative agreement between the measured and theoretical cutting forces has been obtained for all three components when cutting a single tooth space. There is also close quantitative agreement for F_y and the main cutting vertical force F_z, with the peak values (in both directions) within 10%, in spite of measuring errors of order ±50 N due to noise.

The tangential force component F_x shows the greatest discrepancies. This value is mainly influenced by the value of the normal cutting force F_n, particularly at low chip thickness (for which the effect of tool bluntness are greatest). Inclusion of a 'tangential' component of the cutting force (parallel to the cutting edge) might also be worthwhile, even though the effective side rake angle is small at all points.[Abood *et al*]

The cutting forces were measured for spur gears, for both single toothed and full gears. The cutting forces results give a clear picture at the generation process in gear hobbing. The forces for the single toothed gear show that the force acting vertically on the gear blank is the most significant force. The tangential force acts as predicted, in an alternating manner. The radial cutting force is observed to change direction along with process. The peak value is positive at the start of cut, then changes direction to a negative value, reaching a peak value at the mid-face and stays negative. Actually the peak value of all the three forces is reached during the steady state mid-face position, when the hob teeth are in full contact with the blank.

The cutting force behaviour when cutting a full gear is similar to that obtained when cutting a single tooth space. Again the vertical component of the force acting on the gear blank is the most dominant. The tangential force is always positive and it looks like a repeated force. The radial force behaves similarly to a

single tooth, and begins positive before changing direction to a negative force as the hob bites deeper into the metal and stays negative till the end of the process.

7.2 RECOMMENDATIONS FOR FURTHER STUDY

Several different sizes of spur and helical gears were cut on the machine, using both climb and conventional hobbing techniques, although the emphasis was only made on machining spur gears using conventional hobbing. The test results show that the feed rate has a significant effect on the value of the cutting forces, as expected, and that cutting forces increase with a corresponding increase of the axial feed rate. It would be useful to study the effect of the speed of the hob on the cutting forces. Feed rate has also a great effect on the tooth surface profile, as better quality surfaces are resulted when machining with a low feed rate.

Results show that the sharpness of the cutting tool, the hob, has a significant effect on the cutting forces, these being markedly reduced after the hob was sharpened. Using hob shifts during the hob process might have a great effect on the cutting forces and the quality of the tooth profile.

Although the software also predicts the hob torque as well as providing data for predicting hob wear intensity at each point on the cutting edges, tool wear was not estimated at this time. Nevertheless the functionality has been included in the model for future work. The prediction of the cutting forces will also permit the effects of elastic deflections of the system on workpiece accuracy to be investigated, possibly using finite element analysis.

The software can also be readily adapted to investigate the effects of many other parameters and to study their effect on the hobbing process. These would allow the effect of rake angle and the use of a true involute tooth form on the hob teeth to be investigated in the future. The forces measured and estimated were all for spur gears. The model can be easily modified to investigate the nature of the cutting forces when machining helical gears, with different helix angles. Blank material, size of the gear blank, and the number of starts on the hob could also be investigated and study their effect on the cutting forces.

REFERENCES AND BIBLIOGRAPHY

Abood, A.M. Bicker, R. and Pennell, J.A. 'An Analysis of Cutting Forces in Gear Hobbing.' International Conference on Gears VDI-Berichte.1 Nr. 1665, March 2002.

Adam, J.I., 'Cutting Forces and Power on Gear Hobbing Machines.' Collected Papers on Metal Cutting, Book. 82, Mashgiz, Moscow, 1957.

Ashby, R. 'Design of a 3-axis force dynamometer', DU 1371, University of Newcastle upon Tyne, 1991.

Bashkirov, V. N. and Serova, A. A. 'Computer Aided Calculation of the Chip Section in Spur Gear Hobbing.' Soviet Engineering Research, Vol. 4, No. 1 pp 69 -71. 1984.

BGA 'Teaching Pack on Gear Technology', May 1992.

Bhattacharyya, A. and Deb, S.R. 'Mechanics of Gear Hobbing.' Journal of Engineering for Industry Transactions of the ASME, Vol. 92, February 1970, pp 103-108.

Bouzakis, K.D., Kambogiannis, S., Antoniadis, A. and Vidakis,N. 'Gear Hobbing Cutting Process and Tool Wear Prediction Models.' Journal of Manufacturing Science and Engineering Transactions of the ASME, Vol. 124, February 2002.

Broersma, I.R.G. 'Manufacturing and Testing of Gears.' Technical Publications H. Stam, The Netherlands 1969.

Bruins, G.H. and Dräger, H. 'Metal cutting machine tools & tooling.' Vol.1, Carl Hanser, Munich, 1971.

Buckingham, E. 'Analytical Mechanics of Gears', Dover, New York, 1963.

Chang, S.L., Tsay, C.B. and Nagata, S. 'A General Mathematical Model for Gears Cut by CNC Hobbing Machines.' Journal of Mechanical Design Transaction of the ASME, Vol. 119, March 1997.

Churchill PH Hobbing Machines Manual, Churchill Gear Machines Ltd.

Cluff, B.W.,' Gear Process Dynamics.' 7th edition, American Pfauter Limited Partnership, Illionis, 1992.

Colin, A., Jin-Cheng, D., and Miller, J., 'Retrofitting Machine Tools with Computer Control.' Microprocessors and Microsystems, Vol. 109, no 8, October 1985, pp 378-385.

Cooke, D.A.D, and Wellbourn, D.B. 'Forces in gear hobbing –1, spur gears.' Machinery and Production Engineering, pp 475-477, September 1967.

Cooke, D.A.D, and Wellbourn, D.B. 'Forces in gear hobbing –2, helical gears.' Machinery and Production Engineering, pp 258-261, February 1968.

Cranfield Final Technical Report, 'Development of a Computer Controlled Gear Hobbing Machine', DDMS/160303/Reprort, 1982.

Crockett, J.C. 'Gear Cutting Practice, Machines and Tools.' Machinery Publishing Co. Ltd. 1971, UK.

Deb, S.R., De Sarkar, N. and Bhattacharyya, A. 'Investigation of Modified and Conventioanl Design of Gear Hobs.' Proceedings of the 9th AIMTDR Conference IIT – Kanpur- India, December 1980.

Delta_Tau, 'Programmable Multi-Axis Motion Controller (PMAC)'.

Gimpert, D. 'The Gear Hobbing Process.' Gear Technology, Vol. 11, No. 1, pp 68-44, 1994.

Hannam, R.G. and Andrew, C. 'An Analysis of the geometry of Gear Hobbing.' Proceedings of the Institution of Mechanical Engineers, Vol. 182, Pt. 1, No. 25. 1968.

Honda, F. 'Study on the Hobbing Process', Japanese Government Mechanical Laboratory, Report 42, 1961.

Inozemtsev, G.G. 'Hobs with Changed Cutting Edge Geometry.' Machines & Tooling, Vol. 32, No. 4, 1961, pp 22-25.

Jablonowski, J., 'NC Comes to Gear Hobbing.' American Machinist, vol. 120, part 7, 1976, pp 101-104.

Kalpakjian, S. 'Manufacturing Engineering and Technology.' 2nd Edition, Addison-Wesley, 1992.

Khan, A.A. 'Experimental Determination of Relationship of Cutting Force with Cutting Parameters.' Mechanical Engineering Research Bulletin (Dhaka), Vol.7, pp.29-32, 1984.

Khardin, Y.P. 'Cutting forces in hobbing worm wheels.' Machines and Tooling, Vol. 38, Part 2, pp 35-38, 1967.

Kim, D. H., 'Geometry of Hob and Simulation of Generation of the Cylindrical Gears by Conventional or Climb Hobbing Operation', Proceedings of the Institution of Mechanical Engineers, Part D: Journal of Automobile Engineering, v 215, n 4, 2001, p 533-544

König, E., Essel, K, and Witte, L. 'Specific Cutting Force Data for Metal-Cutting' Verein Deutscher Eistenhüttenleute, 1982.

König, W. and Bouzakis, K. 'Determination of the Time Course of the Cutting Force Components in Gear Hobbing.' ASME Paper No. 80-C2/DET-75, 1980.

Koren, Y. 'Design of Computer Control for Manufacturing Systems.' ASME Journal of Engineering for Industry, Vol. 101, No. 3, August 1979, pp 326-332.

Kovar, P.E. 'CNC Basics.' Gear Technology, Vol. 12, No. 1, 1994.

Lancaster, D. 'Active-Filter Cookbook'. Howard W. Sams, Inc., Indianapolis, IN, 1975.

Lichtenauer, G. 'Hobbing of Spur Gears and Helical Gears.' Engineering Manuals, Carl Hurth Maschinen- und Zahnradfabrik, Munich, 1971.

Litvin, FL. 'Gear geometry and Applied Theory', Prentice-Hall, Englewood Cliffs, New Jersey, 1994.

Litvin, FL. 'Theory of Gearing.' NASA Technical Report 88-C-035, 1988.

Milner, D.A. and Raafat, H. 'Gear Hobbing Torque and Power.' ASME Paper No. 78-WA/Prod-33, 1978.

Mitrovič, R. 'Untersuchungen der Zerspankraft beim Wälzfräsen, Unveröffentlichtes Manuskript.' TH Aachen 1974.

Nagafune, S. 'NC Gear Hobbing Machine.' Metalworking Engineering and Marketing. Vol. 4, Part 3, May 1982, pp 72-77.

Nekrasov, S.S. and Saifullin, V. N. 'Hobbing with Large Diameter Multi-start Hobs.' Russian Engineering Journal, No. 6, 1966.

Nelder, J.A. and Mead, R. 'A Simplex Method for Function Minimization.' Computer Journal. 7 (1965), pp. 308–313.

Opitz, H. and Thämer, R. 'Investigations of wear and cutting forces in the machining of gears' (translation) P.E.R.A. Research Report No. 1097, 1963.

Padham, S.S. 'Experimental Investigation of Cutting Torque and Power in Hobbing Process.'M.Sc. Thesis, The University of Aston in Birmingham, 1972.

Pennell, J.A 'Lectures Notes.' University of Newcastle upon Tyne, 1998.

Pfauter, H. 'Pfauter-Wälzfräsen-Teil-1', Springer-Verlag New York, 1976.

Press, W. H., Flannery, B. P., Teukolsky, S. A., and Vetterling, W. T. 'Numerical Recipes'. Cambridge: Cambridge University Press, 1986.

Ramtirov, V. A. and Rashkovich, P. M. 'Program Control Gear-Cutting Machines.' Soviet Engineering Research, Vol. 2, No. 6, 1982, pp 83-87.

Rozenberg, A.M. and Rozenberg, O.A. 'Calculation of Forces Acting in Cutting Ductile Metals', Sverkhtverdye Materialy, No.4, 1987, pp 48-54.

Sakharov, G.N. and Kubark,V.V. 'Forces Developed When Gear-Hobbing With A Generation Motion.' Machines & Tooling Vol. 43, No. 7, 1972.

Severilov, V.S. 'Power Relationships in Gear Hobbing.' Machines & Tooling, Vol. 40, No. 7, 1969, pp 40-43.

Sidorenko, A. K. 'Advances in Gear Hobbing.' Mashgiz, Moscow, 1951.

Sidorenko, A. K. and Adams, J.I 'Gear Production', Mashgiz, Moscow 1961.

Sidorenko, L. S. 'Calculating the Dimension of Chips Removed by the Cutting Edges of a Hob.' Soviet Engineering Research, Vol. 6, No 9 pp 70 -72. 1986.

Sidorenko, L. S. 'Calculation of Cutting Forces in Hobbing Gears.' Soviet Engineering Research, Vol. 12, No. 12, pp. 100 –106, 1992.

Slavîcek, J. 'Stability of hobbing machines.' M.T.D.R. 7th International Machine Tool Design and Research Conference, Birmingham, 1966.

Speyer, K. 'CNC Hobbing : Process, Machine, Control System, Dialog Program.' Landsberg/Lech , Verlag moderne industrie, Germany,1991.

Sülzer, G. 'Bestimmung Der Spanungsquerschintte Beim Wälzfräsen: Determination of the Chip Cross-Section Areas in Hobbing.' Industrie Anszeiger, Vol.96 No. 12, 1974.

Sülzer, G. 'Leistungssteigerung bei der Zylinderradherstellung durch genuae Erfassung Der Zerpspankinematick.' Dissertation TH Aachen, 1973.

Sunajev, B., Gavrilov, P. and Smulevic, A. 'Determination of Cutting Part of Hob and Conditions of Its Economical Utilization.' Production and Exploitations of Cutting Tool, Mashgiz, Moscow, 1954.

Suzuki, T., Ariura, Y. and Umezaki, Y. 'Basic Study on Cutting Forces in Gear Cutting.' JSME International Journal Series C, Vol. 36, No. 4, pp 543-548, 1993.

Terashima, K. and Ueno, T. 'Numerical Analysis of Hobbing in Unfinished Space.' Bulletin of the JSME, Vol. 21, No. 155, May 1978.

Terashima, K., Ueno, T. and Hidaka, K. 'Graphical Analysis of Hobbing in Unfinished Space.' Bulletin of the JSME, Vol. 22, No. 180, June 1980.

Wakuri, A., Ueno, T. and Ainoura, M, 'A Study of Gear Hobbing.' Bulletin of the JSME, Vol. 9, No. 34, 1966.

Watson, H. J. 'Modern Gear Production' Pergamon Press, 1970.

Weck, M. Hurasky-Schönwerth, O. and Winter, W. 'Manufacturing Simulation for the Analysis of the Gear Hobbing Process.' International Conference on Gears VDI-Berichte.1 Nr. 1665, March 2002.

Yang Lin, 'A New Type of Mechanism Scheme for Hobbing Machine and Computer Simulation of Gear Hobbing Process.' Manufacturing Science and Technology for the 21st Century, International Symposium Papers, International Academic Publisher, Beijing, 1994.

APPENDIX A

CONVENTIONAL HOBBING MACHINE TRANSMISSION

The conventional Churchill hobbing machine, Figure A-1, was briefly described in Chapter 5. A more detailed description of the mechanical transmission is given here.

The mechanical transmission for the various motions is illustrated in Figure A-1. The 3-phase, 7.5hp main drive motor is positioned in the top left-hand corner of the machine, and is on a vertical axis. A belt drive and pulley arrangement facilitates three different speed changes, with a tacho-generator used to display the speed on an indicator mounted on the front panel. The coloured lines indicate the transmission paths of the different axes. The blue line indicates the worktable transmission path, the green line the hob transmission path, and the red line that of the vertical feed motion.

Figure A-2 shows the hob shift arrangement, including the flywheel, which was added to minimise the effect on the intermittent cutting action of the hobbing process. Figure A-3 shows the index gearing arrangement, used to change the index ratio between the worktable and the hob, and located in the back of the machine. The mechanical transmission is via a single worm-wheel, which caters for both right hand and left hand hob, achieved by an extra nut in the indexing arrangement.

Figure A-4 shows the feed mechanism for driving the vertical slide. The arrangement is suitable for left and right hand gears as well as both climb cutting and conventional hobbing. A special nut was added for this operation. The feed rate could be changed during cutting, and was applied using an optional vari-feed

system. Figure A-5 shows the differential gearing arrangements, which results in a different range of leads. The arrangement is mounted in the rear column.

Hydraulic actuation is used to control the worktable slide feed, tailstock vertical motion, and hob shift. The system comprises a supply tank, electric motor, pump, relief valves, pressure gauge and oil filter. The worktable dead stop is controlled by two opposed-cylinders and adjusted by rotating a square ended shaft, to adjust the desired depth of cut for both rough and fine cuts.

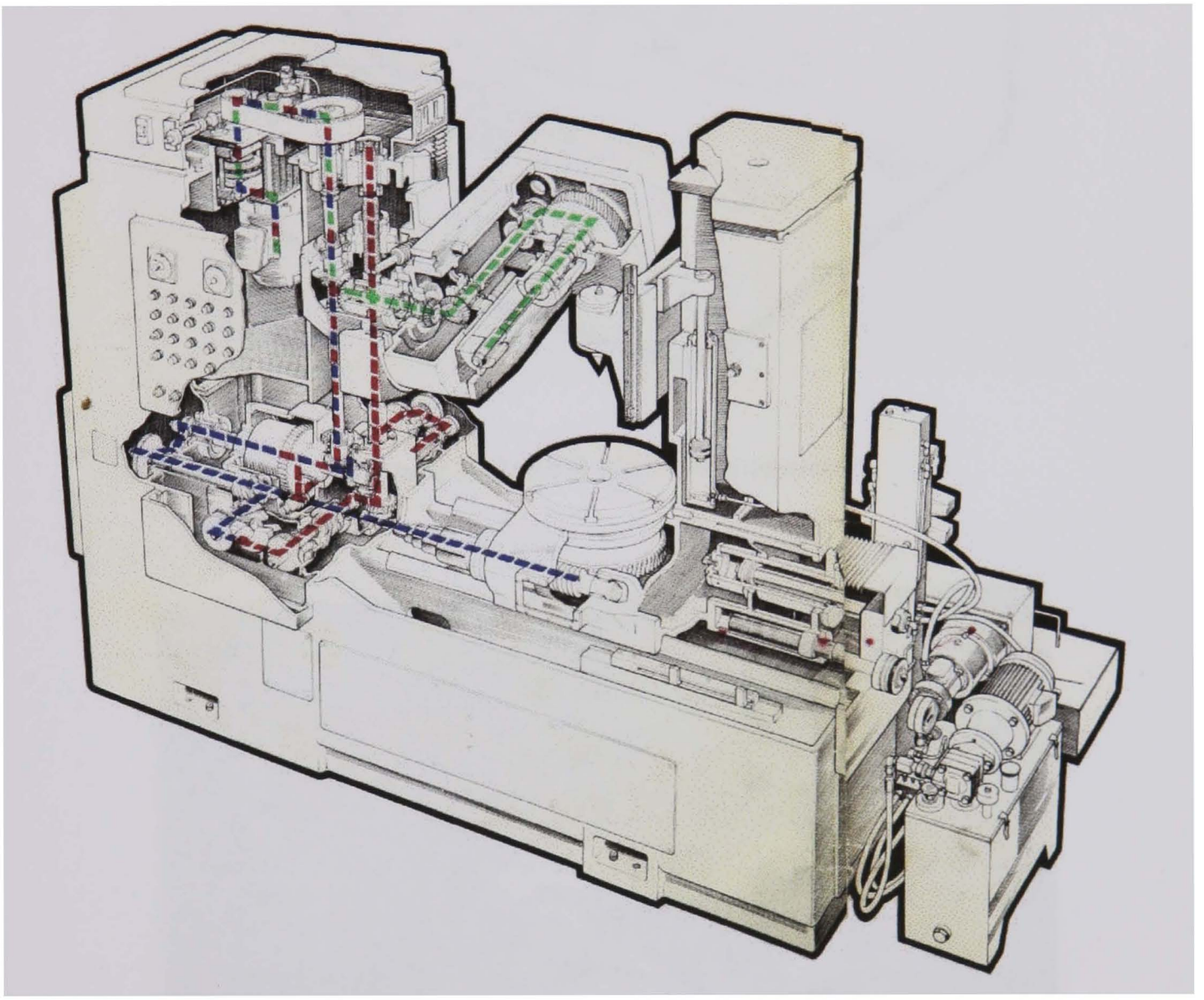

Figure A-1: Conventional Churchill hobbing machine

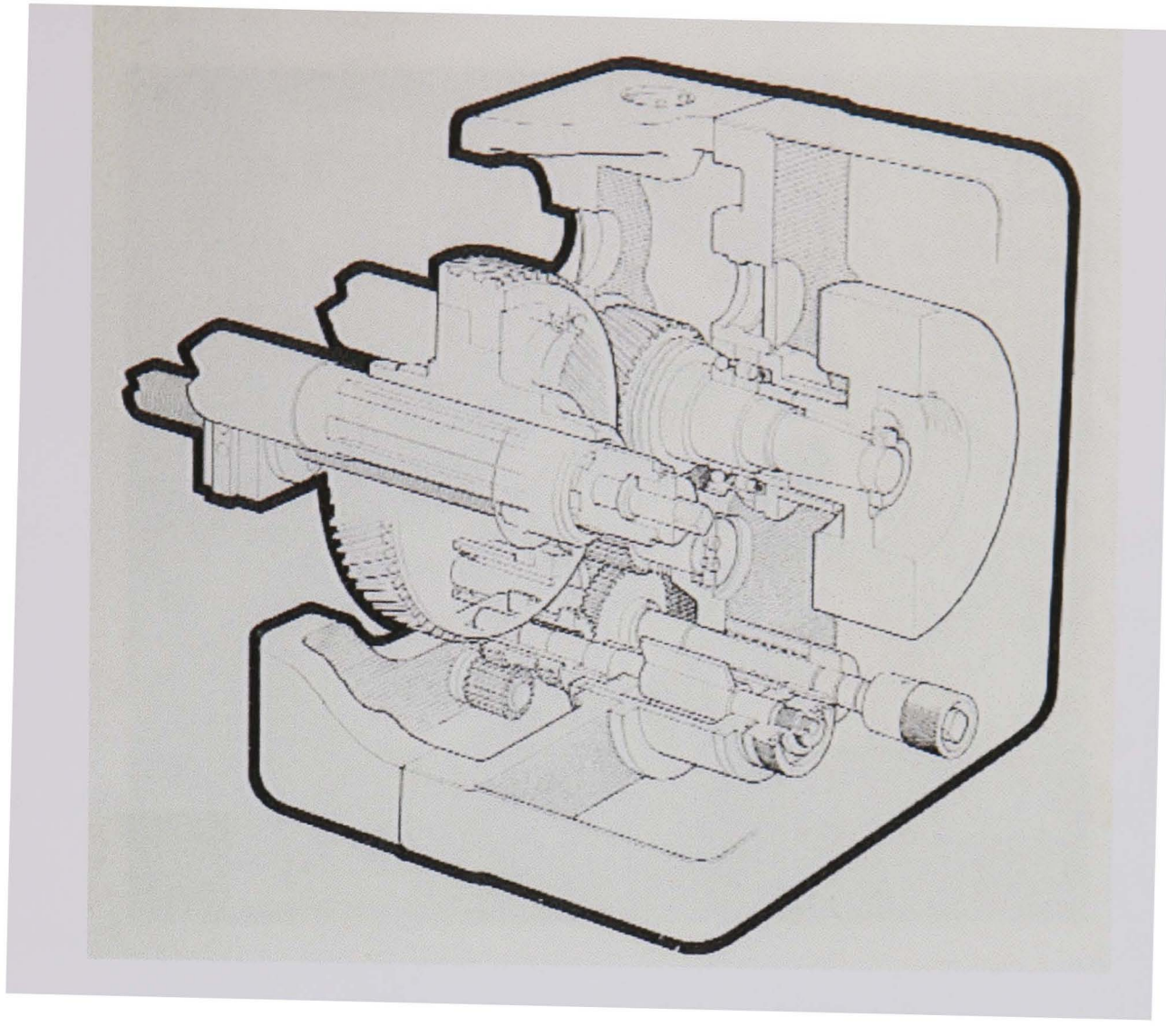

Figure A-2: Hob shift arrangement

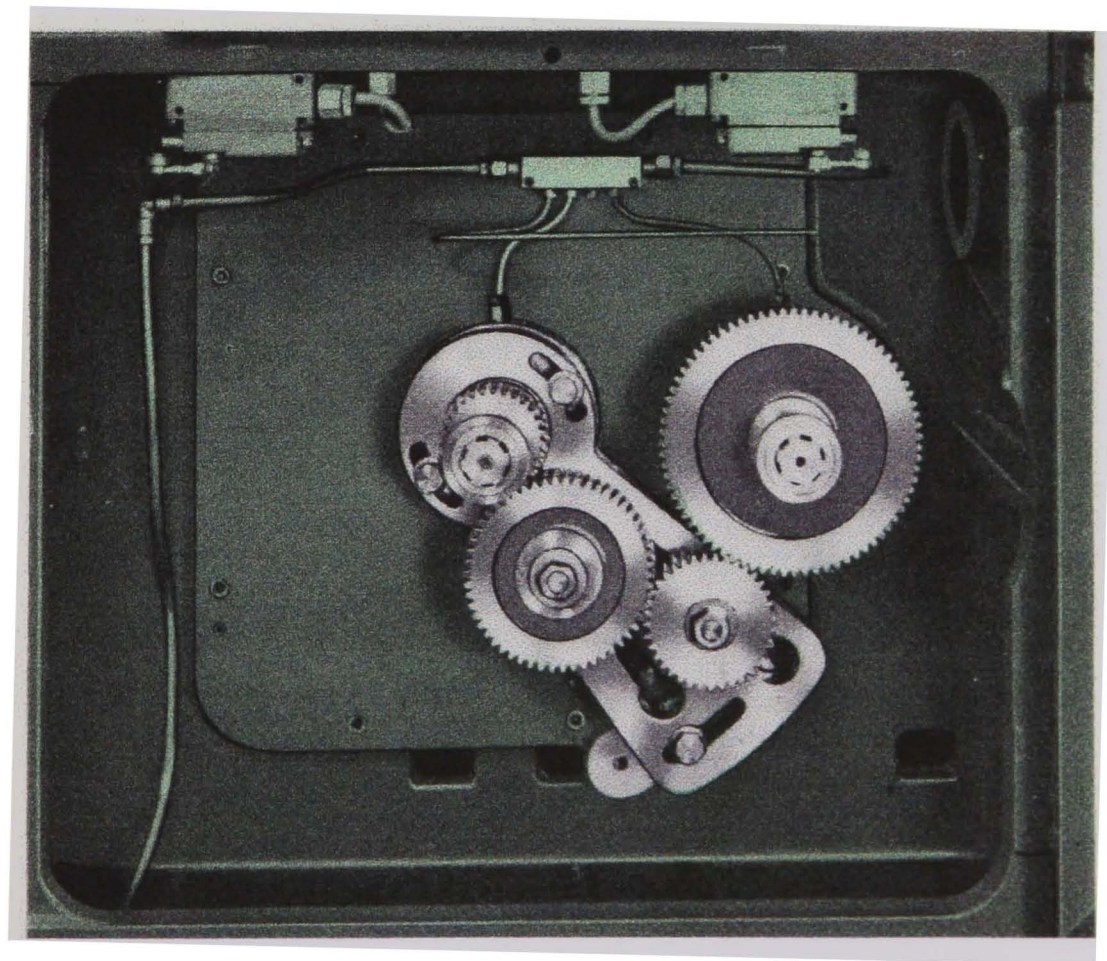

Figure A-3: Index gearing

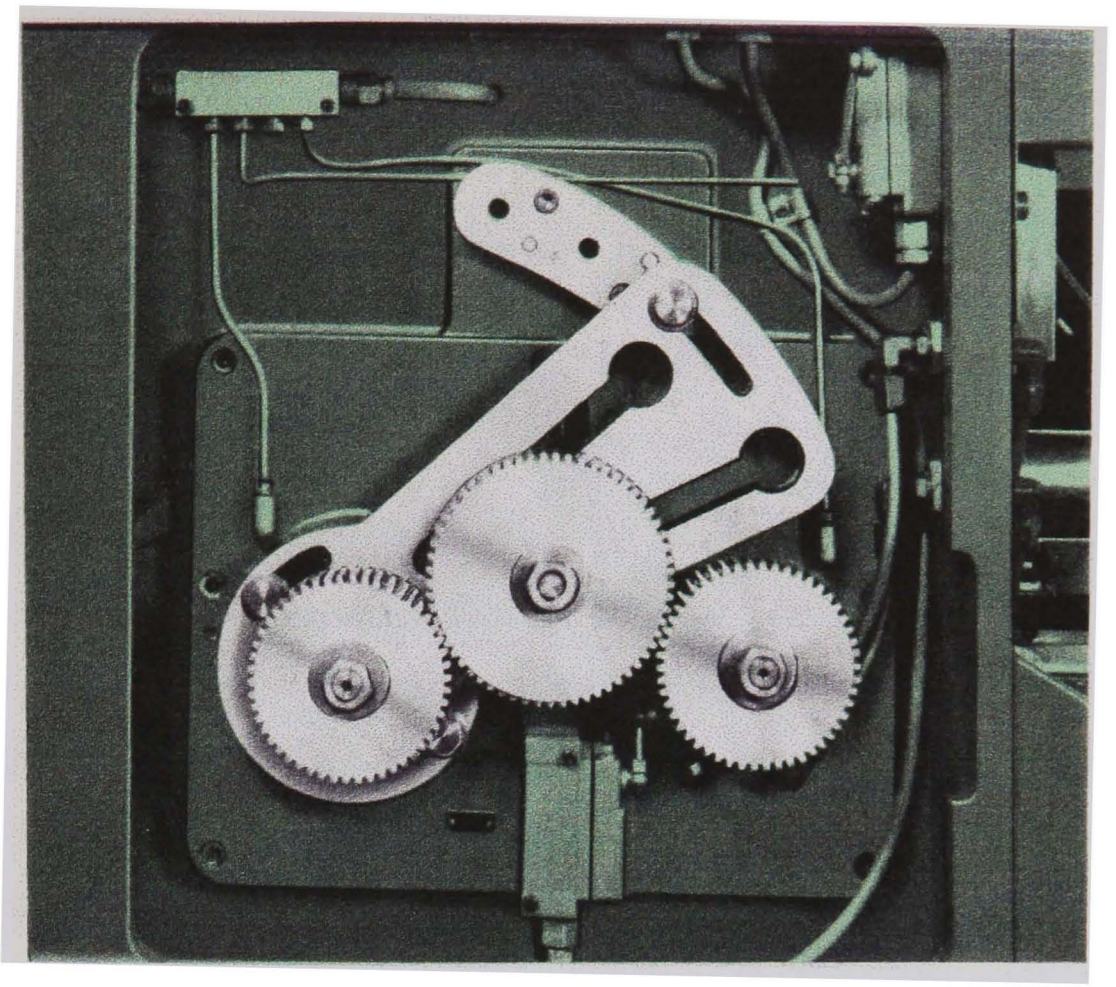

Figure A-4: Vertical drive feed mechanism

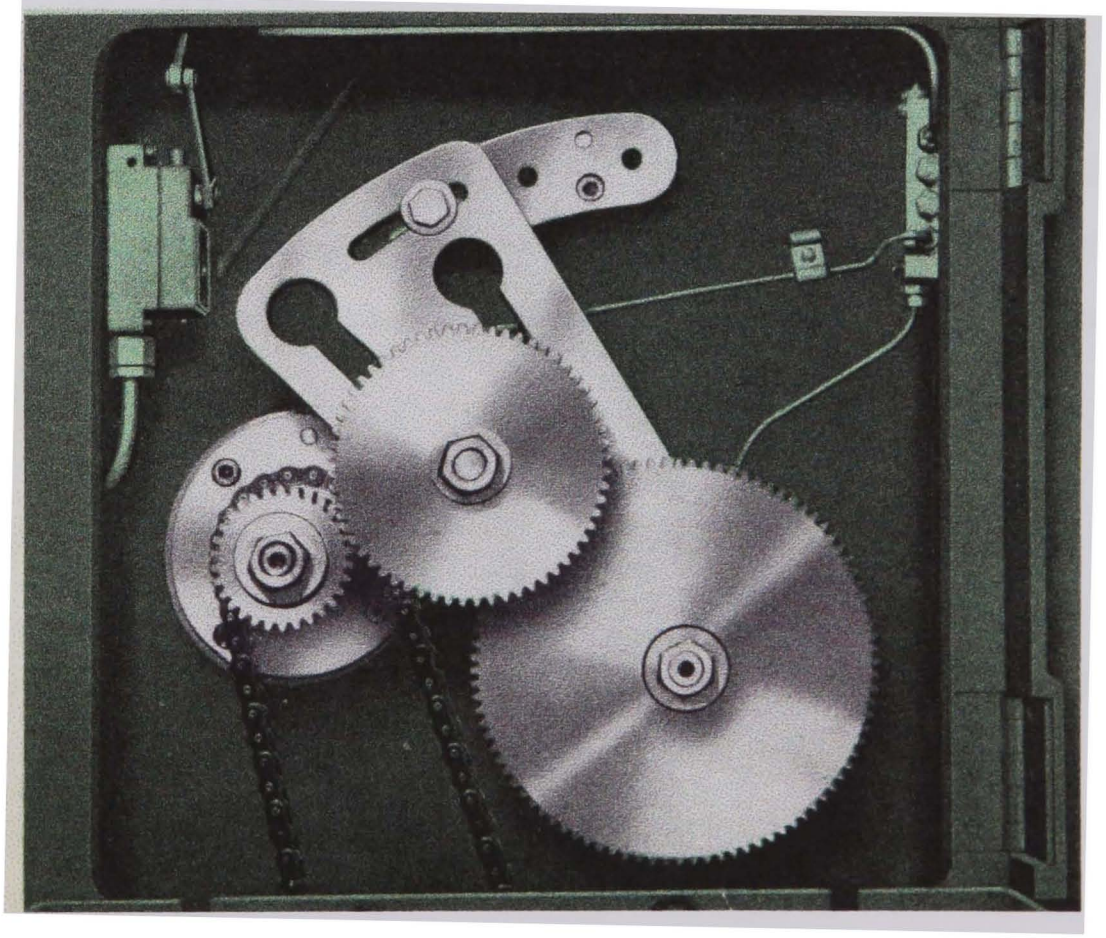

Figure A-5: Differential gearing arrangement

APPENDIX B

PMAC MOTOR TUNING

Fast and stable servo-control system can be achieved with the PMAC multi-axis motion controller. The tuning facility offered with the executive software, PE3.exe, provides an axis tuning capability. There are two main steps in the tuning procedure. The first stage involves the use of a step-response, which allows the user to select the feedback gains for the PID filter parameters. The second stage is the parabolic move, which adjusts the velocity and acceleration feedforward parameter gains in order to minimise the following error.

PMAC axis tuning can be performed either manually or automatically. Manual tuning is achieved by setting the parameters to an appropriate value whereby the operator is able to adjust the step response by studying the resulting plots. Automatic tuning is carried out by PMAC, as it performs multiple and repeated moves and then suggests the values of the system parameters. In this application the manual tuning method was preferred, due to problems with the auto-tuning procedure.

B-1 Step-response

The step response is a commanded position move, which move the motor to a new relative position and then back again over a pre-defined time period. In the step response there are three major PID parameters namely, K_p – Proportional gain *(Ix30)*, K_d - Derivative gain *(Ix31)*, K_i - Integral gain *(Ix33)*. The PID filter equation was explained in Chapter 5.

Figure B-1 and Figure B-2 show the step response of the worktable (motor 2) and the vertical drive (motor 3) respectively. The figures show that both motors are

stable and have very little overshoot, with a relatively fast rise time, and a quick settling time. Considering that the hobbing machine is a large machine with substantial inertia and mass in its moving parts, the PID parameters were adjusted to yield an adequate response. It should be noted that the gravitational mass of the vertical slide contributes to two distinct step responses, depending upon whether the axis is driving up or down, and the eventual chosen parameters were a compromise.

B-2 Parabolic move

Figure B-3 and B-4 show the parabolic move of the worktable and the vertical drive respectively. The parabolic move will show the tracking of the system and the following error between the commanded position and the actual position, which can be adjusted using the velocity K_{vff} *(Ix32)* and acceleration K_{aff} *(Ix35)* feedforward parameters. The figures show a good tracking was achieved for both motors but on the vertical drive, figure B-4, there is an obvious pump in the graph as the motor was moved down but due inertia the motor lagged a bit but recovered so fast.

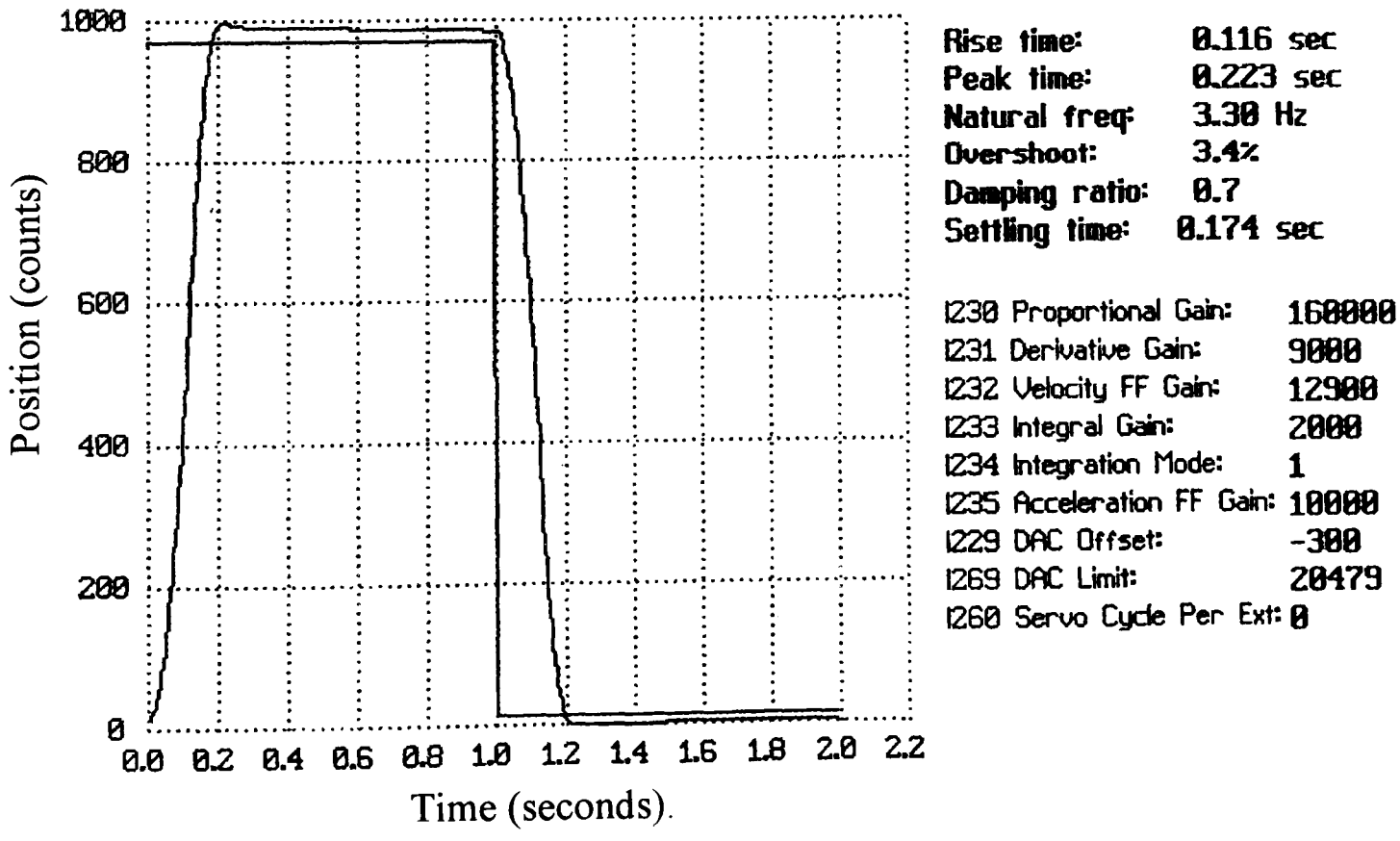

Figure B-1 A step response for the worktable (motor 2)

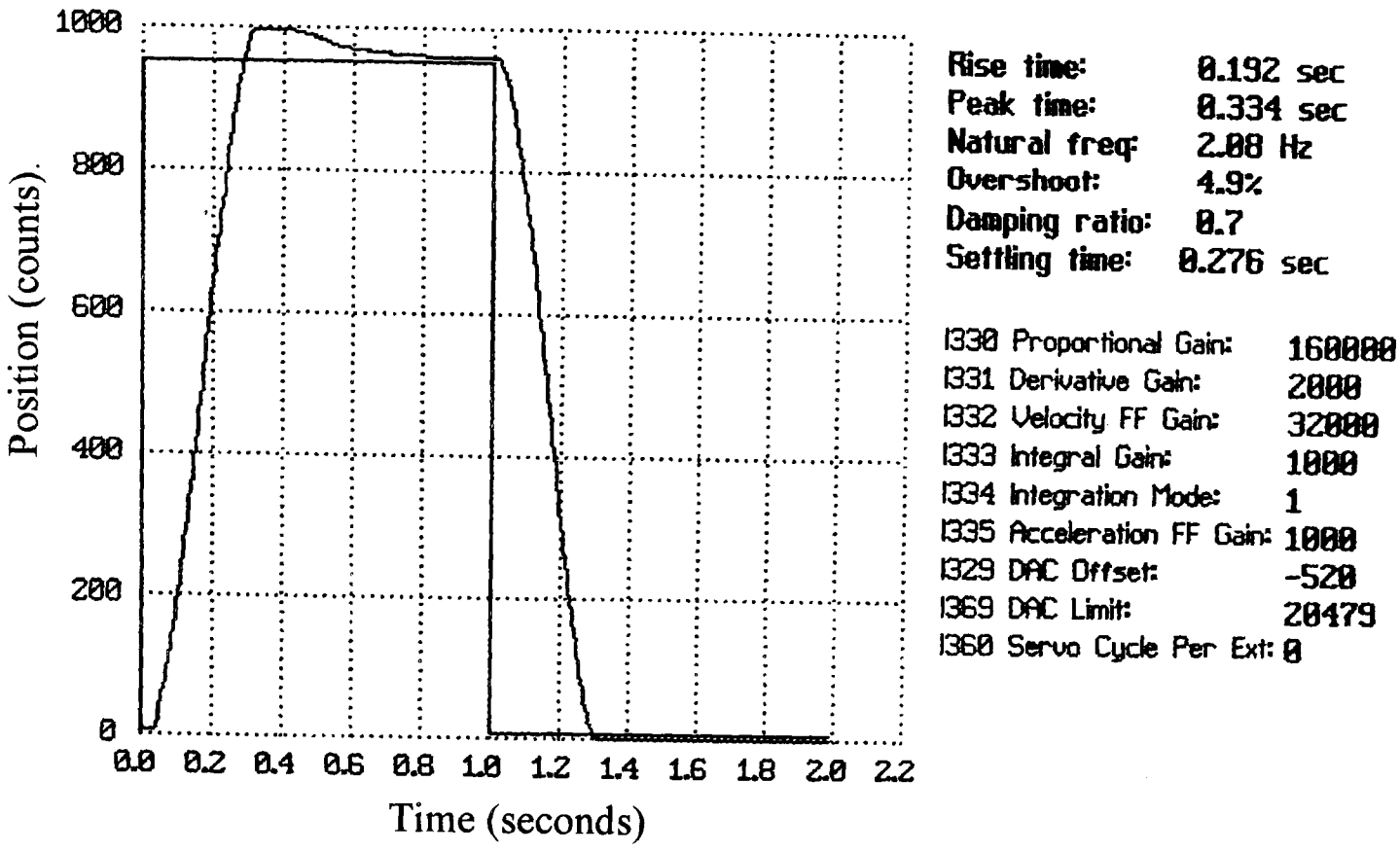

Figure B-2: A step response for the vertical drive (motor 3)

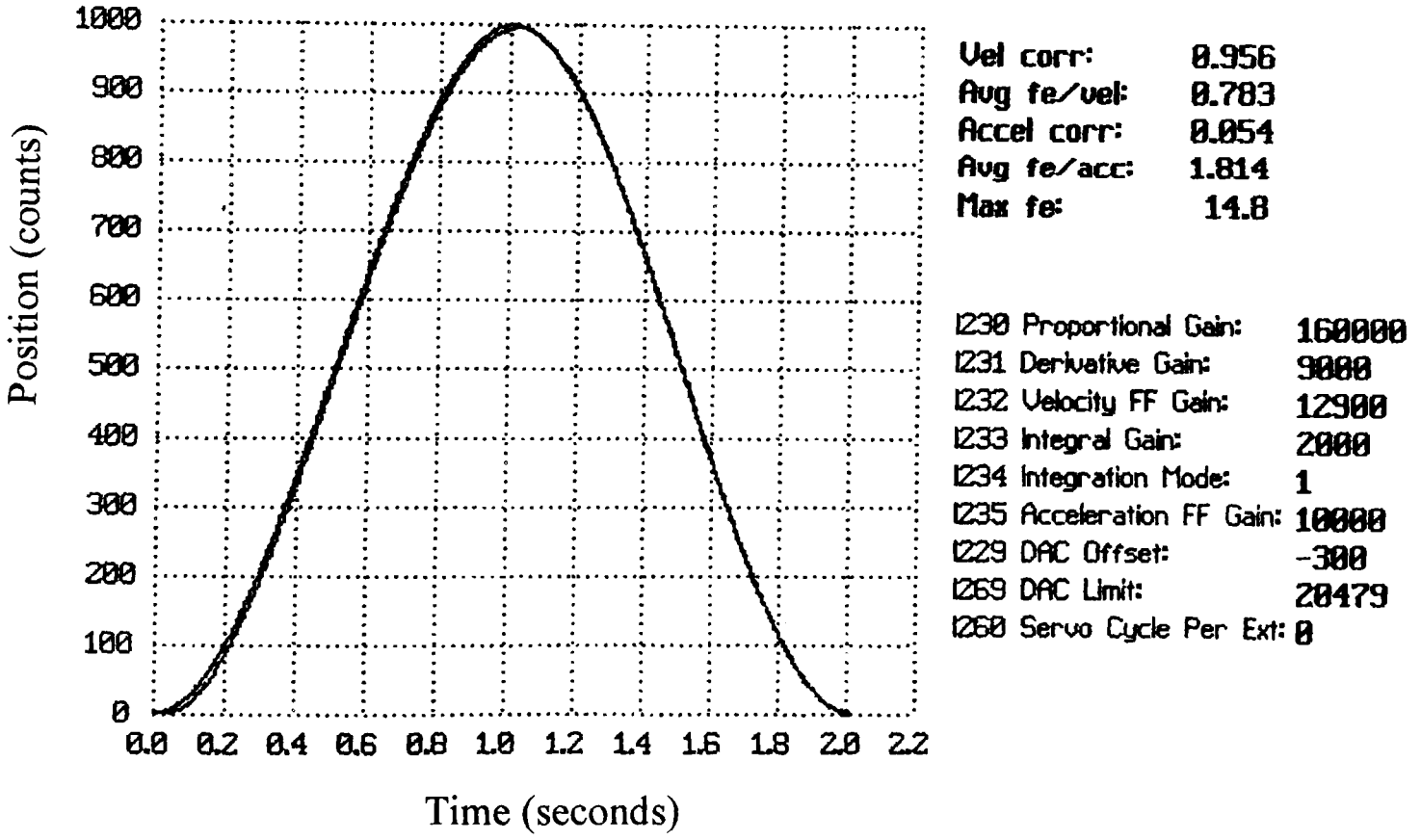

Figure B-3: A parabolic response for the worktable drive (motor 2)

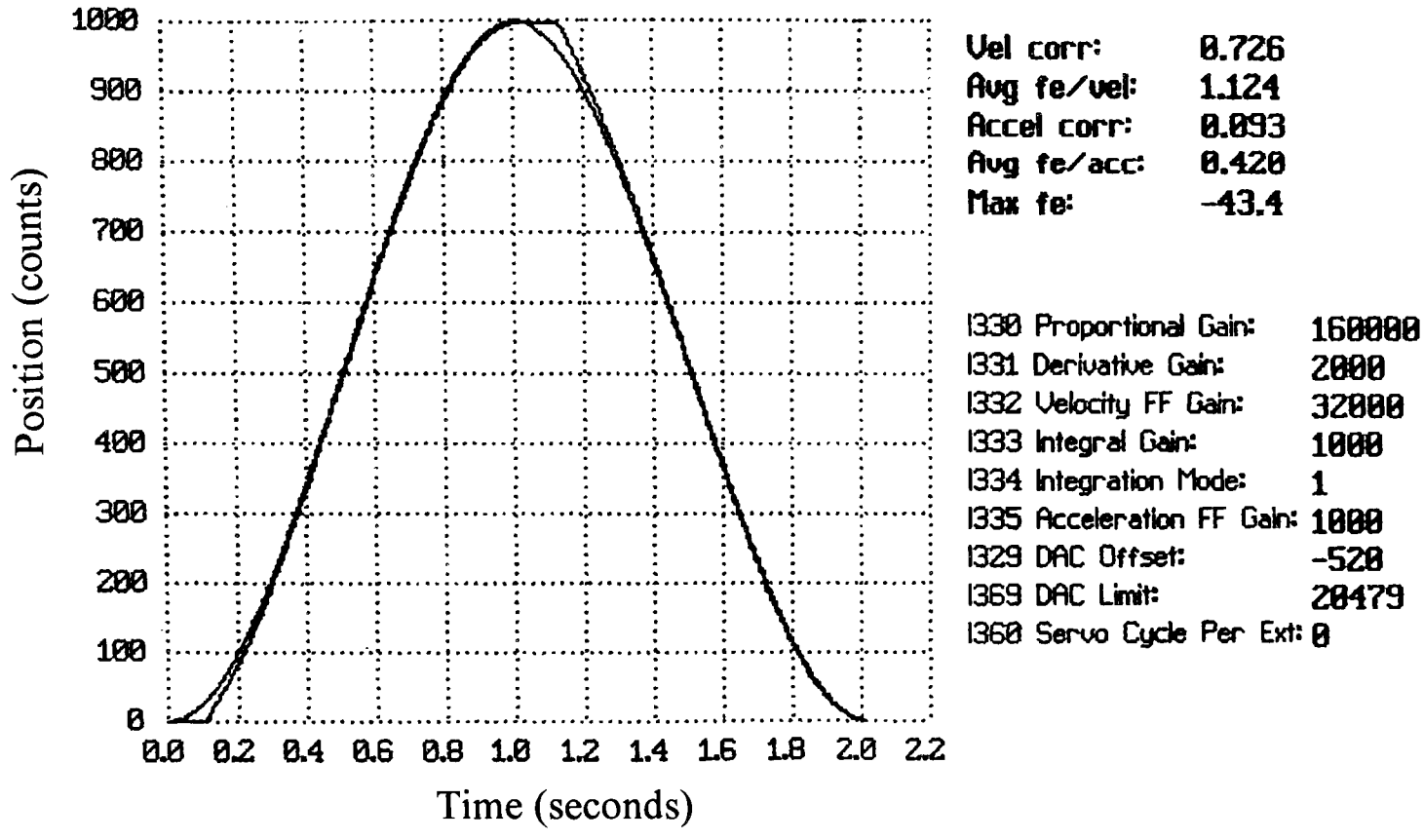

Figure B-4 A parabolic move for the vertical drive (motor 3)

APPENDIX C

FORCE SENSING DYNAMOMETER

In order to measure the cutting forces in the gear hobbing machine a force-transducer was required. Since both the hob and the gear blank are in continuous rotation it was necessary to employ a rotating dynamometer mounted on the worktable, with a telemetry system to transfer force measurements to the data logging facility. It was possible to adapt a 4-axis force sensing dynamometer designed by the Design Unit [Ashby].

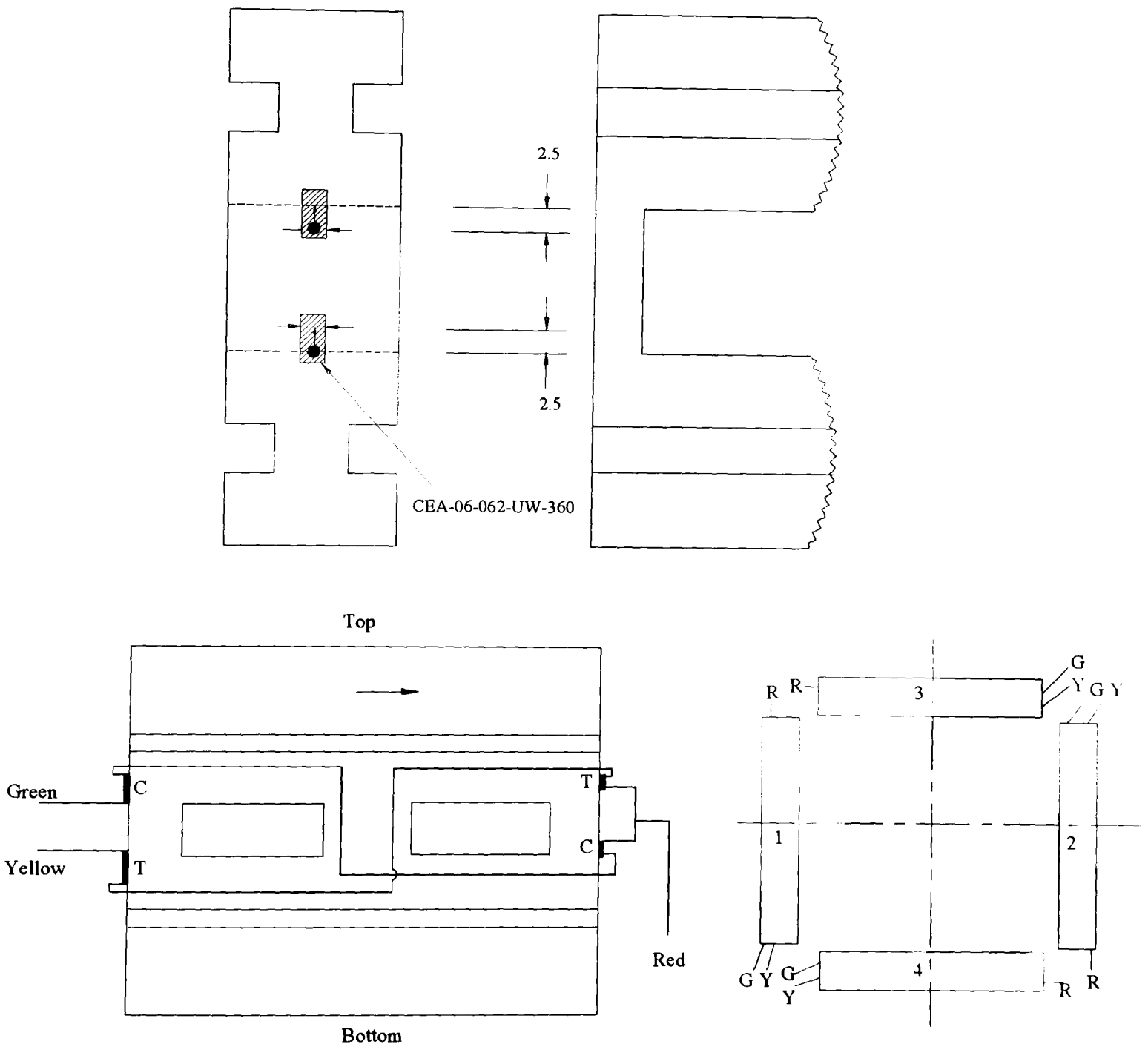

Figure C-1: Gauge positions for the radial sensing elements

The rotating dynamometer has a four component arrangement, and measures the forces in *X, Y, Z* directions and a moment about the *Z-axis*. The *X* and *Y* axes are radial axes, while the *Z* axis is the axial (vertical) axis. General-purpose strain gauges, model (CEA-06-062-UW-360), were used and grouped in a four-gauge Wheatstone full-bridge arrangement to measure one component of force. Figures C-1 and C-2 show the radial and the axial sensing elements arrangement respectively.

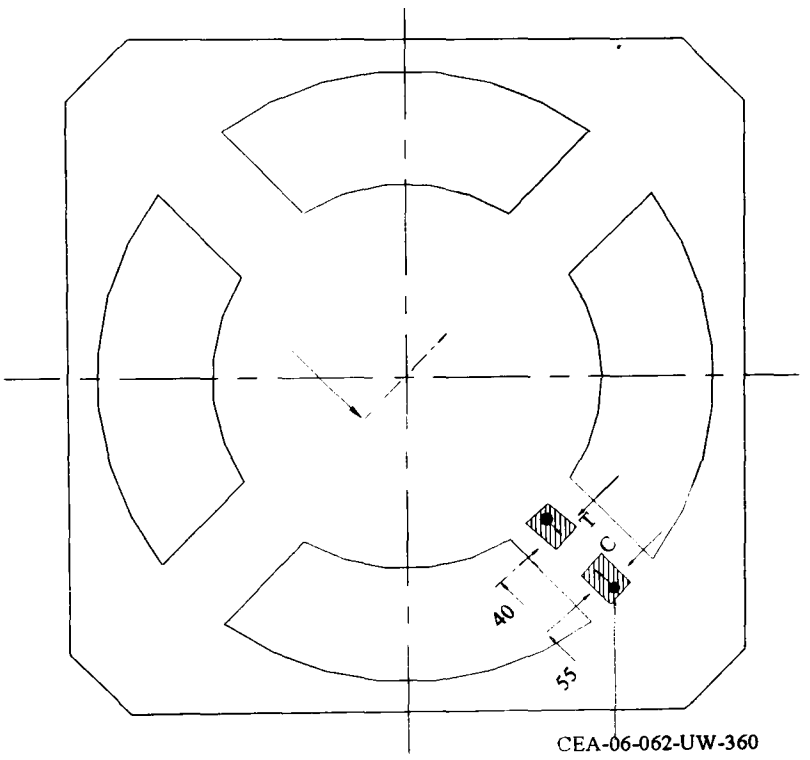

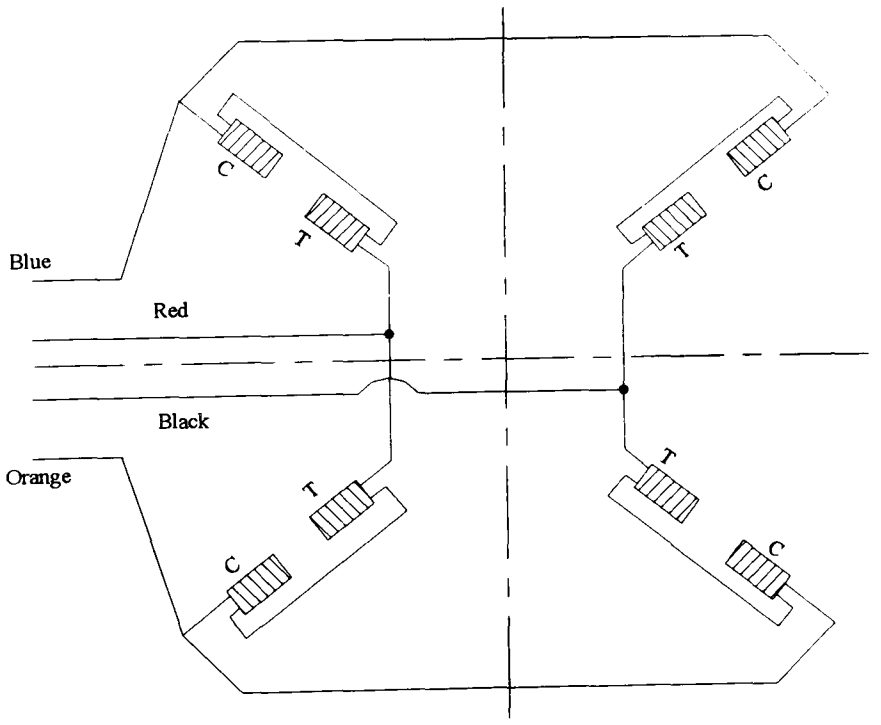

Figure C-2: Gauges position of the axial sensing elements

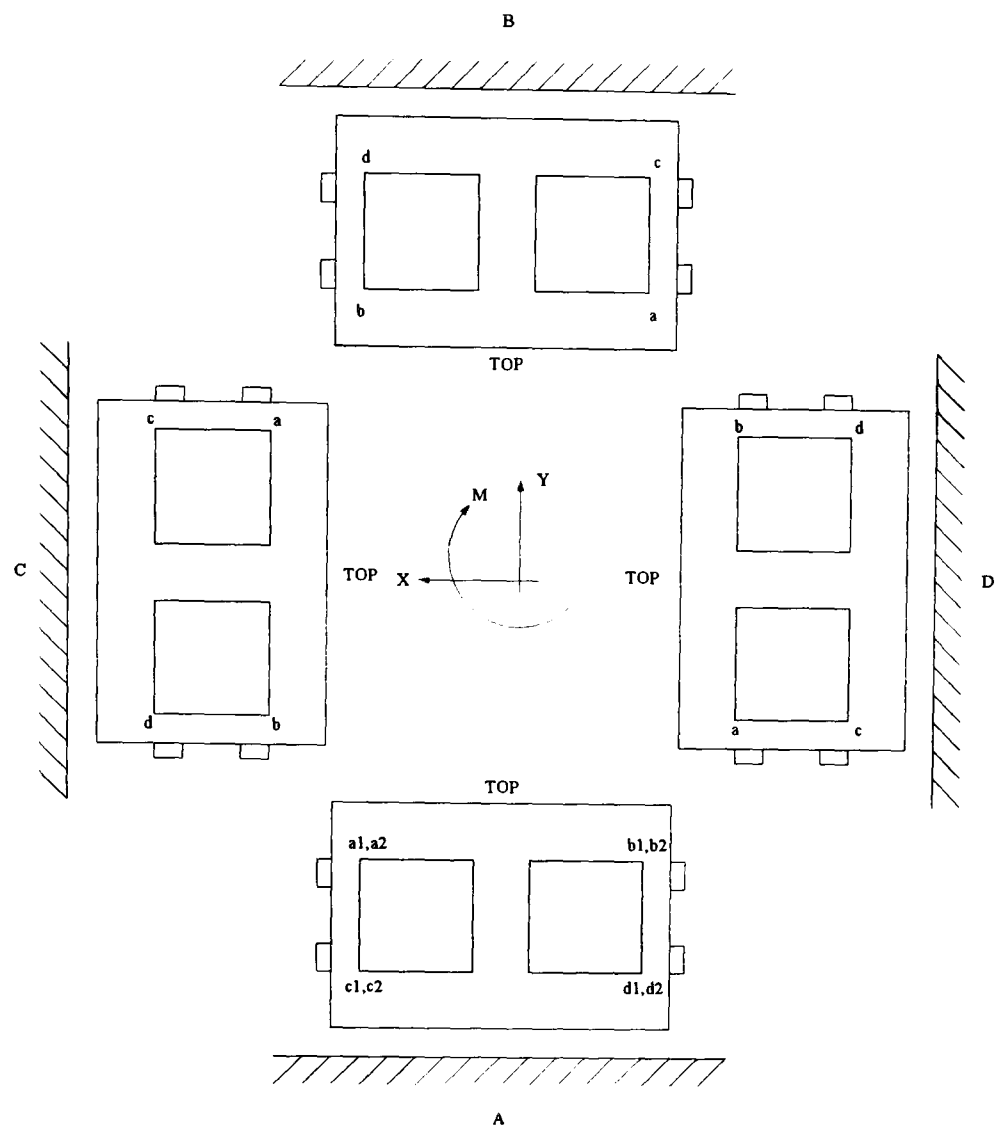

Force X				
	a	b	C	d
A	+	-	-	+
B	-	+	+	-
C/D	0	0	0	0
Force Y				
A	+	-	-	+
B	-	+	+	-
C/D	0	0	0	0
Couple C				
A	+	-	-	+
B	+	-	-	+
C	-1x + (-)	-1x - (+)	-1x – (+)	-1x – (-)
D	-1x + (-)	-1x – (+)	-1x – (+)	-1x + (-)

+ = Tension
- = Compression

Figure C-3: Horizontal and couple sensors and output polarity

The signals from each bridge are amplified using an INA-102 instrumentation amplifier with variable gain for each channel. The original circuit board also has

a dc-dc converter to provide a bi-polar supply for the amplifiers; this converter was later removed as it caused substantial noise and was replaced using an external power supply. Figures C-4 and C-5 show the schematic circuit diagrams in the horizontal and couple sensor and vertical sensors respectively.

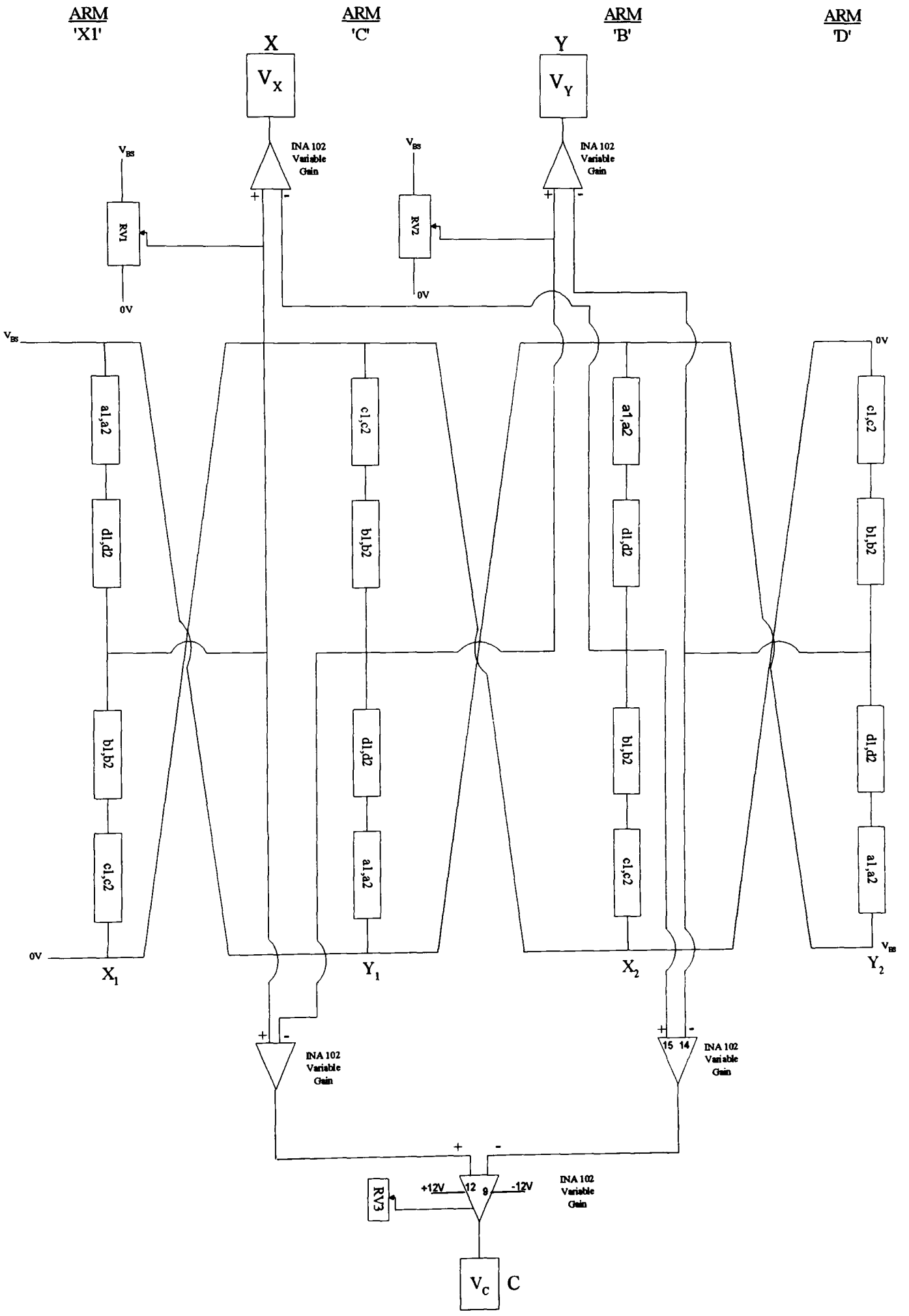

Figure C-4 Horizontal and couple sensors circuit diagram

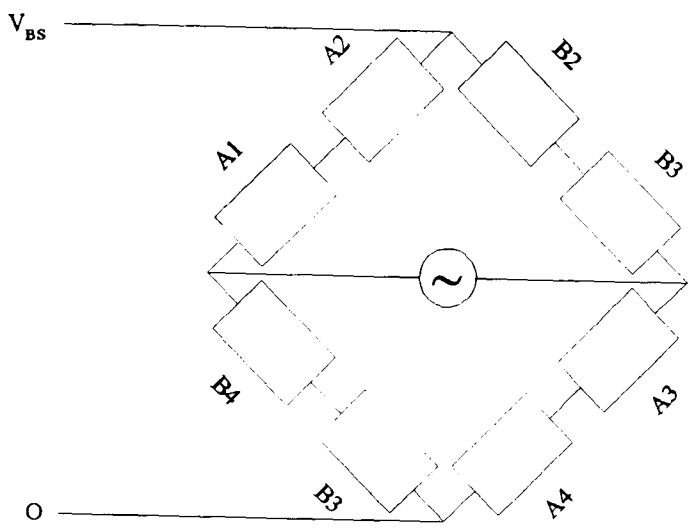

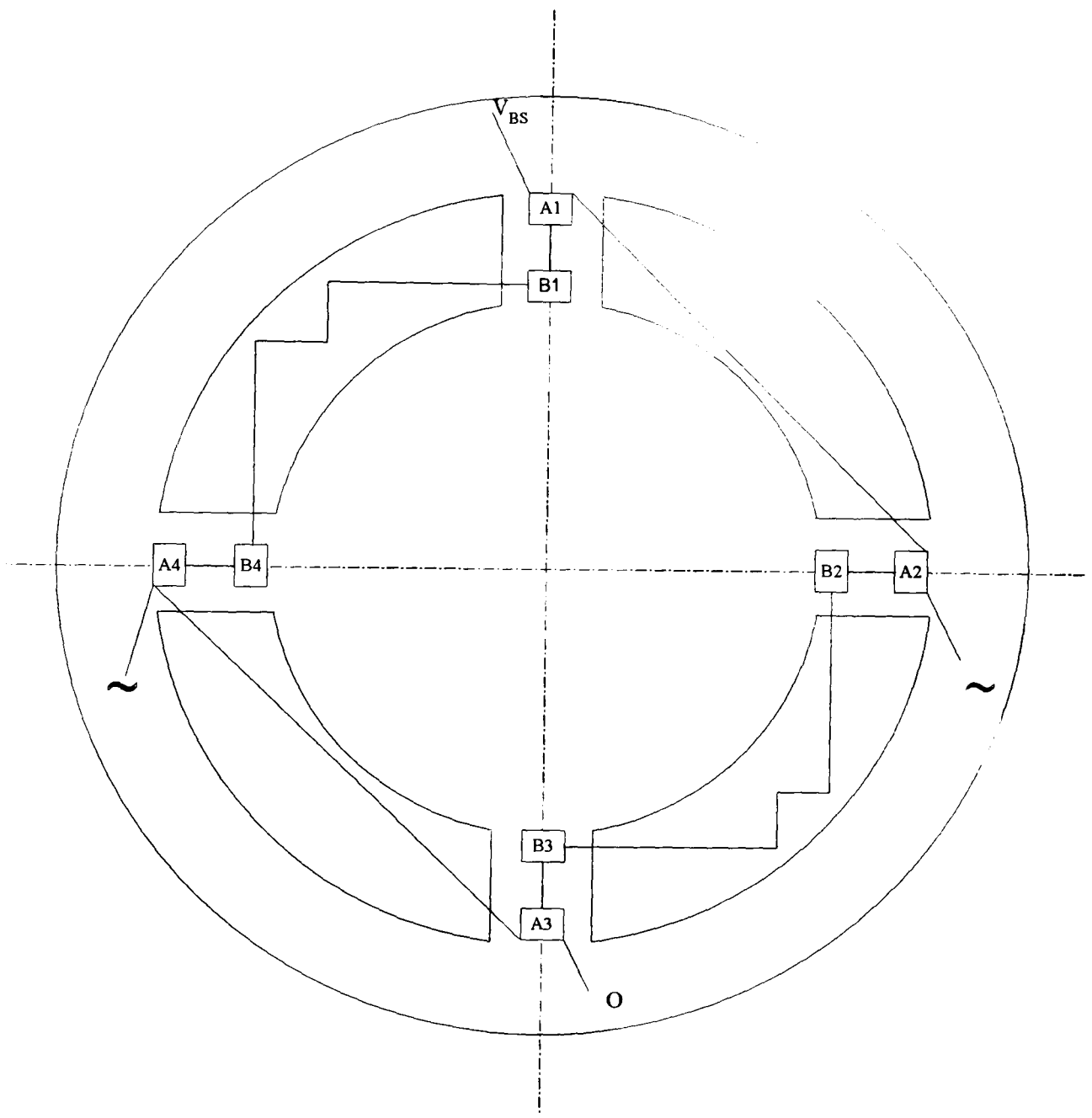

Figure C-5: Vertical sensors circuit diagram

Figure C-6 show the strain gauges arrangement on different arms and also show the circuit board needed to process the signal.

Figure C-6: Dynamometer illustrating sensing elements and gauge arrangements

In order to maintain an electrical contact between the dynamometer and host computer, slip rings were employed. The slip rings are wired directly to the outputs of the strain gauges amplifiers. The slip rings are also used to provide the dynamometer with a regulated dc power supply. Figure C-7 show the slip-ring arrangement.

Figure C-7: Slip rings arrangements

The slip rings rotate with the dynamometer, and the electrical contact brushes are mounted on a circular steel frame which is retained to prevent the brushes from

rotating when the slip rings and the whole dynamometer rotate. A cover was also made with an adequate seal to protect the dynamometer circuit elements from cutting fluid and swarf. Figure C-8 show the dynamometer mounted on the machine worktable and ready for use.

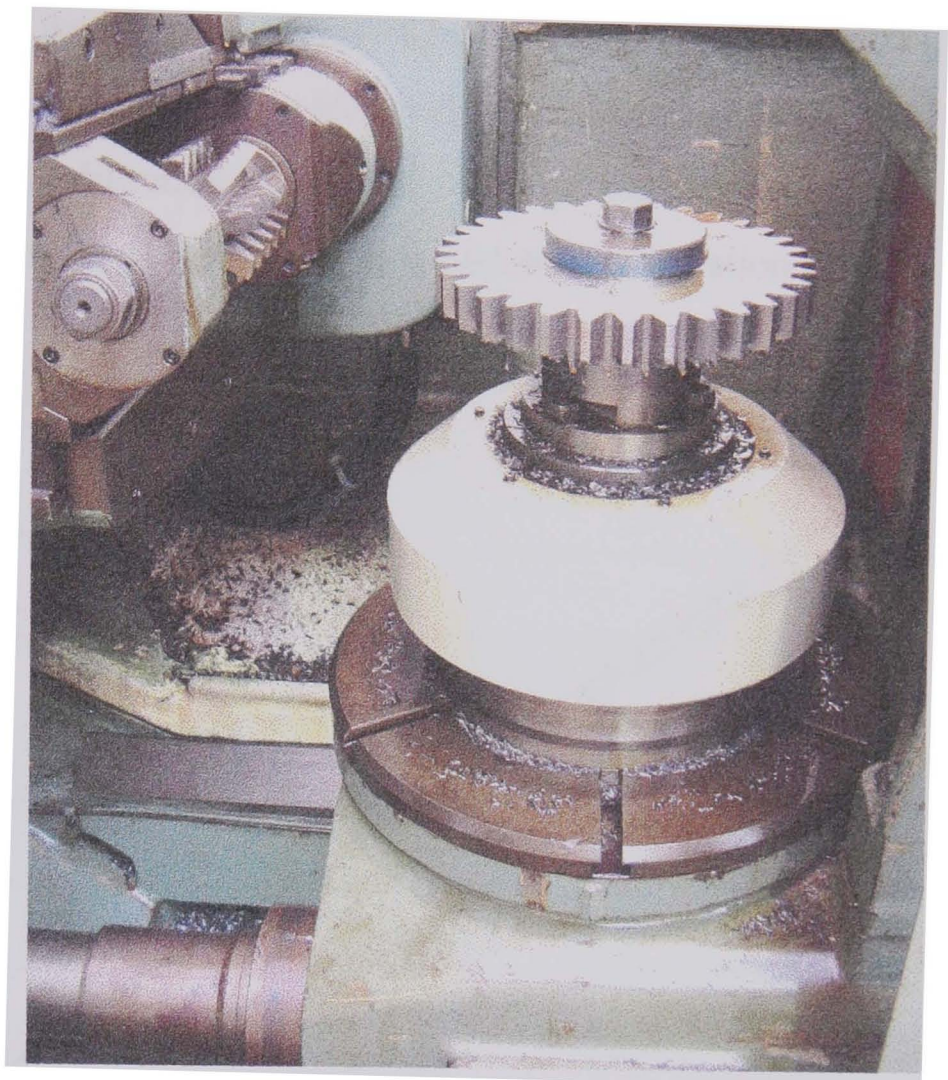

Figure C-8: Force sensing dynamometer

The dynamometer output signals represent the voltage change in each different axis. In order to measure these deflections with their equivalent applied forces a calibration procedure was required. The forces acting on the dynamometer are measured in 3 directions, the vertical and 2 lateral (radial) direction, so forces were applied on these directions and the dynamometer was calibrated.

The vertical force calibration was easier to conduct than that of the radial forces. The dynamometer was place on a tensile/compression test machine and then defined forces were applied and the equivalent output was noted. The radial forces calibration procedure involves using a load cell and a hydraulic pressure ram. The load cell itself was calibrated using the procedure to calibrate the vertical axis. The load cell was attached to the hydraulic ram, and the calibration

procedure was carried out by applying pressure (force) on the *X* and *Y* axes, as the load cell is placed between the pressures ram head and the dynamometer fixture. Forces were applied on both negative and positive side of the axis to gain more reliable calibration. The voltage output from both the load cell and the dynamometer axes were noted. A final graph was produced to represent applied forces acting on each axis (in Newton), as the graph slope units are *mV/N*. Figure C-9 show the calibration graphs for both vertical and lateral axis. Note that the force acting on the *X* and *Y* axes have the same calibration slope.

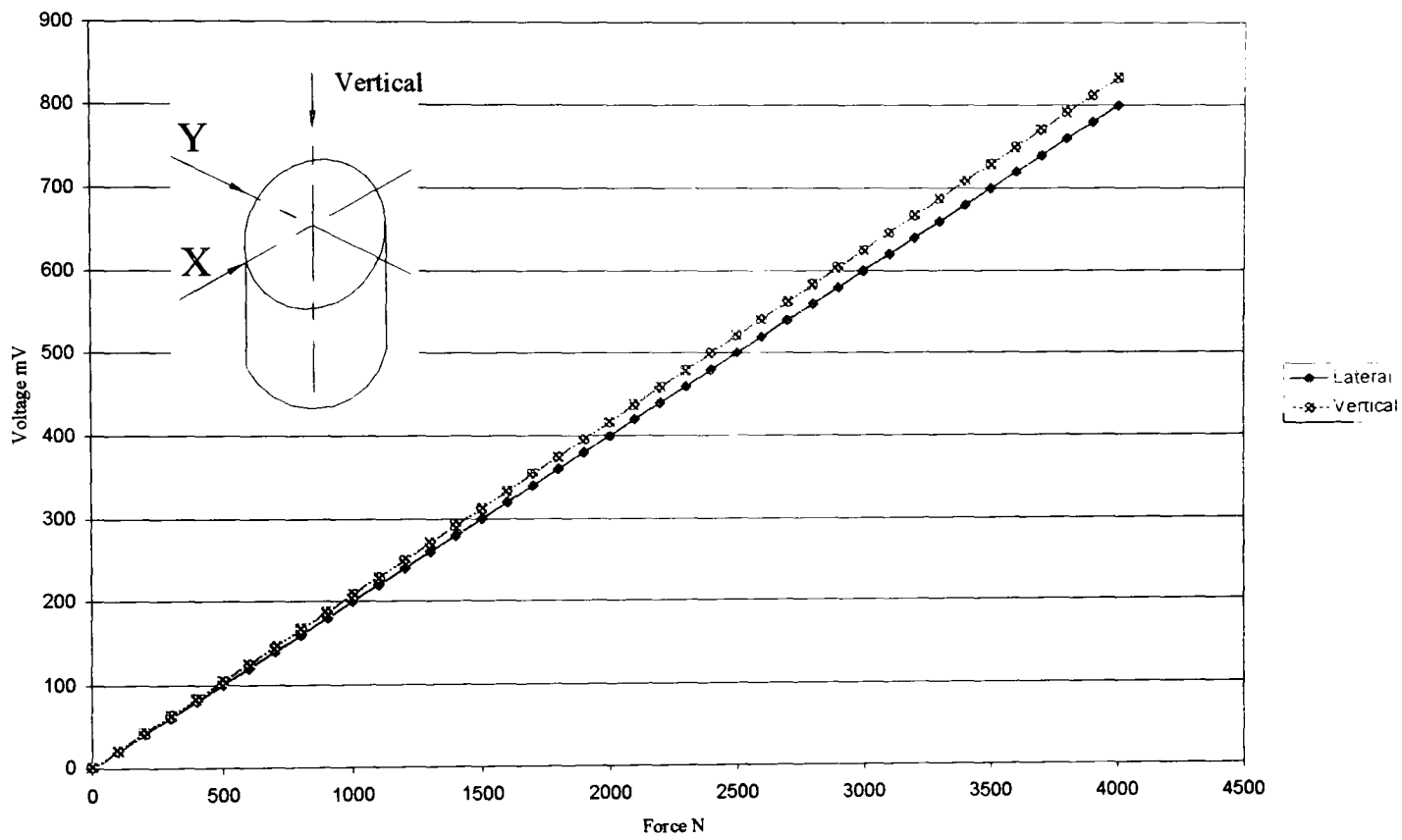

Figure C-9: Dynamometer Calibration

APPENDIX D

LOW-PASS FILTER AND ISOLATION CIRCUITS

D-1 LOW-PASS FILTER

The dynamometer was originally designed for another application [Ashby], and substantial noise was evident on each signal channel. The hobbing machine is a large machine and has several AC and DC motors so the current and noise interference was very noticeable. It was decided to use a second-order low-pass active analogue filter, to reduce the noise, of the Sallen-Key unity gain type. The filter attenuates high frequency components above the cut-off frequency of 200 Hz, which was limited by the data-sampling rate of 466 Hz, to avoid aliasing, and thus complying with Shannon's sampling theorem. The filter comprises a network of resistors and capacitors whose output is used to drive operational amplifier, type LM741CN. The transfer function of the second order filter can be written as [Lancaster]

$$\frac{e_o}{e_i} = \frac{K}{s^2 R1C1R2C2 + s(R1C1 - KR1C1 + R1C2 + R2C2) + 1} \tag{D-1}$$

If R=R1=R2 and C=C1=C2 the above equation could be written as

$$\frac{e_o}{e_i} = \frac{K\omega_n^{\,2}}{s^2 + 2\zeta\omega_n s + \omega_n^{\,2}} \tag{D-2}$$

where

$$\omega_n^{\,2} = \frac{1}{R^2C^2} \left(\text{or } \omega_n = \frac{1}{R\ C}\right) \tag{D-3}$$

$$\text{and } 2\zeta\omega_n = \frac{3-K}{R\ C} \tag{D-4}$$

$$\text{where } K = 3 - 2\zeta \tag{D-5}$$

The above equations allow setting the cut off frequency. The calculation for this project can be calculated as, $R=R1=R2=50K\Omega$ and a nominal $C=16\ nF$.

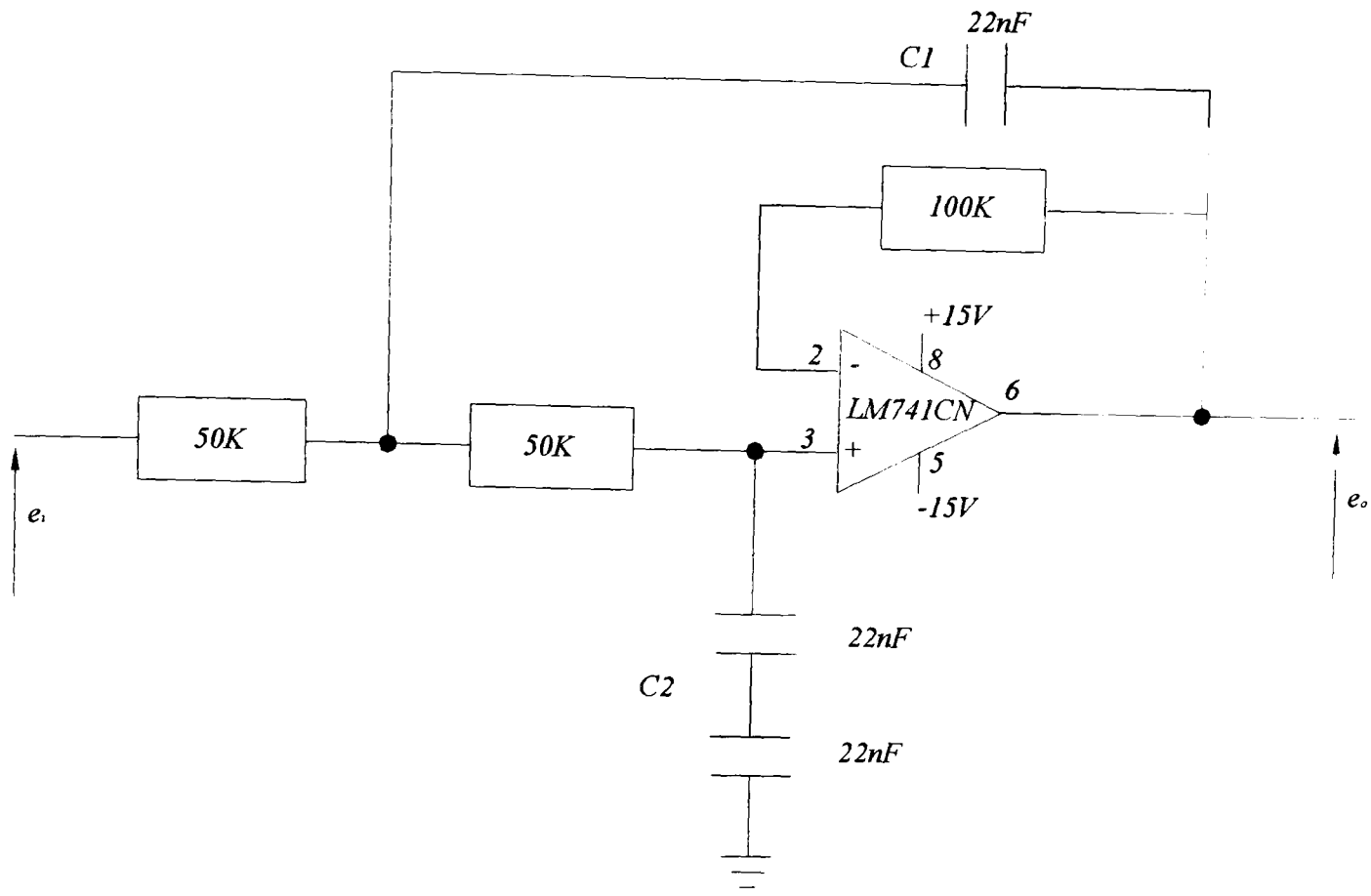

Figure D-1: Low pass filter circuit

If the damping ratio $d = 2\zeta$ (D-6)

Then

$$C1 = C * \frac{2}{d} \quad \text{(D-7)}$$

$$C2 = C * \frac{d}{2} \quad \text{(D-8)}$$

It was decided to choose a value for $d = 1.414$ which will give the flattest amplitude filter, and provides a combined moderately fast initial cut-off and reasonable overshoot. By applying D-7 and D-8 will result

$C1=0.016*1.414= 0.022\ \mu F = 22\ nF$

$C2= 0016*0.707 =0.011\ \mu F = 11\ nF$

and the bandwidth can be calculated using D-3:

$$\omega_n = \frac{1}{CR} = \frac{1}{50*10^3*0.016*10^{-6}} = \frac{10^3}{0.8} = 1250 rad/\sec$$

$$\approx 200 HZ$$

D-2 OPTICAL ISOLATION

The PMAC card provides an optical isolation to all its inputs and output channels, but additional optical isolation was felt necessary in order to maintain a better isolation. This was provided through a dedicated printed circuit board, which was designed for this application.

The board was divided into two main sections for the encoders inputs and amplifier drive signals, and the general I/O signals. The encoders section is connected to J8 on PMAC side and JA on the machine side, whilst the I/O section is connected to J5 on PMAC side and JB on the machine side.

Every encoder provides PMAC with phase and quadrature signal as well as an index or north marker signal, which is high (TRUE) every time the encoder passes through a certain position. The vertical slide encoders provide two additional two signals, for the lower and the upper machine limits. All these signals are buffered using a SN74S244 buffer memory register.

The isolation circuit of each individual channel consists of the TLP521 of optically coupled isolators that comprise infrared light emitting diodes and NPN silicon photo transistors in space efficient dual-in-line plastic packages.

The I/O section circuit is similar to the encoder side circuit but without the buffer, the general output required inverters as polarity was reversed on the machine original design. As PMAC only provides 8 designated outputs, a further were needed to actuate the fine and the rough cut ram. To this end the amplifier enable (AENA1 and AENA4) on J8 were utilized as general output channels. It was decided that no additional optical isolation was required for the DAC signal outputs. The circuit diagram for the digital interface board is shown in figure D-2.

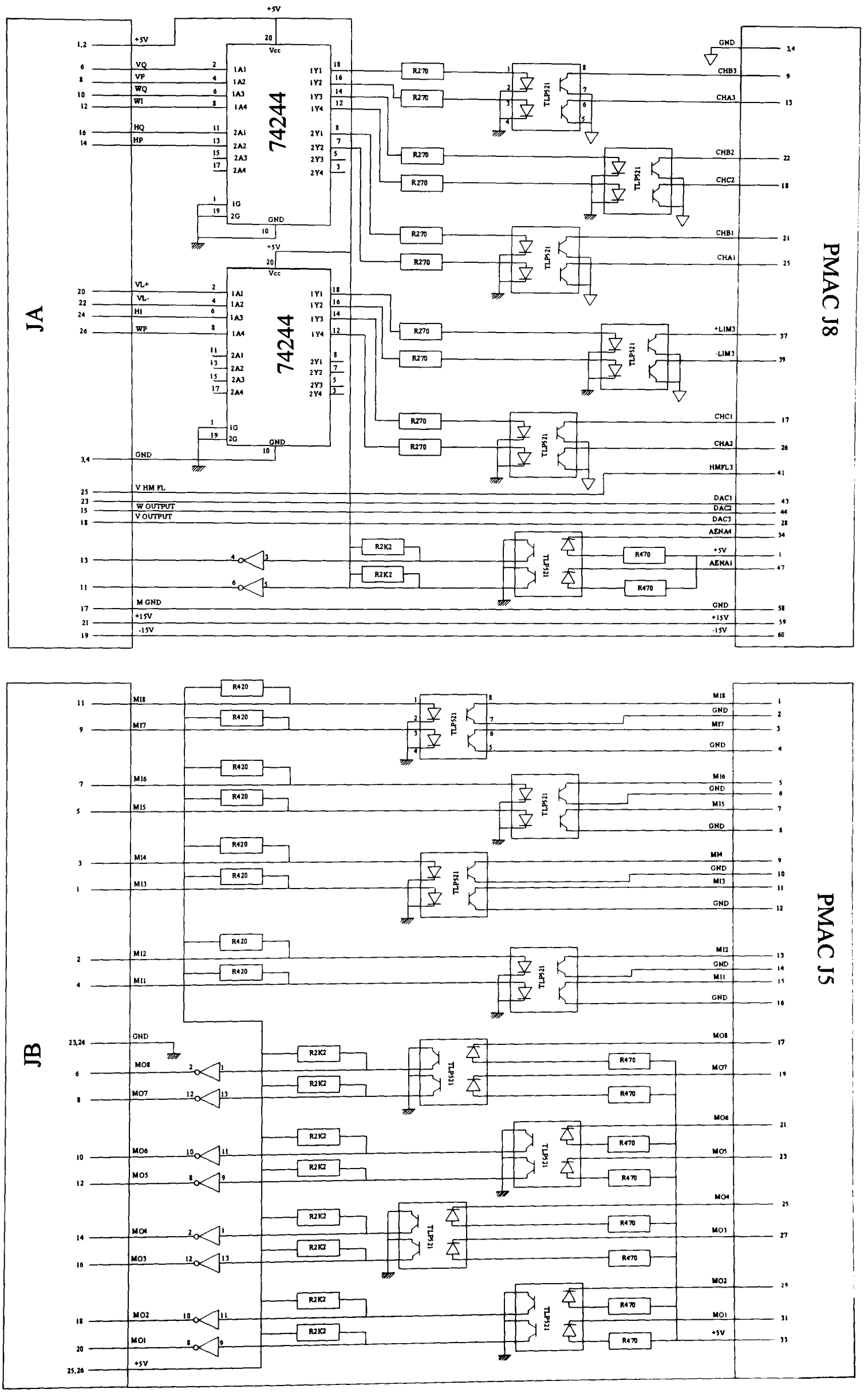

Figure D-2: Optical isolation circuit

APPENDIX E

ALTERNATIVE CUTTING OUT METHODS

By comparing the different surfaces generated by successive hob teeth in a common co-ordinate system fixed in the gear, the actual instantaneous tooth shape can be built up, cut by cut, as the envelope of all previous cuts in each tooth space. The 'cutting out' solution discussed in section 4.9 was selected after having evaluated a number of different possible approaches to the problem, all of which were based on superposing the 'irregular' original *(mk)* grid onto a common regular *(pq)* grid spaced in *0XYZ* co-ordinate system. For completeness it was considered appropriate to include some references to the other approaches evaluated, as follows:

Method 1 - Based on an $(r_p\text{-}z_q)$ Grid

Each surface point P_{pq} is defined by polar co-ordinates $(r_p,\theta_{pq},z_q)_{(1)}$, as illustrated in fig. E1, where

$r_p = \sqrt{x^2{}_{pq(1)} + y^2{}_{pq(1)}}$ for $(p=1 \ldots\ldots p_{max})$

$z = z_q$ for $(q=1 \ldots\ldots q_{max})$

and

$\theta_{pq} = \tan^{-1}(\frac{y_{pq}}{x_{pq}})$ defines the surface position on the circle at (r_p, z_q).

A comparison of where two surfaces intersect the circle ($r=r_p$ in the plane $z=z_q$) then merely requires comparison of the two values of θ_{pq}. This grid can be used for all tooth spaces at any instant. If the gear has Z teeth, and there will be (potentially) 2 Z values of θ_{pq} round the gear for each r_p and z_q. Since each circle potentially intersects the right and left flanks of each tooth. There are thus a large number of values to store, which describe the current 'shape' of the whole gear.

This grid models the tooth flanks as well as the depth of cut on the flanks well. Since the circles $r=r_p$ are never even nearer parallel to the tooth flanks. It will, however, be less successful on the tooth fillet, where cuts may not be recorded unless they exceed Δr in depth, since the root circle will be parallel to the circles $r=r_p$.

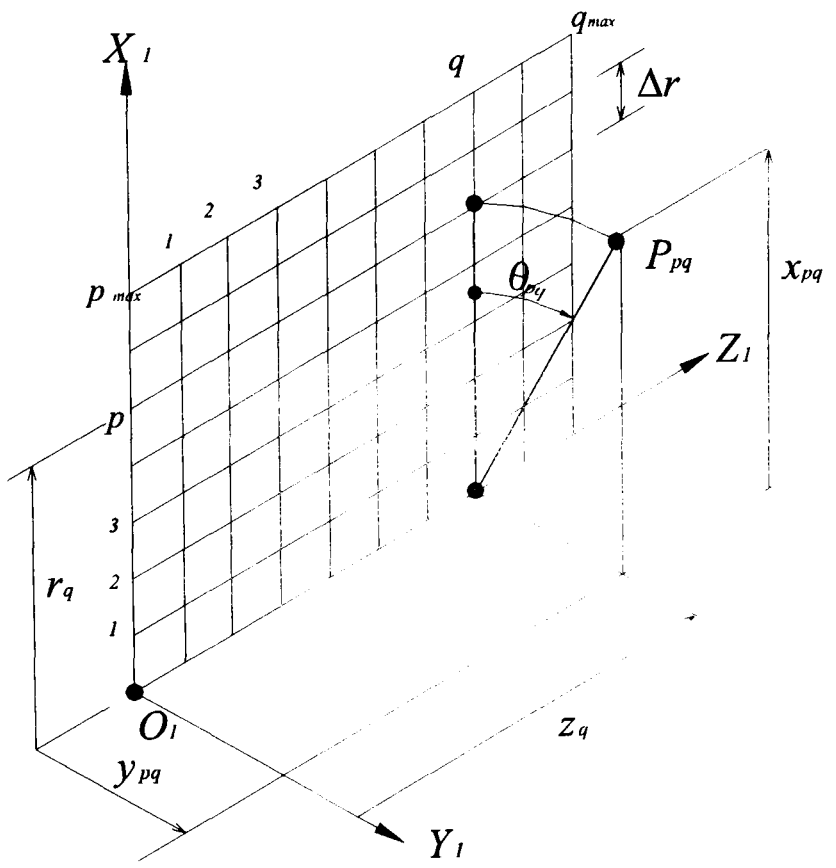

Figure E.1 The r_p-z_q Grid

Method 2- Based on a θ_p-z_q Grid

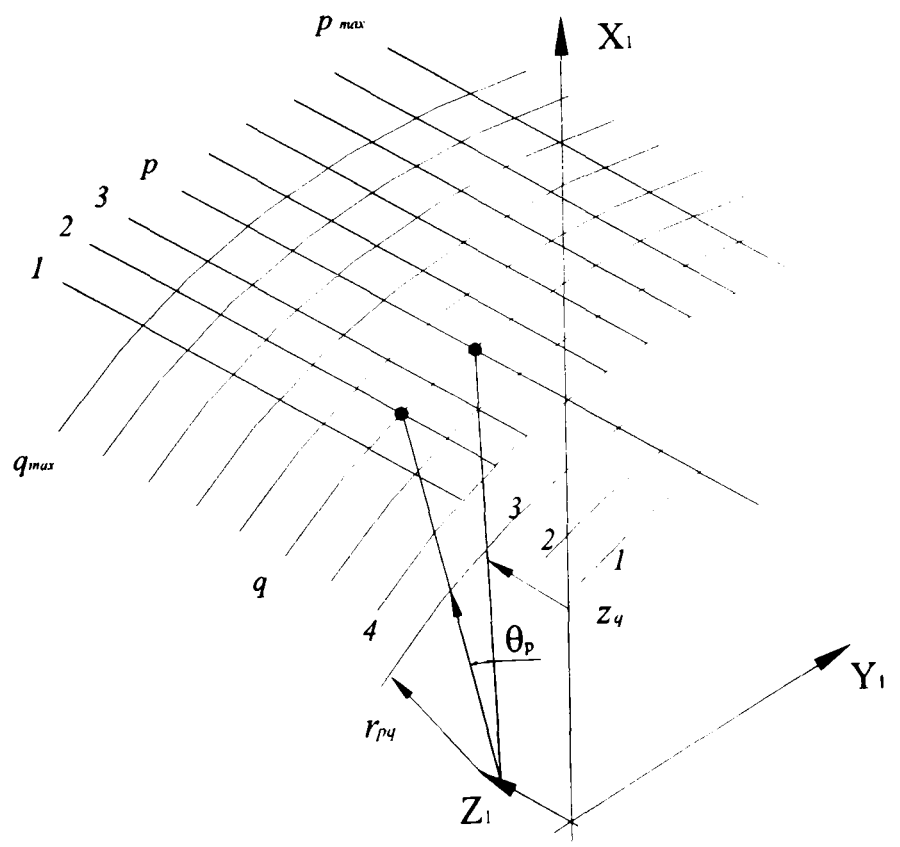

Figure E.2 The θ_p-z_q Grid

Each point P_{pq} lies on a grid at $(\theta_p, z_q)_{(1)}$, as illustrated in fig. E.2, where

$p = (1 \ldots p_{max})$, $q = (1 \ldots\ldots q_{max})$

The position of the point P_{pq} is defined by its radius $r_{pq} = (\sqrt{x_{pq}^2 + y_{pq}^2})_{(1)}$.

Comparison of the two surfaces then involves comparing the radial "depths" of cut (i.e. the values of r_{pq}) along each radial line at $(\theta = \theta_p, z = z_q)$. This grid will provide a good representation of the cuts along the tooth fillet, but those along the flank will be less well represented, since radial lines may be nearly parallel to the flank in the dedendum. There will also be problems if undercutting occurs during generation of the tooth (even if not finally present) since the surfaces could then cut a radial line $(\theta = \theta_p, z = z_q)$ more than once, as shown in fig. E.3.

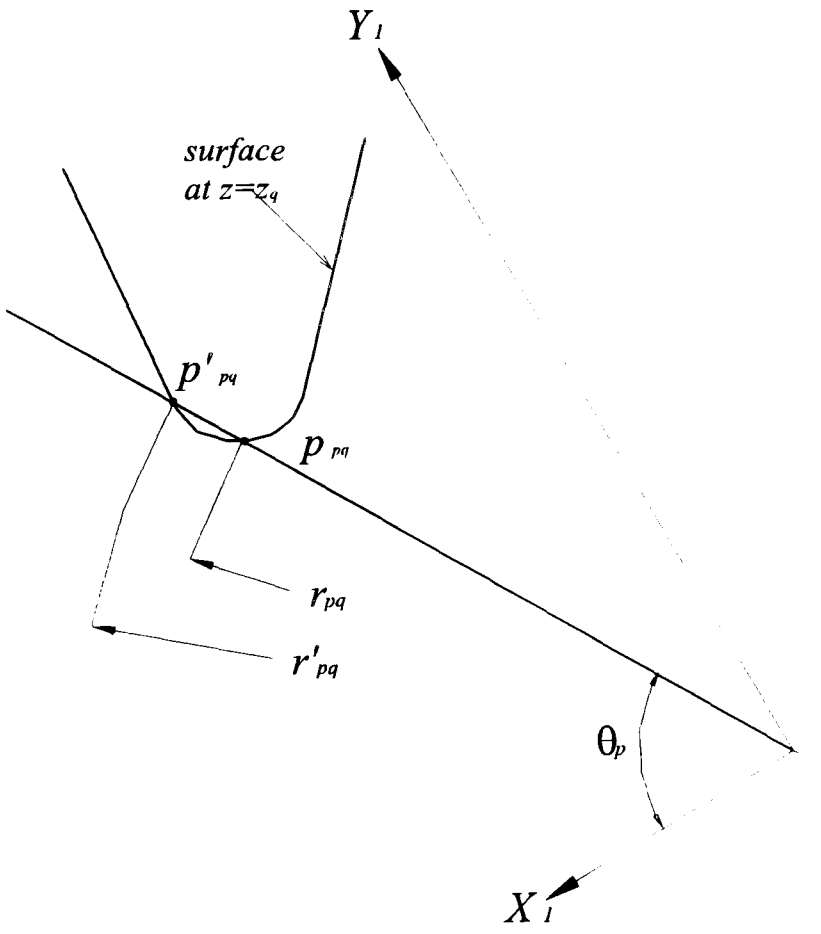

Figure E.3 Problem of undercutting with the θ_p-z_q grid. (Section at $z=z_q$)

Method 3 - The r_p-θ_q Grid

Point P_{pq} lies at $r=r_p$, $\theta = \theta_q$ on a regular polar co-ordinate grid, and as located by its axial position z_{pq}, as shown in fig. E.4. This cylindrical grid quite unsuitable for spur gears, since the 'generators' parallel to OZ_1 at (r_p, θ_q) are

parallel to the tooth surfaces. For helical gears, the lines $(r=r_p,\ \theta = \theta_q)$ parallel to the gear axis would only intersect the flanks at the (relatively small) lead helix angle β_p. This is not a very useful grid to compare two cut surfaces with, since fine cuts on the flanks (less than $r_p\Delta\theta$) or on the fillet (less than Δr) would easily be missed.

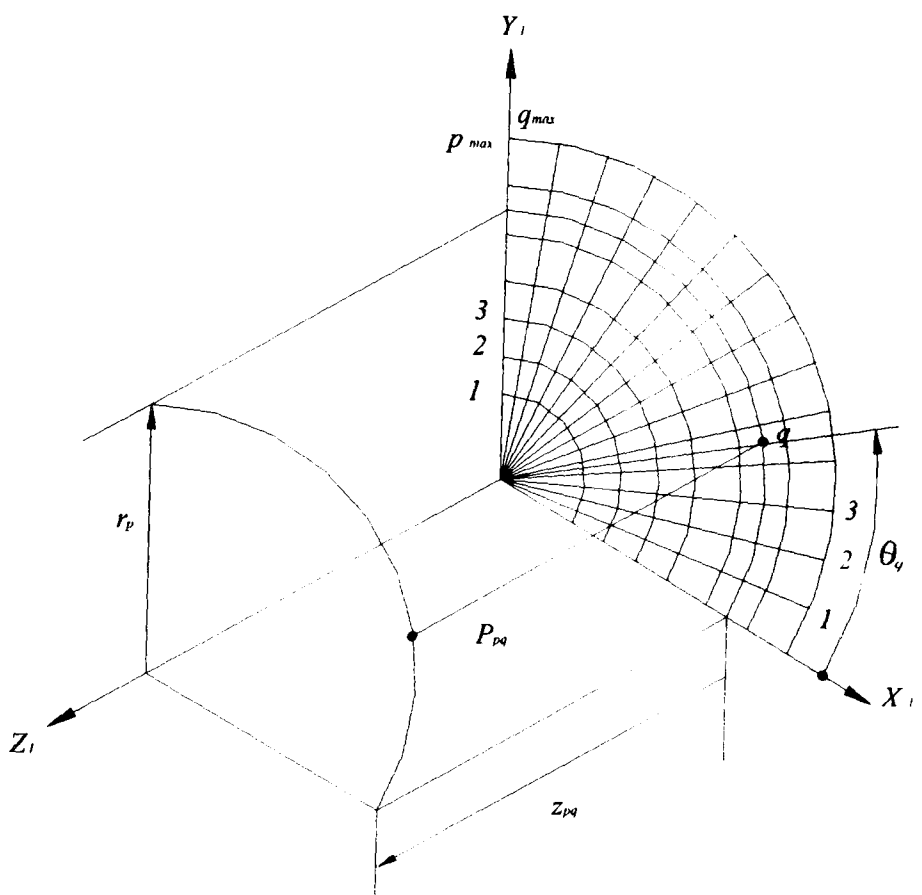

Figure E.4 – The $(r_p$-$\theta_q)$ cylindrical grid

Method 4 - The Inclined (y_p,z_q) grid

In this approach, a (y_p,z_q) grid is used, but is oriented so as to give good discrimination of x_{pq} all along one side of the tooth only (e.g., by choosing $\alpha_{grid} \approx$ 20°-30°, as in figure E.5.

An obvious disadvantage of this system is that a second set of axes $(X_RY_RZ_R)$ is needed for the other flank, while, since the generated points in the (m,k) grid of figure 4.9, do not align exactly with the point of either (p,q), there is also uncertainty (for points around the cutter tip) whether they need to be mapped onto the L or R (p,q) grids on the gear profile.

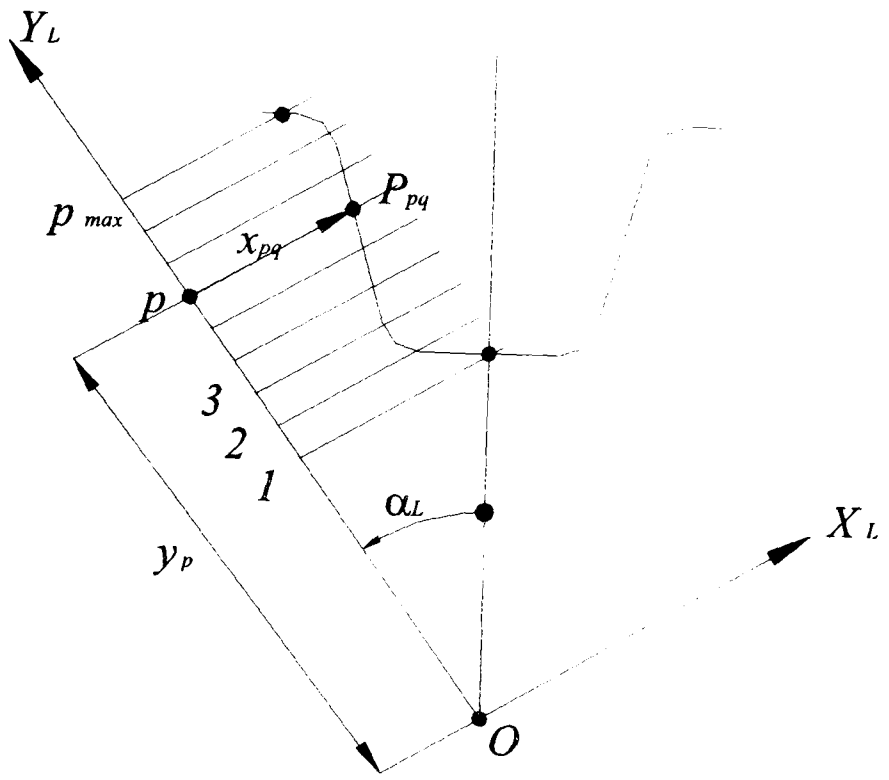

Figure E.5: Section at $z_L=z_q$, through $(y_p\text{-}z_q)$ grid inclined α_L, for L flank.

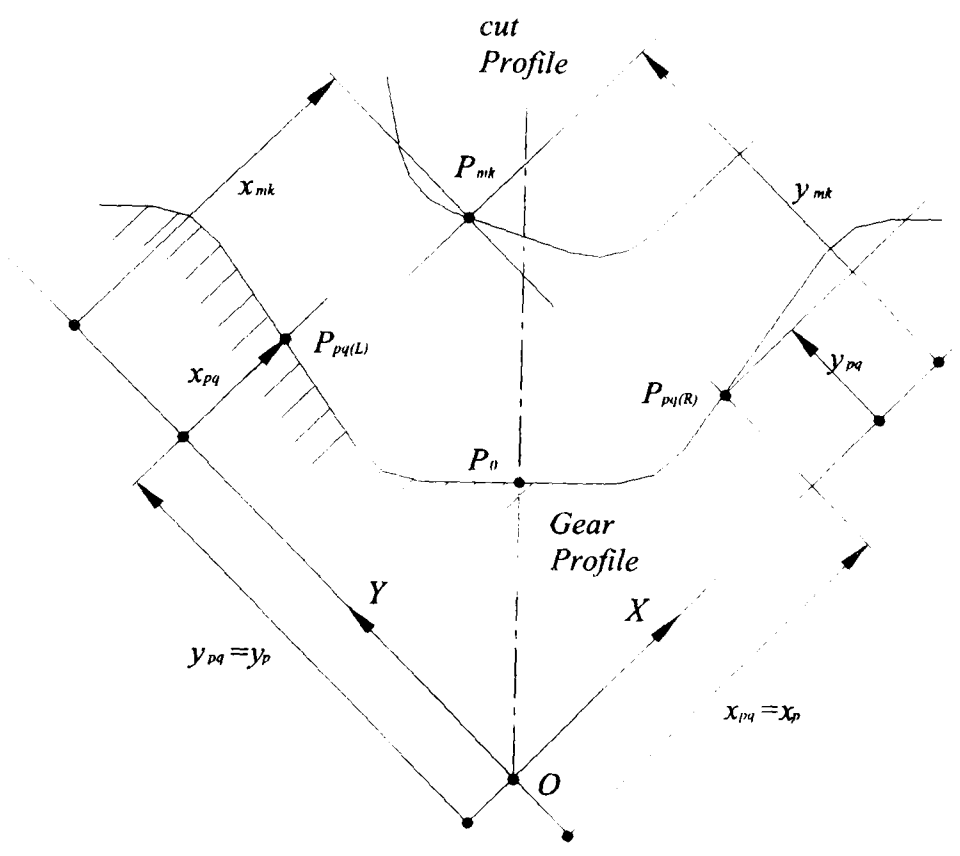

Figure E.6: Inclined 45° $((x_p$ or $y_p))\text{-}z_q)$ grid for both flanks. (Section at $z=z_q$).

This problem can be avoided if a single inclined grid at 45° to the tooth centre line is used, as in figure E6. With this grid, the L flank is represented by a (y_p,z_q) grid with points $P_{pq(L)}$ defined by the values of x_{pq} at (y_p,z_q) (like figure E.5) but points $P_{pq(R)}$ on the R flank defined by values of (y_{pq}) at (y_p,z_q). The central point

P_0 is the point of which $(x_{pq}=y_{pq})$. A generated point $P_{(m,k)}$ on the cut profile with co-ordinates (x_{mk},y_{mk},z_{mk}) is mapped onto the L flank (p,q) grid if $x_{mk} < y_{mk}$, onto R flank, if $x_{mk} \geq y_{mk}$.

This method was used successfully during development of MATLAB software, but tended to give irregularities in calculated the chip thickness near the root P_0, where the two grids 'overlap'. The method was later abandoned in favour of the simple grid described in section 4.9.3, which gives fewer problems overall.

Method 5- Mapping of (θ_{mk}) to (θ_{pq}) as a Cartesian axis

The process of generating the surface produced by one cutting edge yields the co-ordinates in $(X,Y,Z)_{(1)}$ for each of the irregular grid points shown in fig. E.7. Each point P_{mk} can be transformed to $(r,\theta,z)_{(1)}$ co-ordinates giving such that

$$(r_{m,k})_{(1)} = (\sqrt{x^2{}_{m,k} + y^2{}_{m,k}})_{(1)}$$

$$(\theta_{m,k})_{(1)} = (\tan^{-1}(\frac{y_{m,k}}{x_{m,k}}))_{(1)} \qquad \text{(E.1)}$$

$$(z_{m,k})_{(1)} = (Z_{m,k})_{(1)}$$

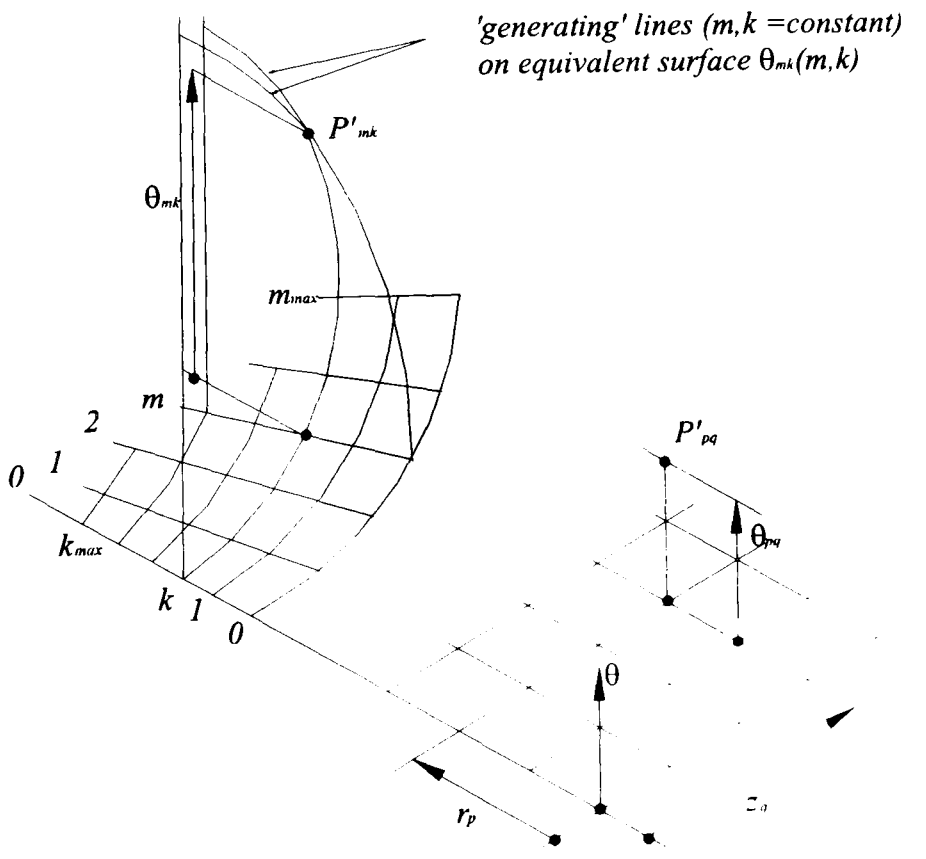

Figure E.7 Interpolation of imaginary 'Cartesian' function $\theta_{mk}(r_{mk},z_{mk})$ onto regular (r_pz_q) grid as $\theta_{pq}(r_p,z_q)$.

In this procedure, the actual surface $(x_{mk},y_{mk},z_{mk})_{(1)}$ is represented by treating θ_{mk} as the third Cartesian axis, so defining Points P'_{mk} on an equivalent 'surface' $\theta_{mk}(r_{mk},z_{mk})$, Figure E.7.

As for the inclined $(y_p\text{-}z_q)$ grid of method 4, separate interpolation of L and R flanks is needed. At the start of computation, $\theta_{pq} = +\infty$ (R flanks) or $= -\infty$ (L flanks). Cutting occurs whenever the interpolated value θ_{pq} for the new (generated) cut is numerically greater than the corresponding value for the gear tooth space. See figure E.8.

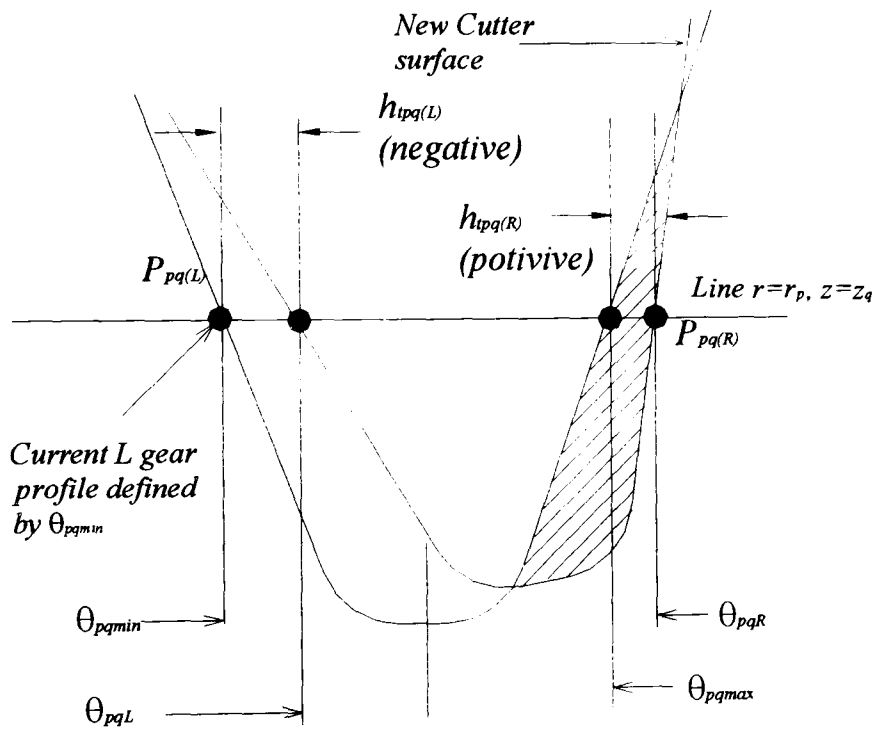

Figure E.8- Cutting only on the right flank ($z=z_q$)

Figure E.8, illustrates a situation when there is no cut on L flank at $P_{pq(L)}$ since

$$\theta_{pkL} > \theta_{pkmin} \tag{E.2}$$

On the R flank however

$$\theta_{pkR} > \theta_{pqmax} \tag{E.3}$$

Cutting therefore occurs (tangential thickness h_{tpq}) when

$$h_{tpq(R)} = r_p(\theta_{pq(R)} - \theta_{pq\max}) \tag{E.4}$$

The cut profile alters the R flank gear profile, so that for the next cut

$$\theta_{pq\max} = \theta_{pq(R)} \tag{E.5}$$

By checking a sufficient number of points (p,q), the depth of cut can be defined over the whole grid. Negative values should also be calculated, (where there is no cut), so that subsequent interpolation is more reliable. If the depth of cut is now plotted over the rectangular grid, a "surface" showing variation of h_t over the cut area will be obtained.

Using the same (B-spline) interpolation procedure, the values of $ht_{(mk)}$ at each of the points P_{mk} of the original (irregular) grid, for each cutter tooth (i,j) can now be calculated, figure E.9.

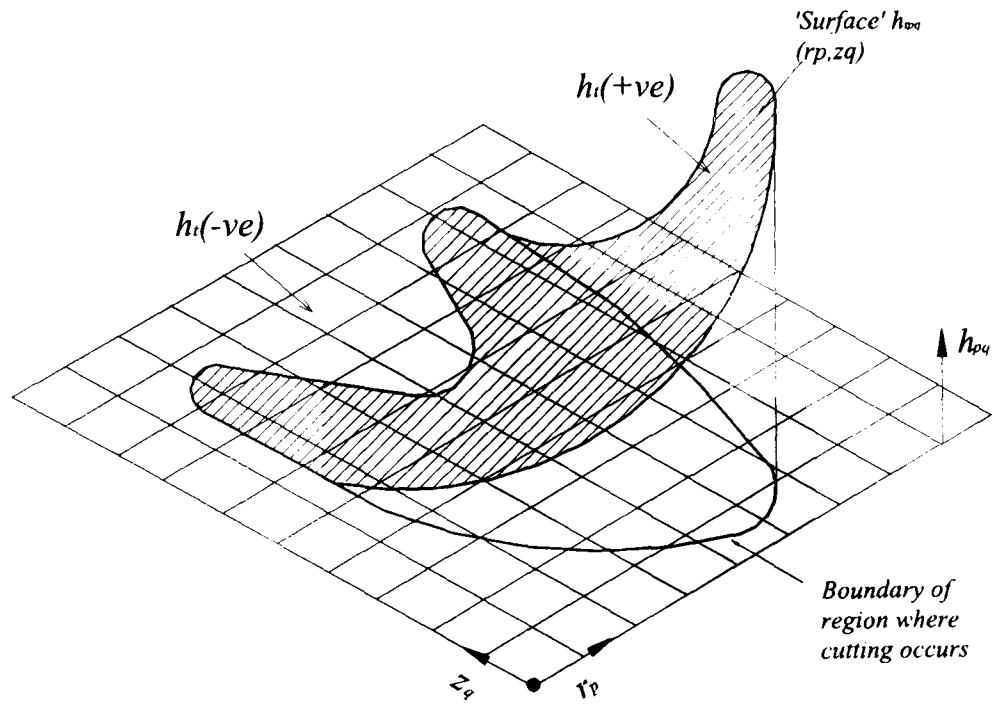

Figure E.9: Mapping from the irregular grid

Since the index k corresponds to a particular point on each hob tooth, the total amount of cutting done over each element of each cutting edge can be summed (over the m time intervals of cutting action separately for each k). The polar co-ordinate $\theta_{i,j,m,k}$ of each point P_{mk} on hob tooth (i,j) is now known, so the 'tangential' tooth thickness h_{tmk} calculated (interpolated) above can be represented as a vector, see figure E.10., giving

$$\bar{h}_{tmk_{(1)}} = h_{tmk}\begin{bmatrix} -\sin\theta_{i,j,m,k} \\ \cos\theta_{i,j,m,k} \\ 0 \end{bmatrix}_{(1)} \qquad \text{(E.6)}$$

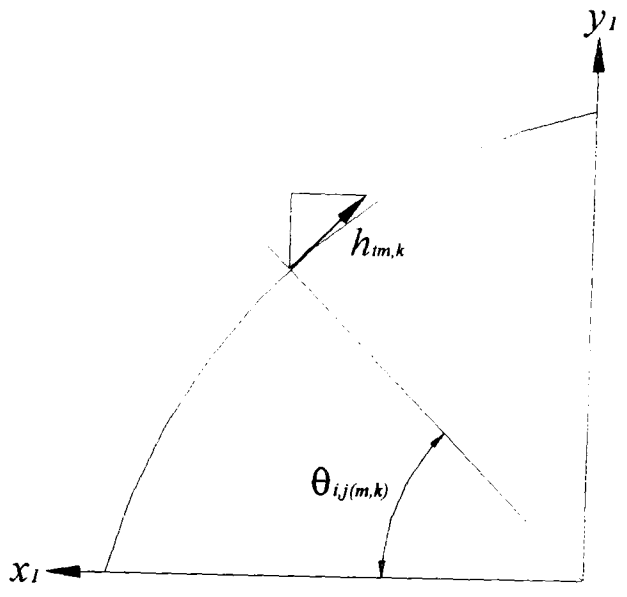

Figure E.10: Tangential h_{tmk} tooth thickness interpolation

The normal chip thickness $h_{m,k}$ is then given by

$$h_{m,k} = h_{t,mk_{(1)}} \bullet \hat{n}_{1(1)} \qquad \text{(E.7)}$$

This method of interpolation of the imaginary surface $\theta_{mk}(r_{mk}, z_{mk})$ seemed to offer few advantages over direct interpolation of the physical cut surfaces, so was not used. Interpolation of the h_{pq} values back onto the original *(mk)* grid was used, as described in section 4.9.3.

Method 6 - The Direct approach

A disadvantage of the methods so far proposed is that each point P_{ijk} on the cutter (in convenient spacing round the cutter) generates inconveniently spaced points on the gear which can not be easily related to the points generated by the other cutting edges. This makes interpolation of the points onto a common co-ordinate grid necessary. It would be helpful if the generated points were all 'regular' grid points. The point P_{ijk} on the cutting edge i,j has co-ordinates in the hob axis (6), given by

$$\bar{r}_{i,j,k_{(6)}} = \begin{bmatrix} r_k \cos\theta_{i,j} \\ r_k \sin\theta_{i,j} \\ \frac{H\theta_{i,j}}{2} \pm \frac{S_k(r_k)}{2} \end{bmatrix} \qquad \text{(E.8)}$$

The only parameter defining the point is its radius r_k (which, in turn, determines s_k section 4.4.1).

The corresponding point P_{ikj} on the gear has co-ordinates in co-ordinate system (1) given by (4.6) and (4.9)

$$\bar{r}_{i,j,k_{(1)}} = \left[T_{1,6}\right] \cdot \bar{r}_{i,j,k_{(6)}} \qquad \text{(E.9)}$$

where the transformation $\left[T_{1,6}\right]$ depends on the hob rotation angle $\phi_0=\phi_m$, which also fixes ϕ_1, from (E.8) and (E.9) it follows that

$$\bar{r}_{i,j,k_{(1)}} = \bar{r}_{i,j,k}(r_k,\phi_0) = \begin{bmatrix} r_{(1)} \cdot (r_k,\phi_m) \\ \theta_{(1)} \cdot (r_k,\phi_m) \\ z_{(1)} \cdot (r_k,\phi_m) \end{bmatrix} \qquad \text{(E.10)}$$

We could thus generate points on (e.g.) the $(r_p\text{-}z_q)$ grid by solving the simultaneous equations:

$$r_{(1)}(r_k,\phi_m) = r_p$$
$$z_{(1)}(r_k,\phi_m) = z_q$$

or

$$f_1(m,k) = r_{(1)}(m,k) - r_p = 0$$
$$f_2(m,k) = z_{(1)}(m,k) - z_q = 0 \qquad \text{(E.11)}$$

for the unknown (r_k, ϕ_m) the solution region. The region in which solutions of E.11 are possible, must first be determined first, since simultaneous, 'numerical'

solution of (E.11) is needed. One technique [Press *et al*] is to form the positive definite function.

$$F(r_k,\phi_0) = (r_1(r_k,\phi_0) - r_p)^2 + (z_1(r_k,\phi_m) - z_q)^2) \tag{E.12}$$

This can be minimised numerically e.g. Nelder & Meade's method, with respect to (r_k, ϕ_m). If a minimum is zero, this yields a solution for (E.11), if minimum >0, then (E.11) has no, real solutions. This is a relatively robust method, provided that

1 - The approximate region in which solutions lie is known.
2- There are no multiple solutions.

Solution of (E.11) or (E.12) for r_k and ϕ_m yields the location r_k of the point P_k on the cutting edge i,j that cuts at (r_p,z_q) and the hob rotation angle (ϕ_m) or time, at which cutting occurs. Note that the points P_{pq} will all, in general, be cut by different points on each hob tooth at different hob rotation angles. The (r_p,z_q) grid still does not match up conveniently with the hob co-ordinate system, in this case, however, since we can not predetermine "equally spaced" points P_k along the cutting edge has been made, or to fix the hob rotation angle ϕ_0 at equal increments of rotation.

Once r_k and ϕ_m have been found for each (r_p,z_q) grid point, the polar co-ordinate θ_{pq} can be calculated from (E.10). Direct comparison of points generated by different teeth is then possible, allowing determination of the tangential depth of cut $h_{t,pq}$ at each grid point, as in (E.4), for each hob tooth i,j. This is also the depth of cut at the corresponding point $(r_k)_{pq}$ at the corresponding hob rotation angle $(\phi_0)_{p,q}$ on tooth i,j of the hob.

Note, however, that these depths of cut, (from which tooth loads, etc. must be deduced), now occur at "randomly" distributed points (r_k) along the cutting edge of tooth (i,j) and moreover, at different hob rotation angles (times). Also a regular time history is not available, for equal $\Delta\phi_m$ increments, of what happens

at each point P_k on the cutting edge, as before. What is available is the grid of points (p×q) given by $(r_k, \phi_m)_{p,q}$ As shown for each of which $h_{t,p,q}$ is known.

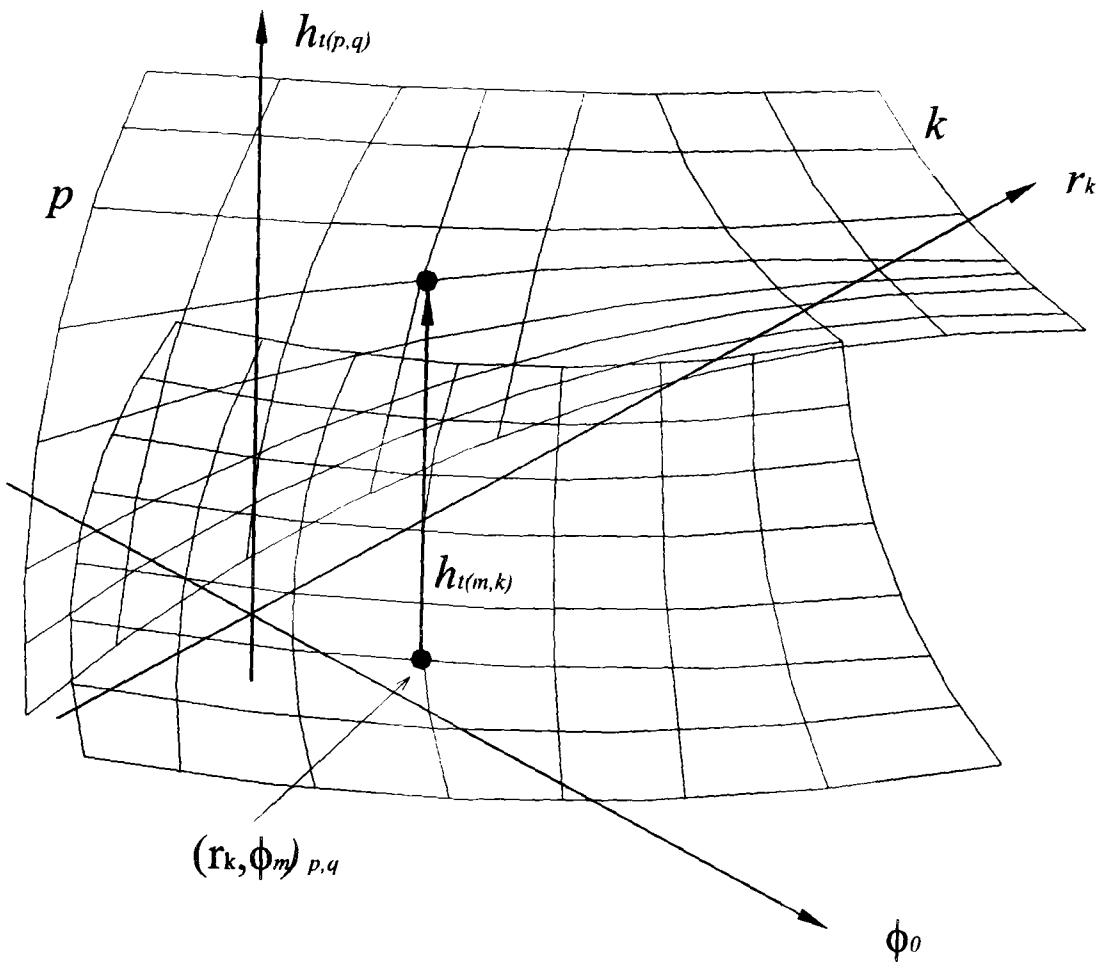

Figure E.11 - The grid of points (p×q) given by $(r_k, \phi_0)_{p,q}$

To calculate $h_{t,(k,m)}$ at regularly spaced points r_k, at equal time intervals $\Delta\phi_0$, an interpolation of the calculated values of $h_{t,p,q}$ is needed. This can be done as previously by using a standard B-spline method, to yield the chip thickness $h_{t,(mk)}$ at each point P_k each cutting edge, at specific angle $(\phi_0)_m$ of the hob rotation. From this point, the solution to determine cutting angles, cutting forces, etc. is exactly the same as before.

This 'direct' method of solution was, in essence, the one used by Terashima (1978, 1980), and, apparently by König (1980), although Weck's later paper (2002), based on König work, suggested that a regular time-spaced grid was later employed, as in this thesis. It is significant that, perhaps because of the lack a regular time-based grid, Terashima did not present results for the time variation of the cutting forces.

Attempts were made to solve equation E.11 numerically, using the MATLAB equation solver, but reliable results could not be obtained. Use of the

minimisation method described above might have been more successful, but this was not investigated further.